

GELMA FOR HYDROGEL FORMULATION
IMPROVING THE PRODUCTION AND EXPLORING ITS VERSATILITY THROUGH
INTERDISCIPLINARITY

Zur Erlangung des akademischen Grades eines
DOKTORS DER INGENIEURWISSENSCHAFTEN (Dr.-Ing.)

von der KIT-Fakultät für Chemieingenieurwesen und Verfahrenstechnik des
Karlsruher Instituts für Technologie (KIT)
genehmigte

DISSERTATION

von
M. Sc. David Andres Grijalva Garces
aus Quito, Ecuador

Erstgutachter: Prof. Dr. Jürgen Hubbuch
Zweitgutachter: Prof. Dr. Norbert Willenbacher

Tag der mündlichen Prüfung: 25.07.2024



This document is licensed under a Creative Commons Attribution 4.0 International License (CC BY 4.0): <https://creativecommons.org/licenses/by/4.0/deed.en>

„What is that about?“

ROBERT M. SAPOLSKY

Acknowledgements

This experimental and writing thesis was a significant amount of work. I thankfully acknowledge every scientific and social interaction during the past years that contributed to the journey of this Ph.D.

I thank Prof. Dr. Jürgen Hubbuch, head of the Biomolecular Separation Engineering department. I want to express my profound appreciation for the opportunity to do this work, which included lengthy discussions about the projects that led to valuable scientific input. Thank you, especially for the freedom to choose the ideas I was keen to follow.

I sincerely thank Prof. Dr. Norbert Willenbacher for his interest in my thesis and his role as a second reviewer. In addition to the scientific work, I am grateful for the excellent talks during my visits to the Institute of Applied Mechanics.

Many thanks to Prof. Dr. Matthias Franzreb for the organizational supervision during some years when our group was part of the Institute of Functional Interfaces. Also, thanks to the members of his group for the pleasant time. Additionally, I thank Dr.-Ing. Nico Leister from the Department of Food Process Engineering for the scientific cooperation.

Special thanks to my colleagues who have contributed substantially to the lovely time at the institute. Thank you for the shared activities that included work in the lab, long hours of supervision of the practical course, and breaks for coffee and cake, to name a few. Thanks to Carsten for his kindness, mentoring, and discussions, which contributed to the origin of ideas central to this thesis. Thanks to Sarah and Barbara for the scientific discussion and their patience regarding the paperwork and bureaucracy. Completing this thesis would not have been possible without the cooperation and support of my colleagues, Svenja and Jasmin. I am so grateful for having the opportunity to meet and work with Lukas and Saskia. I thank them for the relationship in and outside of work.

My students, Anna, Amelie, Johanna, Lea, Christian, and Luise, whose help cannot be overestimated, contributed to this work. I express my gratitude to all of them. I learned so much from them, and I hope they can take something from working with me in the lab and while writing their manuscripts.

I would also like to express my deepest appreciation to the family I made along the way: Julia, Nevena, Theda, Jascha, Jonny, and Moritz. Thanks to my sister, Cristina, and mother, Damariz, for many years of unconditional support. I thank all of them for their support and encouragement, which provided me with a safe space full of love.

Abstract

Biomaterials offer innovative solutions to address diverse challenges in medicine and biotechnology. These materials are engineered to interact with biological systems to improve health outcomes, drug testing, and diagnostics. One class of biomaterials is hydrogels, three-dimensional polymeric networks capable of absorbing and retaining large amounts of water. These resemble the natural extracellular matrix (ECM) in living tissues. Hydrogels can be designed to mimic the biochemical and physical properties of native tissues, making them ideal candidates for a wide range of biomedical applications and biomanufacturing. Gelatin methacryloyl (GelMA) is a promising macromolecule used as the backbone of the polymeric network. GelMA is derived from gelatin, a natural protein obtained from collagen, and modified through methacrylation to introduce residues for photo-crosslinking. This modification grants GelMA tunable properties, including mechanical strength, degradation rate, and bioactivity. Its ability to support cell adhesion, proliferation, and differentiation makes GelMA an excellent scaffold material for tissue engineering and as a platform for biomanufacturing. For this purpose, various advanced manufacturing processes can be applied to create three-dimensional structures with tailored architecture and functionality.

Biomaterials science is a discipline of high complexity and has gained attention in research due to its potential. However, an appropriate transfer of knowledge and the associated methods have been missing, leading to poor comparability across the literature and, hence, a slow translation into clinical stages. The purpose of the thesis is to strengthen the concept of interdisciplinary research. It aims to increase knowledge of GelMA production and explore its compatibility with advanced fabrication methods by developing robust processes and analytical methods, promoting standardized approaches, and providing reproducibility and comparability.

In the first part of this thesis, a new approach is presented in Chapter 3 for functionalizing the most commonly used gelatin to GelMA. The protein from porcine source with a bloom value of 300 g could be processed at room temperature due to urea in the reaction buffer, in contrast to similar studies limited to the range of 35 to 50 °C. At a concentration of 4 M urea, the physical sol-gel transition of gelatin was inhibited. Following the reaction, the purification step consisted of tangential flow filtration. This step accelerated the purification process compared to conventionally applied dialysis. Furthermore, this approach was implemented in Chapter 4 for the derivatization of further raw materials from bovine and fish origin and porcine gelatin with varying bloom strength and, i.e., molecular weight. The degree of functionalization (DoF) is a critical quality attribute for the formulation of hydrogels as it describes the extent of the possible crosslinking. Gelatin source, bloom strength, and batch-to-batch inconsistencies affected the resulting DoF. This property

could be set controllable by variation of the reactant ratio. Moreover, GelMA-based hydrogels were produced, and physical properties were determined. The elasticity and swelling behavior depended on the protein concentration, DoF, and raw material. Regarding the reaction process, robustness was enhanced as the presented method widens the operating range to room temperature. This is advantageous for the scale-up as a thorough mixing in the reactors is guaranteed, hence avoiding temperature profiles that could lead to gelation. A better understanding of the reaction was gained concerning the significance of raw materials. Since the reactants are not miscible, methacrylic anhydride is dispersed as droplets in the gelatin solution. Gelatin is inherently surface active, and the magnitude of its adsorption at the interface depends on molecular weight, molecular weight distribution, and surface charge. As a result, transferring specific production methods requires adaptation according to the raw material.

Furthermore, this part of the thesis included two applications of GelMA. Chapter 3 presents the fabrication of hydrogels for cell culture applications and the determination of their biocompatibility. Cells were cultured over three days, and the viability was determined using fluorescent staining and microscopy. The conventionally used live/dead staining was expanded to include a third fluorophore. The nuclear staining resulted in the tagging of the entire cell population. Automated image processing and analysis have been extensively used in biology to extract cellular features by analyzing separate signals from multiple staining. An automated workflow was developed in this thesis to quantify the viability. Single cells in continuous cellular regions could be identified from overlapping live or dead stains with the nuclear stain. Additionally, automated image analysis enabled the extraction of large data sets as a large number of images could be analyzed, identifying a considerable number of cells. Moreover, GelMA for the microfluidic fabrication of hydrogel microparticles is presented in Chapter 4. These were produced in a single pipeline consisting of a co-flow setup for the droplet generation and a subsequent UV irradiation for photo-crosslinking. The disperse phase consisted of GelMA with concentrations up to 20 % (w/v) in an aqueous solution containing 4 M urea, while the continuous phase was sunflower seed oil. This formulation enabled the experimental execution at room temperature and avoided blockage of the capillaries in submillimeter dimensions without heating the system. Automated image analysis was applied to determine the structural features of droplets and microparticles. Image sequences taken directly at the droplet break-up point were analyzed, and the effect of processing parameters was characterized. The particle size increased with decreasing feed ratio of disperse to continuous phase and increasing GelMA concentration. Moreover, the swelling behavior was studied using a developed image processing workflow that could trace the boundary of particles both in production oil and in cell culture media. The swelling ratio of hydrogel microparticles decreased with increasing polymer concentration. Hence, robust analytical strategies were implemented to characterize biocompatibility droplets and particle size. Automated image analysis proved suitable for the applications. The tools offer time-saving data extraction while increasing reproducibility and reducing operator-dependent errors.

The second part of this thesis revolves around using GelMA in extrusion-based bioprinting, setting comparable experimental settings, and developing robust analytical techniques. For this purpose, polymer solutions comprising GelMA and alginate mixtures were used in Chapter 5. While the concentration of the former was prepared at 3 % (w/v), the concentration of the latter was set at 3 % (w/v) and 4 % (w/v) of the latter. The rheological characterization of the bioink consisted of measuring shear rate-dependent viscosity and applying the power law model to describe this flow behavior. Furthermore, this knowledge enabled the calculation of the required pneumatic pressure to print both bioinks at an equal flow rate. This is a requisite for the comparability of both the structural properties of printed scaffolds and the effect of the biomaterial flow during printing. The

characterization of printing accuracy was performed by imaging and automated image analysis. This analytical strategy was used to extract geometric features of the printed models that consisted of lines, circles, and angles. This approach allowed the determination of metrics at several points along the structure, shortened analytical time, and avoided the possible error of manual data extraction, which is still a common procedure in literature. Moreover, the characterization of processing effects on cells consisted of determining cell viability after mixing cell suspension with biomaterial ink and the printing process itself. Therefore, after each process, the cell-laden polymer solution was diluted, live/dead stains were added, and the cell suspension was analyzed using flow cytometry. This approach, commonly used in biological studies, identifies large numbers of cells. This strategy is advantageous compared to current studies that determine cell viability by manual counting in microscopic images. Furthermore, the characterization of printing accuracy showed no effect of the bioink composition on the geometric features. In contrast, the examination of cell viability revealed that the 1% (w/v) increment led to a significant reduction of viable cells after each single processing step. In the field of bioprinting, the selection of bioinks has been accepted as an either-or question, as properties that enhance structural stability and accuracy are opposed to properties that provide cells with a suitable environment. However, setting an equal flow rate in the presented study challenges this question and leads to identifying a better-performing bioink.

Furthermore, standardized processing settings and analytical methods were established for the study in Chapter 6. This study aimed to evaluate the reproducibility of printing processes within a group of 12 research institutions in Germany. For this purpose, standardized operation procedures were developed for the different operators to follow during printing and the subsequent imaging of structures. In addition, labware, printing components, digital models, and biomaterials were distributed to the participants. Three biomaterials included alginate solutions, GelMA solutions, and a commercially available, ready-to-use ink. The imaging system was also the same for all experiments. After data generation, experimental records and images were centrally stored. The study analysis included a qualitative evaluation of all 2160 images to recognize difficulties during printing and imaging. Identifying patterns in combination with analysis of the provided records reveals that the operators had a significant role during both processes. In addition, three further groups were included to develop independent automated image analysis tools to extract the geometric properties of printed structures. Quantitative data was retrieved from the images as measurements, including but not limited to mean filament width and distributions thereof. The associated coefficients of variation were calculated to assess inter- and intra-laboratory reproducibility. Certain features of the printing equipment could be identified as advantageous for reproducible printing. The use of mechanically operated pistons, automated determination of the nozzle coordinates, and a heating mechanism that enables heating and cooling of the cartridge holder led to an enhancement in the reproducibility of the experiments. The possibility of precise heating and temperature setting was crucial for the GelMA solution printing. Records showed the required increment of pneumatic pressure due to cooling and gelation of the solution. Missing heating elements, as well as electric heating, lead to high variability. In contrast, printers equipped with fluid circulation systems as heating methods could provide more reproducible processes without the intervention of the operator. This led to the conclusion that standardization of printing processes is not yet possible under the current circumstances, as the operator still plays a crucial role in the process due to missing equipment automation. Nonetheless, challenges to be tackled for translating bioprinted scaffolds into clinical stages have been identified.

To summarise this thesis, an improvement was made in the production of GelMA, and the effect of raw materials on the product was studied. A robust processing range in terms of reaction

temperature was proposed. It was demonstrated that GelMA is a versatile biomaterial for preparing hydrogels for cell culture applications and is compatible with advanced processing techniques such as microfluidic fabrication and bioprinting. The precise formulation of the solutions could also enable the processing of GelMA solutions with microdroplets by inhibiting their challenging gelation. By applying methods and principles from other disciplines, comparable experimental settings could be established, and objective, quantitative data was retrieved. Automated image analysis was used to determine macroscopic structural features and identify cells at the microscopic level. Additionally, flow cytometry was introduced as a cell analytical approach that increases the significance of acquired data. Critical features of the bioprinter were identified to manage the printing of GelMA solutions. By reinforcing interdisciplinary research, reliable data can be generated, which is the basis for the translation of the material into clinical stages.

Zusammenfassung

Biomaterialien bieten innovative Lösungen für die verschiedensten Herausforderungen in der Medizin und Biotechnologie. Diese Materialien sind so entwickelt, dass sie mit biologischen Systemen interagieren, um Gesundheitsergebnisse, Medikamententests und Diagnosen zu verbessern. Eine Klasse von Biomaterialien sind Hydrogele, dreidimensionale Polymernetzwerke, die in der Lage sind, große Mengen Wasser zu absorbieren und zu binden. Hydrogele ähneln der natürlichen extrazellulären Matrix (ECM) in lebenden Geweben. Diese können so gestaltet werden, dass sie die biochemischen und physikalischen Eigenschaften von nativem Gewebe nachahmen, was sie zu idealen Kandidaten für ein breites Spektrum biomedizinischer Anwendungen und die biologische Stoffproduktion macht. Gelatine-Methacryloyl (GelMA) ist ein vielversprechendes Makromolekül, das als Grundgerüst des polymeren Netzwerks verwendet wird. GelMA wird aus Gelatine gewonnen, einem natürlichen Protein, das aus Kollagen gewonnen wird, und durch Methacrylierung modifiziert, um Reste für die Photovernetzung einzuführen. Diese Modifizierung verleiht GelMA einstellbare Eigenschaften, darunter mechanische Festigkeit, Abbaurate und Bioaktivität. Seine Fähigkeit, die Zelladhäsion, -proliferation und -differenzierung zu unterstützen, macht GelMA zu einem hervorragenden Gerüstmaterial für das Tissue Engineering und als Plattform für die biologische Stoffproduktion. Zu diesem Zweck können verschiedene fortschrittliche Herstellungsverfahren angewendet werden, um dreidimensionale Strukturen mit maßgeschneiderter Architektur und Funktionalität zu schaffen.

Die Biomaterialwissenschaft ist eine hochkomplexe Disziplin, die aufgrund ihres Potenzials in der Forschung an Aufmerksamkeit gewonnen hat. Es fehlt jedoch ein angemessener Wissenstransfer und die dazugehörigen Methoden, was zu einer schlechten Vergleichbarkeit in der Literatur und damit zu einer langsamen Translation in klinischen Phasen führt. Das Ziel dieser Arbeit ist es, das Konzept der interdisziplinären Forschung zu fördern. Sie zielt darauf ab, das Wissen über die Herstellung von GelMA zu erweitern und die Kompatibilität mit fortschrittlichen Herstellungsmethoden zu erforschen, indem robuste Prozesse und Analysemethoden entwickelt und standardisierte Ansätze gefördert werden, die Reproduzierbarkeit und Vergleichbarkeit gewährleisten.

Im ersten Teil dieser Arbeit wird in Kapitel 3 ein neuer Ansatz zur Funktionalisierung der am häufigsten verwendeten Gelatine zu GelMA vorgestellt. Das Protein aus Schweinefleisch mit einem Bloom-Wert von 30 g konnte dank Harnstoff im Reaktionspuffer bei Raumtemperatur verarbeitet werden, im Gegensatz zu ähnlichen Studien, die auf den Bereich von 35 und 50 °C beschränkt sind. Bei einer Konzentration von 4 M Harnstoff wurde der physikalische Sol-Gel-Übergang der Gelatine gehemmt. Im Anschluss an die Reaktion erfolgte die Aufreinigung durch Querstromfiltration. Dieser Schritt beschleunigte den Aufreinigungsprozess im Vergleich zur konventionell angewandten Dialyse.

Darüber hinaus wurde dieser Ansatz in Kapitel 4 für die Derivatisierung weiterer Rohstoffe von Rindern und Fischen sowie von Schweinegelatine mit unterschiedlicher Gelstärke bzw. Molekulargewicht umgesetzt. Der Funktionalisierungsgrad (*engl. Degree of Functionalization - DoF*) ist ein kritisches Qualitätsmerkmal für die Formulierung von Hydrogelen, da er das Ausmaß der möglichen Vernetzung beschreibt. Die Gelatinequelle, der Bloom-Wert und Variabilität von Charge zu Charge wirkten sich auf den DoF aus. Diese Eigenschaft konnte durch Variation des Reaktantenverhältnisses eingestellt werden. Außerdem wurden Hydrogele auf GelMA-Basis hergestellt und die physikalischen Eigenschaften bestimmt. Die Elastizität und das Quellverhalten hingen von der Proteinkonzentration, der DoF und dem Rohmaterial ab. Im Hinblick auf den Reaktionsprozess wurde die Robustheit verbessert, da die vorgestellte Methode den Betriebsbereich auf Raumtemperatur ausdehnt. Dies ist vorteilhaft für das Scale-up, da eine gründliche Durchmischung in den Reaktoren gewährleistet ist und somit Temperaturprofile vermieden werden, die zu einer Gelierung führen könnten. Es wurde ein besseres Verständnis der Reaktion im Hinblick auf die Bedeutung der Ausgangsstoffe gewonnen. Da die Reaktanten nicht mischbar sind, wird Methacrylsäureanhydrid als Tröpfchen in der Gelatinelösung dispergiert. Gelatine ist von Natur aus grenzflächenaktiv, und das Ausmaß ihrer Adsorption an der Grenzfläche hängt vom Molekulargewicht, der Molekulargewichtsverteilung und der Oberflächenladung ab. Die Übertragung spezifischer Produktionsmethoden erfordert daher eine Anpassung an das jeweilige Rohmaterial.

Darüber hinaus umfasst dieser Teil der Arbeit zwei Anwendungen von GelMA. Kapitel 3 befasst sich mit der Herstellung von Hydrogelen für Zellkulturanwendungen und der Bestimmung ihrer Biokompatibilität. Die Zellen wurden drei Tage lang kultiviert, und ihre Viabilität wurde mittels Fluoreszenzfärbung und Mikroskopie bestimmt. Die herkömmliche Lebend/Tot-Färbung wurde um einen dritten Fluorophor erweitert. Die Zellkernfärbung führte zur Markierung der gesamten Zellpopulation. Automatisierte Bildverarbeitung und -analyse werden in der Biologie häufig eingesetzt, um zelluläre Merkmale zu extrahieren, indem separate Signale aus mehreren Färbungen analysiert werden. In dieser Arbeit wurde ein automatisierter Ablauf entwickelt, um die Lebensfähigkeit zu quantifizieren. Einzelne Zellen in zusammenhängenden Zellregionen konnten durch Überlappung von Lebend- oder Totfärbungen mit der Kernfärbung identifiziert werden. Darüber hinaus ermöglichte die automatisierte Bildanalyse die Extraktion großer Datensätze, da eine große Anzahl von Bildern analysiert werden konnte, wodurch eine bedeutende Anzahl von Zellen identifiziert wurde. Darüber hinaus wird in Kapitel 4 GelMA für die mikrofluidische Herstellung von Hydrogel-Mikropartikeln vorgestellt. Diese wurden in einer einzigen Pipeline hergestellt, die aus einem Co-Flow-Setup für die Tröpfchenbildung und einer anschließenden UV-Bestrahlung zur Fotovernetzung bestand. Die disperse Phase bestand aus GelMA mit Konzentrationen bis zu 20 % (w/v) in einer wässrigen Lösung mit 4 M Harnstoff, während die kontinuierliche Phase Sonnenblumenkernöl war. Diese Formulierung ermöglichte die Versuchsdurchführung bei Raumtemperatur und vermied die Verstopfung der Kapillaren im Submillimeterbereich, ohne das System zu erhitzen. Zur Bestimmung der Strukturmerkmale von Tröpfchen und Mikropartikeln wurde eine automatisierte Bildanalyse eingesetzt. Bildsequenzen, die direkt am Punkt des Tropfenaufbruchs aufgenommen wurden, wurden analysiert, und der Einfluss der Verarbeitungsparameter wurde charakterisiert. Die Partikelgröße nahm mit abnehmendem Einsatzverhältnis von disperser zu kontinuierlicher Phase und steigender GelMA-Konzentration zu. Darüber hinaus wurde das Quellverhalten mit Hilfe eines entwickelten Bildverarbeitungsablauf untersucht, mit dem die Grenzen der Partikel sowohl in Produktionsöl als auch in Zellkulturmedium verfolgt werden konnten. Das Quellungsverhältnis der Hydrogel-Mikropartikel nahm mit steigender Polymerkonzentration ab. Daher wurden robuste Analysestrategien zur Charakterisierung von Biokompatibilitätströpfchen und Partikelgröße implementiert. Die automatisierte Bildanalyse erwies

sich als geeignet für die Anwendungen. Die Tools bieten eine zeitsparende Datenextraktion und erhöhen gleichzeitig die Reproduzierbarkeit und reduzieren bedienerabhängige Fehler.

Der zweite Teil dieser Arbeit befasst sich mit der Anwendung von GelMA beim extrusionsbasierten Bioprinting, die Festlegung vergleichbarer Versuchsbedingungen und die Entwicklung robuster Analysetechniken. Zu diesem Zweck wurden in Kapitel 5 Polymerlösungen aus GelMA und Alginat verwendet. Während die Konzentration des Ersteren bei 3 % (w/v) lag, wurde die Konzentration des Letzteren auf 3 % (w/v) und 4 % (w/v) eingestellt. Die rheologische Charakterisierung der Biotinte bestand in der Messung Viskosität in Abhängigkeit der Scherrate und der Anwendung des Power-Law-Fluidmodell zur Beschreibung dieses Fließverhaltens. Mit diesem Wissen konnte außerdem der erforderliche pneumatische Druck berechnet werden, um beide Biotinten bei gleicher Fließgeschwindigkeit zu drucken. Dies ist eine Voraussetzung für die Vergleichbarkeit sowohl der strukturellen Eigenschaften der gedruckten Gerüsten als auch des Einflusses des Biomaterialflusses während des Drucks. Die Charakterisierung der Druckgenauigkeit erfolgte durch Bildgebung und automatische Bildanalyse. Diese analytische Strategie wurde verwendet, um geometrische Merkmale der gedruckten Modelle zu extrahieren, die aus Linien, Kreisen und Winkeln bestanden. Dieser Ansatz ermöglichte die Bestimmung von Messwerten an mehreren Punkten entlang der Struktur, verkürzte Analysezeit und vermied den möglichen Fehler der manuellen Datenextraktion, die in der Literatur immer noch üblich ist. Darüber hinaus bestand die Charakterisierung der Verarbeitungseffekte auf die Zellen in der Bestimmung der Viabilität der Zellen nach dem Mischen der Zellsuspension mit der Biomaterial-Tinte und nach dem Druckprozess selbst. Daher wurde nach jedem Prozess die zellbeladene Polymerlösung verdünnt, Lebend-/Totfärbungen hinzugefügt und die Zellsuspension mittels Durchflusszytometrie analysiert. Mit diesem Ansatz, der in biologischen Studien häufig verwendet wird, lassen sich große Anzahl von Zellen identifizieren. Diese Strategie ist im Vergleich zu aktuellen Studien, bei denen die Lebensfähigkeit der Zellen durch manuelles Zählen in mikroskopischen Bildern bestimmt wird, von Vorteil. Darüber hinaus zeigte die Charakterisierung der Druckgenauigkeit keinen Einfluss der Zusammensetzung der Biotinte auf die geometrischen Merkmale. Im Gegensatz dazu zeigte die Untersuchung der Zellebensfähigkeit, dass die Erhöhung um 1 % (w/v) zu einer signifikanten Verringerung der lebensfähigen Zellen nach jedem einzelnen Verarbeitungsschritt führte. Im Bereich des Bioprinting wurde die Auswahl von Biotinten als eine Entweder-Oder-Frage akzeptiert, da Eigenschaften, die die strukturelle Stabilität und Genauigkeit verbessern, den Eigenschaften, die den Zellen ein geeignetes Umfeld bieten, gegenüberstehen. Die Einstellung einer gleichen Flussrate in der vorliegenden Studie stellt diese Annahme jedoch in Frage und führt zur Identifizierung einer leistungsfähigeren Biotinte.

Außerdem wurden für die Studie in Kapitel 6 standardisierte Verarbeitungs- und Analysemethoden festgelegt. Ziel dieser Studie war es, die Reproduzierbarkeit der Druckprozesse innerhalb einer Gruppe von 12 Forschungseinrichtungen in Deutschland zu bewerten. Zu diesem Zweck wurden Standardvorgehensweise entwickelt, die von den verschiedenen Bedienern während des Drucks und der anschließenden Bildaufnahme der Strukturen zu befolgen sind. Darüber hinaus wurden Laborutensilien, Druckzubehör, digitale Modelle und Biomaterialien an die Teilnehmer verteilt. Zu den drei Biomaterialien gehörten Alginat- und GelMA-Lösungen sowie eine handelsübliche, einsatzbereite Tinte. Auch das Bildgebungssystem war für alle Experimente gleich. Nach der Datengenerierung wurden die Versuchsaufzeichnungen und Bilder zentral gespeichert. Die Analyse der Studie beinhaltete eine qualitative Auswertung aller 2160 Bilder, um Schwierigkeiten beim Druck und bei der Bildgebung zu erkennen. Die Identifizierung von Mustern in Kombination mit der Analyse der zur Verfügung gestellten Protokollen zeigt, dass die Bediener bei beiden Prozessen eine bedeutende Rolle spielten. Darüber hinaus wurden drei weitere Gruppen für die Entwicklung

unabhängiger automatischer Bildanalysetools zur Extraktion der geometrischen Eigenschaften der gedruckten Strukturen einbezogen. Aus den Bildern wurden quantitative Daten in Form von Messungen gewonnen, einschließlich die mittlere Filamentbreite und deren Verteilungen. Die zugehörigen Variationskoeffizienten wurden berechnet, um die Reproduzierbarkeit zwischen und innerhalb von Laboren zu bewerten. Bestimmte Merkmale der Druckausrüstung konnten als vorteilhaft für den reproduzierbaren Druck identifiziert werden. Die Verwendung von mechanisch betätigten Kolben, die automatische Bestimmung der Düsenkoordinaten und ein Heizmechanismus, der das Aufheizen und Abkühlen des Kartuschenhalters ermöglicht, führten zu einer Verbesserung der Reproduzierbarkeit der Experimente. Die Möglichkeit der präzisen Erwärmung und Temperatureinstellung war für den Druck der GelMA-Lösung entscheidend. Die Aufzeichnungen zeigten den erforderlichen Anstieg des pneumatischen Drucks aufgrund der Abkühlung und Gelierung der Lösung. Fehlende Heizelemente sowie die elektrische Beheizung führen zu einer hohen Variabilität. Im Gegensatz dazu konnten Drucker, die mit Strömungserhitzer als Heizmethode ausgestattet waren, reproduzierbarere Prozesse liefern, ohne dass der Bediener eingreifen musste. Dies führte zu der Schlussfolgerung, dass eine Standardisierung von Druckprozessen unter den derzeitigen Umständen noch nicht möglich ist, da der Bediener aufgrund der fehlenden Automatisierung der Geräte immer noch eine entscheidende Rolle im Prozess spielt. Nichtsdestotrotz wurden Herausforderungen identifiziert, die es zu bewältigen gilt, um gedruckte Gerüste in klinische Stadien zu überführen.

Zusammenfassend wurden die Herstellung von GelMA verbessert und die Auswirkungen der Rohstoffe auf das Produkt untersucht. Es wurde ein robuster Betriebsbereich in Bezug auf die Reaktionstemperatur vorgeschlagen. Es wurde gezeigt, dass GelMA ein vielseitiges Biomaterial für die Herstellung von Hydrogelen für Zellkulturanwendungen ist und mit fortgeschrittenen Verarbeitungstechniken wie der mikrofluidischen Herstellung und dem Bioprinting kompatibel ist. Eine präzise Formulierung der Lösungen könnte auch die Verarbeitung von GelMA-Lösungen zu Mikrotropfen ermöglichen, indem die herausfordernde Gelierung verhindert wird. Durch die Anwendung von Methoden und Prinzipien aus anderen Disziplinen konnten vergleichbare Versuchsbedingungen geschaffen und objektive, quantitative Daten gewonnen werden. Die automatisierte Bildanalyse wurde zur Bestimmung makroskopischer Strukturmerkmale und zur Identifizierung von Zellen auf mikroskopischer Ebene eingesetzt. Zusätzlich wurde die Durchflusszytometrie als zellanalytischer Ansatz eingeführt, der die Signifikanz der gewonnenen Daten erhöht. Kritische Merkmale des Bioprinters wurden identifiziert, um den Druck von GelMA-Lösungen zu ermöglichen. Durch die Förderung der interdisziplinären Forschung können verlässliche Daten generiert werden, die die Grundlage für die Translation der biomaterialien in klinische Phasen bilden.

Contents

Acknowledgements	iii
Abstract	v
Zusammenfassung	ix
Contents	xiii
1 Introduction	1
1.1 Cell Culture Technologies	2
1.1.1 Cell Culture Modalities and Cell Analytics	3
1.2 Biomaterials	6
1.2.1 Extracellular Matrix	7
1.2.2 Cell-Material Interaction	7
1.2.3 Hydrogels	8
1.2.4 Biopolymers	10
1.3 Applications and Analytics	15
1.3.1 Substrates for Cell Culture	15
1.3.2 Microparticles	16
1.3.3 Bioprinting	17
2 Thesis Outline	27
2.1 Research Proposal	27
2.2 Manuscript Overview	30
3 A Novel Approach for the Manufacturing of Gelatin-Methacryloyl	35
David Grijalva Garces, Carsten Philipp Radtke and Jürgen Hubbuch	
3.1 Introduction	36
3.2 Materials and methods	37
3.2.1 GelMA Manufacturing and Characterization	37
3.2.2 Hydrogel Characterization	39
3.2.3 Biocompatibility Assessment	40

3.2.4	Data Handling and Statistical Analysis	41
3.3	Results and discussion	41
3.3.1	GelMA Synthesis and Characterization	41
3.3.2	Hydrogel Characterization	44
3.3.3	Biocompatibility Assessment	46
3.4	Conclusions	47
4	The Effect of Gelatin Source on the Synthesis of Gelatin-Methacryloyl and the Production of Hydrogel Microparticles	53
	David Grijalva Garces, Luise Josephine Appoldt, Jasmin Egner, Nico Leister and Jürgen Hubbuch	
4.1	Introduction	54
4.2	Materials and Methods	55
4.2.1	Hydrogel Characterization	57
4.2.2	Microparticle Fabrication and Characterization	57
4.2.3	Data Handling and Statistical analysis	59
4.3	Results and Discussion	59
4.3.1	GelMA Synthesis and Characterization	59
4.3.2	Hydrogel Characterization	64
4.3.3	Microparticle Generation and Characterization	66
4.4	Conclusions	71
5	Analytics in Extrusion-Based Bioprinting: Standardized Methods Improving Quantification and Comparability of the Performance of Bioinks	79
	Svenja Strauß, David Grijalva Garces and Jürgen Hubbuch	
5.1	Introduction	80
5.2	Materials and Methods	81
5.2.1	Cell Culture	81
5.2.2	Biomaterial Ink and Bioink Preparation	82
5.2.3	Rheological Characterization	82
5.2.4	Printing Performance Evaluation	83
5.2.5	Data Handling and Statistical Analysis	86
5.3	Results and Discussion	86
5.3.1	Rheological Characterization	86
5.3.2	Printing Performance	88
5.4	Conclusions	95
6	On the reproducibility of extrusion-based bioprinting: round robin study on standardization in the field	99
	David Grijalva Garces, Svenja Strauß, Sarah Gretzinger, Barbara Schmiege, Tomasz Jüngst, Jürgen Groll, Lorenz Meinel, Isabelle Schmidt, Hanna Hartmann, Katja Schenke-Layland, Nico Brandt, Michael Selzer, Stefan Zimmermann, Peter Koltay, Alexander Southan, Günter E. M. Tovar, Sarah Schmidt, Achim Weber, Tilman Ahlfeld, Michael Gelinsky, Thomas Scheibel, Rainer Detsch, Aldo R. Boccaccini, Toufik Naolou, Cornelia Lee-Thedieck, Christian Willems, Thomas Groth, Stephan Allgeier, Bernd Köhler, Tiaan Friedrich, Heiko Briesen, Janine Buchholz, Dietrich Paulus, Anselm von Gladiss and Jürgen Hubbuch	
6.1	Introduction	101

6.2	Materials and methods	103
6.2.1	Round robin workflow and design	103
6.2.2	Biomaterials, labware, and geometries	103
6.2.3	Round robin - 3D printing	105
6.2.4	Central data exchange and storage	107
6.2.5	Round robin - Image analysis	107
6.2.6	Data handling and visualization	110
6.3	Results and discussion	110
6.3.1	Round robin - 3D printing	110
6.3.2	Round robin - Image analysis: qualitative	110
6.3.3	Round robin - Image analysis: quantitative	113
6.3.4	Assessment of the reproducibility in 3D bioprinting	114
6.4	Conclusions	120
7	Conclusion and Outlook	125
	References	129
	List of Figures	148
	List of Tables	150
A5	On the reproducibility of extrusion-based bioprinting: round robin study on standardization in the field	155
A5.1	CAD models used during the Round robin – 3D printing test	157
A5.2	Schematic draft of line and circle width	158
A5.3	Exemplary raw images	159

Introduction

Biomaterials science is profoundly significant in advancing various fields. These can be used as prostheses and as carriers of pharmaceutical proteins in medicine, where the biomaterial itself is part of the final product. In combination with living cells, the biomaterial is considered a tissue-engineered product. Tissue models containing biomaterials are also used in diagnostics, studies of disease, and drug discovery. Furthermore, biomaterials can also be used as an aid during the production of biological material for cell therapy and biomanufacturing as a component of bioreactors during cell culture. [1–3] Benefiting from the expertise of biology, materials science, mechanical engineering, and process engineering, biomaterials are developed to interact with biological systems. [3, 4] This type of material includes ceramics, metals, and polymers, both synthetics and naturally derived. Hydrogels stand out among biomaterials for their ability to mimic the native extracellular matrix, providing an ideal environment for cell growth [5, 6]. Gelatin Methacryloyl (GelMA) is an essential component of biomaterials research. Produced through the modification of gelatin, GelMA offers tunable properties suitable for diverse applications, including tissue engineering, drug delivery, and 3D bioprinting [7]. The multidisciplinary approach is vital for comprehending mechanisms during processing and applications to achieve the full potential of biomaterials. However, the transfer of methods between single fields remains incomplete, hindering the integration of expertise from other fields into biomaterials science. The transfer and adaptation of methods are critical to address this limitation, ensuring their applicability and reliability in the framework. Developing robust processes and analytical techniques not only enhance reproducibility in research and development but also can enable translation into clinical applications of tissue-engineered products. This thesis aims to better understand different aspects of GelMA, encompassing its manufacturing processes and compatibility with diverse fabrication techniques. Furthermore, methodologies from other disciplines are applied to ensure the reliability and comparability of the acquired data. This interdisciplinary strategy facilitates progress in elucidating the complex interplay between the processing of biomaterials and the product itself, as well as the interactions between biomaterials and biological systems.

1.1 Cell Culture Technologies

Biomaterials provide essential tools for advancing our understanding of cellular processes and developing innovative therapies for various biomedical applications. Cell culture applications include developmental biology, disease progression, drug testing, and biomanufacturing studies. [8] For any of said purposes, cells are in contact with various materials. This section provides an overview of current cell culture platforms and analytics thereof.

Cells are isolated from native tissues and expanded in bioreactors or tissue culture plates. Similar to in vivo conditions, cells cultured in vitro require nutrients delivered by fluid in the direct surroundings. This liquid, known as cell culture media (CCM), comprises dissolved components such as glucose, amino acids, vitamins, and minerals. Lipids, trace elements, and growth factors are also part of the formulation of any CCM. [8] In the case of in vitro studies of pharmacology and basic biological research, the CCM is supplemented with animal serum as a source of nutrients, as serum contains hormones, growth factors, and carrier proteins. However, this constitutes an issue in research due to batch-to-batch variability of the composition. Of particular interest in the production of biopharmaceuticals is the use of chemically defined CCM, meaning that the content of the media is completely known. In addition to eliminating contamination, the lack of serum in CCM is an advantage in developing robust processes since serum-free media solely contain a known concentration of nutrients. [9] The precise composition of the CCM depends on the cell phenotype used in culture. [10] Cell phenotype also determines metabolism, proliferation as well as morphology [11]. For instance, cells from adipose tissue require glucose and fatty acids as an energy source, whereas the primary energy substrate in the brain is glucose. Furthermore, the energy consumption by neurons is significantly higher than that shown by other cell types. This is because mammals have a large number of neurons where each cell can have up to a thousand synapses, and a significant amount of energy is required to enable solely the communication between cells [12, 13]. Similarly, cancer cells uptake an elevated share of nutrients compared to normal cells. [14, 15] This abnormal type of cell is used in cancer research and the production of therapeutic proteins [16].

According to their use in vitro, three major types of cells are devised. Primary cells are derived from native tissue. This cell type is used to study the in vivo state, as these keep the characteristics shown in the native tissue. Such studies are critical in developmental biology and the study of early-stage disease. Additionally, such cells are tested in the pre-clinical stages of drug discovery as they resemble their native counterparts. Furthermore, cell lines are developed when primary cells are subcultured in controlled environments, leading to a significant increase in proliferation rate. Additionally, cell lines are genetically less heterogeneous than their primary counterparts. Cell lines can be genetically modified to become immortal. This type of cell is known as the immortalized cell strain. This kind of cell is used in the early stages of drug development as they share some attributes of primary cells and do not have ethical concerns compared to animal or human material use. Immortalized and cancer cell strains are also beneficial in the manufacturing of biopharmaceuticals. Both cell types proliferate indefinitely at a high rate in vitro, which is advantageous as it represents a cost-effective and unlimited source of biological material. These production entities are also genetically homogeneous, leading to more robust cell culture processes. [8, 17]

In the case of the production of therapeutic proteins, a production cell strain is selected from several clones. Subsequently, cell banks are created and preserved at temperatures below freezing [8]. Similarly, primary cells can be preserved cryogenically during the transition between donation and research facilities [18]. In both cases, cryoprotectants are included in the formulation of the media. Dimethyl sulfoxide and glycerol are examples thereof. Such supplements inhibit the formation of ice

crystals; therefore, the cells are protected from hypertonic conditions during freezing. Long-term preservation of biological material is performed below -130°C , i.e., within the vapor or liquid phase of nitrogen. Moreover, cells are thawed and expanded in the research or production facility to reach the required amount of cells. This number depends on the intended application. [18, 19] The following section provides an overview of cell culture modalities and cell analytics.

1.1.1 Cell Culture Modalities and Cell Analytics

1.1.1.1 Suspension Cell Culture

To increase the productivity of the manufacturing of therapeutic proteins, cells can be genetically adapted to grow in suspension, i.e., without attachment to a tissue or substrate. One prominent example is the Chinese Hamster Ovary (CHO) cell strain for the production of antibodies. This cell type is cultured in suspension; meaning cells grow in a liquid phase within a stirred bioreactor. The liquid phase in the bioreactor is CCM, which contains nutrients, oxygen, and carbon dioxide. The stirring ensures the homogeneous distribution of components. In the typical production process for monoclonal antibodies, cells are thawed and cultured in bioreactors at a small scale. After a certain number of cells is reached, cells are passaged to the following scale, and so forth, until the cell density for the inoculum of production bioreactors is reached. The passaging of cells is relatively easy, as cells growing in suspension can be easily separated from the liquid media. Typical cell densities in the production of antibodies range from 5×10^6 to 30×10^6 cells mL^{-1} in bioreactors with a capacity up to 10×10^3 L. Cell culture at such large scales can be performed as stirring ensures the supply of nutrients and homogeneous culture conditions at any scale. During the cell culture process, nutrients are consumed, and the concentration of the product and metabolites increases in the bulk phase. This might inhibit the productivity of the host cell strain. However, CCM can be easily replaced with fresh media to enhance the cell culture while keeping the host cells in culture. [11, 16, 17, 20]

Both online and offline, sensors can be implemented to determine the process parameters such as temperature, pH, and gas concentrations. Additionally, the profiles of nutrients, metabolites, and products are monitored. For this purpose, chromatography and mass spectrometry are used. Electrochemical methods and optical sensors are applied to increase the speed of the analysis as well. [21] Profiles of limiting nutrients can be traced to determine the optimal culture time before the renewal of CCM. Moreover, online optical density sensors are widely used in suspension cell strains. Said method is based on light scattering and provides information about cell numbers in culture. [20] However, direct information regarding the metabolic state of cells can only be traced offline. Different techniques can be applied to determine the cellular state, mainly during cell strain development before production. These methods can be divided into two categories: direct or indirect assays. Direct testing consists of the conjugation of a specific marker of the cell with a fluorophore. For example, Annexin-V is used to detect apoptosis as the component interacts only with residues of the cell membrane that are externalized when the cell enters the programmed cell death [22]. The indirect assay to test cell metabolism involves converting an analyte to a colored or fluorescent product. An example of the indirect technique is the MTT (3-(4,5-dimethylthiazol-2-yl)-2,5-diphenyltetrazolium bromide) assay. The dissolved salt can permeate through the intact cell membrane, where the component is reduced by enzymes within the cell. The reaction product, formazan, is a blue-colored component. This method is used to determine the proliferation of cells. [23] Once the component tags the cell marker or is converted to the

measurable component of the assay, light absorbance or fluorescence intensity can be measured using a spectrometer. Alternatively, cells can be visualized and quantified using microscopy. A further method to characterize cells in suspension is flow cytometry [24]. Moreover, the assays involve adding the analytes to the liquid phase around the cells. Hence, the assay analytes readily diffuse and reach the cells to be characterized. [25]

1.1.1.2 Two-Dimensional Cell Culture

In contrast to strains used for biomanufacturing, cells of interest in biological research, cell therapy, and regenerative medicine are cultured in vessels that provide a surface for the cells to attach to. This cell culture modality is known as two-dimensional (2D) cell culture. Surfaces are made mainly out of plastics or glass. These materials are treated with gas plasma for the surface to be hydrophilic or negatively charged. Alternatively, surfaces can be coated with peptides or proteins to enable cell adhesion. The approaches to allow cell adhesion depend on cell type, i.e., on the native origin of the cell. [8, 17] A prominent example of this kind of cell culture is the use of Henrietta Lacks (HeLa) cell line. This method has provided insight into several types of processes of human biology and into cancer pathways [26]. A further example is using Human Embryonic Kidney (HEK) 293 cells. The application of these cells has been manufacturing recombinant proteins and therapeutic viral vectors [27]. Moreover, cryopreserved cells are thawed before use in the research or production facility. Cells attach to the growth surface and proliferate. Cells are passaged before reaching confluency, meaning the complete covering of the growth surface, as cell proliferation stops due to contact inhibition. [8, 17] For cell passaging, cell adhesion peptides on the membrane are enzymatically cleaved using proteases, mainly trypsin, and the ethylenediaminetetraacetic acid (EDTA) binds calcium and magnesium ions that are required for the complex formation within adhesion proteins [28]. Subsequently, the required cells are seeded into the next culture vessel, and fresh CCM is provided. In the large-scale production of cells, scaling the growth area presents a challenge as the number of culture flasks has to be increased. For instance, the production of 1.3×10^{10} embryonic stem cells (ESC) requires a growth surface of $9.75 \times 10^5 \text{ cm}^2$. This large surface involves the use of about 4334 commercially available tissue culture (TC) flasks with a surface of 225 cm^2 (T-225) each. Efforts have been made to increase productivity and reduce the cost of producing such high amounts of cells. For instance, HEK293 cells have been modified to be cultured in suspension [27]. A further approach is the use of microcarriers in a stirred reactor. Microcarriers are spheres made of proteins or polymers in the size range of 50 to 500 μm . The use of such carriers increases the growth surface-to-volume ratio. As discussed above, it enables the use of stirred reactors, which have the advantage of a homogeneous distribution of nutrients, gases, and so forth. [28] Furthermore, the surface for cell attachment can be enlarged in bioreactors with fibers, where cells attach to the fibers, and the CCM flows continuously through the fiber-packed reactor. This also enables the homogeneous and steady supply of nutrients to the biological material. [29] In all named methods, cells adhere to a solid surface and are surrounded by the liquid CCM.

Similar to cell culture in suspension, sensors can determine process conditions in real time, including pH, temperature, and gas concentration. Furthermore, concentration profiles of metabolites and nutrients can be tracked. As adherent cells grow as a monolayer on top of transparent surfaces, microscopy imaging is included in the cell culture setup. This method has the advantage of low contamination risk as no physical probe has to be introduced in the culture vessel. Image acquisition and data analysis can be automated to determine single-cell features such as morphology and size. In addition, metrics of cell groups such as clustering, confluency, and connectivity

can also be quantified. [30] However, as each cell type exhibits different characteristics, the data extraction software has to be adapted and validated for case [31, 32]. Assays to determine metabolic characteristics are similar to those in suspension cell culture. Analytes are added to the liquid media. Subsequently, the fluorescence of colorimetric assays is quantified using a spectrometer or microscope. These assays can be performed directly on cells attached to the substrate. Alternatively, the cells can be harvested before the analytical procedure; cells are labeled in a suspension and analyzed. As the cells are suspended in liquid media, flow cytometry can be applied to detect fluorescent markers. In both cases, analytes diffuse readily to the cells and are uptaken. Most analytes and the associated protocols are developed for this art of cell culture and are established in the field as standards. [11]

1.1.1.3 Three-Dimensional Cell Culture

Cell cultures on 2D substrates have been a helpful approach to understanding basic cellular activities. However, this method cannot mimic the microenvironment of cells in native tissue. Differences have been shown in spatial distribution, morphology, and cytoskeletal structure, as well as in metabolic behavior such as proliferation and differentiation [33, 34]. One example is the cell culture of hepatocytes, cells from the liver. It has been shown that this type of cell survives longer when cultured within collagen gels than when grown on cell culture plates [35]. Therefore, different methods have been developed to generate three-dimensional (3D) structures that attempt to mimic their native extracellular matrix (ECM) and, thus, provide more relevant data regarding biological processes, drug discovery, and disease progression. Hydrogels have been studied as promising candidates for the creation of tissue imitates. [6, 36] Depending on the applications, cryopreserved cells are thawed and prepared before seeding on the 3D substrate. This step can be performed directly after thawing or expansion on cell culture flasks to reach the required quantity of cells. Seeding can be performed pre- or post-fabrication. The first method consists of mixing the cells with a polymer solution that is polymerized in a subsequent space. In contrast, the latter method consists of seeding the cells onto ready-to-use substrates, also known as scaffolds. Both methods are widely used, and both show advantages and disadvantages. Even though cells can be homogeneously distributed into a precursor solution, the polymerization condition of the solution to a scaffold can be detrimental. For the post-fabrication seeding approach, harsh conditions can be applied to form the scaffold. However, the penetration depth of the cells directly after seeding is limited. [37, 38] The cell-laden scaffolds are placed in CCM-containing bioreactors. While the CCM surrounding the scaffold can be easily renewed if needed, the limitation lies in the nutrient and gas supply in the direct cell surrounding. [11] In native tissue, the distance to a blood vessel is around 100 to 200 μm , and any distances higher than that can hinder the diffusion of molecules through the matrices [25, 39]. Therefore, any protocol for 2D cell culture has to be adapted when 3D methods are applied, including the design of scaffolds to contain vessel-like structures within the scaffold.

Furthermore, similar to bioreactors for suspension and 2D cell culture, sensors are applied to monitor nutrient consumption and cell culture conditions. However, the analysis of further cellular features is limited by biological, physical, and technical issues. Since the cells grow in 3D matrices, the surface for the uptake of nutrients and analytes, such as dyes, differs from the surface of cells growing on 2D surfaces. In addition, as is the case for nutrients, the diffusion of analytes through the scaffold material is restricted. The surface properties of the scaffold interact with the surrounding fluid as well as with the solutes. This interaction depends on the charges of both scaffold materials and dissolved components. Therefore, fluorescent dyes might reach the cells at

different times depending on the location away from the liquid-scaffold interface. In the case of assays based on analyte conversion, the detectable compound might not reach the liquid phase. The issue for the detection of expressed factors or metabolites is similar. For instance, the Alamar Blue assay has been widely used in 2D cell cultures. However, differences were shown when applying the same protocol in 2D and 3D cell cultures. These were identified as dependent on time and analyte concentration and were attributed to the differing uptake rates by the cells. [40] Moreover, live/dead fluorescent staining is a further established assay for quantifying cell viability in 2D and 3D cell cultures. Differences were shown in the assay performance that depended on the 3D scaffold material. Cell-free collagen scaffolds led to the detection of increasing fluorescence intensity with increasing sample thickness compared to cell-free PEGylated fibrin scaffolds. [25] These studies imply that cell culture protocols and the associated analytical strategies require adaptation for 3D cell culture. Additionally, validation of adapted protocols might include appropriate controls [40, 41].

1.2 Biomaterials

An intersection between cells and materials arises in developing disease research models and producing tissue-engineered products. To recapitulate tissue properties, biomaterials are used in different combinations to create scaffolds to support cellular functions. Definitions of the term *biomaterials* have been introduced by the National Institutes of Health (NIH) in the United States and the European Society of Biomaterials (ESB). The NIH presented a definition oriented toward the clinical use of said materials, which is "any substance or combination of substances, other than drugs, synthetic or natural in origin, which can be used for any period, which augments or replaces partially or any tissue, organ or function of the body, to maintain or improve the quality of life of the individual" [42]. In contrast, the definition by the ESB is more simple and applicable to research applications: "material intended to interface with biological systems to evaluate, treat, augment or replace any tissue, organ or function of the body" [4].

Disciplines such as biology, materials science, mechanical engineering, and process engineering contribute to biomaterials research and development. For example, biologists contribute their expertise in cellular biology and molecular interactions to study how biomaterials interact with living tissues and cells. Material scientists investigate the structure-property relationships of biomaterials at the molecular level, guiding the design and optimization of biomaterial formulations. Mechanical engineers provide insights into the mechanical properties and behavior of biomaterials under different loading conditions, aiding in the design of load-bearing implants and scaffolds. Process engineers develop scalable manufacturing processes for producing biomaterials on a large scale, ensuring consistency and reproducibility. [1, 3, 43]

Biomaterials have to fulfill many requirements. They are selected based on their biocompatibility, mechanical properties, degradation characteristics, and ability to integrate with the surrounding biological environment. A common difficulty is biocompatibility, defined as "the ability of a material to perform with an appropriate host response in a specific situation." In clinical applications, biomaterials should be non-cytotoxic, non-carcinogenic, and not activate the immune system, naming a few of the criteria. According to the literature in the field of biotechnology, a biocompatible material should not affect cells in any detrimental manner and support cellular activity. Since research also focuses on developing cancer tissues, a biocompatible material reinforces the metabolism of cancer cell lines. [44] Furthermore, biomaterials range from synthetic and natural polymers to ceramics, metals,

and composites. Hydrogels have gained popularity for the development of tissue replicates *in vitro*. The precise formulation and processing of the hydrogel can match the physiological composition and mechanical properties of the host tissue. Despite the diversity of sources, each material presents challenges in the design, manufacturing, and testing in combination with cellular material. [38] An overview of the characteristics of native tissue and the interaction between biomaterials and cells is presented in this section. In addition, a summary of hydrogel formulation and characterization is provided, followed by an overview of the processing and properties of biopolymers.

1.2.1 Extracellular Matrix

The ECM, in which cells reside *in vivo*, consists of many macromolecules. The precise composition of the ECM depends on the organ, but its building blocks can be categorized into three categories. Structural proteins provide the physical stability of the tissue. Collagen is the most abundant protein in the ECM; it forms the backbone of the structure and provides tensile strength due to its molecular structure as a triple helix. Furthermore, elastin supports the matrix as it is associated with collagen and provides recoil to the fibers when stretched. Both offer cell interactive sites. Moreover, organs with increasing elastin-to-collagen ratios show lower stiffness and higher recoil, e.g., cardiovascular muscles [45]. Glycoproteins correspond to non-structural proteins and include fibronectin and laminin. Both proteins enhance the adhesion and migration of cells. Fibronectin connects collagen and cells, especially during tissue development, where the ECM has not yet been completely developed. Laminin has a similar function. It provides adhesion between unequal tissues, which is significant in forming basal membranes. The gaps between the proteins in the ECM are filled with glycosaminoglycans (GAGs) and proteoglycans (PGs). GAGs are hydrophilic polysaccharides with a linear structure. An example thereof is hyaluronic acid (HA). When GAGs are covalently bound to a protein backbone, this class of molecules is called PG. This component of the ECM has a high water-binding capacity and is found throughout all tissues, especially in joints and cartilage. From a cellular perspective, this facilitates the supply of nutrients and growth factors. From a structural point of view, high water content provides lubrication and shock absorption. [46–49]

The mechanical properties of tissue are of great interest. Since the composition of each tissue type varies, so do the mechanical properties. Healthy tissues exhibit elastic moduli that range from 1 to 10^{10} Pa. For instance, brain tissue with an elastic modulus of around 10^3 Pa is in the lower range, whereas bone is in the upper end of the spectrum. Muscle tissue in the heart shows an elastic modulus in the middle range with a value of 16×10^6 Pa. [47, 50] The mechanical properties of tissue also change during disease. An increment up to 150% on the elasticity of cancer tissues has been reported. [50, 51]

1.2.2 Cell-Material Interaction

Cells are isolated from native tissue, where the specific biochemical composition and physical structure depend on the site and species. [51] In cell culture processes, cells are cultured outside the innate environments and adhere to the substrate. Cell metabolic processes such as proliferation, migration, and differentiation can be influenced by external stimuli that arise from biochemical and mechanical cues in the direct microenvironment. [8] Biochemical signals are provided by growth factors, both dissolved in the liquid and bound to the surrounding matrix. *In vitro*, cells show different behaviors depending on the distance to the surface of the scaffold. Additionally, chemotaxis, i.e., the migration of cells along concentration gradients, has been shown. [52] Furthermore, mesenchymal

stem cells (MSCs) can differentiate into osteogenic, chondrogenic, adipogenic, and even neurogenic types. MSC differentiation can be induced *in vitro* by various growth factors and hormones. [53] Mechanics also play a crucial role in cellular metabolism. Cells can perceive the mechanical properties of their environment and convert them into biochemical signals. These processes are referred to as mechanosensing or mechanotransduction. Cells attach to the ECM via focal adhesions (FAs), a protein complex that binds the cytoskeleton with the external microenvironment. The cytoskeleton protein actin is connected with the transmembrane protein integrin. FAs enable the transfer of forces from the microenvironment to the cytoskeleton. Within the cell, the cytoskeletal proteins actin and myosin II contract by crosslinking and form tension fibers to exert tensile forces. [54–56] These structures are enzymatically remodeled in a continuous process and thus adapt to the mechanical properties of the environment. The developing cytoskeleton leads to cellular polarity, a crucial factor for mitosis and migration. Integrin-mediated mechanosensing also activates signaling processes that affect gene and protein expression, including matrix deposition and secretion of proteolytic enzymes. [57, 58] *In vitro* studies have shown a process called durotaxis, in which cells migrate along stiffness gradients [59]. Furthermore, the differentiation of MSCs can be induced by variation in the elasticity of the substrate. While softer substrates in the range of 0.1 to 1 kPa led to neurogenic, stiffer tissues in the range of 25 to 40 kPa led to osteogenic differentiation. [60]

Moreover, cells, such as stromal and epithelial cells, synthesize various biopolymers. Cellular activities also include the expression of proteolytic enzymes that degrade the neighboring matrix and enzymes that crosslink network proteins. This leads to an active remodeling of the cellular microenvironment, which plays a role in biological processes such as migration and proliferation. Additionally, during tissue development, homeostasis, and wound healing, the biochemical and mechanical signals change continuously in space and time. For instance, fibroblasts play a crucial role in wound healing. As these cells proliferate and migrate into blood clots, the temporary ECM is remodeled by protease expression. Breakdown products of this reaction signalize damage and stimulate fibroblast proliferation and collagen synthesis. Fibroblasts differentiate into myofibroblasts to contract the ECM fibers for wound closure. After wound healing, fibroblasts and myofibroblasts undergo apoptosis. [61, 62] Hence, the specific requirements for cell culture of each strain depend on the sources of the biological material and the intended application. [51, 63] For this purpose, hydrogels are formulated with biopolymers to emulate the characteristics of the cellular microenvironment.

1.2.3 Hydrogels

Hydrogels have been investigated as promising candidates for the *in vitro* mimicking of the ECM [5, 6]. Precursor solutions are prepared to form the 3D network. These consist of polymers and solvents. The conformation of the macromolecules in solution depends on the compatibility with the solvent. When the compatibility is high, the volume of the molecule expands, whereas poor compatibility leads to contraction. Furthermore, polymer-polymer interactions are not frequent in dilute polymer solutions, and each molecule interacts primarily with solvent molecules [64, 65]. In concentrated solutions, molecules are entangled, and the chain mobility is reduced. The transition between dilute and concentrated regimes also depends on the molecular weight (MW) of the polymer. High MW molecules entangle at lower concentrations than low MW molecules. [65, 66] Moreover, the dissolution of polymeric materials involves the disentanglement of chains, the diffusion of the solvent into the swelling polymer, and the mass transfer to the solvent. Furthermore, the dissolution rate decreases with increasing MW as the disentanglement of molecules controls the process. Thus, high MW polymers show higher degrees of swelling before the dissolution due to the restricted mobility

at local high concentrations. Dissolving can be enhanced by solvent agitation as the swelling layer decreases in size. [67] In the case of hydrogels, the solvent is an aqueous phase. Solutes such as salts and sugars affect the conformation and, hence, the solubility of the polymer. The solubility decreases with increasing ionic strength and pH values around the isoelectric point (IEP). Furthermore, the viscosity of the precursor solution depends on the formulation, including polymer type, concentration, and MW distribution. The polymer solutions exhibit non-Newtonian behavior, meaning that the viscosity depends on the stress load, rate, and time. Shear-thinning is the phenomenon when the viscosity decreases with increasing shear rate. In solution, polymers are randomly oriented. Polymers can be deformed and oriented along the direction of the applied stress, which leads to lower friction and, hence, a reduction of viscosity. A further property found in some non-Newtonian fluids is yield stress. Due to intra- and inter-molecular interaction, the fluid behaves like a solid at low shear stress. The yield stress is the minimum stress required for the fluid to flow. These effects can be characterized using rotational rheometers. [68, 69]

Furthermore, crosslinkers are also required as a formulation component to produce a 3D network. Physical crosslinks can originate from chain entanglements and ionic and hydrophobic interactions. This crosslink type is a transient bond and advantageous when the hydrogel has to flow as an injection or in bioprinting processes. Chemically crosslinked hydrogels can be produced by photochemical and enzymatic reactions. Further crosslinking methods include the activation of the reaction by catalysis and radiation. [70] In photochemical crosslinking, the reaction starts when the light of a specific wavelength induces the conversion of photo-initiator to free radicals. The reactive species can then react with functional groups of the polymer, such as acrylates and methacrylates. These intermediates are also reactive, which continue to react until the reaction is quenched or the functional groups are saturated. [71] Moreover, the crosslinking conditions can negatively affect the cargo. Mild crosslinking reactions are favorable to avoid protein denaturation and cell inactivation. [72]

As hydrogels are crosslinked matrix, this type of material is insoluble. However, hydrogels swell in the aqueous phase due to the hydrophilic nature of the polymeric backbone. Two counteracting forces govern this process. Spontaneous mixing occurs to reach an equilibrium of chemical potentials inside and outside the hydrogel. Thus, entropy is increased upon mixing. Opposing is the elasticity of the network that results from stretching the polymer molecules. In a stretched state, the possible amount of conformations is reduced. Hence, entropy is reduced. Water is either bound to the polymers or free in between network chains. Hence, the swollen state of a hydrogel is influenced by the crosslink density and the composition of the adjacent liquid. [70] The swelling ratio of the hydrogel is mostly determined as the ratio of the volume in the swollen state to its volume in the dry state [73]. As a significant amount of water is retained, and under the assumption that the density of the hydrogel is the same as that of water, the swelling ratio is calculated by the weight ratio in the swollen state to the dry weight. This approach is mainly adopted in research due to its ease [74, 75]. Hydrogels with high swelling capacities show the advantage of enabling the diffusive transport of molecules, such as nutrients in cell culture or the release of drugs in pharmaceutical applications. [76] The determination of diffusion coefficients of solutes through the polymeric network is essential. Two approaches are used for this purpose. Unbound molecules such as proteins can be loaded within the hydrogel, and the release is traced by analyzing the composition of the adjacent liquid [77, 78] Alternatively, load-free hydrogels are placed in contact with fluid containing fluorescent or light-absorbing molecules. The moving front within the hydrogel is then traced with an appropriate detector. [79, 80]

The physical characterization of hydrogels also includes the determination of the elasticity and stability of the polymeric network. The elastic properties have been reported to increase with increasing crosslink density, which increases with the polymer concentration and MW. Methods based on oscillatory shear and uniaxial compression are mainly applied to determine the elasticity of the hydrogel bulk [81]. Uniaxial tension can also be used. However, technical difficulties arise as softer gels cannot be held in the testing equipment without damaging the sample. Further methods are applied to characterize mechanical properties on shorter length scales. For example, nanoindentation methods such as atomic force microscopy rely on the intrusion of a probe onto the surface of a sample [82, 83]. This limits the method to the surface of hydrogels. Microrheological studies can be performed within polymeric networks to determine local properties in length scales relevant to those at the cellular scale. In such methods, tracer particles are placed, and their motion is analyzed. Both active and passive microrheological methods have been reported. The first technique consists of triggering tracer displacement, e.g., by a focused laser beam in the method of optical tweezers [84, 85]. The latter relies on the Brownian motion of the particles. [86–88]. The multiple particle tracking method also allows the characterization of local heterogeneities within the sample as a high number of particles can be traced [88]. The required mechanical properties can be set by variation of polymer concentration and MW as the crosslink density depends on the number of crosslinking sites and physical entanglements. In tissue engineering, the optimum regarding mechanical properties depends on the growing cell strain. However, increasing the elasticity of hydrogels decreases the swelling capacity. Hence, the diffusion of nutrients through the network is limited [76, 89]. As the expression of enzymes is part of cellular metabolism, hydrogel undergoes degradation. Cells also deposit fibers such as collagen, reinforcing the network. Therefore, knowledge about the degradation kinetics creates favorable conditions during the cell culture period. This phenomenon is characterized by the development of hydrogel weight or elasticity over time [90–92]. Additionally, the composition of the adjacent media can be determined as polymer fragments are released. [93, 94]

1.2.4 Biopolymers

A suitable formulation is required to mimic the biochemical and physical nature of the native ECM. Hydrogel formulation variables include the type of biopolymer, its concentration, and the crosslinking mechanism. The building blocks can be of synthetic and natural origin. While synthetic polymers are cheap and show low or no batch-to-batch variability, these molecules do not provide cell-interactive sites [5, 6]. Biopolymers can be produced biotechnologically or purified from native tissue. The macromolecules provide support for cellular metabolic activities, including adhesion and degradation. However, there are concerns regarding immunogenic response after implantation. Additionally, batch-to-batch variability is an issue in the research and processing of these macromolecules. [48, 49]. This subsection provides an overview of the purification of naturally derived biopolymers and the properties of these macromolecules,

1.2.4.1 Hyaluronic Acid

GAGs are part of the ECM and are characterized by repeating disaccharide units. This molecule is expressed in all vertebrates. The polysaccharide is isolated from tissue. Proteins are removed using proteases and precipitated with organic solvents. The dissolved polysaccharides are then separated from solids via centrifugation. Chromatography is the method used to purify HA from

other GAGs selectively. [95] Rooster comb has the highest HA content in native tissues and is one of the primary sources for the macromolecule [96]. Hyaluronic acid can be produced using recombinant *Streptococcus* and *Lactobacillus* strains to avoid inter-species contamination. However, a low yield in the fermentation and purification processes makes this alternative expensive. [97]

Moreover, the monomer consists of N-acetyl-D-glucosamine, linked to D-glucuronic acid via a $\beta(1,4)$ -glycosidic bond. The length of a disaccharide unit is about 1 nm. Repeating units are linked by a $\beta(1,3)$ -glycosidic bond. [96, 98] HA is enzymatically cleavable [96, 99]. In the human genome, six different genes encode the expression of these enzymes, i.e., hyaluronidase [100]. This unbranched polymer reaches a molecular mass of up to millions of Dalton, i.e., lengths up to a few micrometers. HA is negatively charged in an aqueous solution at physiological pH and ionic strength and has both polar and nonpolar domains, resulting in a highly water-swollen random coil structure. [99, 101]

HA hydrogels can be formed by covalent crosslinking, whereby hydroxyl and carboxyl groups react to form ether or ester bonds. Another method is physical crosslinking with polyvalent cations that interact with negatively charged functional groups from various polymer chains. [101] To increase the mechanical stability of HA hydrogels, the polysaccharide can be modified to enable photo-crosslinking. [102] Methacrylate derivated HA is commonly known in the literature as HAMA and commercially available under the name PhotoHA[®]. In any of the cases, hyaluronic acid of high MW increases the elasticity and decreases the swelling capacity of hydrogels. [101]

1.2.4.2 Alginic acid

Alginic acid is a polysaccharide that has been widely used in research. While the material shows similar properties to HA, alginates are much cheaper. The biopolymer is extracted from algae in alkaline media. Subsequently, sodium or calcium chloride precipitates alginates following centrifugation. A further method for the production of alginates is fermentation. Bacterial alginate can be expressed by *Azotobacter* and *Pseudomonas* and can lead to more defined chemical structures. However, the cost of this approach remains expensive due to low yield in the production and downstream processing. [103–105]

Two monosaccharides compose the linear polymer structure, i.e., α -L-guluronic acid (G) and β -D-mannuronic acid (M). The specific G and M content of alginate depends on the source. The sequence can also be alternating G and M residues or M- or G-blocks. Alginates are highly soluble in the aqueous phase at neutral pH and physiological conditions. The viscosity of the solutions increases with the M content of the biopolymer [103, 105] G-blocks are negatively charged in solution and interact with positively charged ions.

G residues form a physical crosslink in the presence of divalent cations, such as calcium and magnesium. A minimum of 20 consecutive G residues are required for the crosslinking. Physically crosslinked hydrogels show higher elasticity with increasing G content. [103, 104] Additionally, alginate can be functionalized to increase the stability of the network by introducing methacrylate residues to the backbone. Furthermore, alginate hydrogels contain high amounts of liquid and enable the diffusion of nutrients through the network. The polymer has been used for drug delivery and food formulation as the molecule can be broken down via hydrolysis at low pH values. [104, 106] The application in research has been widely accepted for creating tissue replicates as the properties of alginates are structurally similar to those of hyaluronic acid. However, the application of alginate for the composition of tissue-engineered products is limited. Mammals, and more precisely humans, do not express enzymes for the natural degradation of alginates. Additionally, alginate does not

include sites for cell adhesion. Hydrogels containing alginate dissolve after long-term culture periods as crosslinking ions are released to the bulk phase. [49, 104]

1.2.4.3 Collagen

Collagen is extracted from native tissue in acidic or alkaline media. Due to hydrolysis, the crosslinks within the tissue are broken, and collagen is dissolved. Mineral solids and fats are subsequently separated using centrifugation and filtration. [107] The primary source of collagen worldwide is porcine. Furthermore, there are 28 identified types of collagen in human tissue and up to 440 in vertebrates.

Each type of collagen is characterized by triple-helical domains that vary in size and distribution depending on the collagen class, i.e., tissue. Collagen provides structural integrity and adhesion sites for cells to form FAs. The amino acid sequence of collagen consists of repeating glycine units at every third position (X-Y-Gly). The tripeptide sequence is repeated within the chain between 337 and 343 times. The other two amino acids (X and Y) consist mainly of proline and hydroxyproline. Three of these amino acid chains, also called α -chains, form the characteristic structure of collagen molecules. The glycine residues are directed toward the center of the helix, while the X and Y residues are directed outward. This conformation enables the formation of hydrogen bonds that stabilize the right-handed helix structure. With the increasing physiological temperature of the species, the proline and hydroxyproline content increases [108]. Moreover, triple helices consist of about 1000 amino acids that form a 300 nm. long structure with a diameter of about 1.6 nm. Triple helices contain the amino acid sequence for cell adhesion, i.e., arginine-glycine-aspartic acid (RGD). Furthermore, the non-helical regions at both ends of the triple helix are called telopeptides, enabling interactions and crosslinking between helices to form fibrils. Within the fibrils, the triple helices are staggered next to each other. Parallel strands are shifted by 64 to 67 nm along the longitudinal axis of the fibril. Helices in front of each other are separated by a gap of 36 nm. Fibrils can be crosslinked and form a helical structure with diameters up to 500 nm. Collagen fibers are made up of fibrils running parallel to each other. [109–111]

Furthermore, collagen is a hydrophilic protein that can dissolve in an aqueous phase at low temperatures. Increasing temperature above 28 °C leads to the aggregation of collagen helices to fibrils. Therefore, the solutions undergo a transition to a physical hydrogel. [109] For the formation of chemically crosslinked hydrogels, photo-polymerization can be applied using riboflavin as a crosslinking agent [112]. Collagen can also be functionalized with methacrylate groups to enable photochemical crosslinking [113], commercially distributed as PhotoCol[®]. Nomenclature in literature is also ColMA. These methods are applied to increase the elasticity of the resulting hydrogel at higher temperatures or to form hydrogels at low temperatures. As collagen is found in native tissue, its physical properties can be reconstructed in vitro. However, the use of collagen in hydrogel formulation is limited. The non-helical domains of the protein are highly specific in each species. These can trigger immune responses. This phenomenon can be overcome by carefully selecting the collagen source and cell strains. [111, 114] An alternative to the issue is recombinant collagen. This approach is, however, expensive due to a low yield in the expression with bacteria or mammal cell strains, and the molecules show less stability. [115, 116]

1.2.4.4 Gelatin

Collagen can be further processed into gelatin by acidic or alkaline treatment of the collagen-containing solutions. Thereby, large collagen molecules are broken down into shorter polypeptides called gelatin due to hydrolysis. Moreover, enzymatic pre-treatments are also used to cleave telopeptides selectively. Furthermore, gelatin extracted in acid media is known as type A gelatin and shows an IEP at pH 8-9. In contrast, gelatin processed in alkaline media shows IEP at pH 4-5 high pH values lead to converting asparagine and glutamine into aspartic acid and glutamic acid, respectively. This type of gelatin is called type B. Since the extraction conditions are harsh, the molecules in the solution are a mixture of protein chains with varying composition and MW. Increasing processing temperature and time lead to shorter polypeptide chains. [107, 117]

Gelatin molecules unfold to random coils in solution at temperatures higher than physiological temperatures. At lower temperatures, chains refold to helical structures and form physical gels. Triple helices are stabilized by hydrogen bonds, both inter and intramolecular. The kinetics and the magnitude of the gelation are affected by the MW of the protein. Even though there is no direct correlation between MW and gelling properties, studies show that an increasing MW leads to stronger physical gels. Additionally, the elasticity of gelatin hydrogels increases with the protein concentration. [107] Furthermore, since the molecular weight of gelatin is polydisperse, the purified protein is quantitatively characterized by its gel-forming properties. The bloom strength or bloom value characterizes this property. The determination is performed using a standard method. Therefore, the gelatin solution is prepared at 6.67% (w/w) and the measurement is performed at 21 °C. Subsequently, a plunger with a diameter of 12.7 mm is pressed into the surface of a gelatin gel, and the required weight to reach a depth of 4 mm is measured. [118]

Furthermore, the sol-gel transition imposes challenges for the processing and application of gelatin. During processing, heating is required to maintain the solution and avoid physical gelation. In applications at higher temperatures, gelatin hydrogels are not structurally stable. The first difficulty can be addressed by modification of the solvent to inhibit protein-protein interactions, thus inhibiting gelation. The latter issue can be managed by forming covalent bonds to stabilize physical structure. Gelatin networks can be crosslinked using genipin or glutaraldehyde [117]. Alternatively, the protein can be modified to include methacrylate or thiol residues. The functionalized gelatin can then be used to formulate hydrogels with a high water-binding capacity, which is advantageous for biotechnological purposes [119]. For encapsulation of active biological material, the functionalized gelatin enables crosslinking under mild conditions [120]. Additionally, a lower immune reaction is demonstrated by gelatin hydrogels compared to those produced with collagen. Furthermore, recombinant expression systems are used to avoid inter-species contamination, which is crucial for pharmaceutical use. [77]

1.2.4.5 Gelatin-Methacryloyl

The functionalization of gelatin with methacrylate residues, as proposed by Van den Bulcke [121], is a possibility to enable chemical crosslinking. After the modification, the protein is known as gelatin methacryloyl (GelMA). The modification involves adding methacrylic anhydride (MAA) to a gelatin solution under stirring. The methacrylate and methacrylamide residues in the product are bound to former primary amines. The purification of the protein is performed by dialysis. Furthermore, the degree of functionalization (DoF) describes the portion of the free amines substituted after the reaction. The standard method for quantifying the DoF is described by Habeeb [122]. Moreover,

the DoF of GelMA is considered a quality attribute of the product as the residues enable photo-crosslinking, which is crucial for forming stable networks.

Furthermore, the reaction has been thoroughly studied by Lee et al. [123] and Shirahama et al. [124]. It has been shown that a buffered solution at the IEP of the protein enhances the reaction, leading to a reduction of the excess of MAA over gelatin. Additionally, the reaction temperature was limited to the range of 35 to 50 °C and showed no effect on the DoF. Lower temperatures have not been studied as gelation inhibits the distribution of reactants, and higher temperatures can lead to protein degradation due to hydrolysis. Furthermore, a minimal gelatin concentration in the solution is required to distribute MAA evenly during the reaction. At high concentrations, the DoF of the product only depended on the reactant ratio. Hence, the properties of gelatin in solution show an effect on the reaction as the molecules exhibit surface active properties. These depend on the species and extraction parameters and show differences in the IEP and MW of the molecule. Different gelatin sources' production and effects are discussed in more detail in chapters 3 and 4.

The properties of GelMA solutions are similar to those of gelatin solutions. At lower temperatures, GelMA solutions undergo a sol-gel transition. Moreover, hydrogel precursor solutions are prepared by dissolving the polymer with a photo-initiator at higher temperatures. The latter component is required for the formation of covalent bonds after irradiation. Commonly used are the components 2-hydroxy-1-(4-(hydroxyethoxy)phenyl)-2-methyl-1-propanone (Irgacure 2959) and lithium phenyl-2,4,6-trimethylbenzoylphosphinate (LAP). Both compounds dissociate into radicals after exposure to light in the ultraviolet (UV) range. Furthermore, the liquid solution is processed at higher than physiological temperatures and subsequently exposed to UV light. Moreover, the primary structure of collagen α -chains is retained in gelatin and GelMA; thus, cell-interactive sites are available for adhesion and enzymatic cleavage. In addition, the application of GelMA hydrogels triggers a lower immune response than collagen hydrogels. Using photo-polymerization to form cell-loaded hydrogels shows limited suitability as excessive exposure to UV light and the presence of radicals have detrimental effects on the cells. [125, 126] Moreover, the elasticity of the hydrogel increases with the crosslink density, i.e., increasing DoF, MW, and UV irradiation dose.

GelMA hydrogels have been studied for the study of MSC differentiation. These were produced using molding [127, 128] and foaming [129]. More advanced techniques, such as inkjet printing [130], extrusion printing [131], stereolithography [132], and microfluidics [133], have been for the encapsulation of diverse strains for the study of cell proliferation. These were chondrocytes, hepatocytes, fibroblasts, and epithelial cells, respectively. In addition, GelMA has been applied for the load and release of small drugs [134, 135] and therapeutic proteins such as growth factors [127, 136]. GelMA has proven to be a versatile material in various applications as the innate biochemical structure enables cell interaction. Physical properties imposed by the cells can be set by precise formulation of the hydrogels. In addition, physical properties can also be modulated by the crosslinking process. A further attribute is its compatibility with various fabrication processes, including extrusion extrusion-based bioprinting (EBB) [137, 138] stereolithography [139, 140], electrospinning [141, 142], microfluidics [133, 143], molding and casting [135, 144]. The methods are selected according to the demands of the application. Overall, the combination of biocompatibility, tunable properties, and biodegradability makes it a versatile biomaterial with promising applications across different areas of biomedical engineering and tissue regeneration. The versatility makes it a valuable asset in biomaterial research.

1.3 Applications and Analytics

Hydrogels are candidates for creating physical structures that provide cells with the required material properties at the microscopic level. As described above, the physical properties of the biomaterial at the cellular level trigger metabolic processes within cells, i.e., at the subcellular level. On the other hand, cells can also modify the physical properties of the surrounding matrix by expressing enzymes and biopolymers. In addition, these dynamic interactions also have an effect on the diffusivity of cargo. Moreover, hydrogels can be processed to build macroscopic structures that enable the study of said interactions, cultivating established cell lines and acting as carriers of small molecules and pharmaceuticals. This section provides an overview of the manufacturing methods and related analytical approaches relevant to this thesis. In addition, the limitations of said methods are presented, and available strategies from other disciplines are introduced.

1.3.1 Substrates for Cell Culture

Cells are seeded onto or into the polymeric network when studying cells during cell culture using hydrogels as substrates. The effects of the hydrogel components and mechanical stress, such as compression or tension, on the living component are assessed using cell-based assays. The most common method is fluorescent labeling and detection by microscopy. Subsequently, the acquired images are analyzed manually by an operator. Determining viability, i.e., the percentage of living cells is performed by manual counting. This method depends on the operator and is prone to error. Additionally, this is time-consuming and leads to fewer counted specimens in the range of hundreds of cells. [145, 146]

Automated image processing and analysis is one approach to address the issues and increase reproducibility. Therefore, the image can be processed to enhance its quality by increasing contrast or reducing background noise. Subsequently, the image is segmented into single or multiple regions of interest (ROIs). Data extraction is the last step, where specific features are extracted. [146] In cell biology, advanced software has been developed to identify and track the effect of experimental variables on single cells and cell populations. Therefore, the signals of different cellular stains are processed separately, and subsequently, the automated software can identify up to 1.500 morphological properties of single cells. [32] The imaging advantages include reducing contamination risk as the method is non-invasive. [30] For the application of automated image analysis (IA), especially when a high number of images is evaluated, increased working memory is required in the computing hardware, which also affects the analysis time [147].

A challenge regarding the image acquisition hardware is the limited working distance of the microscope and the optical properties of the 3D scaffold, such as opaqueness. Hydrogels also show a background fluorescence and strong light scattering, which can lead to imprecise detection using spectrometers. [11] Flow cytometry is an analytical method widely applied in cell biology based on detecting light scattering and fluorescence. Therefore, a fluidic system transports the cells as a suspension through tubing passing by light sources and detectors. Light scattering is detected at a narrow angle and an angle of 90 degrees, known as forward and side scatter, respectively. The former provides information about the relative size of the cell, while the latter represents the internal complexity or granularity of the cell. Furthermore, fluorescence detection is proportional to the amount of dye bound to the cell component. [24] Advanced equipments can analyze up to 16 different optical parameters simultaneously. Additionally, the number of analyzed cells can reach millions within low sample volumes. Cells must be separated from the scaffold to enable the

analysis of adhesive cell strains. When cells are cultured within hydrogels, the biomaterial must be diluted to be transported within the fluidic system. Additionally, crosslinks can be reversed [148], or the structure can be enzymatically cleaved to soluble components.

1.3.2 Microparticles

Hydrogel microparticles (HMPs) are used as a carrier in the expansion of cells in research and biomanufacturing. Small drug molecules and pharmaceutical proteins like growth factors can also be delivered as cargo within HMPs. [28, 149] The first step in producing HMPs consists of creating droplets that are subsequently crosslinked to hydrogels. Methods such as batch emulsification and spraying are commonly used due to their high throughput and simplicity. However, the resulting droplet size is polydisperse. [150] Using microfluidic systems enables the production of monodisperse droplets. Microfluidic methods reduce the production throughput, which can be increased by out-scaling, i.e., parallelizing multiple systems. [151]

Two immiscible liquids are employed to generate droplets in a bulk phase. An aqueous precursor solution is used as a disperse phase, while the continuous phase is oil. [151] In the co-flow microfluidic method, the disperse phase flows out of an inner capillary into a stream of the continuous phase in an outer tube. A more complex configuration is co-flow-focusing. The design is similar to co-flow; however, the disperse phase meets a second stream of the continuous phase perpendicularly to the flow direction. The focusing stream stabilizes the interface between both phases. [152]. Furthermore, shear stress and interfacial tension induce the formation of droplets [153]. The regimes of droplet generation are called dripping and jetting. In the first case, droplets are created directly at the capillary tip. In the second case, droplets are formed at the end of a thin stream away from the capillary tip. The behavior of these systems can be characterized by dimensionless numbers that describe the relationship between involved forces, as shown in Table 1.1. Inertial and viscous forces must surpass interfacial forces to form a jet, which is the case of high capillary and Weber numbers. Hence, the transition from dripping to jetting and the resulting droplet size depends on the viscosities and feed rates of both phases, interfacial tension in between phases, and the geometry of the used tubes. [154, 155] Furthermore, disperse droplets within a bulk media are unstable and undergo coalescence, where droplet size increases randomly. Droplets can be stabilized using surfactants as a part of the formulation of both phases [156]. Crosslinking is the subsequent step to stabilize the droplets for storage and additionally set the properties of the hydrogel for drug release and cell culture. This process can be performed within the tubes of the microfluidic system or after exiting the system in bulk. For covalently crosslinked HMPs, radical polymerization is achieved by exposure to light as the droplets flow in the stream. Physical crosslinking is performed by mixing the salt-containing phase through secondary capillaries or collecting the emulsion in a salt-containing reservoir [149, 151].

In the field of biomaterials, the characterization of HMPs is limited to imaging and manual detection and extraction of geometric features [157–160]. As mentioned above, manual data extraction from images is time-consuming and error-prone. The recognition and measurement of structures have been widely applied in the field of mechanical engineering as part of quality control [161]. Similarly, the automated evaluation of microstructural features on surfaces of materials [162]. Moreover, in-line analysis of the generated droplets at the break-up point can be performed using the Droplet morphometry and velocimetry (DMV) software [163]. The IA tool was developed for the study of droplets in emulsions. In addition, the encapsulation efficiency in

Table 1.1 Dimensionless number for characterizing droplet generation in microfluidic systems. ρ : fluid density, L : characteristic length, v : characteristic velocity, η : viscosity, σ : interfacial tension.

Ratio	Dimensionless Number	Equation
Inertial to viscous forces	Reynolds number	$\text{Re} = \frac{\rho L v}{\eta}$
Viscous to interfacial forces	Capillary number	$\text{Ca} = \frac{\eta v}{\sigma}$
Inertial to interfacial forces	Weber number	$\text{We} = \text{Re Ca} = \frac{\rho v L^2}{\sigma}$

cell-sorting devices has also been traced [164, 165]. Furthermore, automated IA can be applied to characterizing HMPs in oil and after swelling in aqueous media.

1.3.3 Bioprinting

Extrusion-based bioprinting (EBB) is an advanced manufacturing technique to create 3D structures composed of living cells, biomaterials, and bioactive molecules. Like traditional 3D printing, EBB utilizes a layer-by-layer approach to deposit bioinks, i.e., biopolymer solutions containing living cells onto a substrate according to a digital design or model. [166, 167] By precisely controlling the deposition of bioinks, bioprinters can create complex tissue architectures with spatial control over cell distribution, cell density, and biomaterial composition [168, 169]. While the technology is still in its early stages, ongoing research and advancements in bioprinting techniques, biomaterials, and cell biology drive its development toward clinical translation and commercialization.

The structures to be printed are first designed as a virtual model. The models include freely designed shapes and 3D scans of existing structures. The model is sliced into single layers, and a set of instructions, also called G-code, is generated accordingly to fit the range of movement of the printer. [170] The mechanics of current 3D bioprinters are limited to translation in the three dimensions without rotation around the horizontal plane. Moreover, the biopolymer solutions or bioinks are loaded in cartridges and mounted on the printhead. The biomaterial is extruded through a nozzle using pneumatic pressure or mechanical force. In the pneumatic approach, an increase and drop of pressure induces the movement of a plug along the longitudinal axis of the cartridge, while in the mechanical approach, the displacement is due to the movement of a piston. [38] Pneumatic methods are preferred as these are easy to implement. However, the flow rate cannot be directly set over the pressure setting. In contrast, a piston-driven printer allows for control of flow rate, as the speed of the piston can be set. [171] After the deposition of the biomaterial, the structure can be stabilized by physical or chemical crosslinking and set the mechanical properties of the intended application.

Bioinks are formulated according to the demands of the cell type and the application. While bioprinting offers many advantages, the printing process can subject cells to physical stress, which may impact their viability, functionality, and behavior. Physical stress includes osmotic stress due to drying after the ink exits the nozzle, higher than physiological temperatures during processing, and shear stress during extrusion as the polymer solution flows through the nozzle. [172] Excessive shear stress on cells can lead to necrosis due to cell disruption or changes in cell morphology and phenotype. [173, 174] The shear stress depends on the properties of the polymer solution as well as on the processing parameters and diameter and length of the nozzle, where increased shear rate results from increasing flow rate, viscosity, and decreasing nozzle diameter. Shear thinning behavior

is advantageous for printing cells containing bioinks, as the viscosity and, hence, the shear stress is reduced during the printing process. [172, 175]

Rheological tests measure the flow behavior of bioinks under different conditions, such as shear rate, temperature, and time. This rheological characterization is common in the field of bioprinting. This includes oscillatory and rotational rheometry techniques to determine parameters such as viscosity, yield stress, and viscoelastic behavior. The power law model, also known as Ostwald de-Waele, is used to describe the viscous behavior of the bioink and compare this between different bioink formulations. Equation 1.1 shows the power law relationship, with the model parameters η , $\dot{\gamma}$, K , and n . These correspond to the viscosity, the shear rate, the consistency index, and the power law coefficient, respectively. [175, 176]

$$\eta(\dot{\gamma}) = K \dot{\gamma}^{n-1} \quad (1.1)$$

The experimental setup of frequent studies consists of printing different bio-inks and determining cell viability using equal printing pressures. Higher viscosity is correlated with decreasing viability. No further information is extracted from the rheological characterization. However, it is expected that non-equal flow rates result from different rheological properties, and hence, decreasing cell viability results not only from higher viscosities but also from a higher shear rate. The comparability of the studies is made available by setting equal flow rates, which can be calculated according to Equation 1.2, where Q stands for the volumetric flow rate, R for the nozzle radius, p for the pneumatic pressure, and l for the nozzle length.

$$Q = \bar{v} \pi R^2 = \frac{n\pi}{3n+1} \left(\frac{R^{3n+1} p}{2 K l} \right)^{1/n} \quad (1.2)$$

Furthermore, assessing printing performance involves evaluating the ability of bioinks to maintain shape and how precise the printed shapes are following the printing process. Parameters of filament thickness are quantified to optimize printing conditions. High viscosity, yield stress, and elastic modulus are essential factors for high shape fidelity. Moreover, the analysis of geometric features of printed scaffolds is measured manually [177–179]. As hydrogel biomaterials are water-swollen, image acquisition can be problematic due to light reflection and the transparency of the material. The development of bioinks can be improved by implementing automated IA to determine geometric attributes. Similar approaches can be transferred from, e.g., food process engineering, where image processing is used in processing and production lines to identify quality attributes [180]. While bioprinting offers exciting opportunities for tissue engineering and regenerative medicine, it is essential to carefully consider and optimize printing parameters to minimize the adverse effects of printing on cells and maximize the success of tissue fabrication. Thus, the comparability of the experimental settings has to be considered, and robust processing and analytical strategies have to be developed.

Chapter references

- [1] E. L. S. Fong, B. M. Watson, F. K. Kasper, and A. G. Mikos, „Building Bridges: Leveraging Interdisciplinary Collaborations in the Development of Biomaterials to Meet Clinical Needs“, *Advanced Materials*, vol. 24, no. 36, pp. 4995–5013, 09/2012.
- [2] Y. Xu, C. Chen, P. B. Hellwarth, and X. Bao, „Biomaterials for stem cell engineering and biomanufacturing“, *Bioactive Materials*, vol. 4, no. July 2019, pp. 366–379, 2019.
- [3] W. R. Wagner, S. E. Sakiyama-Elbert, G. Zhang, and M. J. Yaszemski, *Biomaterials Science: An Introduction to Materials in Medicine*, 4th ed., W. R. Wagner, S. E. Sakiyama-Elbert, G. Zhang, and M. J. Yaszemski, Eds. London, United Kingdom: Academic Press, 2020, pp. 1–1586.
- [4] D. F. Williams, „On the nature of biomaterials“, *Biomaterials*, vol. 30, no. 30, pp. 5897–5909, 10/2009.
- [5] R. J. Wade and J. A. Burdick, „Engineering ECM signals into biomaterials“, *Materials Today*, vol. 15, no. 10, pp. 454–459, 10/2012.
- [6] F. Ruedinger, A. Lavrentieva, C. Blume, I. Pepelanova, and T. Scheper, „Hydrogels for 3D mammalian cell culture: a starting guide for laboratory practice“, *Applied Microbiology and Biotechnology*, vol. 99, no. 2, pp. 623–636, 01/2015.
- [7] S. Xiao *et al.*, „Gelatin Methacrylate (GelMA)-Based Hydrogels for Cell Transplantation: an Effective Strategy for Tissue Engineering“, *Stem Cell Reviews and Reports*, vol. 15, no. 5, pp. 664–679, 10/2019.
- [8] S. O’Brien, Y. Park, S. Azarin, and W.-S. Hu, „Cell Culture Bioprocess Technology: Biologics and Beyond“, in *Cell Culture Technology*, C. Kasper, V. Charwat, and A. Lavrentieva, Eds., Cham, Switzerland: Springer, 2018, ch. 1, pp. 1–21.
- [9] F. Eberhardt *et al.*, „Impact of serum-free media on the expansion and functionality of CD19.CAR T-cells“, *International Journal of Molecular Medicine*, vol. 52, no. 1, p. 58, 05/2023.
- [10] K. E. Wellen and C. B. Thompson, „Cellular Metabolic Stress: Considering How Cells Respond to Nutrient Excess“, *Molecular Cell*, vol. 40, no. 2, pp. 323–332, 10/2010.
- [11] V. Charwat and D. Egger, „The Third Dimension in Cell Culture: From 2D to 3D Culture Formats“, in *Cell Culture Technology*, C. Kasper, V. Charwat, and A. Lavrentieva, Eds., Cham, Switzerland: Springer, 2018, ch. 5, pp. 75–90.
- [12] J. W. Deitmer, S. M. Theparambil, I. Ruminot, S. I. Noor, and H. M. Becker, „Energy Dynamics in the Brain: Contributions of Astrocytes to Metabolism and pH Homeostasis“, *Frontiers in Neuroscience*, vol. 13, no. December, pp. 1–7, 12/2019.
- [13] R. C. Vergara *et al.*, „The Energy Homeostasis Principle: Neuronal Energy Regulation Drives Local Network Dynamics Generating Behavior“, *Frontiers in Computational Neuroscience*, vol. 13, no. July, pp. 1–18, 07/2019.
- [14] G. Kroemer and J. Pouyssegur, „Tumor Cell Metabolism: Cancer’s Achilles’ Heel“, *Cancer Cell*, vol. 13, no. 6, pp. 472–482, 06/2008.
- [15] W. G. Kaelin and C. B. Thompson, „Clues from cell metabolism“, *Nature*, vol. 465, no. 7298, pp. 562–564, 06/2010.
- [16] M. Teifel, „Transfektion von Säugerzellen“, in *Gentechnische Methoden*, 1944, Heidelberg, Germany: Spektrum Akademischer Verlag, 2012, pp. 351–383.
- [17] A. Lavrentieva, „Essentials in Cell Culture“, in *Cell Culture Technology*, C. Kasper, V. Charwat, and A. Lavrentieva, Eds., Cham, Switzerland: Springer, 2018, ch. 2, pp. 23–48.
- [18] T. Criswell *et al.*, „Shipping and Logistics Considerations for Regenerative Medicine Therapies“, *Stem Cells Translational Medicine*, vol. 11, no. 2, pp. 107–113, 03/2022.
- [19] B. Rubinsky, „Principles of Low Temperature Cell Preservation“, *Heart Failure Reviews*, vol. 8, no. 3, pp. 277–284, 2003.
- [20] F. Li, N. Vijayasankaran, A. (Shen, R. Kiss, and A. Amanullah, „Cell culture processes for monoclonal antibody production“, *mAbs*, vol. 2, no. 5, pp. 466–479, 09/2010.
- [21] K. R. Kim and W.-H. Yeo, „Advances in sensor developments for cell culture monitoring“, *BMEMat*, vol. 1, no. 4, 12/2023.
- [22] S. Elmore, „Apoptosis: A Review of Programmed Cell Death“, *Toxicologic Pathology*, vol. 35, no. 4, pp. 495–516, 2007.
- [23] M. Ghasemi, T. Turnbull, S. Sebastian, and I. Kempson, „The MTT Assay: Utility, Limitations, Pitfalls, and Interpretation in Bulk and Single-Cell Analysis“, *International Journal of Molecular Sciences*, vol. 22, no. 23, p. 12827, 11/2021.
- [24] A. Adan, G. Alizada, Y. Kiraz, Y. Baran, and A. Nalbant, „Flow cytometry: basic principles and applications“, *Critical Reviews in Biotechnology*, vol. 37, no. 2, pp. 163–176, 02/2017.
- [25] P. Bikmulina *et al.*, „3D or not 3D: a guide to assess cell viability in 3D cell systems“, *Soft Matter*, vol. 18, no. 11, pp. 2222–2233, 2022.

- [26] J. R. Masters, „HeLa cells 50 years on: the good, the bad and the ugly“, *Nature Reviews Cancer*, vol. 2, no. 4, pp. 315–319, 04/2002.
- [27] E. Tan, C. S. H. Chin, Z. F. S. Lim, and S. K. Ng, „HEK293 Cell Line as a Platform to Produce Recombinant Proteins and Viral Vectors“, *Frontiers in Bioengineering and Biotechnology*, vol. 9, no. 12, pp. 1–9, 12/2021.
- [28] S. Derakhti, S. H. Safiabadi-Tali, G. Amoabediny, and M. Sheikhpour, „Attachment and detachment strategies in microcarrier-based cell culture technology: A comprehensive review“, *Materials Science and Engineering: C*, vol. 103, no. 4, p. 109782, 10/2019.
- [29] C. F. Bellani, J. Ajeian, L. Duffy, M. Miotto, L. Groenewegen, and C. J. Connon, „Scale-Up Technologies for the Manufacture of Adherent Cells“, *Frontiers in Nutrition*, vol. 7, no. November, 11/2020.
- [30] A. D. Henn *et al.*, „Cytocentric measurement for regenerative medicine“, *Frontiers in Medical Technology*, vol. 5, no. April, pp. 1–6, 04/2023.
- [31] „CellProfiler: Image analysis software for identifying and quantifying cell phenotypes“, *Genome Biology*, vol. 7, no. 10, R100, 2006.
- [32] M. A. Bray *et al.*, „Cell Painting, a high-content image-based assay for morphological profiling using multiplexed fluorescent dyes“, *Nature Protocols*, vol. 11, no. 9, pp. 1757–1774, 2016.
- [33] E. Cukierman, R. Pankov, and K. M. Yamada, „Cell interactions with three-dimensional matrices“, *Current Opinion in Cell Biology*, vol. 14, no. 5, pp. 633–640, 10/2002.
- [34] F. Pampaloni, E. G. Reynaud, and E. H. K. Stelzer, „The third dimension bridges the gap between cell culture and live tissue“, *Nature Reviews Molecular Cell Biology*, vol. 8, no. 10, pp. 839–845, 10/2007.
- [35] M. J. Gomez-Lechón *et al.*, „Long-term expression of differentiated functions in hepatocytes cultured in three-dimensional collagen matrix“, *Journal of Cellular Physiology*, vol. 177, no. 4, pp. 553–562, 12/1998.
- [36] J. Lee, M. J. Cuddihy, and N. A. Kotov, „Three-Dimensional Cell Culture Matrices: State of the Art“, *Tissue Engineering Part B: Reviews*, vol. 14, no. 1, pp. 61–86, 03/2008.
- [37] J. L. Drury and D. J. Mooney, „Hydrogels for tissue engineering: scaffold design variables and applications“, *Biomaterials*, vol. 24, no. 24, pp. 4337–4351, 11/2003.
- [38] J. Malda *et al.*, „25th Anniversary Article: Engineering Hydrogels for Biofabrication“, *Advanced Materials*, vol. 25, no. 36, pp. 5011–5028, 09/2013.
- [39] W. Sun *et al.*, „The bioprinting roadmap“, *Biofabrication*, vol. 12, no. 2, p. 022002, 04/2020.
- [40] M. Gargotti, U. Lopez-Gonzalez, H. J. Byrne, and A. Casey, „Comparative studies of cellular viability levels on 2D and 3D in vitro culture matrices“, *Cytotechnology*, vol. 70, no. 1, pp. 261–273, 02/2018.
- [41] F. Bonnier *et al.*, „Cell viability assessment using the Alamar blue assay: A comparison of 2D and 3D cell culture models“, *Toxicology in Vitro*, vol. 29, no. 1, pp. 124–131, 02/2015.
- [42] P. Chandra, J. J. Yoo, and S. J. Lee, „Biomaterials in regenerative medicine: Challenges in technology transfer from science to process development“, in *Translational Regenerative Medicine*, Cambridge, United Kingdom: Elsevier, 2015, ch. 13, pp. 151–167.
- [43] M. Vallet-Regí, „Evolution of Biomaterials“, *Frontiers in Materials*, vol. 9, no. March, pp. 1–5, 03/2022.
- [44] D. F. Williams, „On the mechanisms of biocompatibility“, *Biomaterials*, vol. 29, no. 20, pp. 2941–2953, 07/2008.
- [45] A. J. Ryan and F. J. O’Brien, „Insoluble elastin reduces collagen scaffold stiffness, improves viscoelastic properties, and induces a contractile phenotype in smooth muscle cells“, *Biomaterials*, vol. 73, pp. 296–307, 12/2015.
- [46] C. Bason, M. Gallorini, and A. C. Berardi, „The Extracellular Matrix, Growth Factors and Morphogens in Biomaterial Design and Tissue Engineering“, in *Extracellular Matrix for Tissue Engineering and Biomaterials*, A. C. Berardi, Ed., 1st ed., Cham, Switzerland: Humana Cham, 2018, ch. 1, pp. 3–26.
- [47] C. F. Guimarães, L. Gasperini, A. P. Marques, and R. L. Reis, „The stiffness of living tissues and its implications for tissue engineering“, *Nature Reviews Materials*, vol. 5, no. 5, pp. 351–370, 02/2020.
- [48] M. Gómez-Florit, R. M. Domingues, S. M. Bakht, B. B. Mendes, R. L. Reis, and M. E. Gomes, „Natural Materials“, in *Biomaterials Science*, Fourth Ed., London, United Kingdom: Elsevier, 2020, pp. 361–375.
- [49] K. Schenke-Layland, S. Liescher, and S. L. Layland, „Use of Extracellular Matrix Proteins and Natural Materials in Bioengineering“, in *Biomaterials Science*, Fourth Ed., London, United Kingdom: Elsevier, 2020, pp. 401–413.
- [50] G. Singh and A. Chanda, „Mechanical properties of whole-body soft human tissues: a review“, *Biomedical Materials*, vol. 16, no. 6, p. 062004, 11/2021.
- [51] T. H. Qazi *et al.*, „Programming hydrogels to probe spatiotemporal cell biology“, *Cell Stem Cell*, vol. 29, no. 5, pp. 678–691, 05/2022.

- [52] L. G. Griffith and M. A. Swartz, „Capturing complex 3D tissue physiology in vitro“, *Nature Reviews Molecular Cell Biology*, vol. 7, no. 3, pp. 211–224, 03/2006.
- [53] C. Sobacchi, E. Palagano, A. Villa, and C. Menale, „Soluble Factors on Stage to Direct Mesenchymal Stem Cells Fate“, *Frontiers in Bioengineering and Biotechnology*, vol. 5, no. MAY, pp. 1–9, 05/2017.
- [54] E. Cukierman, R. Pankov, D. R. Stevens, and K. M. Yamada, „Taking Cell-Matrix Adhesions to the Third Dimension“, *Science*, vol. 294, no. 5547, pp. 1708–1712, 11/2001.
- [55] V. Vogel and M. Sheetz, „Local force and geometry sensing regulate cell functions“, *Nature Reviews Molecular Cell Biology*, vol. 7, no. 4, pp. 265–275, 04/2006.
- [56] K. A. Jansen, D. M. Donato, H. E. Balcioglu, T. Schmidt, E. H. Danen, and G. H. Koenderink, „A guide to mechanobiology: Where biology and physics meet“, *Biochimica et Biophysica Acta (BBA) - Molecular Cell Research*, vol. 1853, no. 11, pp. 3043–3052, 11/2015.
- [57] P. Kollmannsberger, C. M. Bidan, J. W. C. Dunlop, and P. Fratzl, „The physics of tissue patterning and extracellular matrix organisation: how cells join forces“, *Soft Matter*, vol. 7, no. 20, p. 9549, 2011.
- [58] K. Burridge and C. Guilly, „Focal adhesions, stress fibers and mechanical tension“, *Experimental Cell Research*, vol. 343, no. 1, pp. 14–20, 04/2016.
- [59] C.-M. Lo, H.-B. Wang, M. Dembo, and Y.-l. Wang, „Cell Movement Is Guided by the Rigidity of the Substrate“, *Biophysical Journal*, vol. 79, no. 1, pp. 144–152, 07/2000.
- [60] A. J. Engler, S. Sen, H. L. Sweeney, and D. E. Discher, „Matrix Elasticity Directs Stem Cell Lineage Specification“, *Cell*, vol. 126, no. 4, pp. 677–689, 08/2006.
- [61] G. Broughton, J. E. Janis, and C. E. Attinger, „The Basic Science of Wound Healing“, *Plastic and Reconstructive Surgery*, vol. 117, no. SUPPLEMENT, 12S–34S, 06/2006.
- [62] B. Li and J. H. Wang, „Fibroblasts and myofibroblasts in wound healing: Force generation and measurement“, *Journal of Tissue Viability*, vol. 20, no. 4, pp. 108–120, 11/2011.
- [63] D. Dado and S. Levenberg, „Cell–scaffold mechanical interplay within engineered tissue“, *Seminars in Cell & Developmental Biology*, vol. 20, no. 6, pp. 656–664, 08/2009.
- [64] P. E. Rouse, „A Theory of the Linear Viscoelastic Properties of Dilute Solutions of Coiling Polymers“, *The Journal of Chemical Physics*, vol. 21, no. 7, pp. 1272–1280, 07/1953.
- [65] R. H. Colby, „Structure and linear viscoelasticity of flexible polymer solutions: comparison of polyelectrolyte and neutral polymer solutions“, *Rheologica Acta*, vol. 49, no. 5, pp. 425–442, 05/2010.
- [66] M. Rubinstein, R. H. Colby, and A. V. Dobrynin, „Dynamics of semidilute polyelectrolyte solutions“, *Physical Review Letters*, vol. 73, no. 20, pp. 2776–2779, 1994.
- [67] B. A. Miller-Chou and J. L. Koenig, „A review of polymer dissolution“, *Progress in Polymer Science*, vol. 28, no. 8, pp. 1223–1270, 08/2003.
- [68] T. Osswald and N. Rudolph, *Polymer Rheology*. München, Germany: Carl Hanser Verlag GmbH & Co. KG, 11/2014, pp. 101–141.
- [69] F. Irgens, *Rheology and non-newtonian fluids*. Berlin, Heidelberg, Germany: Springer International Publishing, 2013, vol. 9783319010533, pp. 1–190.
- [70] N. A. Peppas and A. S. Hoffman, „Hydrogels“, in *Biomaterials Science*, 1, Fourth Edi, London: Elsevier, 2020, pp. 153–166.
- [71] K. S. Lim, J. H. Galarraga, X. Cui, G. C. J. Lindberg, J. A. Burdick, and T. B. F. Woodfield, „Fundamentals and Applications of Photo-Cross-Linking in Bioprinting“, *Chemical Reviews*, vol. 120, no. 19, pp. 10662–10694, 10/2020.
- [72] N. Peppas, „Hydrogels in pharmaceutical formulations“, *European Journal of Pharmaceutics and Biopharmaceutics*, vol. 50, no. 1, pp. 27–46, 07/2000.
- [73] J. Jung and J. Oh, „Swelling characterization of photo-cross-linked gelatin methacrylate spherical microgels for bioencapsulation“, *e-Polymers*, vol. 14, no. 3, pp. 161–168, 05/2014.
- [74] Z. Wang, Z. Tian, F. Menard, and K. Kim, „Comparative study of gelatin methacrylate hydrogels from different sources for biofabrication applications“, *Biofabrication*, vol. 9, no. 4, p. 044101, 08/2017.
- [75] M. B. Aljaber, F. Verisqa, Z. Keskin-Erdogan, K. D. Patel, D. Y. S. Chau, and J. C. Knowles, „Influence of Gelatin Source and Bloom Number on Gelatin Methacryloyl Hydrogels Mechanical and Biological Properties for Muscle Regeneration“, *Biomolecules*, vol. 13, no. 5, p. 811, 05/2023.
- [76] N. A. Peppas, J. Z. Hilt, A. Khademhosseini, and R. Langer, „Hydrogels in Biology and Medicine: From Molecular Principles to Bionanotechnology“, *Advanced Materials*, vol. 18, no. 11, pp. 1345–1360, 06/2006.
- [77] M. Sutter, J. Siepmann, W. E. Hennink, and W. Jiskoot, „Recombinant gelatin hydrogels for the sustained release of proteins“, *Journal of Controlled Release*, vol. 119, no. 3, pp. 301–312, 2007.

- [78] T. Nii, „Strategies using gelatin microparticles for regenerative therapy and drug screening applications“, *Molecules*, vol. 26, no. 22, pp. 1–10, 2021.
- [79] P. Kofinas, „Hydrogels prepared by electron irradiation of poly(ethylene oxide) in water solution: unexpected dependence of cross-link density and protein diffusion coefficients on initial PEO molecular weight“, *Biomaterials*, vol. 17, no. 15, pp. 1547–1550, 1996.
- [80] L. Wenger and J. Hubbuch, „Investigation of Lysozyme Diffusion in Agarose Hydrogels Employing a Microfluidics-Based UV Imaging Approach“, *Frontiers in Bioengineering and Biotechnology*, vol. 10, no. March, pp. 1–12, 03/2022.
- [81] K. S. Anseth, C. N. Bowman, and L. Brannon-Peppas, „Mechanical properties of hydrogels and their experimental determination“, *Biomaterials*, vol. 17, no. 17, pp. 1647–1657, 01/1996.
- [82] J. R. Tse and A. J. Engler, „Preparation of Hydrogel Substrates with Tunable Mechanical Properties“, *Current Protocols in Cell Biology*, vol. 47, no. 1, pp. 1–16, 06/2010.
- [83] C. T. McKee, J. A. Last, P. Russell, and C. J. Murphy, „Indentation Versus Tensile Measurements of Young’s Modulus for Soft Biological Tissues“, *Tissue Engineering Part B: Reviews*, vol. 17, no. 3, pp. 155–164, 06/2011.
- [84] M. A. Kotlarchyk, E. L. Botvinick, and A. J. Putnam, „Characterization of hydrogel microstructure using laser tweezers particle tracking and confocal reflection imaging“, *Journal of Physics: Condensed Matter*, vol. 22, no. 19, p. 194 121, 05/2010.
- [85] A. Sheikhi and R. J. Hill, „Hydrogel–colloid interfacial interactions: a study of tailored adhesion using optical tweezers“, *Soft Matter*, vol. 12, no. 31, pp. 6575–6587, 2016.
- [86] K. M. Schultz and E. M. Furst, „Microrheology of biomaterial hydrogelators“, *Soft Matter*, vol. 8, no. 23, p. 6198, 2012.
- [87] J. Roether, S. Bertels, C. Oelschlaeger, M. Bastmeyer, and N. Willenbacher, „Microstructure, local viscoelasticity and cell culture suitability of 3D hybrid HA/collagen scaffolds“, *PLOS ONE*, vol. 13, no. 12, J. D. Schieber, Ed., e0207397, 12/2018.
- [88] J. Hafner *et al.*, „Monitoring matrix remodeling in the cellular microenvironment using microrheology for complex cellular systems“, *Acta Biomaterialia*, vol. 111, pp. 254–266, 07/2020.
- [89] M. W. Tibbitt and K. S. Anseth, „Hydrogels as extracellular matrix mimics for 3D cell culture“, *Biotechnology and Bioengineering*, vol. 103, no. 4, pp. 655–663, 07/2009.
- [90] R. Ravichandran *et al.*, „Functionalised type-I collagen as a hydrogel building block for bio-orthogonal tissue engineering applications“, *Journal of Materials Chemistry B*, vol. 4, no. 2, pp. 318–326, 2016.
- [91] Z. Li *et al.*, „Tuning Alginate-Gelatin Bioink Properties by Varying Solvent and Their Impact on Stem Cell Behavior“, *Scientific Reports*, vol. 8, no. 1, p. 8020, 05/2018.
- [92] S. Naghieh, M. Sarker, N. K. Sharma, Z. Barhoumi, and X. Chen, „Printability of 3D Printed Hydrogel Scaffolds: Influence of Hydrogel Composition and Printing Parameters“, *Applied Sciences*, vol. 10, no. 1, p. 292, 2019.
- [93] J. A. Burdick, C. Chung, X. Jia, M. A. Randolph, and R. Langer, „Controlled Degradation and Mechanical Behavior of Photopolymerized Hyaluronic Acid Networks“, *Biomacromolecules*, vol. 6, no. 1, pp. 386–391, 01/2005.
- [94] B. Sarker *et al.*, „Evaluation of Fibroblasts Adhesion and Proliferation on Alginate-Gelatin Crosslinked Hydrogel“, *PLoS ONE*, vol. 9, no. 9, M. Yamamoto, Ed., e107952, 09/2014.
- [95] M. K. Cowman, H.-G. Lee, K. L. Schwertfeger, J. B. McCarthy, and E. A. Turley, „The Content and Size of Hyaluronan in Biological Fluids and Tissues“, *Frontiers in Immunology*, vol. 6, no. JUN, pp. 1–8, 06/2015.
- [96] G. Kogan, L. Šoltés, R. Stern, and P. Gemeiner, „Hyaluronic acid: a natural biopolymer with a broad range of biomedical and industrial applications“, *Biotechnology Letters*, vol. 29, no. 1, pp. 17–25, 12/2006.
- [97] M. A. Torres-Acosta *et al.*, „Comparative Economic Analysis Between Endogenous and Recombinant Production of Hyaluronic Acid“, *Frontiers in Bioengineering and Biotechnology*, vol. 9, no. July, pp. 1–14, 07/2021.
- [98] J. A. Burdick and G. D. Prestwich, „Hyaluronic Acid Hydrogels for Biomedical Applications“, *Advanced Materials*, vol. 23, no. 12, pp. 41–56, 03/2011.
- [99] B. P. Toole, „Hyaluronan: from extracellular glue to pericellular cue“, *Nature Reviews Cancer*, vol. 4, no. 7, pp. 528–539, 07/2004.
- [100] A. B. Csoka, G. I. Frost, and R. Stern, „The six hyaluronidase-like genes in the human and mouse genomes“, *Matrix Biology*, vol. 20, no. 8, pp. 499–508, 12/2001.
- [101] M. N. Collins and C. Birkinshaw, „Hyaluronic acid based scaffolds for tissue engineering—A review“, *Carbohydrate Polymers*, vol. 92, no. 2, pp. 1262–1279, 02/2013.
- [102] K. A. Smeds and M. W. Grinstaff, „Photocrosslinkable polysaccharides for in situ hydrogel formation“, *Journal of Biomedical Materials Research*, vol. 54, no. 1, pp. 115–121, 01/2001.
- [103] I. Donati and S. Paoletti, „Material Properties of Alginates“, in *Biology and Applications*, B. H. A. Rehm, Ed., Springer Berlin Heidelberg, 2009, ch. 1, pp. 1–53.

- [104] K. Y. Lee and D. J. Mooney, „Alginate: Properties and biomedical applications“, *Progress in Polymer Science*, vol. 37, no. 1, pp. 106–126, 01/2012.
- [105] M. B. Łabowska, I. Michalak, and J. Detyna, „Methods of extraction, physicochemical properties of alginates and their applications in biomedical field - A review“, *Open Chemistry*, vol. 17, no. 1, pp. 738–762, 2019.
- [106] A. D. Augst, H. J. Kong, and D. J. Mooney, „Alginate Hydrogels as Biomaterials“, *Macromolecular Bioscience*, vol. 6, no. 8, pp. 623–633, 08/2006.
- [107] R. Schrieber and H. Gareis, *Gelatine Handbook*. Weinheim, Germany: Wiley, 02/2007.
- [108] P. Privalov, E. Tiktopulo, and V. Tischenko, „Stability and mobility of the collagen structure“, *Journal of Molecular Biology*, vol. 127, no. 2, pp. 203–216, 01/1979.
- [109] M. Djabourov, J.-P. Lechaire, and F. Gaill, „Structure and rheology of gelatin and collagen gels“, *Biorheology*, vol. 30, no. 3-4, pp. 191–205, 08/1993.
- [110] J. Brinckmann, „Collagens at a Glance“, in *Topics in Current Chemistry*, vol. 247, 04/2005, pp. 1–6.
- [111] „The Collagen Suprafamily: From Biosynthesis to Advanced Biomaterial Development“, *Advanced Materials*, vol. 31, no. 1, 2019.
- [112] A. Tirella, T. Liberto, and A. Ahluwalia, „Riboflavin and collagen: New crosslinking methods to tailor the stiffness of hydrogels“, *Materials Letters*, vol. 74, pp. 58–61, 05/2012.
- [113] H. Liang, S. J. Russell, D. J. Wood, and G. Tronci, „Monomer-Induced Customization of UV-Cured Atelocollagen Hydrogel Networks“, *Frontiers in Chemistry*, vol. 6, no. DEC, pp. 1–14, 12/2018.
- [114] J. M. Lee, S. K. Q. Suen, W. L. Ng, W. C. Ma, and W. Y. Yeong, „Bioprinting of Collagen: Considerations, Potentials, and Applications“, *Macromolecular Bioscience*, vol. 21, no. 1, pp. 1–18, 01/2021.
- [115] N. J. Bulleid, D. C. A. John, and K. E. Kadler, „Recombinant expression systems for the production of collagen“, *Biochemical Society Transactions*, vol. 28, no. 4, pp. 350–353, 08/2000.
- [116] S. Browne, D. I. Zeugolis, and A. Pandit, „Collagen: Finding a Solution for the Source“, *Tissue Engineering Part A*, vol. 19, no. 13-14, pp. 1491–1494, 07/2013.
- [117] A. A. Karim and R. Bhat, „Fish gelatin: properties, challenges, and prospects as an alternative to mammalian gelatins“, *Food Hydrocolloids*, vol. 23, no. 3, pp. 563–576, 2009.
- [118] I. Haug and K. Draget, „Gelatin“, in *Handbook of Food Proteins*, 1964, G. Phillips and P. Williams, Eds., Woodhead Publishing, 2011, pp. 92–115.
- [119] K. Y. Lee and D. J. Mooney, „Hydrogels for Tissue Engineering“, *Chemical Reviews*, vol. 101, no. 7, pp. 1869–1880, 07/2001.
- [120] T. Göckler *et al.*, „Tuning Superfast Curing Thiol-Norbornene-Functionalized Gelatin Hydrogels for 3D Bioprinting“, *Advanced Healthcare Materials*, vol. 10, no. 14, pp. 1–13, 07/2021.
- [121] A. I. Van Den Bulcke, B. Bogdanov, N. De Rooze, E. H. Schacht, M. Cornelissen, and H. Berghmans, „Structural and rheological properties of methacrylamide modified gelatin hydrogels“, *Biomacromolecules*, vol. 1, no. 1, pp. 31–38, 2000.
- [122] A. Habeeb, „Determination of free amino groups in proteins by trinitrobenzenesulfonic acid“, *Analytical Biochemistry*, vol. 14, no. 3, pp. 328–336, 03/1966.
- [123] B. H. Lee, H. Shirahama, N.-J. Cho, and L. P. Tan, „Efficient and controllable synthesis of highly substituted gelatin methacrylamide for mechanically stiff hydrogels“, *RSC Advances*, vol. 5, no. 128, pp. 106 094–106 097, 2015.
- [124] H. Shirahama, B. H. Lee, L. P. Tan, and N.-J. Cho, „Precise Tuning of Facile One-Pot Gelatin Methacryloyl (GelMA) Synthesis“, *Scientific Reports*, vol. 6, no. 1, p. 31 036, 08/2016.
- [125] H. Xu, J. Casillas, S. Krishnamoorthy, and C. Xu, „Effects of Irgacure 2959 and lithium phenyl-2,4,6-trimethylbenzoylphosphinate on cell viability, physical properties, and microstructure in 3D bioprinting of vascular-like constructs“, *Biomedical Materials*, vol. 15, no. 5, p. 055 021, 08/2020.
- [126] A. K. Nguyen, P. L. Goering, R. K. Elespuru, S. Sarkar Das, and R. J. Narayan, „The Photoinitiator Lithium Phenyl (2,4,6-Trimethylbenzoyl) Phosphinate with Exposure to 405 nm Light Is Cytotoxic to Mammalian Cells but Not Mutagenic in Bacterial Reverse Mutation Assays“, *Polymers*, vol. 12, no. 7, p. 1489, 07/2020.
- [127] M. Kirsch *et al.*, „Gelatin-Methacryloyl (GelMA) Formulated with Human Platelet Lysate Supports Mesenchymal Stem Cell Proliferation and Differentiation and Enhances the Hydrogel’s Mechanical Properties“, *Bioengineering*, vol. 6, no. 3, p. 76, 08/2019.
- [128] S.-B. Han, J.-K. Kim, G. Lee, and D.-H. Kim, „Mechanical Properties of Materials for Stem Cell Differentiation“, *Advanced Biosystems*, vol. 4, no. 11, pp. 1–17, 11/2020.
- [129] S. Liu, M. Jin, Y. Chen, L. Teng, D. Qi, and L. Ren, „Air-In-Water Emulsion Solely Stabilized by Gelatin Methacryloyl and Templating for Macroporous Nanocomposite Hydrogels“, *Macromolecular Chemistry and Physics*, vol. 220, no. 9, pp. 1–9, 05/2019.

- [130] E. Hoch, T. Hirth, G. E. Tovar, and K. Borchers, „Chemical tailoring of gelatin to adjust its chemical and physical properties for functional bioprinting“, *Journal of Materials Chemistry B*, vol. 1, no. 41, pp. 5675–5685, 2013.
- [131] M. Cuvellier *et al.*, „3D culture of HepaRG cells in GelMa and its application to bioprinting of a multicellular hepatic model“, *Biomaterials*, vol. 269, p. 120611, 2021.
- [132] Z. Wang, R. Abdulla, B. Parker, R. Samanipour, S. Ghosh, and K. Kim, „A simple and high-resolution stereolithography-based 3D bioprinting system using visible light crosslinkable bioinks“, *Biofabrication*, vol. 7, no. 4, p. 045009, 12/2015.
- [133] T. Tang *et al.*, „Microfluidic Fabrication of Gelatin Acrylamide Microgels through Visible Light Photopolymerization for Cell Encapsulation“, *ACS Applied Bio Materials*, vol. 6, no. 6, pp. 2496–2504, 06/2023.
- [134] J. Liu, T. Tagami, and T. Ozeki, „Fabrication of 3D-Printed Fish-Gelatin-Based Polymer Hydrogel Patches for Local Delivery of PEGylated Liposomal Doxorubicin“, *Marine Drugs*, vol. 18, no. 6, p. 325, 06/2020.
- [135] M. Vigata, C. Meinert, N. Bock, B. L. Dargaville, and D. W. Hutmacher, „Deciphering the Molecular Mechanism of Water Interaction with Gelatin Methacryloyl Hydrogels: Role of Ionic Strength, pH, Drug Loading and Hydrogel Network Characteristics“, *Biomedicines*, vol. 9, no. 5, p. 574, 05/2021.
- [136] A. H. Nguyen, J. McKinney, T. Miller, T. Bongiorno, and T. C. McDevitt, „Gelatin methacrylate microspheres for controlled growth factor release“, *Acta Biomaterialia*, vol. 13, pp. 101–110, 02/2015.
- [137] K. Hölzl, S. Lin, L. Tytgat, S. Van Vlierberghe, L. Gu, and A. Ovsianikov, „Bioink properties before, during and after 3D bioprinting“, *Biofabrication*, vol. 8, no. 3, p. 032002, 09/2016.
- [138] W. Liu *et al.*, „Extrusion Bioprinting of Shear-Thinning Gelatin Methacryloyl Bioinks“, *Advanced Healthcare Materials*, vol. 6, no. 12, pp. 1–11, 06/2017.
- [139] R. Gauvin *et al.*, „Microfabrication of complex porous tissue engineering scaffolds using 3D projection stereolithography“, *Biomaterials*, vol. 33, no. 15, pp. 3824–3834, 05/2012.
- [140] Z. Wang *et al.*, „Visible Light Photoinitiation of Cell-Adhesive Gelatin Methacryloyl Hydrogels for Stereolithography 3D Bioprinting“, *ACS Applied Materials & Interfaces*, vol. 10, no. 32, pp. 26859–26869, 08/2018.
- [141] J. Visser *et al.*, „Reinforcement of hydrogels using three-dimensionally printed microfibrils“, *Nature Communications*, vol. 6, no. 1, p. 6933, 04/2015.
- [142] J. Liang, H. Chen, Z. Guo, P. Dijkstra, D. Grijpma, and A. Poot, „Tough fibrous mats prepared by electrospinning mixtures of methacrylated poly(trimethylene carbonate) and methacrylated gelatin“, *European Polymer Journal*, vol. 152, no. February, 2021.
- [143] W. J. Seeto, Y. Tian, S. Pradhan, P. Kerscher, and E. A. Lipke, „Rapid Production of Cell-Laden Microspheres Using a Flexible Microfluidic Encapsulation Platform“, *Small*, vol. 15, no. 47, pp. 1–13, 11/2019.
- [144] K. Yue, G. Trujillo-de Santiago, M. M. Alvarez, A. Tamayol, N. Annabi, and A. Khademhosseini, „Synthesis, properties, and biomedical applications of gelatin methacryloyl (GelMA) hydrogels“, *Biomaterials*, vol. 73, pp. 254–271, 2015.
- [145] F. Piccinini, A. Tesei, C. Arienti, and A. Bevilacqua, „Cell Counting and Viability Assessment of 2D and 3D Cell Cultures: Expected Reliability of the Trypan Blue Assay“, *Biological Procedures Online*, vol. 19, no. 1, p. 8, 12/2017.
- [146] R. Szeliski, *Computer Vision* (Texts in Computer Science May). Cham, Switzerland: Springer International Publishing, 2022, ch. 3, pp. 85–151.
- [147] V. Wiesmann, D. Franz, C. Held, C. Münzenmayer, R. Palmisano, and T. Wittenberg, „Review of free software tools for image analysis of fluorescence cell micrographs“, *Journal of Microscopy*, vol. 257, no. 1, pp. 39–53, 01/2015.
- [148] S. Gretzinger, N. Beckert, A. Gleadall, C. Lee-Thedieck, and J. Hubbuch, „3D bioprinting – Flow cytometry as analytical strategy for 3D cell structures“, *Bioprinting*, vol. 11, no. March, e00023, 09/2018.
- [149] A. C. Daly, L. Riley, T. Segura, and J. A. Burdick, „Hydrogel microparticles for biomedical applications“, *Nature Reviews Materials*, vol. 5, no. 1, pp. 20–43, 2020.
- [150] A. L. Liu and A. J. García, „Methods for Generating Hydrogel Particles for Protein Delivery“, *Annals of Biomedical Engineering*, vol. 44, no. 6, pp. 1946–1958, 06/2016.
- [151] E. Amstad, „Emulsion Drops as Templates for the Fabrication of Microparticles and Capsules“, in *Droplet Microfluidics*, C. Ren and A. Lee, Eds., The Royal Society of Chemistry, 11/2020, pp. 261–289.
- [152] A. Dewandre, J. Rivero-Rodriguez, Y. Vitry, B. Sobac, and B. Scheid, „Microfluidic droplet generation based on non-embedded co-flow-focusing using 3D printed nozzle“, *Scientific Reports*, vol. 10, no. 1, p. 21616, 12/2020.
- [153] N. Qin, „Fundamentals“, in *Droplet Microfluidics*, C. Ren and A. Lee, Eds., The Royal Society of Chemistry, 11/2020, pp. 15–44.
- [154] A. S. Utada, L.-Y. Chu, A. Fernandez-Nieves, D. R. Link, C. Holtze, and D. A. Weitz, „Dripping, Jetting, Drops, and Wetting: The Magic of Microfluidics“, *MRS Bulletin*, vol. 32, no. 9, pp. 702–708, 09/2007.
- [155] A. S. Utada, A. Fernandez-Nieves, J. M. Gordillo, and D. A. Weitz, „Absolute Instability of a Liquid Jet in a Coflowing Stream“, *Physical Review Letters*, vol. 100, no. 1, p. 014502, 01/2008.

- [156] T. F. Tadros, *Volume 1 Interfacial Phenomena and Colloid Stability, Basic Principles*. Berlin, Germany: De Gruyter, 12/2015.
- [157] C. B. Highley, K. H. Song, A. C. Daly, and J. A. Burdick, „Jammed Microgel Inks for 3D Printing Applications“, *Advanced Science*, vol. 6, no. 1, p. 1801076, 01/2019.
- [158] E. X. Ng, M. Wang, S. H. Neo, C. A. Tee, C. H. Chen, and K. J. Van Vliet, „Dissolvable Gelatin-Based Microcarriers Generated through Droplet Microfluidics for Expansion and Culture of Mesenchymal Stromal Cells“, *Biotechnology Journal*, vol. 16, no. 3, pp. 1–10, 2021.
- [159] J. Huang *et al.*, „One-step generation of core–shell biomimetic microspheres encapsulating double-layer cells using microfluidics for hair regeneration“, *Biofabrication*, vol. 15, no. 2, p. 025007, 04/2023.
- [160] Z. Lin *et al.*, „Bioactive Decellularized Extracellular Matrix Hydrogel Microspheres Fabricated Using a Temperature-Controlling Microfluidic System“, *ACS Biomaterials Science and Engineering*, vol. 8, no. 4, pp. 1644–1655, 2022.
- [161] S. Dutta, S. K. Pal, and R. Sen, „Digital Image Processing in Machining“, in *Modern Mechanical Engineering*, J. P. Davim, Ed., 1st ed., Berlin, Heidelberg, Germany: Springer, 2014, pp. 367–410.
- [162] B. L. DeCost and E. A. Holm, „A computer vision approach for automated analysis and classification of microstructural image data“, *Computational Materials Science*, vol. 110, pp. 126–133, 12/2015.
- [163] A. S. Basu, „Droplet morphometry and velocimetry (DMV): A video processing software for time-resolved, label-free tracking of droplet parameters“, *Lab on a Chip*, vol. 13, no. 10, pp. 1892–1901, 2013.
- [164] J.-C. Baret *et al.*, „Fluorescence-activated droplet sorting (FADS): efficient microfluidic cell sorting based on enzymatic activity“, *Lab on a Chip*, vol. 9, no. 13, p. 1850, 2009.
- [165] M. Chabert and J.-L. Viovy, „Microfluidic high-throughput encapsulation and hydrodynamic self-sorting of single cells“, *Proceedings of the National Academy of Sciences*, vol. 105, no. 9, pp. 3191–3196, 03/2008.
- [166] J. Groll *et al.*, „A definition of bioinks and their distinction from biomaterial inks“, *Biofabrication*, vol. 11, no. 1, p. 013001, 11/2018.
- [167] J. Groll *et al.*, „A definition of bioinks and their distinction from biomaterial inks“, *Biofabrication*, vol. 11, no. 1, p. 013001, 11/2018.
- [168] K. Dubbin, A. Tabet, and S. C. Heilshorn, „Quantitative criteria to benchmark new and existing bio-inks for cell compatibility“, *Biofabrication*, vol. 9, no. 4, p. 044102, 09/2017.
- [169] „Biofabrication: A Guide to Technology and Terminology“, *Trends in Biotechnology*, vol. 36, no. 4, pp. 384–402, 04/2018.
- [170] F. Wulle *et al.*, „Multi-axis 3D printing of gelatin methacryloyl hydrogels on a non-planar surface obtained from magnetic resonance imaging“, *Additive Manufacturing*, vol. 50, no. December 2021, p. 102566, 02/2022.
- [171] L. Wenger, S. Strauß, and J. Hubbuch, „Automated and dynamic extrusion pressure adjustment based on real-time flow rate measurements for precise ink dispensing in 3D bioprinting“, *Bioprinting*, vol. 28, no. July, e00229, 12/2022.
- [172] G. Gillispie *et al.*, „Assessment methodologies for extrusion-based bioink printability“, *Biofabrication*, vol. 12, no. 2, p. 022003, 02/2020.
- [173] R. Chang, J. Nam, and W. Sun, „Effects of Dispensing Pressure and Nozzle Diameter on Cell Survival from Solid Freeform Fabrication–Based Direct Cell Writing“, *Tissue Engineering Part A*, vol. 14, no. 1, pp. 41–48, 01/2008.
- [174] A. A. Foster, L. M. Marquardt, and S. C. Heilshorn, „The diverse roles of hydrogel mechanics in injectable stem cell transplantation“, *Current Opinion in Chemical Engineering*, vol. 15, pp. 15–23, 02/2017.
- [175] N. Paxton, W. Smolan, T. Böck, F. Melchels, J. Groll, and T. Jungst, „Proposal to assess printability of bioinks for extrusion-based bioprinting and evaluation of rheological properties governing bioprintability“, *Biofabrication*, vol. 9, no. 4, p. 044107, 11/2017.
- [176] A. Blaeser, D. F. Duarte Campos, U. Puster, W. Richtering, M. M. Stevens, and H. Fischer, „Controlling Shear Stress in 3D Bioprinting is a Key Factor to Balance Printing Resolution and Stem Cell Integrity“, *Advanced Healthcare Materials*, vol. 5, no. 3, pp. 326–333, 02/2016.
- [177] Y. He, F. Yang, H. Zhao, Q. Gao, B. Xia, and J. Fu, „Research on the printability of hydrogels in 3D bioprinting“, *Scientific Reports*, vol. 6, no. 1, p. 29977, 07/2016.
- [178] T. Gao *et al.*, „Optimization of gelatin–alginate composite bioink printability using rheological parameters: a systematic approach“, *Biofabrication*, vol. 10, no. 3, p. 034106, 06/2018.
- [179] A. A. Aldana, F. Valente, R. Dilley, and B. Doyle, „Development of 3D bioprinted GelMA–alginate hydrogels with tunable mechanical properties“, *Bioprinting*, vol. 21, no. June 2020, e00105, 03/2021.
- [180] T. Brosnan and D. W. Sun, „Improving quality inspection of food products by computer vision - A review“, *Journal of Food Engineering*, vol. 61, no. 1 SPEC. Pp. 3–16, 2004.

Thesis Outline

2.1 Research Proposal

Biomaterials play a crucial role in developing advanced medical devices, tissue-engineered constructs, drug delivery systems, and diagnostic tools, ultimately contributing to improved healthcare outcomes and quality of life for patients. Among biomaterials, hydrogels emerge as a versatile class of materials capable of holding substantial amounts of water within their three-dimensional network structures. Hydrogels mimic the natural extracellular matrix of tissues and organs, providing an ideal environment for cell growth. Hydrogels can be tailored to exhibit specific mechanical and physical properties, biodegradability, and bioactivity, making them suitable for a wide range of biomedical applications. One notable biopolymer for formulating hydrogels that has emerged as a key research focus is Gelatin Methacryloyl, also called GelMA. This protein merges the biocompatibility of gelatin with the tunable mechanical properties afforded by the functionalization. This unique combination allows GelMA to be used for specific applications, including tissue engineering, regenerative medicine, drug delivery, and 3D bioprinting. Despite the wide range of applications of GelMA, there is still a lack of knowledge regarding the effect of the raw materials from different sources and their molecular weight on the quality attributes of GelMA. Furthermore, biomaterials science merges the knowledge of previous research in single fields such as biology, mechanical engineering, process engineering, and material science in a field of high complexity. Existing methods and techniques from each of these disciplines can be applied to research on biomaterials and their application. However, the transfer of methods between the disciplines has only taken place partially, if at all. This fragmentation of knowledge and the partial transfer of methods between single fields pose significant challenges that might slow down the progression of research and hinder translation to the clinical stage. Here, by validating methods and techniques from different fields, researchers can enhance the robustness and accuracy of their studies. Additionally, establishing automated, standardized procedures and protocols can improve reproducibility, comparability, and reliability across studies.

This thesis focuses on gaining comprehensive knowledge of various aspects of GelMA, including its production, utilization with different fabrication methods, and integration of existing methods from single research fields. For this purpose, robust processes and analytical strategies were implemented to establish the reproducibility and comparability of the gathered data. This interdisciplinary approach allows for transferring knowledge and techniques across disciplines, facilitating advancements in understanding the interactions between biomaterials and biological systems and optimizing fabrication processes.

The first part of the thesis focuses on the synthesis of GelMA and its application to hydrogel formulation for cell culture and microfluidic fabrication techniques. Here, the sol-gel transition of the solutions limits gelatin processing as the solutions require stable heating. In Chapter 3, an approach is developed for gelatin processing at room temperature by suitable formulation of the synthesis buffer. In addition, tangential flow filtration is applied for the purification process. Moreover, the synthesis approach is adopted in the following study presented in Chapter 4. Here, the effects of diverse raw materials with different bloom strengths and from various species on the product are studied. GelMA is used for hydrogel formulation in both studies, and elastic moduli are determined by variation in protein concentration, degree of functionalization, and raw material.

Furthermore, automated image processing is implemented as an objective and reproducible analysis. GelMA hydrogels are used as cell culture substrates in Chapter 3, and the biocompatibility is determined. Therefore, cell viability is determined using cellular staining, microscopy, and automated image analysis. Besides the traditional live/dead staining component, nuclear staining that tags both active and inactive cells is introduced. This analytical strategy enables the distinction of single cells in an automated manner since the independent signals are used, and the extracted data is merged to identify single cells in overlapping regions. Moreover, hydrogel microparticles are produced using GelMA in Chapter 4. Gained knowledge of the buffer composition is applied to produce GelMA droplets at room temperature at concentrations up to 20% (w/v) without the clogging of thin capillaries. The effect of process parameters such as GelMA concentration and feed rates of disperse and continuous phases on the size of droplets is determined using automated image analysis. The swelling behavior of hydrogel microparticles in cell culture media is analyzed using further automated workflow for data extraction from images.

The second part of the thesis presents the application of GelMA for the formulation of polymer solutions in extrusion-based bioprinting. The assessment of printing performance regarding structural properties and the effects on cells is currently unreliable. Experimental procedures for the studies on the printing performance of bioink include the setting of equal printing parameters and manual extraction of geometric features of printed structures. By variation of the formulation, the rheological properties of the inks differ, and, therefore, the flow rate during extrusion also varies. In addition, the manual extraction of data reduces the reliability of the analysis. Additionally, the printing effects on cells are determined using microscopy and manual identification of cells. In Chapter 5, the study includes the rheological characterization of two bioinks based on a constant GelMA concentration and a 1% (w/v) variation of alginate concentration. The volumetric flow rate is set equal for both bioinks according to the specific flow behavior. Regarding printing accuracy, automated image processing is implemented to analyze three basic geometries. The effects of processing steps on cell viability are assessed by diluting the bioinks, cellular staining, and subsequent data acquisition using a flow cytometer. The processing steps comprise mixing a cell suspension with a biopolymer solution and printing the bioink.

Furthermore, comparability across studies is limited in the current literature, which can be addressed by standardizing procedures and analytical strategies. The following study presented

in Chapter 6 evaluates the possibility of standardization of extrusion-based bioprinting within a consortium of 12 research facilities. For this purpose, standard operating procedures are established for printing and image acquisition. Additionally, biomaterials, including a GelMA solution, labware, and printing models, are distributed across all participating laboratories. A qualitative assessment of the produced data consisting of 2160 images is performed to identify possible complications during the printing and imaging steps. Moreover, quantitative data extraction is performed using three different image analysis workflows as automated methods. Based on the extracted data, including geometric properties of the printed structures, the reproducibility of intra- and inter-laboratory printing processes is evaluated. This analytical approach also identifies critical instrument functions of the printer. Advantageous functions include the precise temperature setting in the cartridge holder, automated coordinate determination, and mechanically driven extrusion mechanisms. Regarding the GelMA-based bioink, the printed structures showed enhanced reproducibility when printers were equipped with fluid circulation systems enabling heating and cooling. Lower reproducibility was demonstrated in the case of printers supplied solely with electric heating.

2.2 Manuscript Overview

Within the scope of this thesis, four manuscripts were prepared and subsequently published. Each manuscript is presented briefly with a summary and the corresponding citation. As a result, the publications are slightly changed and adapted to the format and layout of this thesis. Moreover, two of the following manuscripts were prepared in collaboration with colleagues to enhance their quality. As a result, the first authorship was shared, i.e., contributed equally. Detailed information on the contributions and the signature of each author is included as a supplement to the examination copy of this thesis. Two manuscripts, Chapter 5 and Chapter 6, can also be found in the thesis of the co-author Svenja Strauß.

Chapter 3

A Novel Approach for the Manufacturing of Gelatin-Methacryloyl..... 35

David Grijalva Garces, Carsten Philipp Radtke and Jürgen Hubbuch

published in Polymers, Volume 14(24), 2022, Article 5424

<https://doi.org/10.3390/polym14245424>

This study presents an approach that enables gelatin processing at room temperature, below the sol-gel transition temperature of gelatin solutions. For this purpose, the functionalization of gelatin to gelatin methacryloyl (GelMA) included urea in the reaction buffer. Moreover, the degree of functionalization (DoF) of GelMA is considered a quality attribute of the protein. The presented approach allowed for an accurate adjustment of the DoF by adjusting the ratio of reactant volume to gelatin concentration. Furthermore, varying the concentration of GelMA and its DoF led to fabricated hydrogels with customized elasticity. Moreover, GelMA was applied to formulate hydrogels for cell culture. The biocompatibility of these hydrogels was evaluated and compared to hydrogels produced using the conventional method of GelMA synthesis. Therefore, an image processing and analysis workflow was developed to distinguish single nuclei from overlapping cells. Subsequently, the position of the nuclei was merged with the live /dead staining data to determine the number of cells and the biocompatibility of the biomaterial. Moreover, NIH 3T3 fibroblasts were cultured on the hydrogels during a three-day incubation period, and cell viability was comparable to that of the control group. This study demonstrates that the robustness of the synthesis can be enhanced, as no heating is required during processing. Additionally, an automated analytical strategy is applied to determine cell viability reliably.

Chapter 4

The Effect of Gelatin Source on the Synthesis of Gelatin-Methacryloyl and the Production of Hydrogel Microparticles..... 53

David Grijalva Garces, Luise Josephine Appoldt, Jasmin Egner, Nico Leister and Jürgen Hubbuch

published in Gels, Volume 9(12), 2023, Article 927

<https://doi.org/10.3390/gels9120927>

Since gelatin is derived from native tissue, the properties of the raw materials fluctuate depending on the source and the purification process. In this study, gelatin modification was conducted following the previously developed approach. Eight different gelatin products were functionalized to gelatin methacryloyl (GelMA). The reaction between gelatin and methacrylic anhydride is a two-phase reaction. Hence, raw materials have a significant effect as gelatin is inherently surface active. It was observed that the bloom strength and the source of gelatin influenced the degree of functionalization (DoF). Additionally, batch-to-batch variability of the raw materials proved to affect the product. Furthermore, GelMA was used to prepare hydrogels and characterize their elasticity. The mechanical property depended on the DoF, bloom strength, and raw material source. Moreover, microfluidic production was used to generate droplets that serve as a template for forming hydrogel microparticles. The use of urea in solution enabled the generation of particles as a single pipeline at room temperature. By inhibiting the gelation and, hence, blocking capillaries, high GelMA concentration could be used. Furthermore, automated image processing determined droplet and particle size by identifying the interface between disperse and continuous phases. Moreover, the size of droplets was controlled by adjusting the continuous to disperse phase ratio, while the GelMA concentration influenced the swelling behavior of hydrogel microparticles. This study expands the knowledge of processing parameters related to the quality attribute of GelMA. In addition, bloom strength is a further parameter that influences the elasticity of hydrogels. Furthermore, GelMA, combined with urea, is suitable for microfluidics fabrication at high concentrations. Automated image processing was also applied for the data extraction.

Chapter 5

Analytics in Extrusion-Based Bioprinting: Standardized Methods Improving Quantification and Comparability of the Performance of Bioinks 79

Svenja Strauß*, David Grijalva Garces* and Jürgen Hubbuch

* contributed equally

published in Polymers, Volume 15(8), 2023, Article 1829

<https://doi.org/10.3390/polym15081829>

The compromise between the structural and biological properties of printed scaffolds has been accepted in bioprinting. However, the comparability across studies in extrusion-based bioprinting has proven to be a limitation in the development of bioink. Therefore, this study proposed a method to assess the printing performance of two different biomaterial inks by setting an equal flow rate and granting comparability. Gelatin methacryloyl (GelMA) and alginate were used for the bioink formulation; both inks differed by 1% (w/v) alginate concentration. The rheological characterization of both bioinks enabled the determination of printing settings in a pneumatically driven extrusion printer. Printing accuracy was determined using automated image analysis to extract geometric features of simple structures, i.e., lines, circles, and angles. No significant differences were found regarding the accuracy of printed structures using both bioinks. Furthermore, the effects of processing steps on cells were determined by live/dead staining and fluorescence detection using a flow cytometer. Processing steps included the mixing of the biopolymer solutions with cell suspensions. Flow cytometry was used as an analytical tool to increase the relevance of the acquired data by increasing the number of quantified cells. While the bioinks showed no effects on the accuracy, the bioink of higher viscosity led to a significant decrease in cell viability after each process. The study presents a straightforward method for characterizing the bioinks by setting a

comparable experimental setup. Furthermore, automated image processing proved to be a suitable data extraction method, including a large number of images. Following the developed approach, it could be shown that no compromise has to be taken to determine the better-performing formulation.

This study was a collaboration between Svenja Strauß and me, and the resulting manuscript is also included in her thesis. The methodology and experimental design of the study were planned together. While her focus lay on developing robust tools for the image acquisition and automated image analysis of printed structures, my focus was the formulation and rheological characterization of the polymer solutions used. Cell culture and cell analytics were also my focus in the study. Data evaluation, visualization, and writing of the original draft were done as a joint work. All authors have read and approved the published version of the manuscript.

Chapter 6

On the reproducibility of extrusion-based bioprinting: round robin study on standardization in the field..... 99

David Grijalva Garces*, Svenja Strauß*, Sarah Gretzinger, Barbara Schmiege, Tomasz Jüngst, Jürgen Groll, Lorenz Meinel, Isabelle Schmidt, Hanna Hartmann, Katja Schenke-Layland, Nico Brandt, Michael Selzer, Stefan Zimmermann, Peter Koltay, Alexander Southan, Günter E. M. Tovar, Sarah Schmidt, Achim Weber, Tilman Ahlfeld, Michael Gelinsky, Thomas Scheibel, Rainer Detsch, Aldo R. Boccaccini, Toufik Naolou, Cornelia Lee-Thedieck, Christian Willems, Thomas Groth, Stephan Allgeier, Bernd Köhler, Tiaan Friedrich, Heiko Briesen, Janine Buchholz, Dietrich Paulus, Anselm von Gladiss and Jürgen Hubbuch *contributed equally

published in Biofabrication, Volume 16(1), 2024, Article 015002
<https://doi.org/10.1088/1758-5090/acfe3b>

The limited comparability of the studies in bioprinting limits not only the development of printable biomaterials but also the translation to clinical stages. Standardization is a crucial step in developing processes and analytical strategies to enable the achievement of medical applications. This study aims to evaluate the currently possible degree of standardization of bioprinting processes within a group of 12 research entities in the field of bioprinting in Germany. The models to be printed, labware, and biomaterial inks, including alginate and gelatin methacryloyl (GelMA), were distributed centrally. Additionally, standardized operational procedures for printing and data acquisition were written to set a comparable framework in the study. In addition, three independent academic groups developed a robust analytical strategy to extract unbiased data. This consisted of automated image processing that extracted geometric features describing the printed structure, such as filament width. Furthermore, a qualitative analysis of the acquired images was performed to identify possible experimental deviations. The quantitative analysis using automated image analysis was used to evaluate the reproducibility of the geometric features by calculating the coefficient of variation. High variability in an inter- and intralaboratory comparison suggested that current bioprinting methods are not reproducible yet. In addition, advantageous functions of the printing equipment could be identified. Lower variability was shown for laboratories using instruments with mechanically driven extrusion mechanisms, systems that precisely set temperature, and automated coordinate calibration units.

This manuscript presents a collaborative study between 15 research institutions and was published with shared first authorship between Svenja Strauß and me. The study is also shown in her thesis.

Among the participants of the study, the group at the Karlsruhe Institute of Technology (KIT) played the role of project administration and organization. Furthermore, experimental procedures for data generation were performed at 12 laboratories, including KIT. Moreover, data extraction was performed by three additional groups. The laboratories not associated with KIT worked under subcontracts. The KIT team comprised Sarah Gretzinger, Barbara Schmiege, Svenja Strauß, Jürgen Hubbuch, and me. Sarah Gretzinger, Barbara Schmiege, and Jürgen Hubbuch focused on the administrative work, including but not limited to communicating with participants and scheduling the transfer of materials and equipment. Svenja Strauß and I performed data processing, data analysis, and the preparation of graphical illustrations. The first draft of the manuscript was done in collaboration, as well. All authors have read and approved the published final version of the manuscript.

3

A Novel Approach for the Manufacturing of Gelatin-Methacryloyl

David Grijalva Garces^{1,2}, Carsten Philipp Radtke² and Jürgen Hubbuch^{1,2}

¹ Institute of Functional Interfaces, Karlsruhe Institute of Technology (KIT), Eggenstein-Leopoldshafen, Germany

² Institute of Engineering in Life Sciences, Section IV: Biomolecular Separation Engineering, Karlsruhe Institute of Technology (KIT), Karlsruhe, Germany

Abstract

Gelatin and its derivatives contain cell adhesion moieties as well as sites that enable proteolytic degradation, thus allowing cellular proliferation and migration. The processing of gelatin to its derivatives and/or gelatin-containing products is challenged by its gelation below 30 °C. In this study, a novel strategy was developed for the dissolution and subsequent modification of gelatin to its derivative gelatin-methacryloyl (GelMA). This approach was based on the presence of urea in the buffer media, which enabled the processing at room temperature, i.e., lower than the sol-gel transition point of the gelatin solutions. The degree of functionalization was controlled by the ratio of reactant volume to the gelatin concentration. Hydrogels with tailored mechanical properties were produced by variations of the GelMA concentration and its degree of functionalization. Moreover, the biocompatibility of hydrogels was assessed and compared to hydrogels formulated with GelMA produced by the conventional method. NIH 3T3 fibroblasts were seeded onto hydrogels and the viability showed no difference from the control after a three-day incubation period.

3.1 Introduction

Hydrogels are widely used as scaffolds for tissue engineering (TE) as the polymeric network resembles the extracellular matrix (ECM) within native tissue. For this purpose, hydrophilic polymers are covalently or physically crosslinked in order to create a water-swollen network [89, 181]. The building blocks for hydrogel formulation can be purified from native tissue or produced synthetically. Naturally derived polymers show higher biocompatibility and can promote cellular adhesion and proliferation, whereas synthetic polymers have the advantage of low batch-to-batch variation compared to polymers extracted from natural sources [5, 6]. The composition of the network influences cellular behavior not only by biochemical cues but also by the resulting physical structure and mechanical properties of the surrounding matrix [56, 182].

Gelatin is derived from collagen, the most abundant protein in the native ECM, by acidic or alkaline treatment. The use of gelatin as a cell culture carrier is limited by the sol-gel transition of gelatin solutions at physiological temperatures [119]. In order to increase the stability of gelatin hydrogels at higher temperatures, the protein backbone can be chemically crosslinked. One approach for this purpose is the functionalization of gelatin with methacrylamide and methacrylate residues [121]. The resulting product, gelatin methacryloyl, also known as GelMA, retains sites for cell adhesion as well as for enzymatic degradation that are present in collagen and gelatin [183]. The use of photo-crosslinkable GelMA has gained popularity in the fields of TE and biofabrication [183]. The versatile GelMA has been used in cancer research [184], drug encapsulation and delivery [135], and in bioprinting. Therefore, bioinks containing solely GelMA are used [185], as well as bioink blends with other proteins like collagen [186] or in combination with polysaccharides such as alginate and gellan gum [179, 187].

To meet the increasing demand for biomaterials required for TE applications, the manufacturing of hydrogel components requires a thorough understanding of the process parameters to reach a certain quality attribute [42]. In the case of GelMA, an aspect of particular interest is the degree of functionalization (DoF) of the biopolymer as the functional residues are relevant during photo-crosslinking. Since GelMA was first introduced by Van den Bulcke [121] over two decades ago, lab-scale studies have shown increasing reproducibility and efficiency during GelMA manufacturing, where aqueous gelatin in aqueous solution reacts with methacrylic anhydride (MAA). Lee [123] and

Shirahama [124] studied the effect of the pH of the protein solution on the produced GelMA. As reaction by-products are acidic, the pH of the solution decreases, thus inhibiting the progress of the reaction. By introducing a carbonate-bicarbonate (CB) buffer at the isoelectric point (IEP) of type A gelatin, these methods showed a reduction of MAA excess over free amino groups from 30- to 2.2-fold. The study by Shirahama [124] also observed the effect of reaction temperature, which proved to have no influence on the DoF. This study was limited to the range of 35 to 50 °C as a lower temperature would allow the solution to form a physical gel, thus leading to inefficient mixing and distribution of reactants. To the best of our knowledge, no studies have reported the possibility of GelMA production at temperatures lower than 35 °C.

In this work, we propose a GelMA manufacturing process including a chaotropic salt, i.e., urea, as a buffer component at pH 9 that enables the processing of gelatin at room temperature. GelMA with various degrees of functionalization was produced and used as the basis for hydrogel formulation. Furthermore, the effect of polymer concentration and DoF on the elasticity and swelling behavior of hydrogels was characterized. Additionally, the suitability of GelMA hydrogels for cell culture was assessed by the cultivation of NIH 3T3 fibroblasts. Therefore, an automated image processing workflow was developed for the identification of single cells and the determination of cell viability. Fibroblasts were incubated on GelMA hydrogels produced by the presented method for a three-day period. GelMA produced by the conventional method was used as a control.

3.2 Materials and methods

3.2.1 GelMA Manufacturing and Characterization

3.2.1.1 Synthesis and Purification

For the dissolution of gelatin and subsequent synthesis of GelMA, a 0.25 M carbonate-bicarbonate (CB) buffer was prepared according to the method of Lee [123] and Shirahama [124]. Buffer components were purchased from Merck (Darmstadt, Germany). CB buffer was composed of 0.023 M sodium carbonate and 0.227 M sodium bicarbonate, pH 9 was adjusted with 1 M sodium hydroxide (NaOH) or 1 M hydrochloric acid (HCl). This buffer system was used for the dissolution of gelatin (Type A, 300 bloom strength, Sigma-Aldrich, St. Louis, MI, USA) to a concentration of 10% (w/v) at 40 °C under stirring. Subsequently, the reaction was performed at 40 °C by the addition of methacrylic anhydride (MAA, 94%, Sigma-Aldrich) dropwise with a syringe pump (Nemesys, CETONI, Korbussen, Germany) over a period of 100 min. The MAA-to-gelatin ratio was 100 $\mu\text{L g}^{-1}$. The reaction was carried out for additional 20 min. The process was terminated by 2-fold dilution with ultrapure water and pH adjustment to pH 7.4. The reaction mixture was purified with 3.5 kDa molecular weight cutoff dialysis tubing (Thermo Fisher Scientific, Waltham, MA, USA) in an ultrapure water reservoir for 4 days at 40 °C. The conductivity of the water in the reservoir was measured with a conductivity meter (CDM230, Radiometer Analytical SAS, Villeurbanne, France). By the end of the dialysis, the conductivity of the reservoir equaled the conductivity of fresh ultrapure water with a value of 5 $\mu\text{S cm}^{-1}$. This approach for the production of GelMA is referred to as the conventional approach throughout this manuscript. A second buffer system comprised of 0.25 M CB buffer and 4 M urea (Merck) was prepared. The pH of the solution was adjusted to pH 9. In the urea-containing CB buffer, gelatin was dissolved to 10% (w/v) at room temperature (RT) under stirring, no external heating sources were used. Subsequently, the reaction started by adding MAA dropwise to the appropriate amount. A summary of the produced

Table 3.1 Overview of the experimental set-up for the synthesis of gelatin methacryloyl (GelMA), and the sample nomenclature used throughout this manuscript. CB: carbonate-bicarbonate, DoF: degree of functionalization RT: room temperature.

Synthesis Buffer	MAA-to-Gelatin Ratio $\mu\text{L/g}$	Reaction Temperature	DoF -	Nomenclature
0.25 M CB	100	50 °C	0.926	50C100MA
0.25 M CB, 4 M urea	100	RT	0.963	RT100MA
0.25 M CB, 4 M urea	50	RT	0.657	RT50MA
0.25 M CB, 4 M urea	25	RT	0.176	RT25MA
0.25 M CB, 4 M urea	12.5	RT	0.044	RT12.5MA

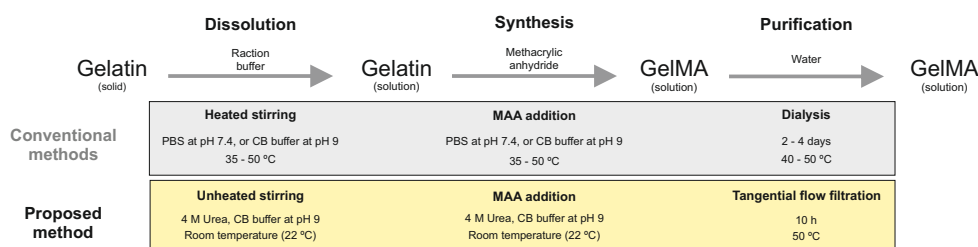


Figure 3.1 Synthesis and purification of gelatin methacryloyl (GelMA). Conventional methods require the heating of the phosphate-buffered saline (PBS) or the carbonate-bicarbonate (CB) buffer for the dissolution of gelatin. Similarly, the synthesis of GelMA requires heated stirring of the biopolymer solution in order to ensure homogeneous mixing and distribution of the added methacrylic anhydride (MAA). Reaction by-products as well as buffer salts are removed using a dialysis membrane at temperatures above the gelation temperature of GelMA [121, 123, 124]. The presented method allows for the dissolution of gelatin and the synthesis of GelMA at room temperature under stirring as the urea-containing CB buffer inhibits the formation of a physical gel. Subsequently, GelMA is purified in a tangential flow filtration unit at 50 °C, thereby reducing the processing time to hours.

samples within this study is provided in Table 3.1. The reaction mixture was then purified against ultrapure water in a tangential flow filtration (TFF) unit (Tandem 1082, Sartorius, Göttingen, Germany) equipped with a 2 kDa molecular weight cutoff membrane (Vivaflow® 200, Hydrosart®, Sartorius). The TFF process took place at 50 °C. During purification, the retentate pressure was set to 0.2 MPa, as recommended by the manufacturer as the maximal operating pressure. The purification was stopped after 10 diafiltration volumes. The conductivity of the retentate was equal to the conductivity of ultrapure water by the end of the purification. After each run, the TFF membrane was cleaned with ultrapure water, a 0.1 M sodium hydroxide solution, and a 15% (v/v) ethanol (Merck) solution. The GelMA solutions produced by both methods were frozen at -80 °C and lyophilized at -55 °C and 0.66 Pa for 4 days. Solid GelMA was stored at RT until further use. The methodology used for the synthesis and purification of GelMA in this study is schematically presented in Figure 3.1.

3.2.1.2 DoF Determination

The degree of functionalization (DoF) was determined based on the trinitrobenzenesulfonic (TNBS) acid (Sigma-Aldrich) method by Habeeb [122]. A 0.1 M CB Buffer (0.009 M sodium carbonate, 0.091 M sodium bicarbonate) was prepared and used as a reaction buffer containing 0.01% (w/v) TNBS. Glycine (Sigma-Aldrich) standards, a gelatin reference, and GelMA samples were dissolved in ultrapure water. A volume of 250 μL of each sample was mixed with an equal volume of the TNBS reagent solution and incubated for 2 h at 40 $^{\circ}\text{C}$. The reaction was stopped by addition of 250 μL of a 10% (w/v) sodium dodecyl sulfate (Sigma-Aldrich) solution and 125 μL of a 1 M HCl solution. The absorbance of each sample was measured at 335 nm using a microplate reader (infiniteM200, Tecan Group, Männedorf, Switzerland). The gelatin and GelMA samples were prepared at 0.1, 0.3, 0.5, and 0.8 mg mL^{-1} . The concentration of primary amino groups in the samples was determined in comparison to a glycine standard curve, which was measured at 3, 5, 8, 10, and 20 $\mu\text{g mL}^{-1}$, and normalized to the respective protein concentration. The DoF was estimated as the difference between the number of free amines present in gelatin ($c_{\text{NH}_2, \text{gelatin}}$), i.e., before the functionalization, and the amount in the produced GelMA ($c_{\text{NH}_2, \text{GelMA}}$), i.e., after the reaction, divided by the number of free amines in the raw gelatin, as shown in Equation (3.1).

$$\text{Degree of Functionalization} / - = \frac{c_{\text{NH}_2, \text{gelatin}} - c_{\text{NH}_2, \text{GelMA}}}{c_{\text{NH}_2, \text{gelatin}}} \quad (3.1)$$

The experimental setup for the characterization of the synthesized GelMA samples consisted of three experimental runs at each MAA-to-gelatin ratio. The absorbance measurements were performed for each independently synthesized batch.

3.2.2 Hydrogel Characterization

3.2.2.1 Preparation

Prior to the addition of GelMA, the photo-initiator lithium phenyl-2,4,6-trimethylbenzoylphosphinate (LAP, Sigma-Aldrich) was dissolved to the final concentration of 0.5% (w/v) in Dulbecco's phosphate buffered saline (DPBS, without calcium and magnesium, 1 \times , pH 7.4, Thermo Fisher Scientific). GelMA synthesized at different MAA/gelatin ratios was used for hydrogel preparation by dissolving the lyophilized material to 5, 10, and 15% (w/v). The resulting hydrogel precursor solution was incubated at 37 $^{\circ}\text{C}$ until complete dissolution of GelMA. A volume of 235 μL GelMA solution was transferred to cylindrical polytetrafluoroethylene (PTFE) molds (diameter 10 mm, height 3 mm). The samples were polymerized by exposure to a UV lamp (365 nm, OSRAM, Munich, Germany) with an irradiation dose of 2850 mJ cm^{-2} . Polymerized GelMA hydrogels were incubated in DPBS until further analysis.

3.2.2.2 Physical Characterization

The rheological and swelling behavior of the hydrogels were characterized in this study. The viscoelastic properties of cell-free hydrogels were characterized based on their storage and loss modulus as a function of frequency. The cylindrical hydrogels were placed between the plate-plate geometry (diameter 10 mm) of a rotational rheometer (Physica MCR301, Anton Paar, Graz, Austria). The gap height was adjusted to 2.5 mm. All conditions were tested within the linear viscoelastic (LVE) regime covering the frequency range of 0.5 to 50 rad s^{-1} at a stress amplitude of 0.5 Pa.

The swelling behavior of the crosslinked hydrogels was characterized by the ratio of the weight of the hydrogel in the swollen state ($m_{swollen}$) to the weight in the dry state (m_{dry}), as shown in Equation 3.2. The weight in the swollen state was determined after the equilibration of hydrogels in DPBS. In order to weigh the samples in the dry state, GelMA hydrogels were frozen at $-80\text{ }^{\circ}\text{C}$ overnight and lyophilized for 24 h.

$$\text{Swelling Ratio/-} = \frac{m_{swollen}}{m_{dry}} \quad (3.2)$$

Data for the physical characterization study shown below were acquired from measurements performed with three experimental runs with a set of three samples (i.e., technical replicates) each. For each experimental run, GelMA hydrogels from independently synthesized batches were prepared.

3.2.3 Biocompatibility Assessment

3.2.3.1 Cell Culture

Culture media and supplements were purchased from Gibco™ (Thermo Fisher Scientific). NIH 3T3 mouse fibroblasts (CLS Cell Lines Service, Eppelheim, Germany) were cultured in Dulbecco's Modified Eagle Medium (DMEM, high glucose, GlutaMAX™) supplemented with 10% (v/v) FBS (fetal bovine serum), 50 U mL^{-1} penicillin, and $50\text{ }\mu\text{g mL}^{-1}$ streptomycin. Cells were seeded in tissue culture flasks and maintained at $37\text{ }^{\circ}\text{C}$ in a humidified, 5% CO_2 atmosphere. Subcultivation proceeded at 70 to 80% confluence.

3.2.3.2 Cell Seeding on Hydrogel Coated Well Plates

The biocompatibility of GelMA hydrogels manufactured at room temperature was investigated. Hydrogels formulated with GelMA produced by the conventional method were used as a control. For these experiments, hydrogels were prepared with GelMA at a reactant ratio of 100 μL MAA per gram gelatin. Lyophilized GelMA was dissolved in ultrapure water to a 2% (w/v) solution at $50\text{ }^{\circ}\text{C}$. Warm GelMA solutions were sterile filtered using $0.2\text{ }\mu\text{m}$ polyethersulfone (PES) filters (diameter 50 mm, Merck) in a laminar flow cabinet. The sterile solutions were frozen at $-80\text{ }^{\circ}\text{C}$ and lyophilized as described in Section 3.2.1.1. Hydrogel precursor solutions were then prepared at a concentration of 10% (w/v) as mentioned in Section 3.2.2.1. The bottoms of 12-well plates (Thermo Fisher) with a surface area of 3.5 cm^2 were coated with GelMA by transferring a volume of $350\text{ }\mu\text{L}$ to each well and a subsequent crosslinking under UV exposure. Cells were detached from culture flasks with Trypsin/ethyleneaminetetraacetic acid (Gibco), centrifuged, and resuspended in fresh media. The seeding density on the hydrogel-coated plates was set to 80×10^3 cells per well within a total media volume of 2 mL. Cell-laden samples were kept at incubation conditions until further analysis.

3.2.3.3 Cell Staining and Imaging

The biocompatibility was assessed after one and after three days of incubation. Staining compounds were purchased from Thermo Fisher (Invitrogen). The cell-laden samples were washed with DPBS prior to staining. The samples were covered with 2 mL of staining solution comprised of calcein-AM, propidium iodide, and Hoechst 33342 with concentrations 0.1, 1.5, and $1.66\text{ }\mu\text{M}$, respectively. Incubation followed for 15 min at $37\text{ }^{\circ}\text{C}$. Imaging was performed immediately after staining using an inverted microscope (Axio Observer.Z1, Carl Zeiss, Oberkochen, Germany).

3.2.3.4 Cell Counting and Viability

In order to obtain an objective determination of the number of cells, an image processing workflow was developed using Matlab[®] R2021b (TheMathWorks, Natick, MA, USA). The acquired green signal originated from calcein retained within the cellular membrane, whereas the red signal arose from stained DNA of cells with compromised membranes. The blue signal of stained nuclear DNA is present in all cells, both viable and dead, as Hoechst 33342 is membrane permeable. The three signals were used as input for the image processing workflow. The preprocessing of the images consisted of individual binarisation of each signal. The identification of single nuclear regions on the binary image of the blue channel was performed by the watershed segmentation method. Binary images from the green and red signals were used as masks on the blue signal. Nuclei behind the green mask and behind the red mask were considered nuclei of viable and dead cells, respectively. The image processing workflow is shown schematically in Figure 3.2. Cell viability was calculated according to Equation (3.3), where the number of viable cells (N_{viable}) was divided by the total number of cells consisting of both viable and dead cells (N_{dead}). The experimental setup consisted of three experimental runs (i.e., biological replicates). For each biological replicate, GelMA precursor solutions from independently synthesized batches were used. Two independent hydrogel samples (i.e., technical replicates) and at least 6 images were recorded of each sample.

$$\text{Cell viability}/\% = 100 * \frac{N_{viable}}{N_{viable} + N_{dead}} \quad (3.3)$$

3.2.4 Data Handling and Statistical Analysis

Data evaluation, image processing, statistical analysis, and data visualization were done with Matlab[®] R2021b. Results are shown as a mean \pm standard deviation. The normal distribution of data sets was verified using the Jarque–Bera test with the α -value set to 0.05. A one-way analysis of variance (ANOVA) was performed in order to find significant differences. A p -value below 0.05 was classified as statistically significant.

3.3 Results and discussion

3.3.1 GelMA Synthesis and Characterization

In order to use the biopolymer as a cell culture carrier, gelatin was modified to GelMA. Type A Gelatin was used as starting material for the production of GelMA. The protein was dissolved in a CB buffer solution at pH 9. After the complete dissolution of the gelatin, MAA was added continuously. Both steps were performed under thorough stirring at 50 °C. After the reaction was stopped, the purification of the GelMA took place using dialysis tubing in an ultrapure water reservoir at 40 °C. A second approach for the dissolution and synthesis of GelMA was performed. For this purpose, gelatin was dissolved at RT in a CB buffer at pH 9 that contained 4 M urea. The dissolution of gelatin in the urea-containing buffer solely required stirring. The presence of urea in the buffer also allowed the efficient mixing of MAA during the synthesis, which was also performed at RT. In contrast, the purification set-up for this approach did require the heating of the TFF unit to 50 °C. The DoF of GelMA produced at MAA-to-gelatin ratio of 100 $\mu\text{L g}^{-1}$ was determined. GelMA synthesized in the CB buffer (50C100MA) exhibited a DoF of 0.926 ± 0.057

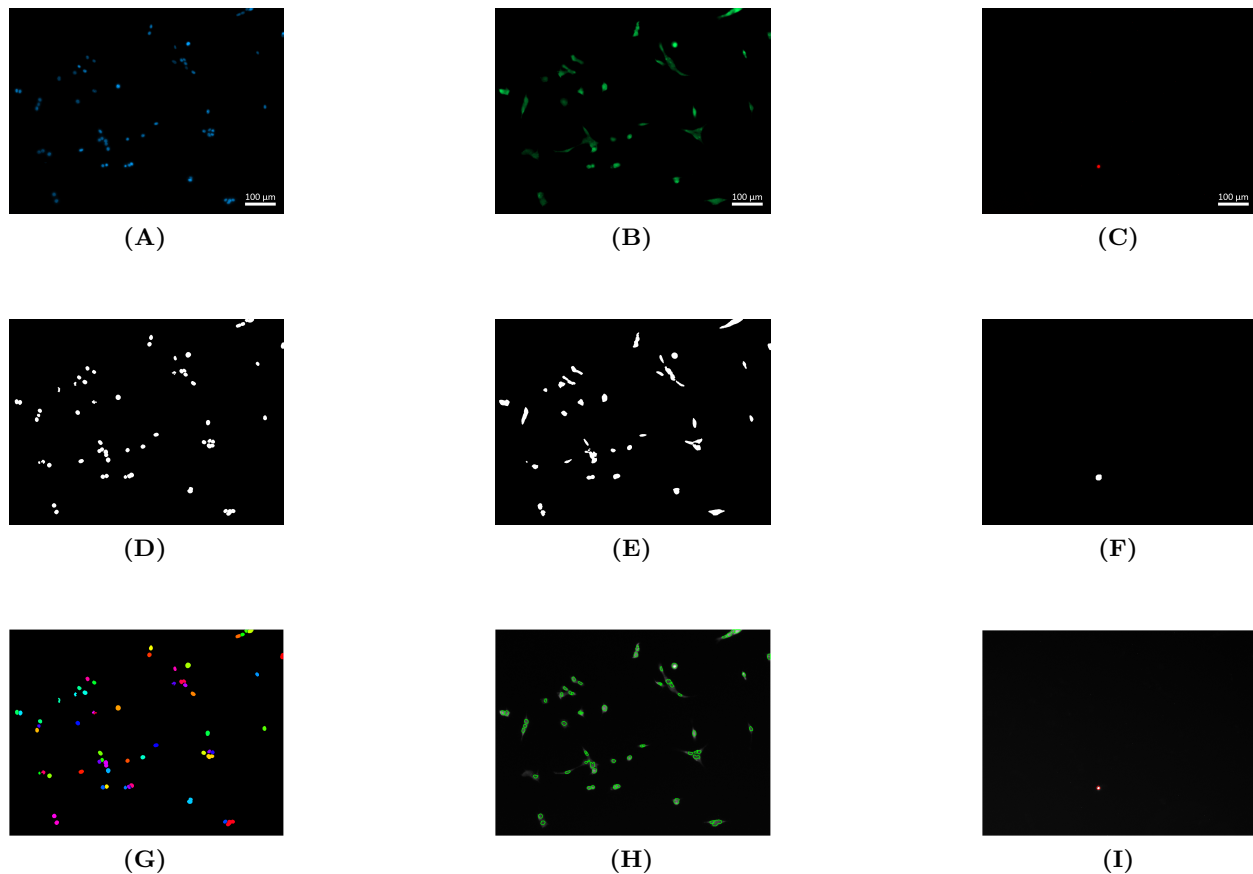


Figure 3.2 Image processing workflow for cell counting. (A–C) Single signal images used as inputs for the image processing workflow. Scale bar: 100 μm . (A) Nuclear DNA stained using membrane-permeable Hoechst 33342, (B) calcein-AM converted to calcein and retained in the cytoplasm, and (C) DNA stained using membrane-impermeable propidium iodide. The input images are preprocessed to binary data. (D–F) Resulting binary images of the regions of interest. (D) Nuclear region within all cells, (E) cytoplasmic region within viable cells, and (F) nuclear region within dead cells. (G) Single nuclear regions are identified with a watershed segmentation algorithm. The identified nuclei behind the produced mask from the calcein stain are considered viable, whereas nuclei behind the mask from the propidium iodide stain are considered dead cells. (H) Outline of nuclei of cells identified as viable shown in green as a composite with the raw image. (I) Outline of nuclei of cells identified as dead shown in red as a composite with the raw image.

and did not significantly differ from GelMA produced in the urea containing CB buffer (RT100MA), which showed a DoF of 0.963 ± 0.027 , as presented on Table 3.1 and Figure 3.3.

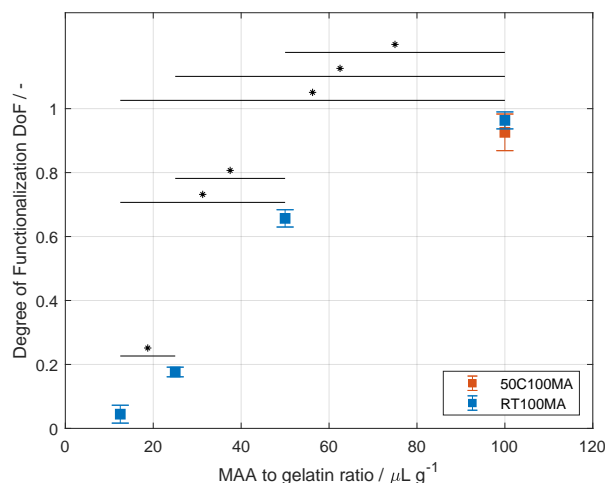


Figure 3.3 Degree of functionalization (DoF) of produced gelatin methacryloyl (GelMA) batches the DoF was determined by the TNBS method [122]. No difference was found between samples produced a room temperature and samples produced at $50\text{ }^{\circ}\text{C}$ at $100\text{ }\mu\text{L g}^{-1}$. The DoF increased significantly with increasing the methacrylic anhydride (MAA)-to-gelatin ratio. Asterisks denote a significant difference between samples ($p < 0.05$).

As MAA reacts with neutral free amine groups, a pH value higher than the isoelectric point of gelatin had to be maintained during the reaction. The typical isoelectric point of type A gelatin lies between pH 7 and pH 9. Therefore, the functionalization process was performed at pH 9 in a buffered solution, similar to the methods by Lee [123] and Shirahama [124]. These and previous studies report the processing of gelatin at temperatures above the gelation point of gelatin solutions [121, 188, 189]. A brief overview of the synthesis parameters found in the literature is schematically shown in Figure 3.1. Gelatin undergoes a sol-gel transition due to inter- and intramolecular interactions of the biopolymer as the protein backbone forms helical structures similar to those found in collagen [190, 191]. In order to process gelatin at RT, urea was used in the reaction buffer. Urea causes the unfolding of proteins as the hydrophobic interaction between protein chains is disrupted [192–194]. This effect was used in order to ensure the sol state at RT, thus enabling the homogeneous mixing of MAA during the synthesis of GelMA. The purification of GelMA produced at RT required heating of the complete TFF set-up, GelMA, and water reservoirs, as well as the membrane. The decreasing concentration of urea during purification allows the re-folding of GelMA protein coils to helical structures, i.e., the transition from a solution to a gel [121]. Nevertheless, the purification time was reduced to about ten hours compared to the several days required by the dialysis process. It is noteworthy to mention that the purity of the samples should be analyzed using other methodologies in future studies, as in the presented study the purification was indirectly controlled by measuring the conductivity of the liquid used during purification, and no direct quantification of the purity of the sample was performed. In addition, there were no significant differences between the DoF of GelMA produced by both methods, and the values are in the same range as previous studies [123, 124, 188]. Additionally, Shirahama [124] also showed that the produced GelMA was not influenced by the reaction temperature in the range from 35 to $50\text{ }^{\circ}\text{C}$. The DoF of GelMA produced at higher

temperatures is comparable to the DoF of GelMA synthesized by the presented approach at RT; thus, this finding could indicate that the reaction kinetics is controlled by the molecular weight and molecular weight distribution of the used gelatin, rather than by the reaction temperature. Differences in molecular weight can arise not only from the species of the gelatin source but also from the bloom strength and even from batch-to-batch variations of the same gelatin product. The DoF of type B GelMA produced with bovine gelatin has been studied in the literature showing a higher value than that of type A GelMA produced with porcine gelatin [195]. This is due to the fact that the pH of the buffered solution remains above the IEP of bovine gelatin during the reaction. The presented method of reaction buffer containing urea should also be implemented in future studies for the comparison of the properties of GelMA from different species as well as varying bloom strength.

The effect of the MAA-to-gelatin ratio was also studied for the developed synthesis at RT and is shown in Figure 3.3. All synthesized batches are summarized in Table 3.1. The ratio was varied from 12.5 to 100 $\mu\text{L g}^{-1}$, where the increasing ratio leads to higher DoF ranging from 0.044 ± 0.028 to 0.963 ± 0.027 . Statistically significant differences between the DoF values were found for all data sets ($p < 0.05$). The effect of the increasing ratio is in accordance with other studies [123, 124, 188, 189]. Based on the reactant ratio, the resulting GelMA product can be controlled in a reproducible manner as required for the formulation of hydrogels.

3.3.2 Hydrogel Characterization

GelMA hydrogels can be covalently crosslinked to generate hydrogels with structural properties according to the required application. In cell culture, the physical properties of the matrix environment are known to influence cellular migration, proliferation, and differentiation [59, 196, 197]. Hydrogels were prepared as described previously and the resulting storage modulus was determined by oscillatory frequency sweeps on a rheometer. Holding the DoF constant, the elastic modulus showed a significant increase with higher polymer concentration ($p < 0.05$), as shown in Figure 3.4. The moduli of RT100MA hydrogels at 5, 10, and 15% (w/v) were 1.4, 11.2, and 29.4 kPa, respectively. The same trend was observed with all used samples, i.e., RT50MA, RT25MA, and RT12.5MA. The increase of the elastic modulus corresponds to a higher crosslink density in the polymeric network [81]. The higher GelMA content leads to an increased availability of crosslinking sites as well as an increasing amount of physical entanglements. This behavior is comparable with other studies [195, 198, 199].

The elasticity of the hydrogels was influenced by the DoF, this effect is presented in Figure 3.4 as well. Hydrogels prepared from the samples RT50MA, RT25MA, and RT12.5MA with DoFs of 0.657, 0.176, and 0.044, respectively, show a significant increase of elasticity with increasing DoF at a constant GelMA concentration ($p < 0.05$). At a concentration of 15% (w/v), the moduli increased from 1.8 to 29.4 kPa with increasing DoFs. The elasticity of hydrogels produced from RT100MA and RT50MA was in the same range and did not differ significantly at any tested GelMA concentration, even though the DoFs of both samples differed significantly. The DoF of GelMA RT100MA was 0.963, while the DoF of the RT50MA sample was 0.657.

The results observed from the samples RT50MA, RT25MA, and RT12.5MA are in accordance with other studies [195, 198, 199]. The increasing elasticity of the hydrogels at a constant polymer concentration is attributed to the higher crosslink density proceeding from the higher amount of methacrylamide and methacrylate residues. The missing difference between the samples prepared with RT50MA and RT100MA could arise from the crosslinking condition used in this study. The

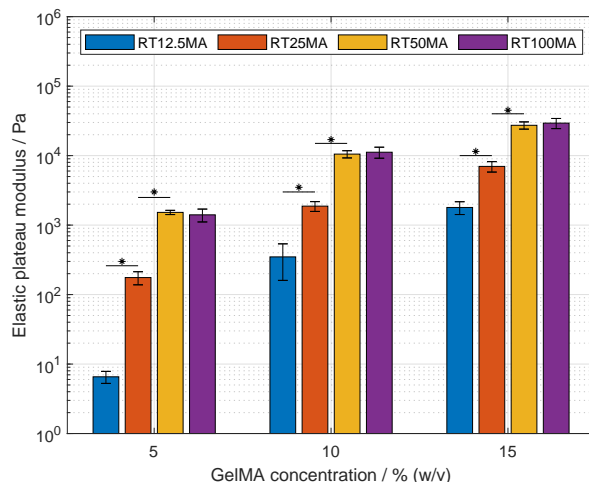


Figure 3.4 Elastic plateau modulus of gelatin methacryloyl (GelMA) hydrogels at various concentrations. The elasticity of hydrogels increased significantly with higher GelMA concentrations of the same synthesized sample ($p < 0.05$). These differences are not shown for the purpose of clarity. Significant differences between the elastic modulus of samples at a constant GelMA concentration are denoted with an asterisk ($p < 0.05$).

irradiation dose was set to 2850 mJ cm^{-2} and the concentration of the photo-initiator was set to 0.5% (w/v). The irradiance dose is higher than those used in similar studies by Van Den Bulcke [121], Nichol [198], and Pepelanova [188] which were set to 10, 6.9, and 1200 mJ cm^{-2} , respectively. The concentration of the used photo-initiator was also higher than the concentration presented by Van Den Bulcke (0.006% (w/v)) [121], Schuurman (0.05% (w/v)) [185], and Lee (0.1% (w/v)) [195]. In free radical polymerization, the reaction rate is proportional to the irradiance and photo-initiator concentration, as studied by O’Connell [199]. The fast generation of free radicals, which initiates the chain polymerization, is opposed by the increasing elasticity of the matrix, i.e., the decreasing mobility of the polymeric network and the lower diffusivity of free radicals. Thus, reaching a limit of the created crosslinks.

The swelling behavior of hydrogels reflects the ability of the polymeric network to bind and retain aqueous media. This property influences the diffusion of nutrients to the cells and metabolic by-products away from the cells [76]. As shown in Figure 3.5, it was observed that the swelling ratio of hydrogels was influenced by the used GelMA concentration as well as the DoF. Maintaining a constant DoF, an increasing amount of GelMA significantly reduced the swelling capacity of the network ($p < 0.05$). Furthermore, a higher DoF led to lower swelling ratios at a constant concentration. This effect was significant between the samples RT50MA, RT25MA, and RT12.5MA ($p < 0.05$). Similar to the observation during the characterization of the mechanical properties, the swelling ratios of hydrogels produced with GelMA RT50MA and RT100MA did not differ significantly. The effect of GelMA concentration and DoF on the swelling capacity of GelMA hydrogels have also been demonstrated by other studies [127, 135, 198, 200] and are in agreement with the observations presented in this study. The driving mechanism of swelling is the osmotic pressure difference between the fluid within the network and the outer solution, which is opposed by the elasticity of the network preventing the dissolution due to its crosslinked structure [76, 201]. Therefore, more elastic hydrogels produced with higher GelMA concentrations or higher DoFs have a

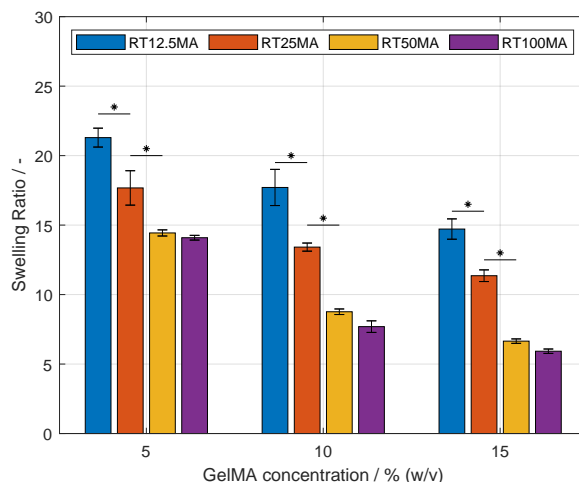


Figure 3.5 Equilibrium swelling ratio of gelatin methacryloyl (GelMA) hydrogels at various concentrations. The swelling behavior increased significantly with higher GelMA concentrations of the same synthesized sample ($p < 0.05$). These differences are not shown for the purpose of clarity. Significant differences between the swelling ratio of samples at a constant GelMA concentration are denoted with an asterisk ($p < 0.05$).

lower swelling capability due to the higher crosslink density. As previously described, the similarity between the swelling ratio of the hydrogel samples RT50MA and RT100MA could be explained by the crosslinking conditions. It has to be kept in mind that the physical properties of a crosslinked GelMA hydrogel also depend on the properties of the used gelatin before functionalization such as the animal source, the bloom strength, and the crosslinking conditions [188, 195, 202]. By variation of the gelatin bloom strength, and, therefore, variation of the molecular weight of the biopolymer, the range of elasticity of the produced hydrogels could be expanded in further investigations. The GelMA hydrogels produced in this study proved to be suitable for mimicking the physical properties of tissue. Such properties can be adjusted in a controllable manner over the concentration of biopolymer and/or DoF in order to adjust the hydrogel to the specific cell type requirements.

3.3.3 Biocompatibility Assessment

GelMA hydrogels were used as carriers for NIH 3T3 fibroblasts in culture. The biocompatibility of synthesized GelMA as a hydrogel was determined via quantification of the cell viability after one, and after three days in cultivation. For this purpose, fluorescent staining and subsequent imaging of the samples was performed. The acquired images were imported into Matlab[®] and evaluated using the image processing workflow, as described in Section 3.2.3.4. During processing, the detected signals were binarized separately. Single nuclei in contiguous regions were identified using a watershed segmentation tool. Nuclei of cells under the binary mask proceeding from the green channel were counted as live cells, whereas nuclei under the red mask were classified as dead cells. The image processing workflow enabled the objective and automated analysis of the gained frames. The developed tool is intended to reduce the time required for the analysis of images. Moreover, the automated identification of cells is also advantageous as it increases reproducibility and reduces observer-dependent errors [147, 203, 204]. The used image processing workflow allowed

the analysis of relatively large data sets, which consisted of at least 40 frames with more than 1500 identified cells for each tested material. In contrast, similar studies in the field of tissue engineering and biofabrication are limited to a relatively low number of counted cells [74, 195] and/or a low number of acquired images by microscopy [185, 205].

Figure 3.6 shows the viability of cells seeded onto 10% (w/v) GelMA hydrogels. Cells growing on GelMA synthesized according to the conventional method at 50 °C (50C100MA) showed viabilities of 94.8% and 94.5% after one and three days, respectively. The viability of cells on GelMA produced at room temperature (RT100MA) was quantified to a value of 95.8% after one day of incubation, and a value of 93.3% after three days.

The viability of cells after one day did not significantly differ from the viability after three days for either hydrogel. Hence, no significant difference in viability was observed between cells growing on GelMA 50C100MA and on GelMA RT100MA. This approach of GelMA production at room temperature enabled the synthesis of a biocompatible material for hydrogel formulation. The high viability is in accordance with similar studies that use GelMA produced following conventional methods [74, 195, 198, 202]. In the field of tissue engineering, the applications of hydrogels also include cell growth within the produced scaffold as well as cellular invasion in scaffolds. Such studies should be performed with GelMA produced according to the presented methodology.

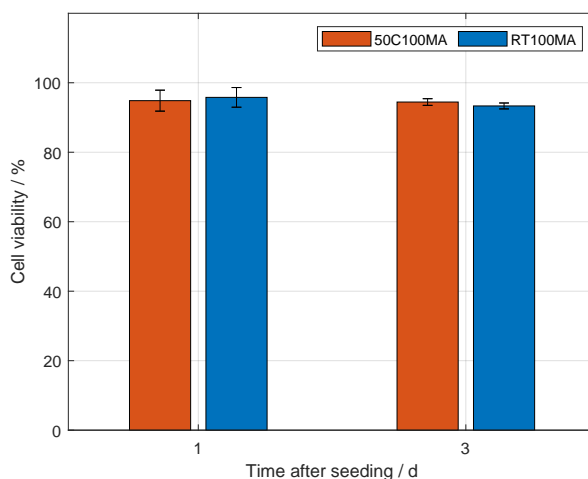


Figure 3.6 Cell viability of NIH 3T3 fibroblasts on gelatin methacryloyl (GelMA) coated well plates. GelMA produced similar to the method of Shirahama [124] at 50 °C (50C100MA) was used as a control in comparison with GelMA produced by the novel approach presented in this study, i.e., at room temperature (RT100MA). The viability of cells seeded onto both hydrogels samples did not differ significantly after one and three days.

3.4 Conclusions

In the field of tissue engineering, the use of GelMA-based hydrogels is well established due to the biocompatible nature of the biomaterial. The current manufacturing of products containing gelatin and gelatin derivatives requires heating, as gelatin solutions undergo a transition to a gel state at lower temperatures. This study presents a novel approach to functionalize gelatin to GelMA at room temperature. This process was possible due to the presence of urea in the synthesis buffer, as urea

decreases the protein-protein interaction, thereby inhibiting the gelation of the solution and allowing efficient mixing of the reactants. GelMA with different degrees of functionalization was produced in a controllable manner by variation of the reactant ratio. By variation of the concentration of GelMA and its DoF, hydrogels were prepared with elastic properties in the range of 1.8 to 24 kPa, thus enabling the precise adaptation to specific cell type requirements. Moreover, the determination of cell viability was performed by imaging and a subsequent image processing workflow that allowed the time-saving analysis of several frames. GelMA produced at room temperature proved to be suitable for cell culture applications with the cell line NIH 3T3 and no difference was observed in comparison to GelMA produced by the conventional method at elevated temperatures, i.e., 50 °C. The possibility to manufacture GelMA at room temperature shows several advantages. First, gelatin solutions are prone to the growth of microorganisms and would require cooling during longer transition periods between operations such as gelatin dissolution and GelMA synthesis. The presence of urea in the solution can be helpful during mentioned time intervals as urea is known to inhibit microbial growth. Second, the growing demand for biomaterials and related products such as bioinks requires suitable means to produce them efficiently in large quantities. Processing at room temperature, i.e., without heating, could facilitate the transition to large-scale production as undesired temperature profiles in reactors can lead to poor mixing and improper distribution of reactants, thus leading to non-reproducible processes. Thirdly, and of significant importance, the production of GelMA for clinical stages might face conditions imposed by regulatory agencies. These require detailed information on the range of operating conditions that will result in the production of materials meeting quality criteria. In the case of GelMA, the presented approach widens the operating range in terms of temperature in order to achieve the aimed degree of functionalization, and, therefore, the robustness of the synthesis process is enhanced.

Conflict of interest

The authors declare that they have no known competing financial interests or personal relationships that could have appeared to influence the work reported in this paper.

Author contributions

Conceptualization, D.G.G.; methodology, D.G.G.; formal analysis, D.G.G. and C.P.R.; data curation, D.G.G.; software, D.G.G.; writing—original draft preparation, D.G.G.; writing—review and editing, C.P.R. and J.H.; visualization, D.G.G.; supervision, J.H.; project administration, J.H.; funding acquisition, J.H. All authors have read and agreed to the published version of the manuscript.

Acknowledgments

We would like to thank Amelie Wirth and Johanna Ossmann for their valuable contributions in the form of experimental work for this project. We acknowledge support by the KIT-Publication Fund of the Karlsruhe Institute of Technology.

Data availability statement

The raw data supporting the conclusions of this article as well as the written codes for Matlab® will be made available on request, inquiries can be directed to the corresponding author

Chapter references

- [5] R. J. Wade and J. A. Burdick, „Engineering ECM signals into biomaterials“, *Materials Today*, vol. 15, no. 10, pp. 454–459, 10/2012.
- [6] F. Ruedinger, A. Lavrentieva, C. Blume, I. Pepelanova, and T. Scheper, „Hydrogels for 3D mammalian cell culture: a starting guide for laboratory practice“, *Applied Microbiology and Biotechnology*, vol. 99, no. 2, pp. 623–636, 01/2015.
- [42] P. Chandra, J. J. Yoo, and S. J. Lee, „Biomaterials in regenerative medicine: Challenges in technology transfer from science to process development“, in *Translational Regenerative Medicine*, Cambridge, United Kingdom: Elsevier, 2015, ch. 13, pp. 151–167.
- [56] K. A. Jansen, D. M. Donato, H. E. Balcioğlu, T. Schmidt, E. H. Danen, and G. H. Koenderink, „A guide to mechanobiology: Where biology and physics meet“, *Biochimica et Biophysica Acta (BBA) - Molecular Cell Research*, vol. 1853, no. 11, pp. 3043–3052, 11/2015.
- [59] C.-M. Lo, H.-B. Wang, M. Dembo, and Y.-l. Wang, „Cell Movement Is Guided by the Rigidity of the Substrate“, *Biophysical Journal*, vol. 79, no. 1, pp. 144–152, 07/2000.
- [74] Z. Wang, Z. Tian, F. Menard, and K. Kim, „Comparative study of gelatin methacrylate hydrogels from different sources for biofabrication applications“, *Biofabrication*, vol. 9, no. 4, p. 044101, 08/2017.
- [76] N. A. Peppas, J. Z. Hilt, A. Khademhosseini, and R. Langer, „Hydrogels in Biology and Medicine: From Molecular Principles to Bionanotechnology“, *Advanced Materials*, vol. 18, no. 11, pp. 1345–1360, 06/2006.
- [81] K. S. Anseth, C. N. Bowman, and L. Brannon-Peppas, „Mechanical properties of hydrogels and their experimental determination“, *Biomaterials*, vol. 17, no. 17, pp. 1647–1657, 01/1996.
- [89] M. W. Tibbitt and K. S. Anseth, „Hydrogels as extracellular matrix mimics for 3D cell culture“, *Biotechnology and Bioengineering*, vol. 103, no. 4, pp. 655–663, 07/2009.
- [119] K. Y. Lee and D. J. Mooney, „Hydrogels for Tissue Engineering“, *Chemical Reviews*, vol. 101, no. 7, pp. 1869–1880, 07/2001.
- [121] A. I. Van Den Bulcke, B. Bogdanov, N. De Rooze, E. H. Schacht, M. Cornelissen, and H. Berghmans, „Structural and rheological properties of methacrylamide modified gelatin hydrogels“, *Biomacromolecules*, vol. 1, no. 1, pp. 31–38, 2000.
- [122] A. Habeeb, „Determination of free amino groups in proteins by trinitrobenzenesulfonic acid“, *Analytical Biochemistry*, vol. 14, no. 3, pp. 328–336, 03/1966.
- [123] B. H. Lee, H. Shirahama, N.-J. Cho, and L. P. Tan, „Efficient and controllable synthesis of highly substituted gelatin methacrylamide for mechanically stiff hydrogels“, *RSC Advances*, vol. 5, no. 128, pp. 106 094–106 097, 2015.
- [124] H. Shirahama, B. H. Lee, L. P. Tan, and N.-J. Cho, „Precise Tuning of Facile One-Pot Gelatin Methacryloyl (GelMA) Synthesis“, *Scientific Reports*, vol. 6, no. 1, p. 31 036, 08/2016.
- [127] M. Kirsch *et al.*, „Gelatin-Methacryloyl (GelMA) Formulated with Human Platelet Lysate Supports Mesenchymal Stem Cell Proliferation and Differentiation and Enhances the Hydrogel’s Mechanical Properties“, *Bioengineering*, vol. 6, no. 3, p. 76, 08/2019.
- [135] M. Vigata, C. Meinert, N. Bock, B. L. Dargaville, and D. W. Huttmacher, „Deciphering the Molecular Mechanism of Water Interaction with Gelatin Methacryloyl Hydrogels: Role of Ionic Strength, pH, Drug Loading and Hydrogel Network Characteristics“, *Biomedicines*, vol. 9, no. 5, p. 574, 05/2021.
- [147] V. Wiesmann, D. Franz, C. Held, C. Münzenmayer, R. Palmisano, and T. Wittenberg, „Review of free software tools for image analysis of fluorescence cell micrographs“, *Journal of Microscopy*, vol. 257, no. 1, pp. 39–53, 01/2015.
- [179] A. A. Aldana, F. Valente, R. Dilley, and B. Doyle, „Development of 3D bioprinted GelMA-alginate hydrogels with tunable mechanical properties“, *Bioprinting*, vol. 21, no. June 2020, e00105, 03/2021.
- [181] B. V. Slaughter, S. S. Khurshid, O. Z. Fisher, A. Khademhosseini, and N. A. Peppas, „Hydrogels in Regenerative Medicine“, *Advanced Materials*, vol. 21, no. 32-33, pp. 3307–3329, 09/2009.
- [182] D. E. Ingber, „Cellular mechanotransduction: putting all the pieces together again“, *The FASEB Journal*, vol. 20, no. 7, pp. 811–827, 05/2006.
- [183] B. J. Klotz, D. Gawlitta, A. J. Rosenberg, J. Malda, and F. P. Melchels, „Gelatin-Methacryloyl Hydrogels: Towards Biofabrication-Based Tissue Repair“, *Trends in Biotechnology*, vol. 34, no. 5, pp. 394–407, 05/2016.
- [184] E. Kaemmerer, F. P. Melchels, B. M. Holzapfel, T. Meckel, D. W. Huttmacher, and D. Loessner, „Gelatin methacrylamide-based hydrogels: An alternative three-dimensional cancer cell culture system“, *Acta Biomaterialia*, vol. 10, no. 6, pp. 2551–2562, 06/2014.
- [185] W. Schuurman *et al.*, „Gelatin-Methacrylamide Hydrogels as Potential Biomaterials for Fabrication of Tissue-Engineered Cartilage Constructs“, *Macromolecular Bioscience*, vol. 13, no. 5, pp. 551–561, 05/2013.
- [186] H. Stratesteffen, M. Köpf, F. Kreimendahl, A. Blaeser, S. Jockenhoevel, and H. Fischer, „GelMA-collagen blends enable drop-on-demand 3D printability and promote angiogenesis“, *Biofabrication*, vol. 9, no. 4, p. 045 002, 09/2017.

- [187] V. H. M. Mouser, F. P. W. Melchels, J. Visser, W. J. A. Dhert, D. Gawlitta, and J. Malda, „Yield stress determines bioprintability of hydrogels based on gelatin-methacryloyl and gellan gum for cartilage bioprinting“, *Biofabrication*, vol. 8, no. 3, p. 035003, 07/2016.
- [188] I. Pepelanova, K. Kruppa, T. Scheper, and A. Lavrentieva, „Gelatin-Methacryloyl (GelMA) Hydrogels with Defined Degree of Functionalization as a Versatile Toolkit for 3D Cell Culture and Extrusion Bioprinting“, *Bioengineering*, vol. 5, no. 3, p. 55, 07/2018.
- [189] M. Zhu, Y. Wang, G. Ferracci, J. Zheng, N.-J. Cho, and B. H. Lee, „Gelatin methacryloyl and its hydrogels with an exceptional degree of controllability and batch-to-batch consistency“, *Scientific Reports*, vol. 9, no. 1, p. 6863, 05/2019.
- [190] I. Pezron, M. Djabourov, and J. Leblond, „Conformation of gelatin chains in aqueous solutions: 1. A light and small-angle neutron scattering study“, *Polymer*, vol. 32, no. 17, pp. 3201–3210, 01/1991.
- [191] S. B. Ross-Murphy, „Structure and rheology of gelatin gels: recent progress“, *Polymer*, vol. 33, no. 12, pp. 2622–2627, 01/1992.
- [192] Q. Zou, S. M. Habermann-Rottinghaus, and K. P. Murphy, „Urea effects on protein stability: Hydrogen bonding and the hydrophobic effect“, *Proteins: Structure, Function, and Genetics*, vol. 31, no. 2, pp. 107–115, 05/1998.
- [193] M. C. Stumpe and H. Grubmüller, „Interaction of Urea with Amino Acids: Implications for Urea-Induced Protein Denaturation“, *Journal of the American Chemical Society*, vol. 129, no. 51, pp. 16126–16131, 12/2007.
- [194] A. Das and C. Mukhopadhyay, „Urea-Mediated Protein Denaturation: A Consensus View“, *The Journal of Physical Chemistry B*, vol. 113, no. 38, pp. 12816–12824, 09/2009.
- [195] B. Lee, N. Lum, L. Seow, P. Lim, and L. Tan, „Synthesis and Characterization of Types A and B Gelatin Methacryloyl for Bioink Applications“, *Materials*, vol. 9, no. 10, p. 797, 09/2016.
- [196] E. Hadjipanayi, V. Mudera, and R. A. Brown, „Close dependence of fibroblast proliferation on collagen scaffold matrix stiffness“, *Journal of Tissue Engineering and Regenerative Medicine*, vol. 3, no. 2, pp. 77–84, 02/2009.
- [197] R. A. Marklein and J. A. Burdick, „Controlling Stem Cell Fate with Material Design“, *Advanced Materials*, vol. 22, no. 2, pp. 175–189, 01/2010.
- [198] J. W. Nichol, S. T. Koshy, H. Bae, C. M. Hwang, S. Yamanlar, and A. Khademhosseini, „Cell-laden microengineered gelatin methacrylate hydrogels“, *Biomaterials*, vol. 31, no. 21, pp. 5536–5544, 07/2010.
- [199] C. D. O’Connell *et al.*, „Tailoring the mechanical properties of gelatin methacryloyl hydrogels through manipulation of the photocrosslinking conditions“, *Soft Matter*, vol. 14, no. 11, pp. 2142–2151, 2018.
- [200] S. Krishnamoorthy, B. Noorani, and C. Xu, „Effects of Encapsulated Cells on the Physical–Mechanical Properties and Microstructure of Gelatin Methacrylate Hydrogels“, *International Journal of Molecular Sciences*, vol. 20, no. 20, p. 5061, 10/2019.
- [201] J. Ricka and T. Tanaka, „Swelling of ionic gels: quantitative performance of the Donnan theory“, *Macromolecules*, vol. 17, no. 12, pp. 2916–2921, 12/1984.
- [202] M.-Y. Shie, J.-J. Lee, C.-C. Ho, S.-Y. Yen, H. Y. Ng, and Y.-W. Chen, „Effects of Gelatin Methacrylate Bio-ink Concentration on Mechano-Physical Properties and Human Dermal Fibroblast Behavior“, *Polymers*, vol. 12, no. 9, p. 1930, 08/2020.
- [203] N. Malpica *et al.*, „Applying watershed algorithms to the segmentation of clustered nuclei“, *Cytometry*, vol. 28, no. 4, pp. 289–297, 12/1998.
- [204] S. Eggert and D. W. Huttmacher, „In vitro disease models 4.0 via automation and high-throughput processing“, *Biofabrication*, vol. 11, no. 4, p. 043002, 07/2019.
- [205] S. Sharifi, H. Sharifi, A. Akbari, and J. Chodosh, „Systematic optimization of visible light-induced crosslinking conditions of gelatin methacryloyl (GelMA)“, *Scientific Reports*, vol. 11, no. 1, p. 23276, 12/2021.

4

The Effect of Gelatin Source on the Synthesis of Gelatin-Methacryloyl and the Production of Hydrogel Microparticles

David Grijalva Garces^{1,2}, Luise Josephine Appoldt², Jasmin Egner², Nico Leister³ and Jürgen Hubbuch^{1,2}

- ¹ Institute of Functional Interfaces, Karlsruhe Institute of Technology (KIT), Eggenstein-Leopoldshafen, Germany
- ² Institute of Engineering in Life Sciences, Section IV: Biomolecular Separation Engineering, Karlsruhe Institute of Technology (KIT), Karlsruhe, Germany
- ³ Institute of Engineering in Life Sciences, Section I: Food Process Engineering, Karlsruhe Institute of Technology (KIT), Karlsruhe, Germany

Abstract

Gelatin methacryloyl (GelMA) is widely used for the formulation of hydrogels in diverse biotechnological applications. After the derivatization of raw gelatin, the degree of functionalization (DoF) is an attribute of particular interest as the functional residues are necessary for crosslinking. Despite progress in the optimization of the process found in the literature, a comparison of the effect of raw gelatin on the functionalization is challenging as various approaches are employed. In this work, the modification of gelatin was performed at room temperature (RT), and eight different gelatin products were employed. The DoF proved to be affected by the bloom strength and by the species of gelatin at an equal reactant ratio. Furthermore, batch-to-batch variability of the same gelatin source had an effect on the produced GelMA. Moreover, the elasticity of GelMA hydrogels depended on the DoF of the protein as well as on bloom strength and source of the raw material. Additionally, GelMA solutions were used for the microfluidic production of droplets and subsequent crosslinking to hydrogel. This process was developed as a single pipeline at RT using protein concentrations up to 20% (w/v). Droplet size was controlled by the ratio of the continuous to dispersed phase. The swelling behavior of hydrogel particles depended on the GelMA concentration.

4.1 Introduction

Hydrogels are polymeric networks with a high water-binding and retaining capacity. Since the backbone of the hydrogels is crosslinked polymers, the structural stability of the hydrogel is preserved in aqueous phase [76]. These properties enable the transport of dissolved molecules within the physical structure which can be beneficial for a variety of biotechnological applications such as the immobilization of enzymes [206] and microorganisms [207, 208] in bioreactors, as well as cell culture for studies of cellular metabolism [89]. For these diverse purposes, advanced manufacturing strategies are applied for the creation of defined physical structures such as microparticles in microfluidics [149] and tissue models in bioprinting [209].

A suitable biomaterial for the production of hydrogels is gelatin, which is extracted from collagen [119]. Furthermore, the molecular weight and molecular weight distribution of gelatin not only depend on the sources but also on the processing conditions such as treatment time, pH, and temperature. Gelatin extracted in acidic media, and media extracted using alkaline milieus, shows isoelectric points (IEP) at pH 8–9, and pH 4–5, respectively [107, 117]. After processing, the protein backbone retains sites for cell adhesion as well as for enzymatic cleavage such as those present in collagen [119]. A challenging property of gelatin for certain applications is the transition of the gelatin solution to a gel below a physiological temperature. A way to handle the limited structural stability of hydrogels at elevated temperatures is the formation of covalent bonds between the proteins. For this purpose, gelatin is functionalized to gelatin methacryloyl (GelMA). The methacrylate and methacrylamide residues present in GelMA enable the creation of crosslinked networks via photopolymerization [121]. The first draft of the process was proposed by Van den Bulcke *et al.* [121]. The study included the addition of methacrylic anhydride (MAA) to the gelatin solution in phosphate-buffered saline (PBS) at pH 7.5 under stirring at 50 °C. Significant progress has been made by research groups to identify the effect of process parameters on the resulting degree of functionalization (DoF) of GelMA. Lee *et al.* [123] and Shirahama *et al.* [124] have presented a thorough characterization of the reaction using porcine gelatin. In these studies, the MAA-to-gelatin ratio was significantly reduced by using carbonate bicarbonate (CB) buffer at

pH values above the IEP of porcine gelatin. This enhancement is due to the fact that free amino groups are not charged. Additionally, Shirahama *et al.* [124] studied the derivatization of gelatin in a temperature range from 35 to 50 °C with no difference in the produced DoF. Our previous study complemented the findings of both groups by producing porcine GelMA at room temperature (RT) while keeping the MAA-to-gelatin ratio at the same value [210]. Despite the improvement of the synthesis process concerning porcine GelMA, more work is required to compare the effect of raw material on the final product. To the best of our knowledge, a wide range of raw materials including a variation in species and bloom strength have only been reported once [75]. However, the used synthesis buffer was composed of 0.1 M CB buffer, lower than the optimum reported by Shirahama *et al.* [124]. Further studies have compared the use of porcine and bovine gelatin pairwise. However, making a comparison across studies is challenging. This is because the applied methods vary in terms of buffer composition and pH (PBS at pH 7.4 [211–213] or CB at pH 9 [75, 188, 195]), as well as buffering capacity (0.1 M [75, 195] or 0.25 M CB [188]).

As GelMA contains cell adhesion sites, hydrogel microparticles can be used for cellular expansion and differentiation. Commonly used methods for the expansion of adherent cell types are based on the use of tissue culture (TC) flasks. This limits the production of large quantities of cells as the required physical space increases linearly with the number of required flasks. In contrast, a significant advantage is shown by the expansion of cells using microcarriers. Hydrogel microparticles offer a high growth surface-to-volume ratio and can be implemented into stirred bioreactors [214]. The application of GelMA when compared to underivatized gelatin has the advantage that crosslinking can be performed via photopolymerization in a single stage when producing hydrogel microparticles. In contrast, particle production with gelatin requires multiple stages [158]. The challenging property of GelMA solutions, however, is the sol–gel transition below 30 °C. This issue has been addressed in the literature by using relatively low concentrations of the protein, i.e., below 10 % (w/v) [73, 74, 215], or by heating the entire microfluidic systems [74, 133]. In the first part of this work, we apply the previously presented method to produce GelMA at room temperature. To characterize the effect of the raw material on the produced GelMA, we use a wide range of gelatin products. Porcine gelatin of five different products was tested. The samples included two separate batches of the most commonly studied gelatin product, i.e., porcine gelatin, 300 g bloom strength. Additionally, fish gelatin as well as two bovine products with varying bloom values were incorporated into the study. Furthermore, the produced GelMA was used for the formulation of hydrogels. The elasticity as a function of the source of the raw material was characterized. As a second part of the study, fish and porcine GelMA were used for the microfluidic production of droplets and the subsequent crosslinking to hydrogel microparticles. The manufacturing of microparticles was performed on a single pipeline at room temperature. The resulting droplet size was controlled by variation in the feed ratio of continuous to disperse phase, as well as by variation in GelMA type and concentration. In addition, the swelling behavior of hydrogel microparticles in aqueous media was determined.

4.2 Materials and Methods

4.2.0.1 Precursor Solution for the Synthesis of Gelatin-Methacryloyl

Gelatin products were purchased from Sigma-Aldrich (St. Louis, MI, USA), and the relevant product information is listed in Table 4.1. The buffer for the dissolution and synthesis of GelMA was prepared following the method by Grijalva Garces *et al.* [210]. Buffer components for the synthesis of GelMA were acquired from Merck (Darmstadt, Germany). The buffer composition

was 0.25 M carbonate bicarbonate (CB) and 4 M urea. After the dissolution of the salts, the pH of the solution was adjusted to pH 9 using 1 M sodium hydroxide (NaOH) or 1 M hydrochloric acid (HCl). Gelatin was dissolved in the synthesis buffer to a concentration of 10 % (w/v) at room temperature under stirring.

4.2.0.2 Rheological Characterization of Gelatin Solutions

The viscosity of the solutions at 10 % (w/v) gelatin in synthesis buffer was measured using a rotational rheometer (Physica MCR301, Anton Paar, Graz, Austria). For the characterization of the gelatin solutions, the configuration of the rheometer included a cone-plate geometry (diameter 60 mm, cone angle 0.5°), and a solvent trap in order to avoid sample drying during the measurements. The viscosity was determined within the shear rate range of 0.5 to 500 s^{-1} .

The viscosity values of the gelatin solutions provided below were determined as triplicates. Each value was measured from an independently prepared solution. Values are shown as mean and standard deviation.

4.2.0.3 Synthesis and Purification

The synthesis was performed at room temperature under stirring. The reaction was started by adding methacrylic anhydride (MAA, 94 %, Sigma-Aldrich) to the gelatin solutions. The MAA-to-gelatin ratio was $100\text{ }\mu\text{L g}^{-1}$ for all gelatin samples. Additionally, porcine gelatin was modified to GelMA with a ratio of $40\text{ }\mu\text{L g}^{-1}$. Throughout this study, sample nomenclature includes 100MA, and 40MA depending on the used MAA-to-gelatin ratio. The reaction was carried out for 60 min. The process was terminated by two-fold dilution with ultrapure water and a subsequent pH adjustment to pH 7.4. The diluted reaction mixture was then dialyzed with a 3.5 kDa molecular weight cut-off tubing (Thermo Fisher Scientific, Waltham, MA, USA) in an ultrapure water reservoir. This purification took place for 4 days at 40°C . GelMA solutions were frozen at -80°C overnight and lyophilized. Solid GelMA samples were stored at room temperature until further use.

4.2.0.4 Determination of Degree of Functionalization

The degree of functionalization (DoF) of GelMA samples was determined based on the method by Habeeb [122]. Therefore, glycine (Sigma-Aldrich), gelatin materials, and GelMA samples were dissolved in ultrapure water. Glycine standards for the determination of a standard curve were prepared at 3, 5, 8, 10, and $20\text{ }\mu\text{g mL}^{-1}$. Gelatin references and GelMA samples were dissolved in ultrapure water at 0.1, 0.3, 0.5, and 0.8 mg mL^{-1} . A 0.1 M CB buffer at pH 8.5 was used as a reaction buffer containing 0.01 % (w/v) trinitrobenzenesulfonic (TNBS) acid (Sigma-Aldrich). A volume of 250 mL of the TNBS reagent solution was mixed with an equal volume of the gelation as well as GelMA samples. Incubation followed for 2 h at 40°C . The reaction was terminated by addition of 250 μL of a 10 % (w/v) sodium dodecyl sulfate (Sigma-Aldrich) solution and 125 μL of a 1 M HCl solution. A microplate reader (infiniteM200, Tecan Group, Männedorf, Switzerland) for the measurement of the sample absorbance at 335 nm. The concentration of free amines in the samples was determined in comparison to a glycine calibration curve and normalized to the respective gelatin concentration. The DoF was calculated according to Equation (4.1). The difference between the number of free amino groups present in gelatin ($c_{\text{NH}_2,\text{gelatin}}$), i.e., before the functionalization, and the amount in the produced GelMA ($c_{\text{NH}_2,\text{GelMA}}$), i.e., after the reaction, was divided by the number of free amines in the raw gelatin.

$$\text{Degree of Functionalization} / - = \frac{c_{NH_2, gelatin} - c_{NH_2, GelMA}}{c_{NH_2, gelatin}} \quad (4.1)$$

The production and characterization of GelMA samples consisted of three experimental runs using each gelatin source. The measurement of absorbance in order to determine the DoF was performed for each independently synthesized batch. The values are shown as mean and standard deviation.

4.2.1 Hydrogel Characterization

4.2.1.1 Precursor Solution for the Production of Hydrogels

GelMA samples synthesized from different sources and MAA-to-gelatin ratios were used for hydrogel preparation. For this purpose, a solution containing 0.1 % (w/v) the photo-initiator lithium phenyl-2,4,6-trimethylbenzoylphosphinate (LAP, Sigma-Aldrich) was prepared in Dulbecco's phosphate-buffered saline (DPBS, without calcium and magnesium, 1×, pH 7.4, Thermo Fisher Scientific). Subsequently, the lyophilized material was dissolved to 10 % (w/v) in LAP containing DPBS at 40 °C. GelMA solutions were transferred to cylindrical polytetrafluoroethylene (PTFE) molds (diameter 10 mm, height 3 mm) by pipetting a volume of 235 μL . The samples were then crosslinked to hydrogels by exposure to an ultraviolet (UV) light-emitting diode (LED, 365 nm, OSRAM, Munich, Germany) with an irradiation intensity of 12 mW cm^{-2} for 3 min. GelMA hydrogels were equilibrated in DPBS until further analysis.

4.2.1.2 Mechanical Characterization

The viscoelastic properties of hydrogels were characterized using a rotational rheometer Physica MCR301. A plate-plate geometry (diameter 10 mm) and a solvent trap were part of the configuration of the rheometer. The cylindrical hydrogels were placed on the bottom plate and the top plate was positioned to a gap height of 2.5 mm. Storage and loss moduli were measured within the linear viscoelastic (LVE) regime covering the frequency range of 0.5 to 50 rad s^{-1} . A constant stress amplitude was set to 0.5 Pa. The data of the mechanical characterization were acquired from three experimental runs with three samples each. For each run, GelMA hydrogels from independently produced batches were prepared. The data are presented below as the mean and standard deviation of the elastic plateau modulus.

4.2.2 Microparticle Fabrication and Characterization

4.2.2.1 Precursor Solution for the Production of Microparticles

The manufacturing of GelMA hydrogel microparticles at room temperature was investigated. For these experiments, porcine GelMA, i.e., p300 I, and fish GelMA at a reactant ratio of 100 μL MAA per gram gelatin were used. A 4 M urea solution was prepared for the dissolution of porcine GelMA. Subsequently, the photoinitiator LAP was dissolved to 1 % (w/v). Lyophilized porcine GelMA was added to the mixture and dissolved under stirring. The precursor solution containing fish GelMA was prepared by dissolving the lyophilized material in ultrapure water containing 1 % (w/v) LAP. Samples from both sources were prepared at 10, 15, and 20 % (w/v). The precursor solutions were protected from light prior to their use in the disperse phase in the microfluidic device as described below. The tested samples and the used concentrations are summarized in Table 4.2. Sunflower seed oil (Sigma-Aldrich) was employed as continuous phase.

4.2.2.2 Rheological Characterization of Disperse and Continuous Phase

The shear-rate dependent viscosity of sunflower seed oil and the GelMA solutions was characterized as described in Section 4.2.0.2. For these measurements, the solvent trap served additionally as protection from light to avoid photo-crosslinking during the measurement.

The viscosity of the oil phase was measured as triplicates from the same bulk. The value is presented as the mean and associated standard deviation. Regarding the rheological characterization of the GelMA solutions, the viscosity was determined at each concentration as triplicates. Each value was acquired from the prepared solution from each independently synthesized batch.

4.2.2.3 Microfluidic Production of Droplets and Crosslinking to Microparticles

The setup for the production of GelMA droplets and the subsequent crosslinking process is shown schematically in Figure 4.4(A). The disperse and continuous phases, i.e., GelMA solutions and sunflower seed oil, respectively, were filled in high-precision glass syringes (SETonic, Ilmenau, Germany). A Nemesys syringe pump was used to control the feed rates using the software QmixElements v20140605 (both CETONI, Korbussen, Germany). The rate of the oil phase was set to a constant value of 120 mL min^{-1} for all experiments. The tested GelMA concentrations and the corresponding feed rates, as well as the feed ratio, defined as the ratio of the feed rate of the continuous phase to that of the disperse phase, are listed in Table 4.2.

For the formation of GelMA droplets, a microfluidic device with glass capillaries was employed, as shown in Figure 4.4(B). A detailed description of the equipment is provided by Leister *et al.* [216]. The setup consisted of one outer and two inner glass capillaries (World Precision Instruments, Friedberg, Germany). The inner capillaries (outer diameter 1 mm, inner diameter 0.58 mm) were modified by pulling with a micro-pipette puller (P-1000, Sutter Instruments, Novato, CA, USA). The tip diameter of the capillary for the disperse phase was $170 \mu\text{m}$, while the tip diameter of the second capillary used as the outlet of dispersed droplets in oil was $340 \mu\text{m}$. The inner capillaries as well as the outer capillary (length 15 mm, inner diameter 1.56 mm) were treated with 2-[methoxy(polyethyleneoxy)6-9-propyl]tris(dimethylamino)silane (Gelest Inc., Morrisville, PA, USA) in order to render the surface hydrophobic. The capillaries were attached in the polyoxymethylene (POM) module as published by Bandulasena *et al.* [217]. The distance between inner capillaries was set to $170 \mu\text{m}$. The outlet of the microfluidic device was connected to a polyvinyl chloride (PVC) tubing (outer diameter 1.8 mm, inner diameter 1 mm, Deutsch & Neumann, Hennigsdorf, Germany). The tubing was arranged as a loop under four UV LEDs (OSRAM), where photo-crosslinking took place with a total irradiation intensity of 25.6 mW cm^{-2} . An image of the tubing placed under UV light is provided in Figure 4.4(C). The produced hydrogel microparticles in oil were collected and stored at room temperature until further analysis.

4.2.2.4 Determination of Droplet Size

Image sequences of the formation of droplets at the break-up point were acquired using a monochrome camera (DMK 33U, The Imaging Source Europe, Bremen, Germany) equipped with a $1\times$ lens (TMN 1.0/50, The Imaging Source Europe) using the software IC capture V2.5 (The Imaging Source Europe). The acquisition rate was set to 10 frames per second. The resulting droplet sizes were determined using “Droplet Morphometry and Velocimetry” (DMV) software [163] by analyzing at least 150 frames. The coordinates of the center of each droplet, as well as the respective droplet diameter in each frame, were exported. Detected objects with a center below or above the

longitudinal axis of the capillaries at the direct proximity of the break-up point were considered outliers and removed from the distributions. The data distribution of at least 50 droplets per sample is shown below as box plots including median, upper, and lower quartile, as well as maxima and minima within a 1.5-fold interquartile range.

4.2.2.5 Determination of Hydrogel Swelling Behavior

For the determination of the swelling behavior of the hydrogel microparticles, the samples from both GelMA sources produced with a feed ratio of $5\times$ were collected. DPBS was added to the particle/oil mixture and centrifuged at 500 rcf. The excessive oil and DPBS were removed keeping the particles in the bottom of the centrifuge tube. The microparticles were suspended in fresh DPBS and centrifuged. This wash series was performed four times. Microparticles were then equilibrated overnight in DPBS. Hydrogel microparticles and the corresponding oil phase and DPBS were placed on a microscopy slide for image acquisition. The imaging setup consisted of a monochrome camera (Genie Nano M2420 Mono, Teledyne Dalsa, Waterloo, ON, Canada) equipped with a $10\times$ objective (Nikon, Tokyo, Japan). For the quantification of the particle size, an image processing and analysis workflow was developed using Matlab[®] R2023a (TheMathWorks Inc., Natick, MA, USA) with the library Image Processing Toolbox 11.7. The variation in pixel intensities compared to the nine-by-nine surrounding pixels was analyzed using the local entropy filter. The output images contain high-intensity values in the regions of high-intensity variation, i.e., the interface between microparticles and bulk media. Particle diameters were detected on said output processed images. The swelling behavior of the hydrogel microparticles was characterized by the ratio of media diameter after swelling in DPBS ($d_{p,DPBS}$) to the median diameter in oil ($d_{p,Oil}$), as shown in Equation (4.2). The data sets presented below correspond to the swelling ratio of at least 40 hydrogel particles of each sample.

$$\text{Volumetric Swelling Ratio } \% = \frac{d_{p,DPBS}^3}{d_{p,Oil}^3} \quad (4.2)$$

4.2.3 Data Handling and Statistical analysis

Image processing, data evaluation, data visualization, and statistical analysis of the data sets were performed with Matlab[®] R2023a (TheMathWorks Inc., Natick, MA, USA). One-way analysis of variance (ANOVA) was performed in order to determine significant differences. A p -value below 0.05 was considered as statistically significant.

4.3 Results and Discussion

4.3.1 GelMA Synthesis and Characterization

As demonstrated previously, the dissolution of porcine gelatin of 300 g bloom strength in urea-containing buffer was possible solely under stirring at room temperature [210]. This method was applicable for dissolving porcine gelatin of various bloom strengths, and two different gelatin products from bovine tissue. All used gelatin products are listed in Table 4.1. The dissolution at room temperature was due to the fact that urea disrupts protein-protein hydrophobic interactions and causes gelatin to unfold to coils in solution [192–194]. Even though gelatin from cold-water fish does not form a physical gel above 5 to 10 °C due to the lower content of proline and hydroxyproline [107,

Table 4.1 Overview of gelatin types for the synthesis of gelatin methacryloyl (GelMA). The products were purchased from Sigma-Aldrich; the corresponding product information is provided including source, Bloom strength is according to the manufacturer, as is the sample nomenclature used throughout this manuscript.

Product number	Batch number	Source	Bloom strength	Nomenclature
G6144	SLCH4483	porcine	80-120 g	p80
G2625	SLCC4273	porcine	175 g	p175
G1890	SLCC7838	porcine	300 g	p300 I
G1890	SLBX2973	porcine	300 g	p300 II
39465	BCBW7164	porcine	ultrahigh	pUH
G7765	038K0681	fish	–	f
G6650	SLCM1231	bovine	50-120 g	b50
G9382	SLCF9893	bovine	225 g	b225

218], the same synthesis buffer was used for the sake of comparability during the synthesis of GelMA. As the rheological behavior of protein solution affects the distribution of reactants during a stirred reaction, the viscosity of the gelatin solutions in the synthesis buffer was measured. Figure 4.1 provides the corresponding results.

The viscosity of solutions containing porcine gelatin increased significantly from 11.80 ± 0.17 mPa s to 53.93 ± 0.25 mPa s with increasing bloom strength of the gelatin product. The latter value was shown by the solution using a porcine source labeled as gelatin with ultrahigh (UH) gel strength by the supplier. Two batches from the same product with a bloom strength of 300 g were acquired and used for the measurements of viscosity. The solution produced with p300 I and p300 II gelatin showed a viscosity of 46.63 ± 0.42 mPa s and 39.43 ± 0.25 mPa s, respectively. These two values were significantly different ($p < 0.05$). Fish gelatin solution showed a viscosity of 13.26 ± 0.06 mPa s. The viscosity of the solutions comprising bovine gelatin showed an increase in viscosity with increasing bloom strength of the product from 14.07 ± 0.06 mPa s to 28.60 ± 0.10 mPa s. Statistically significant differences between the viscosity values were found between all data sets ($p < 0.05$). The increase in viscosity of gelatin solutions with increasing bloom strength is in accordance with other studies [218, 219]. This is because the bloom value correlates with the molecular weight (MW) of gelatin [107]. Therefore, an increasing molecular weight leads to increasing intramolecular friction and to a higher amount of entanglements of proteins in solution, and, thus, higher viscosity [68, 220]. In the case of gelatin pUH, no bloom value is stated by the producer. However, it was assumed that the MW is higher than that of gelatin p300 I and p300 II due to the ultrahigh gel strength. This was confirmed by the higher viscosity of the solution. Similarly, no bloom value is provided for fish gelatin. This is because the determination of gel strength is performed following a standardized method at 21 °C. Therefore, no bloom value can be measured for this product. The viscosity of the fish gelatin solution was around the values of viscosity of porcine gelatin p80 and bovine gelatin b50. Thus, the MW of fish gelatin was around the same magnitude as that of bovine and porcine gelatin of lower bloom strengths, as has been observed in the literature [218].

Although it has been mentioned in the literature that the DoF of GelMA might vary when different types of gelatin are used [130], not many reports have been presented on this topic. In this study, GelMA was synthesized using different gelatin products with varying species of origin and

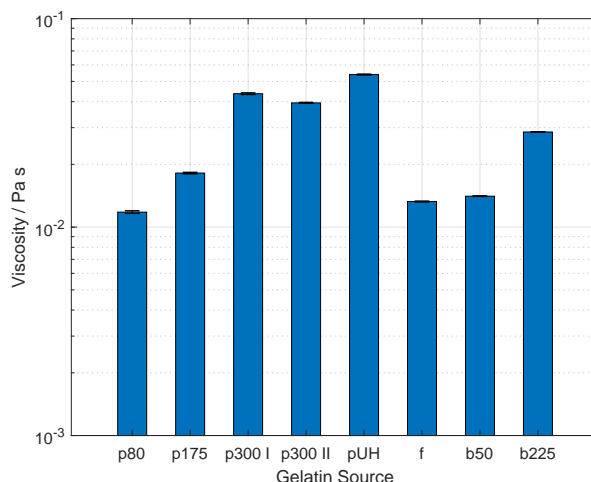


Figure 4.1 Viscosity of solution comprising gelatin at 10 % (w/v) in reaction buffer, i.e., 0.25 M carbonate bicarbonate (CB) buffer, and 0.25 M urea, measured at room temperature. Sample nomenclature is provided in Table 4.1. The viscosity increased with increasing bloom strength of both porcine and bovine gelatin. Additionally, the viscosity of gelatin solutions prepared with the same product but different batches, i.e., p300 I, and p300 II, showed a significant difference. Statistically significant differences between the viscosity values were found between all data sets ($p < 0.05$). Values are shown as mean and standard deviation. Each gelatin solution was tested three times from independently prepared samples.

various values of bloom strength. Table 4.1 provides relevant information on the tested products. The DoFs of the produced samples are shown in Figure 4.2. In the first part of the study regarding the synthesis of GelMA, the previous method using a urea-containing buffer to process gelatin at room temperature was simplified [210]. In contrast to the said study where MAA was continuously fed during the reaction, the complete amount of reactant was added at the beginning of the reaction in the present study. Additionally, the reaction time was shortened to 60 min. The GelMA sample p300 I was produced using the same gelatin product and batch. At a MAA-to-gelatin ratio from $100 \mu\text{L g}^{-1}$ (100MA), the DoF exhibited a value of 0.899 ± 0.010 . This value is not significantly different from the data shown previously with a value of 0.963 ± 0.027 [210]. Reaching a similar DoF in spite of the reduction in reaction time is comparable to the study by Shirahama *et al.* [124], as it was shown that the reaction is completed within 60 min when the complete volume of MAA is added at the starting point. As mentioned above, porcine gelatin with a bloom strength of 300 g has been widely studied for the production of GelMA [188, 213, 221]. Moreover, batch-to-batch variability is known to be a drawback of naturally derived polymers [5, 6]. To test the effect of such inconsistencies, a second batch of the same product was used to synthesize GelMA p300 II. The DoF showed a value 0.832 ± 0.021 at 100MA, significantly lower than that of GelMA p300 I ($p < 0.05$). Furthermore, the feasibility of using the developed method with porcine gelatin of varying bloom strength and the effects thereof were studied at $100 \mu\text{L g}^{-1}$ (100MA). The DoF values of GelMA were 0.732 ± 0.014 , and 0.810 ± 0.007 for the samples produced with gelatin of lower bloom strength, i.e., samples p80-100MA, and p175-100MA, respectively. These values differed significantly from each other and from the DoF of GelMA p300 I-100 MA ($p < 0.05$). Additionally,

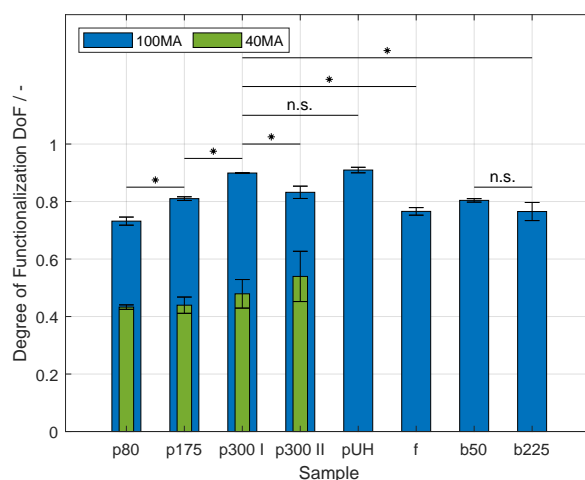


Figure 4.2 Degree of functionalization (DoF) of produced gelatin methacryloyl (GelMA). Sample nomenclature regarding the used raw materials is provided in Table 4.1. The DoF was determined by the trinitrobenzenesulfonic (TNBS) acid method [122]. At a methacrylic anhydride (MAA)-to-gelatin ratio of $100 \mu\text{L g}^{-1}$ (100MA), asterisks denote a significant difference between synthesized samples ($p < 0.05$). No significant differences are denoted with the abbreviation n.s. ($p > 0.05$). Moreover, the DoF of porcine GelMA decreased significantly with decreasing MAA-to-gelatin ratio from 100 to $40 \mu\text{L g}^{-1}$ (40MA) ($p < 0.05$). At a MAA-to-gelatin ratio of $40 \mu\text{L g}^{-1}$ (40MA), no significant differences regarding the DoF were proven ($p > 0.05$). These differences are not shown for the purpose of clarity. Values are shown as mean and standard deviation. The functionalization of each gelatin type was carried out separately three times. The DoF of each batch was determined.

porcine gelatin with ultrahigh gel strength was modified to GelMA with a DoF of 0.910 ± 0.010 . However, these data did not differ significantly from the data of the sample p300 I-100MA.

Gelatin p300 I and p300 II were derived from porcine skin with an acidic treatment (Type A) due to the high-fat content of the tissue [117, 218]. Individual differences within a species could lead to differences in MW and MW distribution. Additionally, slight differences in processing could also affect the properties of porcine gelatin as has been shown by Duconseille *et al.* [222]. The study showed that minor differences in the raw material and processing steps have a significant impact on the biochemical composition. In the reaction of gelatin to GelMA, the organic compound MAA is added to the aqueous gelatin solution. As both liquids are not miscible, thorough stirring is required to disperse the reactant to fine droplets. This issue has been addressed in the literature [124, 144, 221]. Hence, gelatin shows surface active properties leading to the adsorption of molecules to the created interface [223, 224]. During stirring, MAA droplets are formed, which then collapse at different rates depending on the adsorption rate of gelatin to the interface and on the stabilization mechanism of the droplets. For instance, Shirahama *et al.* [124] mentioned that it was not feasible to evenly distribute MAA within a 1% (w/v) gelatin solution as not enough protein was in solution to stabilize the MAA droplets. Furthermore, the adsorbed amount is dependent on the MW and MW distribution [156]. Additionally, the MW of the adsorbed protein affects the stabilization mechanism of the created droplets [156, 223]. As the reaction took place in a buffered solution at pH 9, around the isoelectric point (IEP) of porcine gelatin, the stabilization mechanism is mostly steric. The magnitude of stabilization as well as the amount of adsorbed protein both increase

with increasing MW. Consequently, the stabilization provided by gelatin of higher MW, i.e., higher bloom value, yields a higher interface and therefore a higher reaction rate leading to higher values of DoF. A study was presented by Aljaber *et al.* [75], where porcine gelatin of 300 g as well as 175 g bloom strength was used to produce GelMA, and showed a higher DoF for the material of higher bloom value, which is in accordance with the presented data in this study.

The possibility to transfer the developed approach to raw materials other than porcine gelatin was tested using fish gelatin from cold water as well as two bovine gelatin products with different gel strengths. The buffer system and the processing at room temperature proved to be applicable to fish and bovine gelatin. As mentioned above, the presence of urea in the buffer inhibits the formation of helical structures of the gelatin from bovine tissue, i.e., the transition from solution to a gel. At a MAA-to-gelatin ratio from $100 \mu\text{L g}^{-1}$ (100MA), the DoF of fish GelMA showed a value of 0.766 ± 0.013 . Furthermore, the effect of various values of bloom strength was studied using bovine gelatin at $100 \mu\text{L g}^{-1}$. The DoF values of GelMA were 0.804 ± 0.006 , and 0.765 ± 0.013 for the samples produced with gelatin of lower bloom strength, i.e., samples b50-100MA, and b225-100MA, respectively. The DoF of both bovine GelMA samples as well as fish GelMA differed significantly from the DoF of GelMA p300 I-100MA ($p < 0.05$). The effect of increasing bloom strength on the resulting DoF of bovine GelMA was not significant. As fish gelatin is extracted using acidic media [117], the IEP of the protein is similar to that of porcine gelatin. The determined DoF of GelMA f-100MA is in the same range as the DoF of porcine GelMA with the lowest bloom strength, i.e., p80-100MA. This comparable result is due to the fact that the MW of fish gelatin lies around the MW of gelatin p80, as was mentioned above regarding the results of the viscosity of both gelatin solutions. Hence, the stabilization of MAA droplets could take place at a similar magnitude. It has been shown by Lee *et al.* [123] that the reaction is most effective when the free amino groups are not charged; therefore, the pH during the reaction as well as the IEP of gelatin plays a significant role during the production of GelMA. In the literature, a higher DoF of bovine GelMA compared to that of porcine GelMA has been reported [211, 213]. Both studies performed the reaction using phosphate-buffered saline, leading to the crucial difference in the surface charge of both proteins. The IEP of bovine gelatin lies around pH 4–5 due to the alkaline pre-treatment of bovine tissue where asparagine and glutamine are converted to aspartic acid and glutamic acid, respectively, [107, 117]. Therefore, at pH 7 the reaction rate of bovine GelMA is much higher than the rate of porcine gelatin.

Further studies producing GelMA using CB solutions have shown similar DoF values for porcine and bovine products. Lee *et al.* [195] prepared GelMA using porcine gelatin with 175 g bloom strength and bovine gelatin with 225 g. Both samples showed similar DoF values, which is in accordance with the presented study. Aljaber *et al.* [75] prepared GelMA using porcine gelatin with 300 g bloom strength, which had a higher DoF than the GelMA produced from bovine gelatin. Although the bloom strength of the bovine protein was not stated in that study, the results are in accordance with the results shown in this manuscript. As mentioned above, MAA and aqueous gelatin solutions are not miscible, and gelatin molecules are adsorbed to the created interface. The aqueous solution is buffered at pH 9; consequently, the bovine protein is negatively charged, making it less suitable for the stabilization of MAA droplets compared to the neutrally charged porcine gelatin [225]. This could lead to bigger droplets decreasing the amount of total interface for the reaction to GelMA, and, therefore decreasing the DoF of both bovine samples. The stabilization mechanism of MAA droplets could explain the missing difference regarding the DoF of GelMA b50 and b225. Additionally, proteins of lower MW show an electrostatic stabilizing effect because of the negatively charged surface, while the stabilizing mechanism of proteins with higher MW is

rather steric [223]. As a result, both gelatin types could stabilize the created interface at similar magnitudes, thus showing similar DoF values.

The effect of the MAA-to-gelatin ratio was also studied using four gelatin raw materials, i.e., p80, p175, p300 I, and p300 II. The DoF of each GelMA sample at $40 \mu\text{L g}^{-1}$ (40MA) decreased significantly compared to each counterpart at 100MA ($p < 0.05$). This result is in accordance with similar studies [123, 124, 188]. Holding the MAA-to-gelatin ratio constant at 40 MA, the DoF did not differ significantly by increasing bloom strength. As the volume of the reactant decreases, the created interface becomes smaller and the stabilization efficiency provided by the proteins is equally effective.

This study shows that the gelatin source as well as bloom strength and even batch-to-batch variations have a significant impact on the process. As the adsorption of the gelatin molecules at the interface to MAA is highly influenced by the MW and MW distribution, the setting of an optimal reactant ratio will depend on the used raw material. Our findings imply process parameters developed using a certain raw material cannot be simply transferred to the operation with a different one. In the case of GelMA, the process parameters to meet a certain DoF have to be adapted according to the gelatin material to be used. Further understanding of the reaction is required taking into account the properties of gelatin at the interface to the reactant. The stirring conditions should also be thoroughly studied, as the droplet size depends on the energy input to the process. As previously stated regarding the use of the protein in the field of tissue engineering, detailed information about the range of operating conditions to meet certain quality attributes is required. This is a requisite by regulatory authorities to reach clinical stages.

4.3.2 Hydrogel Characterization

GelMA solutions can be covalently crosslinked to hydrogels. This possibility is crucial when the intended application takes place at elevated temperatures. As shown in the literature, the elasticity of the produced hydrogels is influenced by the protein concentration and its DoF [121, 210, 226]. This study aimed to characterize the effect of the source as well as the effect of diverse values of bloom strength of the raw material on the resulting mechanical properties. For this purpose, hydrogels were prepared at 10% (w/v) as described above, and the storage modulus was determined by oscillatory frequency sweeps on a rheometer. The associated values are presented in Figure 4.3.

The elastic moduli of the hydrogels prepared with porcine GelMA 100MA increased significantly with the bloom strength of the respective gelatin raw material ($p < 0.05$). The moduli were 2.15 ± 0.16 kPa, 5.85 ± 1.11 kPa, and 9.04 ± 0.85 kPa, for GelMA samples p80-100MA, p175-100MA, and p300 I-100MA, respectively. The hydrogels produced with p300 II exhibited an elastic modulus of 7.60 ± 0.91 kPa, and the data did not differ significantly from the data produced with p300 I-100MA, i.e., the same gelatin product used as raw material proceeding from a different batch. Similarly, the elastic moduli of GelMA hydrogels p300 I and p300 II did not differ significantly from that of hydrogels produced with GelMA pUH-100MA. This effect is in accordance with the work of Aljaber *et al.* [75]. The study showed an increase in elastic as well as compressive moduli by increasing the bloom of the raw material from 175 g to 300 g. The increasing elasticity corresponds to higher crosslink density in the polymeric network. This resistance to the deformation is influenced by both covalent bonds and physical entanglements [68, 81]. GelMA with higher bloom strength showed a higher DoF, and thus a higher amount of methacrylamide and methacrylate residues. Furthermore, as the bloom value of the protein increases, so too does the MW, which leads to an increment in the amount of physical entanglements, as well. Although significant differences in

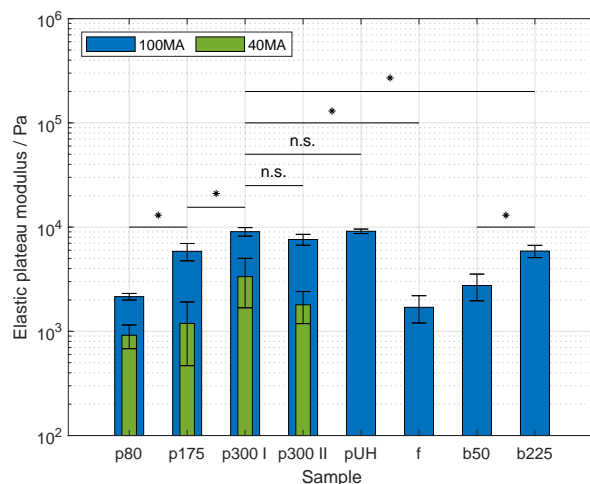


Figure 4.3 Elastic plateau modulus of gelatin methacryloyl (GelMA) hydrogels of various sources at 10 % (w/v). Sample nomenclature regarding the used raw materials is provided in Table 4.1. At a methacrylic anhydride (MAA)-to-gelatin ratio of $100 \mu\text{L g}^{-1}$ (100MA), asterisks denote a significant difference between synthesized samples ($p < 0.05$). No significant differences are denoted with the abbreviation n.s. ($p > 0.05$). Furthermore, the elasticity of the hydrogels produced with porcine GelMA decreased significantly with decreasing MAA-to-gelatin ratio from 100 to $40 \mu\text{L g}^{-1}$ (40MA) ($p < 0.05$). At a MAA-to-gelatin ratio of $40 \mu\text{L g}^{-1}$ (40MA), no significant differences regarding the hydrogel elasticity were shown ($p > 0.05$). These differences are not shown for the purpose of clarity. Data are shown as mean and corresponding standard deviation. Each batch of GelMA was used for the formulation of hydrogels. Three samples of each batch were tested.

viscosity at the same gelatin concentration were measured meaning a difference in the MW and MW distribution, the missing difference by means of the elasticity of samples p300 I, p300 II, and pUH could arise from the crosslinking conditions in the present study. The irradiation dose was set to 2167 mJ cm^{-2} . This condition is much higher than the presented methods in similar studies [121, 188, 198]. As studied by O’Connell et al. [199], the reaction rate is proportional to the irradiance and photo-initiator concentration in free radical polymerization. As a result, the diffusivity of radicals and the accessibility of crosslinking sites are rapidly lowered by the increasing elasticity of the polymeric matrix, thus limiting the formation of covalent bonds.

Not only the elastic moduli of hydrogels made of porcine GelMA were determined, but also those of fish and bovine GelMA. The samples prepared with f-100MA, and b50-100MA showed elastic moduli values of $1.69 \pm 0.50 \text{ kPa}$, and $2.75 \pm 0.79 \text{ kPa}$, respectively. These data sets were not significantly different from each other. The elastic moduli of b225-100MA hydrogels had a value of $5.88 \pm 0.79 \text{ kPa}$, significantly higher than that of GelMA f-100MA and b50-100MA hydrogels ($p < 0.05$). The data measured from the b225-100MA hydrogel were significantly lower than the data acquired from hydrogels p300 I, p300 II, pUH ($p < 0.05$). The lower elasticity of fish GelMA in comparison to porcine GelMA and bovine GelMA has been shown in the literature. While both Young *et al.* [213] and Aljaber *et al.* [75] state the use of porcine gelatin with 300 g bloom strength, only Young *et al.* mention the bloom value of bovine gelatin, i.e., 225 g. In both cases, hydrogels prepared with fish GelMA show the lowest elasticity. Due to the fact that the DoF of p80-100MA, f-100MA, and b50-100MA were similar, the covalent crosslinks and chain entanglements contribute

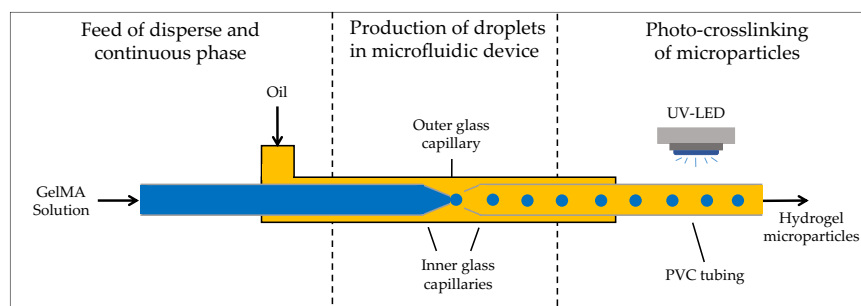
equally to the elasticity of the hydrogels. Moreover, the effect of increasing elasticity with increasing bloom strength of porcine gelatin is exhibited by the samples prepared with bovine GelMA, as well. As both bovine GelMA samples proved to have a similar DoF, the increasing elasticity of the hydrogel b225-100MA is a consequence of the larger amount of physical entanglements due to the higher MW of the protein.

The effect of the DoF on the elasticity of hydrogels was characterized using porcine GelMA. The samples prepared with GelMA 40MA were significantly less elastic than the counterparts produced with GelMA 100MA ($p < 0.05$). The behavior is attributed to the fact of the lower amount of methacrylamide and methacrylate residues required for photo-crosslinking at an equal GelMA concentration. The effect of DoF on elasticity has been reported in similar studies [195, 198, 199, 210]. Future research should include the characterization of the relationship between the properties of the GelMA backbone, i.e., MW and DoF, and hydrogel properties, i.e., elasticity. Additionally, the protein composition can also be taken into account as the protein sources vary in terms of species. Hence, variability regarding the amount of hydrophilic amino acids along the protein affects the mechanical properties of the hydrogel as well.

4.3.3 Microparticle Generation and Characterization

GelMA has proved to be a versatile material in a wide range of applications, e.g., three-dimensional cell culture in studies of disease and tissue engineering [183]. The formation of physical gels at room temperature imposes a challenge for the manufacturing of GelMA-containing products. Similar to gelatin solutions, GelMA solutions form physical gels due to inter- and intramolecular interactions leading to the formation of helical structures. Regarding the elasticity of physical gels, the effect is less pronounced in GelMA compared to raw gelatin; however, the transition temperature remains that of unmodified gelatin [121]. Because the gelation occurs below physiological temperature, the production of GelMA structures with techniques such as bioprinting [227], electrospinning [228], and microfluidics [229] relies on the addition of further polymers to the formulation in order to adapt the precursor solution to the particular method. Alternatively, the production equipment is heated above the gelation point [74, 133]. The aim of this part of the study was the production of GelMA droplets using a microfluidic device at room temperature. For the production of droplets, fish GelMA was dissolved in ultrapure water as the protein solution did not form a physical gel at room temperature. In contrast, porcine GelMA was dissolved in 4 M urea solution to inhibit the gel formation as the process took place at room temperature, i.e., below the gel transition temperature. The processing of GelMA to hydrogel microparticles consists of two consecutive steps. Firstly, GelMA droplets are produced within an oil stream using a microfluidic device. Subsequently, the droplets in oil are covalently crosslinked to hydrogels under UV irradiation as fluid flows within light-transmitting tubing. A schematic draft of the process is provided in Figure 4.4. The tested samples and corresponding concentrations as well as the feed rates of both continuous and disperse phases are listed in Table 4.2.

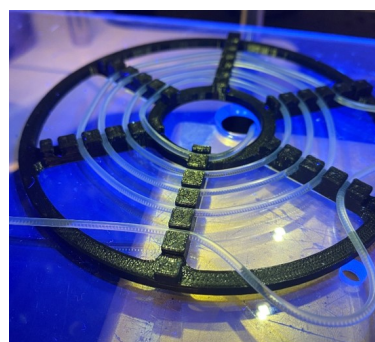
As the droplet formation process is influenced by the viscosity of both inner and outer phases, the viscosity of solutions prepared with fish GelMA and porcine GelMA, as well as the viscosity of sunflower seed oil, were measured. The data on the viscosity of GelMA solutions are shown in Figure 4.5. The viscosity of the oil exhibited a value of 60.5 ± 0.2 mPa·s, which is shown as a line across the figure. A significant increase in viscosity was shown with an increasing concentration of both fish and porcine samples, i.e., samples f-100MA, and p300 I-100MA, respectively, ($p < 0.05$). The values of viscosity of the fish at the concentrations 10, 15, and 20 % (w/v) were 5.2 ± 0.1 mPa·s,



(A)



(B)



(C)

Figure 4.4 Schematic of the microfluidic setup used in this study. (A) Disperse phase and continuous phase, i.e., Gelatin methacryloyl (GelMA) and sunflower seed oil, respectively, were fed into the microfluidic device using a syringe pump. The droplet production took place within an outer glass capillaries, where two inner capillaries were placed. The left and right inner capillaries had diameters of $170\ \mu\text{m}$ and $340\ \mu\text{m}$, respectively. The dispersed droplets in oil were crosslinked to hydrogel microparticles under ultraviolet (UV) light-emitting diodes (LED). Figure adapted from Leister *et al.* [216]. The complete experimental setup was used at room temperature. (B) Image of the used microfluidic device. (C) Image of the light-transmitting tubing under UV irradiance for the crosslinking of hydrogel microparticles.

$9.9 \pm 0.2\ \text{mPa}\cdot\text{s}$ and $17.4 \pm 0.6\ \text{mPa}\cdot\text{s}$, respectively. Solutions containing fish GelMA showed lower values of viscosity compared to those of porcine GelMA at the same protein concentration with values of $24.7 \pm 2.0\ \text{mPa}\cdot\text{s}$, $61.1 \pm 6.1\ \text{mPa}\cdot\text{s}$ and $133.0 \pm 19.2\ \text{mPa}\cdot\text{s}$. Furthermore, the viscosity of solutions of both GelMA types at 10% (w/v) are significantly lower than the viscosity of the solution with the corresponding gelatin product shown in Figure 4.5.

The effect of increasing porcine GelMA on the viscosity is in accordance with literature [226]. The viscosity of the solution is affected by the amount of bound water which increases with protein concentration. Additionally, the friction between protein chains and the number of physical entanglements of protein chains increases with the concentration [68, 220]. The higher values of porcine GelMA solution compared to those of fish GelMA solution have not been reported in the literature, but it is expected since the viscosity of porcine gelatin solutions is higher than that of fish gelatin, as shown above. Additionally, the solution of fish GelMA did not contain urea since fish GelMA does not form a physical gel at room temperature. This fact could also account for the higher viscosity of the porcine GelMA solutions in this study as urea increases the viscosity as

Table 4.2 Composition of disperse phase as employed for the production of hydrogel microparticles as well as the feed rate and feed ratio of continuous phase to disperse phase. The feed rate of the continuous phase consisting of sunflower seed oil was set to 120 mL min^{-1} .

GelMA Sample	Concentration % (w/v)	Feed Rates mL min^{-1}	Feed Ratios \times
f-100MA	15	12, 24, 60	10, 5, 2
f-100MA	20	12, 24, 60	10, 5, 2
p300 I-100MA	10	12, 24, 60	10, 5, 2
p300 I-100MA	15	12, 24, 60	10, 5, 2
p300 I-100MA	20	8, 24, 60	15, 10, 5

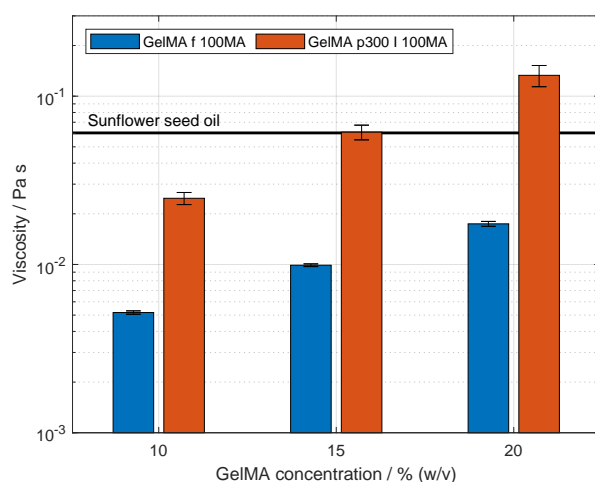


Figure 4.5 Viscosity of gelatin methacryloyl (GelMA) solutions and sunflower seed oil measured at room temperature. Sample nomenclature is provided in Table 4.2. The mean value and standard deviation of the viscosity of sunflower seed oil are shown as a black region. The viscosity of oil was measured three times from the same bulk. Fish GelMA was dissolved in ultrapure water, and porcine GelMA was dissolved in 4 M urea solution. The viscosity of both GelMA types was acquired at 10, 15, and 20% (w/v). The viscosity of the solutions increased significantly with increasing concentration of both types of GelMA ($p < 0.05$). Significant differences were found between the viscosity of the solutions at a constant GelMA concentration ($p < 0.05$). The values are presented as mean and standard deviation. GelMA solutions were measured three times at each concentration. At a constant concentration, GelMA from an independently synthesized batch was used.

well [230]. The decreasing viscosity of the solution after the modification of gelatin to GelMA is in accordance with literature [211, 226] and is attributed to the reduction in hydrophilic interaction between the GelMA backbone and the surrounding aqueous phase.

GelMA droplets were produced at the tip of glass capillaries within the microfluidic system. Exemplary images of the droplets at the break-up point are shown in Figure 4.6(A),(B). The droplets were formed in a co-flow configuration using the second capillary as a flow restriction to facilitate the droplet formation. Directly after droplet break-up, the particle size was determined using high-speed image acquisition and using automated image analysis to determine the droplet size.

The effect of feed ratio as well as GelMA type and concentration were tested. The associated data are shown in Figure 4.6C. Droplets were generated with fish GelMA at 15 and 20 % (w/v). At both concentrations, increasing the feed ratio led to significantly lower droplet sizes. A similar effect was exhibited in the production of droplets with porcine GelMA solution at room temperature. For GelMA droplets at 10 and 15 % (w/v), the decreasing droplet size was significant. At 20 % (w/v) porcine GelMA, the same trend with respect to the lower concentrations was shown; however, the effect of increasing the feed ratio was not significant. In the literature, GelMA droplets for the production of microparticles have been studied at concentrations up to 10 % (w/v) [73, 159, 215]. Such low concentration has been used due to the thermal gelation of GelMA solutions at room temperature. Additionally, the heating of the microfluidic devices has been implemented in other studies to maintain the solutions as a liquid [74, 133]. In the presented study, droplets of porcine GelMA solution with a protein concentration of 20 % (w/v) could be produced at room temperature. The processing without heating of the devices was feasible due to the presence of urea in the solution. Moreover, the effect of increasing feed rate leading to decreasing droplet size is in accordance with the literature [73, 133, 159, 215]. This is due to the viscous drag of the oil phase in contrast to the decreasing inertial and interfacial force of the disperse phase [231]. Moreover, the study by Wang *et al.* [74] mentioned the higher droplet size for the solution comprising porcine GelMA compared to the solution containing fish GelMA. Furthermore, the study by Samanipour *et al.* [215] stated the increasing diameter of particles generated by increasing the GelMA concentration at the same feed rate. These effects were justified as due to an increase in viscosity—the former due to the higher viscosity of the protein of porcine origin and the latter due to the increment of the protein concentration. The droplet formation was in the dripping regime. In our study, this effect of the viscosity on particle size was partially exhibited, but it was not a trend overall. Additionally, the mechanism of droplet formation shifted with increasing viscosity of the protein solutions from dripping to jetting regime as shown in Figure 4.6(A),(B), respectively. In our study, the high GelMA concentration lowers the interface tension at a higher magnitude, and therefore the inner phase is more prone to forming a jet stream. Additionally, the viscosity of the oil was not considerably higher than the viscosities of the GelMA solutions. Especially for the sample at 20 % (w/v), where the viscosity of the inner phase exceeds the oil viscosity, the required feed ratios were even higher for the break-up of droplets. These conditions even lead to the widening of the jets, leading to higher droplet sizes [232].

Particles generated at a feed ratio of $5\times$ were collected for further analysis regarding the swelling behavior in DPBS. For this purpose, images were taken of the droplets in oil, and after equilibration in DPBS. These images are shown in Figure 4.7(A),(B), respectively. The particle diameters in both media were determined using an image processing and analysis workflow developed in Matlab[®]. Moreover, the volumetric swelling ratio was calculated according to Equation (4.2), and the associated results are shown in Figure 4.7(C). The swelling ratio of fish GelMA particles decreased from 4.10 ± 1.00 to 1.35 ± 0.35 with increasing GelMA concentration. Similarly, the swelling behavior of particles composed of porcine GelMA decreased with increasing protein concentration. The volumetric swelling ratio of the 10 % (w/v), 15 % (w/v), and 20 % (w/v) hydrogel particles were 4.72 ± 0.77 , 3.12 ± 0.05 , and 2.81 ± 0.01 . The effect of GelMA concentration on the swelling capacity of hydrogels has been shown in similar studies [185, 200, 202]. The swelling process is driven by the osmotic pressure difference between the aqueous phase within the polymeric network and the bulk phase. Counteracting the swelling process is the elasticity of the crosslinked network, which increases with increasing concentration of the protein [76, 201]. As mentioned above, the increasing elasticity originates from the higher amount of both covalent bonds and physical entanglements [81].

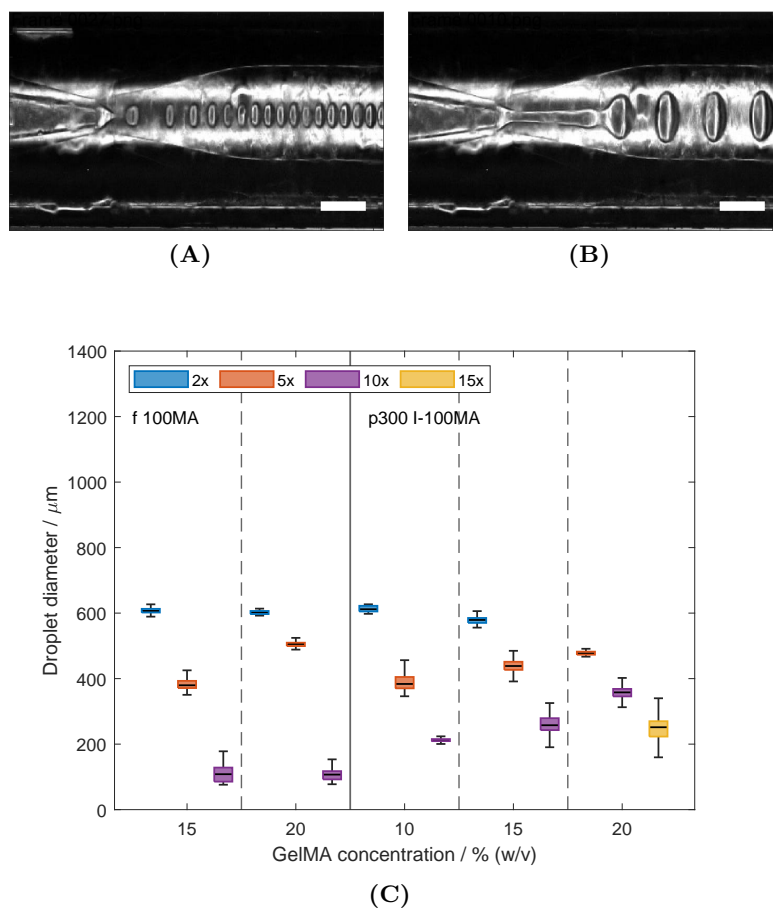


Figure 4.6 Production of gelatin methacryloyl (GelMA) droplets in a microfluidic device. Fish and porcine GelMA were used in the disperse phase, whereas sunflower seed oil was used in the continuous phase. Sample nomenclature is provided in Table 4.2. The feed rate of the continuous phase was set to 120 mL min⁻¹. (A,B) Microscopic images of the break-up points of GelMA droplets. Scale bar: 500 μm. (A) 15% (w/v) Fish GelMA with a feed rate of 12 mL min⁻¹, i.e., 10× feed ratio. (B) 20% (w/v) Fish GelMA with a feed rate of 24 mL min⁻¹, i.e., 5× feed ratio. (C) Droplet size of disperse phase composed of fish and porcine GelMA, i.e., samples f-100MA and p300 I-100MA, at different concentrations and different feed ratios. The droplet size was measured directly after formation using the “Droplet Morphometry and Velocimetry” (DMV) software [163]. The data were collected from at least 50 droplets of each GelMA sample. Values of the droplet size distribution are shown as a boxplot, where the middle line indicates the median and the edges of the boxes represent the 25 and 75 percentiles. Whiskers indicate maxima and minima within a 1.5-fold interquartile range. Moreover, the droplet size decreased with increasing feed ratio of continuous to disperse phase at each tested composition.

The presented study shows the production of GelMA droplets and the subsequent crosslinking to hydrogel particles in a single step at room temperature. Fish GelMA and porcine GelMA were used for this purpose, including GelMA concentrations that have not been studied in the literature due to the complexity of the material and its thermal gelation at temperatures below physiological conditions. Further studies regarding droplet production and subsequent crosslinking should include a thorough characterization of the mechanisms of droplet formation including the calculation of dimensionless numbers such as the capillary and Weber number. The droplet formation is influenced by the composition of both phases, which depends on the intended application. Surfactants could be used for the stabilization of GelMA droplets, as the small molecules adsorb rapidly to newly created interfaces, and, hence, avoiding coalescence. For encapsulation of cells as well as biopharmaceuticals, fish GelMA at high concentrations could be used as it can be processed at room temperature without the use of urea as an additive. This is of significant importance as urea induces protein denaturation and cell disruption. Regarding cell delivery, research implies the biocompatibility of used surfactants; therefore, the determination of non-critical concentrations to avoid cytotoxic effects should be included. Furthermore, porcine GelMA can be implemented for the production of microcarriers. As previously reported, cells can attach to the GelMA hydrogels after the purification of GelMA. Hence, hydrogel microparticles can be used for the expansion of adherent cells. This approach increases the area-to-volume ratio of bioreactors compared to the commonly used TC flasks. Similarly, such microcarriers can be implemented for the selective differentiation of stem cells depending on the hydrogel formulation and its stiffness [56, 158]. In the present study, the robustness of the production process is increased as the system is not sensitive to temperature fluctuations that could lead to the gelation of the GelMA-containing solutions. Particularly, hydrogel particles at concentrations of 15 and 20 % (w/v) were produced, higher than previously reported in the literature. Hence, stiffer hydrogels could be prepared, which is required for the differentiation and expansion of certain cell phenotypes. Additionally, as GelMA hydrogels can be enzymatically degraded, cells can be easily harvested and separated from the aqueous media.

4.4 Conclusions

Gelatin methacryloyl is well established for the formulation of hydrogels, finding application in biotechnology, tissue engineering, and biofabrication. The studies on the manufacturing progress have been focused on the use of porcine gelatin as raw material. However, a comparison across the literature of the effects of raw materials on the final product is challenging, as various approaches are employed including differences in the composition of reaction buffer, pH, and buffering capacity. Additionally, the molecular weight of the protein has not been the focus of the reports. In the first part of this study, we produced GelMA at room temperature applying the previously reported method, where urea is used in the reaction buffer to inhibit the thermal gelation of the protein solution. This principle was successfully applied to the operation with a variety of raw materials other than the one used in our previous report. Moreover, insights were gained into the effects of batch-to-batch variability, as two different batches of the same porcine gelatin product were used, and the degree of functionalization of the two products differed. Furthermore, the bloom value, and hence the molecular weight of porcine gelatin, proved to have a significant impact on the degree of functionalization, which decreased with decreasing bloom strength. Additionally, fish gelatin and two bovine gelatin products with varying bloom values were modified to GelMA. The DoF of the products was lower than that of porcine GelMA with high bloom. Our findings underline the

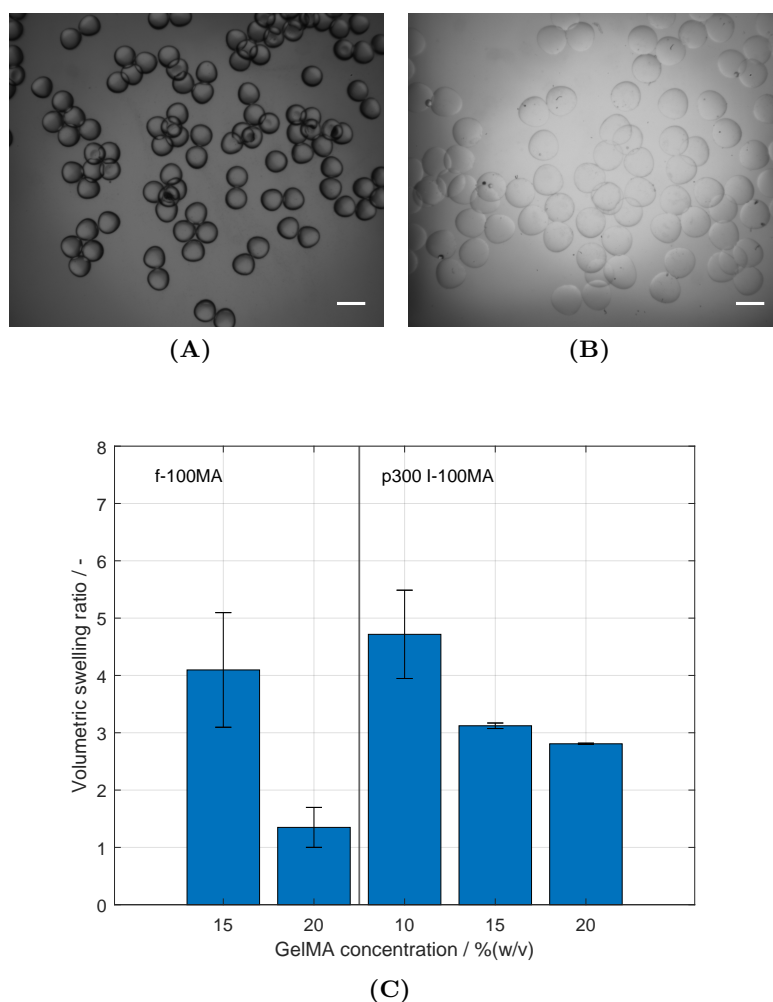


Figure 4.7 Volumetric swelling ratio of gelatin methacryloyl (GelMA) microparticles. Fish and porcine GelMA particles were produced at a feed ratio of continuous to disperse phase of 5 \times . Sample nomenclature is provided in Table 4.2. (A,B) Microscopic images of GelMA microparticles. Scale bar: 1000 μm . (A) 20% (w/v) fish GelMA particles collected after photo-crosslinking in the sunflower seed oil phase. (B) 20% (w/v) fish GelMA after swelling to equilibrium in Dulbecco's phosphate-buffered saline (DPBS). (C) Volumetric swelling ratio (VSR) of GelMA particles composed of fish and porcine GelMA, i.e., samples f-100MA and p300 I-100MA. The swelling ratio was calculated according to Equation (4.2). Moreover, the swelling behavior decreased with increasing GelMA concentration of each type. Values are presented as mean and corresponding standard deviation. The particles size for the calculation of the swelling behavior was detected from at least 40 particles of each sample.

significant impact of the raw material on the processing of gelatin to GelMA. As the reactants are not miscible, stirring is required to disperse methacrylic anhydride droplets in the gelatin solution. The protein adsorption at the interface, where the reaction takes place, depends on the molecular weight, molecular weight distribution, as well as protein charge. Therefore, the optimization of process parameters is highly dependent on raw materials, and a developed process cannot simply be transferred to the operation with a different raw material. Further research should take into account the properties of gelatin at the interface to the reactant. Furthermore, the produced GelMA materials of varying species and bloom strength were used for the formulation of hydrogels, and the elasticity of the polymeric network was characterized. By variation in the degree of functionalization, GelMA hydrogels showed increasing elastic moduli. In addition, the molecular weight of the raw materials affected the elasticity. Decreasing the bloom strength of GelMA hydrogels led to less elastic behavior.

As a second part of the presented study, two GelMA types were used for the microfluidic generation of droplets and the subsequent crosslinking to hydrogel particles. Both processes were performed on a single pipeline at room temperature. Therefore, fish GelMA was dissolved in water and porcine GelMA was dissolved in urea solution to maintain a solution at room temperature. The droplets could be produced at higher GelMA concentrations than that found in the literature. Moreover, the droplet size decreased with an increasing feed ratio of the continuous to disperse phase at each tested concentration. The swelling behavior of crosslinked particles was characterized. Hydrogel particles exhibited a higher swelling degree with decreasing GelMA concentration. Future studies should include the formulation of GelMA using surfactants as well as the adaptation of the modular microfluidic device to stabilize the droplets by other means. Additionally, further understanding of the mechanisms of GelMA droplet generation is required, specifically how process parameters affect dripping and jetting regimes.

Conflict of interest

The authors declare that they have no known competing financial interests or personal relationships that could have appeared to influence the work reported in this paper.

Author contributions

Conceptualization, D.G.G.; methodology, D.G.G. and N.L.; Investigation, D.G.G, L.J.A. and J.E; formal analysis, D.G.G.; data curation, D.G.G; software, D.G.G.; writing—original draft preparation, D.G.G.; writing—review and editing, L.J.A, J.E., N.L, and J.H; visualization, D.G.G.; supervision, J.H.; project administration, J.H.; funding acquisition, J.H.

All authors have read and agreed to the published version of the manuscript

Acknowledgments

We would like to thank Katharina Jonas for her valuable contribution in the form of preparation of the glass capillaries, and Goran Vladislavljević for providing the microfluidic module used in this study. Additionally, the authors are thankful for the thorough review of the manuscript by Svenja Strauß. We acknowledge support by the KIT-Publication Fund of the Karlsruhe Institute of Technology.

Data availability statement

The raw data supporting the conclusions of this article as well as the written codes for Matlab® will be made available on request. Inquiries can be directed to the corresponding author.

Chapter references

- [5] R. J. Wade and J. A. Burdick, „Engineering ECM signals into biomaterials“, *Materials Today*, vol. 15, no. 10, pp. 454–459, 10/2012.
- [6] F. Ruedinger, A. Lavrentieva, C. Blume, I. Pepelanova, and T. Scheper, „Hydrogels for 3D mammalian cell culture: a starting guide for laboratory practice“, *Applied Microbiology and Biotechnology*, vol. 99, no. 2, pp. 623–636, 01/2015.
- [56] K. A. Jansen, D. M. Donato, H. E. Balcioglu, T. Schmidt, E. H. Danen, and G. H. Koenderink, „A guide to mechanobiology: Where biology and physics meet“, *Biochimica et Biophysica Acta (BBA) - Molecular Cell Research*, vol. 1853, no. 11, pp. 3043–3052, 11/2015.
- [68] T. Osswald and N. Rudolph, *Polymer Rheology*. München, Germany: Carl Hanser Verlag GmbH & Co. KG, 11/2014, pp. 101–141.
- [73] J. Jung and J. Oh, „Swelling characterization of photo-cross-linked gelatin methacrylate spherical microgels for bioencapsulation“, *e-Polymers*, vol. 14, no. 3, pp. 161–168, 05/2014.
- [74] Z. Wang, Z. Tian, F. Menard, and K. Kim, „Comparative study of gelatin methacrylate hydrogels from different sources for biofabrication applications“, *Biofabrication*, vol. 9, no. 4, p. 044 101, 08/2017.
- [75] M. B. Aljaber, F. Verisqa, Z. Keskin-Erdogan, K. D. Patel, D. Y. S. Chau, and J. C. Knowles, „Influence of Gelatin Source and Bloom Number on Gelatin Methacryloyl Hydrogels Mechanical and Biological Properties for Muscle Regeneration“, *Biomolecules*, vol. 13, no. 5, p. 811, 05/2023.
- [76] N. A. Peppas, J. Z. Hilt, A. Khademhosseini, and R. Langer, „Hydrogels in Biology and Medicine: From Molecular Principles to Bionanotechnology“, *Advanced Materials*, vol. 18, no. 11, pp. 1345–1360, 06/2006.
- [81] K. S. Anseth, C. N. Bowman, and L. Brannon-Peppas, „Mechanical properties of hydrogels and their experimental determination“, *Biomaterials*, vol. 17, no. 17, pp. 1647–1657, 01/1996.
- [89] M. W. Tibbitt and K. S. Anseth, „Hydrogels as extracellular matrix mimics for 3D cell culture“, *Biotechnology and Bioengineering*, vol. 103, no. 4, pp. 655–663, 07/2009.
- [107] R. Schrieber and H. Gareis, *Gelatine Handbook*. Weinheim, Germany: Wiley, 02/2007.
- [117] A. A. Karim and R. Bhat, „Fish gelatin: properties, challenges, and prospects as an alternative to mammalian gelatins“, *Food Hydrocolloids*, vol. 23, no. 3, pp. 563–576, 2009.
- [119] K. Y. Lee and D. J. Mooney, „Hydrogels for Tissue Engineering“, *Chemical Reviews*, vol. 101, no. 7, pp. 1869–1880, 07/2001.
- [121] A. I. Van Den Bulcke, B. Bogdanov, N. De Rooze, E. H. Schacht, M. Cornelissen, and H. Berghmans, „Structural and rheological properties of methacrylamide modified gelatin hydrogels“, *Biomacromolecules*, vol. 1, no. 1, pp. 31–38, 2000.
- [122] A. Habeeb, „Determination of free amino groups in proteins by trinitrobenzenesulfonic acid“, *Analytical Biochemistry*, vol. 14, no. 3, pp. 328–336, 03/1966.
- [123] B. H. Lee, H. Shirahama, N.-J. Cho, and L. P. Tan, „Efficient and controllable synthesis of highly substituted gelatin methacrylamide for mechanically stiff hydrogels“, *RSC Advances*, vol. 5, no. 128, pp. 106 094–106 097, 2015.
- [124] H. Shirahama, B. H. Lee, L. P. Tan, and N.-J. Cho, „Precise Tuning of Facile One-Pot Gelatin Methacryloyl (GelMA) Synthesis“, *Scientific Reports*, vol. 6, no. 1, p. 31 036, 08/2016.
- [130] E. Hoch, T. Hirth, G. E. Tovar, and K. Borchers, „Chemical tailoring of gelatin to adjust its chemical and physical properties for functional bioprinting“, *Journal of Materials Chemistry B*, vol. 1, no. 41, pp. 5675–5685, 2013.
- [133] T. Tang *et al.*, „Microfluidic Fabrication of Gelatin Acrylamide Microgels through Visible Light Photopolymerization for Cell Encapsulation“, *ACS Applied Bio Materials*, vol. 6, no. 6, pp. 2496–2504, 06/2023.
- [144] K. Yue, G. Trujillo-de Santiago, M. M. Alvarez, A. Tamayol, N. Annabi, and A. Khademhosseini, „Synthesis, properties, and biomedical applications of gelatin methacryloyl (GelMA) hydrogels“, *Biomaterials*, vol. 73, pp. 254–271, 2015.
- [149] A. C. Daly, L. Riley, T. Segura, and J. A. Burdick, „Hydrogel microparticles for biomedical applications“, *Nature Reviews Materials*, vol. 5, no. 1, pp. 20–43, 2020.
- [156] T. F. Tadros, *Volume 1 Interfacial Phenomena and Colloid Stability, Basic Principles*. Berlin, Germany: De Gruyter, 12/2015.
- [158] E. X. Ng, M. Wang, S. H. Neo, C. A. Tee, C. H. Chen, and K. J. Van Vliet, „Dissolvable Gelatin-Based Microcarriers Generated through Droplet Microfluidics for Expansion and Culture of Mesenchymal Stromal Cells“, *Biotechnology Journal*, vol. 16, no. 3, pp. 1–10, 2021.
- [159] J. Huang *et al.*, „One-step generation of core-shell biomimetic microspheres encapsulating double-layer cells using microfluidics for hair regeneration“, *Biofabrication*, vol. 15, no. 2, p. 025 007, 04/2023.
- [163] A. S. Basu, „Droplet morphometry and velocimetry (DMV): A video processing software for time-resolved, label-free tracking of droplet parameters“, *Lab on a Chip*, vol. 13, no. 10, pp. 1892–1901, 2013.

- [183] B. J. Klotz, D. Gawlitta, A. J. Rosenberg, J. Malda, and F. P. Melchels, „Gelatin-Methacryloyl Hydrogels: Towards Biofabrication-Based Tissue Repair“, *Trends in Biotechnology*, vol. 34, no. 5, pp. 394–407, 05/2016.
- [185] W. Schuurman *et al.*, „Gelatin-Methacrylamide Hydrogels as Potential Biomaterials for Fabrication of Tissue-Engineered Cartilage Constructs“, *Macromolecular Bioscience*, vol. 13, no. 5, pp. 551–561, 05/2013.
- [188] I. Pepelanova, K. Kruppa, T. Scheper, and A. Lavrentieva, „Gelatin-Methacryloyl (GelMA) Hydrogels with Defined Degree of Functionalization as a Versatile Toolkit for 3D Cell Culture and Extrusion Bioprinting“, *Bioengineering*, vol. 5, no. 3, p. 55, 07/2018.
- [192] Q. Zou, S. M. Habermann-Rottinghaus, and K. P. Murphy, „Urea effects on protein stability: Hydrogen bonding and the hydrophobic effect“, *Proteins: Structure, Function, and Genetics*, vol. 31, no. 2, pp. 107–115, 05/1998.
- [193] M. C. Stumpe and H. Grubmüller, „Interaction of Urea with Amino Acids: Implications for Urea-Induced Protein Denaturation“, *Journal of the American Chemical Society*, vol. 129, no. 51, pp. 16 126–16 131, 12/2007.
- [194] A. Das and C. Mukhopadhyay, „Urea-Mediated Protein Denaturation: A Consensus View“, *The Journal of Physical Chemistry B*, vol. 113, no. 38, pp. 12 816–12 824, 09/2009.
- [195] B. Lee, N. Lum, L. Seow, P. Lim, and L. Tan, „Synthesis and Characterization of Types A and B Gelatin Methacryloyl for Bioink Applications“, *Materials*, vol. 9, no. 10, p. 797, 09/2016.
- [198] J. W. Nichol, S. T. Koshy, H. Bae, C. M. Hwang, S. Yamanlar, and A. Khademhosseini, „Cell-laden microengineered gelatin methacrylate hydrogels“, *Biomaterials*, vol. 31, no. 21, pp. 5536–5544, 07/2010.
- [199] C. D. O’Connell *et al.*, „Tailoring the mechanical properties of gelatin methacryloyl hydrogels through manipulation of the photocrosslinking conditions“, *Soft Matter*, vol. 14, no. 11, pp. 2142–2151, 2018.
- [200] S. Krishnamoorthy, B. Noorani, and C. Xu, „Effects of Encapsulated Cells on the Physical–Mechanical Properties and Microstructure of Gelatin Methacrylate Hydrogels“, *International Journal of Molecular Sciences*, vol. 20, no. 20, p. 5061, 10/2019.
- [201] J. Ricka and T. Tanaka, „Swelling of ionic gels: quantitative performance of the Donnan theory“, *Macromolecules*, vol. 17, no. 12, pp. 2916–2921, 12/1984.
- [202] M.-Y. Shie, J.-J. Lee, C.-C. Ho, S.-Y. Yen, H. Y. Ng, and Y.-W. Chen, „Effects of Gelatin Methacrylate Bio-ink Concentration on Mechano-Physical Properties and Human Dermal Fibroblast Behavior“, *Polymers*, vol. 12, no. 9, p. 1930, 08/2020.
- [206] J. Kunkel and P. Asuri, „Function, Structure, and Stability of Enzymes Confined in Agarose Gels“, *PLoS ONE*, vol. 9, no. 1, P. K. Agarwal, Ed., e86785, 01/2014.
- [207] M. C. Gutiérrez *et al.*, „Hydrogel scaffolds with immobilized bacteria for 3D cultures“, *Chemistry of Materials*, vol. 19, no. 8, pp. 1968–1973, 2007.
- [208] T. Takei, K. Ikeda, H. Ijima, and K. Kawakami, „Fabrication of poly(vinyl alcohol) hydrogel beads crosslinked using sodium sulfate for microorganism immobilization“, *Process Biochemistry*, vol. 46, no. 2, pp. 566–571, 2011.
- [209] S. V. Murphy and A. Atala, „3D bioprinting of tissues and organs“, *Nature Biotechnology*, vol. 32, no. 8, pp. 773–785, 08/2014.
- [210] D. Grijalva Garces, C. P. Radtke, and J. Hubbuch, „A Novel Approach for the Manufacturing of Gelatin-Methacryloyl“, *Polymers*, vol. 14, no. 24, p. 5424, 12/2022.
- [211] L. Sewald *et al.*, „Beyond the Modification Degree: Impact of Raw Material on Physicochemical Properties of Gelatin Type A and Type B Methacryloyls“, *Macromolecular Bioscience*, vol. 18, no. 12, pp. 1–10, 2018.
- [212] S. Pahoff, C. Meinert, O. Bas, L. Nguyen, T. J. Klein, and D. W. Hutmacher, „Effect of gelatin source and photoinitiator type on chondrocyte redifferentiation in gelatin methacryloyl-based tissue-engineered cartilage constructs“, *Journal of Materials Chemistry B*, vol. 7, no. 10, pp. 1761–1772, 2019.
- [213] A. T. Young, O. C. White, and M. A. Daniele, „Rheological Properties of Coordinated Physical Gelation and Chemical Crosslinking in Gelatin Methacryloyl (GelMA) Hydrogels“, *Macromolecular Bioscience*, vol. 20, no. 12, pp. 1–15, 12/2020.
- [214] H. Tavassoli, S. N. Alhosseini, A. Tay, P. P. Chan, S. K. Weng Oh, and M. E. Warkiani, „Large-scale production of stem cells utilizing microcarriers: A biomaterials engineering perspective from academic research to commercialized products“, *Biomaterials*, vol. 181, pp. 333–346, 10/2018.
- [215] R. Samanipour, Z. Wang, A. Ahmadi, and K. Kim, „Experimental and computational study of microfluidic flow-focusing generation of gelatin methacrylate hydrogel droplets“, *Journal of Applied Polymer Science*, vol. 133, no. 29, p. 43 701, 08/2016.
- [216] N. Leister, C. Yan, and H. P. Karbstein, „Oil Droplet Coalescence in W/O/W Double Emulsions Examined in Models from Micrometer- to Millimeter-Sized Droplets“, *Colloids and Interfaces*, vol. 6, no. 1, p. 12, 02/2022.

- [217] M. V. Bandulasena, G. T. Vladislavljević, and B. Benyahia, „Versatile reconfigurable glass capillary microfluidic devices with Lego® inspired blocks for drop generation and micromixing“, *Journal of Colloid and Interface Science*, vol. 542, pp. 23–32, 2019.
- [218] B. H. Leuenberger, „Investigation of viscosity and gelation properties of different mammalian and fish gelatins“, *Topics in Catalysis*, vol. 5, no. 4, pp. 353–361, 1991.
- [219] E. Van Den Bosch and C. Gielens, „Gelatin degradation at elevated temperature“, *International Journal of Biological Macromolecules*, vol. 32, no. 3-5, pp. 129–138, 2003.
- [220] H. Münstedt and F. R. Schwarzl, *Deformation and Flow of Polymeric Materials*. Berlin/Heidelberg, Germany: Springer Berlin Heidelberg, 2014.
- [221] D. Loessner *et al.*, „Functionalization, preparation and use of cell-laden gelatin methacryloyl-based hydrogels as modular tissue culture platforms“, *Nature Protocols*, vol. 11, no. 4, pp. 727–746, 2016.
- [222] A. Duconseille, D. Andueza, F. Picard, V. Santé-Lhoutellier, and T. Astruc, „Variability in pig skin gelatin properties related to production site: A near infrared and fluorescence spectroscopy study“, *Food Hydrocolloids*, vol. 63, pp. 108–119, 2017.
- [223] J. Olijve, F. Mori, and Y. Toda, „Influence of the molecular-weight distribution of gelatin on emulsion stability“, *Journal of Colloid and Interface Science*, vol. 243, no. 2, pp. 476–482, 2001.
- [224] J. O’Sullivan, B. Murray, C. Flynn, and I. Norton, „The effect of ultrasound treatment on the structural, physical and emulsifying properties of animal and vegetable proteins“, *Food Hydrocolloids*, vol. 53, pp. 141–154, 02/2016.
- [225] T. F. Tadros, *Volume 2 Interfacial Phenomena and Colloid Stability, Industrial Applications*. Berlin, Germany: De Gruyter, 12/2015.
- [226] E. Hoch, C. Schuh, T. Hirth, G. E. Tovar, and K. Borchers, „Stiff gelatin hydrogels can be photo-chemically synthesized from low viscous gelatin solutions using molecularly functionalized gelatin with a high degree of methacrylation“, *Journal of Materials Science: Materials in Medicine*, vol. 23, no. 11, pp. 2607–2617, 2012.
- [227] F. P. Melchels, W. J. Dhert, D. W. Hutmacher, and J. Malda, „Development and characterisation of a new bioink for additive tissue manufacturing“, *Journal of Materials Chemistry B*, vol. 2, no. 16, pp. 2282–2289, 2014.
- [228] Y. Yang, T. Xu, Q. Zhang, Y. Piao, H. P. Bei, and X. Zhao, „Biomimetic, Stiff, and Adhesive Periosteum with Osteogenic–Angiogenic Coupling Effect for Bone Regeneration“, *Small*, vol. 17, no. 14, pp. 1–10, 04/2021.
- [229] C. Colosi *et al.*, „Microfluidic Bioprinting of Heterogeneous 3D Tissue Constructs Using Low-Viscosity Bioink“, *Advanced Materials*, vol. 28, no. 4, pp. 677–684, 01/2016.
- [230] S. Halonen, T. Kangas, M. Haataja, and U. Lassi, „Urea-Water-Solution Properties: Density, Viscosity, and Surface Tension in an Under-Saturated Solution“, *Emission Control Science and Technology*, vol. 3, no. 2, pp. 161–170, 06/2017.
- [231] J. Guerrero, Y.-W. Chang, A. A. Fragkopoulos, and A. Fernandez-Nieves, „Capillary-Based Microfluidics—Coflow, Flow-Focusing, Electro-Coflow, Drops, Jets, and Instabilities“, *Small*, vol. 16, no. 9, p. 1904344, 03/2020.
- [232] A. S. Utada, A. Fernandez-Nieves, H. A. Stone, and D. A. Weitz, „Dripping to jetting transitions in coflowing liquid streams“, *Physical Review Letters*, vol. 99, no. 9, pp. 1–4, 2007.

5

Analytics in Extrusion-Based Bioprinting: Standardized Methods Improving Quantification and Comparability of the Performance of Bioinks

Svenja Strauß^{1,2*}, David Grijalva Garces^{1,2*} and Jürgen Hubbuch^{1,2}

¹ Institute of Functional Interfaces, Karlsruhe Institute of Technology (KIT), Eggenstein-Leopoldshafen, Germany

² Institute of Engineering in Life Sciences, Section IV: Biomolecular Separation Engineering, Karlsruhe Institute of Technology (KIT), Karlsruhe, Germany

* Contributed equally

Abstract

Three-dimensional bioprinting and especially extrusion-based printing as a most frequently employed method in this field is constantly evolving as a discipline in regenerative medicine and tissue engineering. However, the lack of relevant standardized analytics does not yet allow an easy comparison and transfer of knowledge between laboratories regarding newly developed bioinks and printing processes. This work revolves around the establishment of a standardized method, which enables the comparability of printed structures by controlling for the extrusion rate based on the specific flow behavior of each bioink. Furthermore, printing performance was evaluated by image-processing tools to verify the printing accuracy for lines, circles, and angles. In addition, and complementary to the accuracy metrics, a dead/live staining of embedded cells was performed to investigate the effect of the process on cell viability. Two bioinks, based on alginate and gelatin methacryloyl, which differed in 1% (w/v) alginate content, were tested for printing performance. The automated image processing tool reduced the analytical time while increasing reproducibility and objectivity during the identification of printed objects. During evaluation of the processing effect of the mixing of cell viability, NIH 3T3 fibroblasts were stained and analyzed after the mixing procedure and after the extrusion process using a flow cytometer, which evaluated a high number of cells. It could be observed that the small increase in alginate content made little difference in the printing accuracy but had a considerably strong effect on cell viability after both processing steps.

5.1 Introduction

Artificially generated scaffolds loaded with cellular material in the field of tissue engineering find their application as implants to replace damaged tissue and as models to study diseases or the effect of active compounds [233, 234]. In this context, hydrogels are commonly employed, as these biomaterials form a highly swollen network in the aqueous phase resembling the physical structure of the extracellular matrix [181]. The biochemical composition of such tissue analog can be formulated according to the specific application. Therefore, naturally derived polymers, such as polysaccharides, e.g., alginate and hyaluronic acid, as well as proteins, e.g., collagen and gelatin, are suitable components [235]. Biofabrication methods, such as three-dimensional (3D) bioprinting, have gained attention in this field, as a wide range of material compositions can be used, and the method is relatively easy to scale-up [38]. So-called bioinks are produced for this purpose, which comprise polymer solutions with embedded cells [167]. Extrusion-based bioprinting (EBB) processes have to fulfill several requirements for the layer-by-layer generation of 3D structures intended for the application as tissue analogs. From the structural point of view, predefined geometries, which can be traced back to a series of simple structures that are stacked on top of each other, have to be produced accurately. In the final stages, the bioinks should retain the fabricated shape. During and after the printing process, high cell viability has to be maintained as the cells undergo mechanical stress during the process. The created network must support both vascularization and metabolic activities during cell culture. Meeting the structural and biological requirements has been accepted as a compromise. This is because parameters that increase the stability of printed scaffolds have a negative impact on cell viability, as those increase shear stress [234, 236, 237]. Although the rheological characterization of bioinks is a standard in bioprinting, the gained information is rarely exploited in the settings of printing parameters [138, 238, 239]. The common systematics of printability studies relies on a constant pneumatic pressure and/or printing speed while using different bioink compositions [138,

240, 241], and no relationship between those parameters is presented. Other studies simply set the printing parameters for each tested bioink in a rather arbitrary manner [195, 239]. Furthermore, the aforementioned approaches may result in unequal amounts of extruded material since the rheological properties of the bioinks depend on the polymer content and the type of polymer. Therefore, such methodologies do not allow an adequate comparison of the structural characteristics from the printed scaffolds based solely on the material properties. This issue was addressed in the review by Gillispie *et al.* [172]. Furthermore, methodologies for the evaluation of printed structures are lacking standards as well. Methods in that field consist of the manual extraction of the metrics of the produced structures [178, 179, 242–244]. Such methods are prone to observer-dependent errors and are not reproducible. One possible post-printing analysis method circumventing this drawback is automated image analysis. This method shows the advantages of automation, leading to higher reproducibility as well as objectivity. In addition, images and extracted data undergo long-term storage. These methods are well established for quality control in production processes [245, 246]. There have been advances in the image analysis field, but workflows still include several manual observer-dependent steps [243]. The determination of cellular viability mostly consists of evaluation of images acquired by microscopy. On the one hand, specific characteristics, such as the morphology and size of the cells can be extracted from the images, but on the other hand, the images represent only a small portion of the printed structure. Studies in the field are limited to a low number of cells in the range of hundreds of cells [185, 247]. The reproducibility as well as the significance of the results regarding cell viability can be increased by the implementation of automated image processing workflows, as well [204, 248]. A further option to quantify several thousand cells is flow cytometry as already tested in a few studies in the field [148, 249]. The lack of standardized printing methodologies as well as techniques for the evaluation of the printing performance of bioinks presents a limitation in the development of formulations as a comparison within and between laboratories.

In this work, we aim to establish robust and objective methods for the evaluation of the printing performance of biomaterial inks and bioinks. The rheological properties of two biomaterial inks were characterized in order to determine the relationship between the printing speed and pneumatic pressure of each biomaterial ink and, therefore, control the flow rate within experiments. The assessment of the printing performance considered the accuracy of printing single-layer structures, i.e., lines, circles, and angles. For this purpose, automated image processing workflows were developed to extract geometrical features from the produced structures. The developed tools were used in order to characterize the effect of the bioink composition as well as the presence of cells on the resulting geometry. As a second part of the investigation of the printing performance, the viability of cells embedded in the bioink was determined directly after the mixing step and after bioprinting via staining and data acquisition by means of flow cytometry.

5.2 Materials and Methods

5.2.1 Cell Culture

NIH 3T3 mouse fibroblasts (CLS Cell Lines Service GmbH, Eppelheim, Germany) were incubated in Dulbecco's Modified Eagle Medium (DMEM, high glucose, GlutaMAX™) supplemented with 10% (w/v) fetal bovine serum (FBS), 50 U mL⁻¹ penicillin, and 50 µg mL⁻¹ streptomycin. Cell culture media and supplements were acquired from Gibco™ (Thermo Fisher Scientific, Waltham, MA, USA). Fibroblasts were cultured in tissue culture (TC) flasks at 37 °C in a humidified atmosphere containing 5% CO₂. Cells were passaged upon reaching 70 to 80% confluency.

5.2.2 Biomaterial Ink and Bioink Preparation

Gelatin methacryloyl (GelMA) was produced from Type A Gelatin (300 bloom strength, Sigma-Aldrich, St. Louis, MO, USA) according to the method published by Grijalva Garces *et al.* [210]. The degree of functionalization of used GelMA was 65 % determined by the method by Habeeb [122]. Alginic acid sodium salt was obtained from Sigma-Aldrich (A2033, from brown algae). The adequate quantities of biomaterial were dissolved in Dulbecco's Phosphate Buffered Saline (DPBS, without calcium and magnesium, Thermo Fisher Scientific) and mixed at 3500 rpm for 5 min in a SpeedMixer® (Hauschild GmbH & Co. KG, Hamm, Germany). The biomaterial ink was filled directly to a final volume of 3 mL into 10 mL cartridges (Nordson Corporation, Westlake, OH, USA) for cell-free printing. Not all formulations employed in this study contained cells, which is why they are referred to as 'biomaterial inks' instead of 'bioink' for the sake of clarity. Alginic acid and GelMA solutions for the cell-containing experiments were prepared as mentioned above. However, the initial concentration was higher, taking into account the dilution of the biomaterial ink after the mixing of the cell suspension with the cell-free biomaterial ink. The concentrated biomaterial ink was transferred to 5 mL syringes (B. Braun SE, Melsungen, Germany). Cells were harvested from the TC flasks with trypsin/ethylenediaminetetraacetic acid (Gibco™), centrifuged at 300 rcf for 5 min, and resuspended in 150 μ L fresh DPBS. Subsequently, the cell suspension was transferred into 3 mL syringes (B. Braun). The syringe filled with biomaterial ink and the cell-containing syringe were connected via a Luer-Lock adapter and mixed by pushing five times back and forth between both syringes. The cell-laden bioink was then loaded into the 10 mL cartridges for printing and sealed with pneumatic pistons (Nordson Corp.). The first formulation was prepared with 3 % (w/v) alginate and with 3 % (w/v) GelMA (A3G3), the second 4 % (w/v) alginate and 3 % (w/v) GelMA (A4G3). The final cell count was set to 2×10^6 cells mL⁻¹ for the bioinks. A summary of the formulations with the respective components is shown in Table 5.1.

Table 5.1 Biomaterial ink compositions as employed in this study and abbreviations used throughout this work. Power law exponent and consistency index according to the Ostwald–de Waele relationship were determined as mentioned in Section 5.2.3 and used for the calculation of the specific pneumatic pressure for printing performance experiments.

Abbr.	Alginate (% (w/v))	GelMA (% (w/v))	Power Law Exponent n	Consistency Index K (Pa s ^{n})	Pneumatic Pressure (kPa)
A3G3	3	3	0.35	146.39	80.5
A4G3	4	3	0.32	284.09	129.1

5.2.3 Rheological Characterization

The rheological behavior of the polymer solutions was characterized based on the shear rate-dependent viscosity. For this purpose, a rotational rheometer Physica MCR301 (Anton Paar GmbH, Graz, Austria) with a cone-plate geometry (diameter 25 mm, cone angle 1°) was used. Additionally, a solvent trap was used to prevent the sample drying during measurements. The viscosity of both cell-free formulations, i.e., A3G3 and A4G3, was determined as a function of the shear rate in the range of 1×10^{-1} to 1×10^3 s⁻¹. The data of the viscous behavior were fitted according to the Ostwald–de Waele relationship, and the values of the power law exponent n and the consistency index K were determined for this model using Origin 2021 (OriginLab Corporation, Northampton,

MA, USA). The rheological characterization was carried out as three biological replicates ($n = 3$) with a set of three technical triplicates ($n = 3$) each, resulting in data sets of nine replicates. For each biological replicate, an independently prepared solution was used.

In order to control the extrusion rate, i.e., the deposited material amount, the Ostwald–de Waele relationship was coupled with the Hagen–Poiseuille equation for the volumetric flow rate Q through a cylindrical capillary, see Equation (5.1), where R and l represent the capillary radius and length, respectively. The geometric variables of the capillary were taken according to the nozzle (inner diameter 0.61 mm, length 12.7 mm, Nordson Corp.) intended for the printing process. For evaluation of the printing accuracy in Section 5.2.4.1, the printing speed was set equal to the mean velocity \bar{v} during extrusion at 10 mm s^{-1} , and the required pneumatic pressure p was calculated. The pneumatic pressures used for printing of both formulations are given in Table 5.1.

$$Q = \bar{v} \pi R^2 = \frac{n\pi}{3n+1} \left(\frac{R^{3n+1} p}{2 K l} \right)^{1/n} \quad (5.1)$$

5.2.4 Printing Performance Evaluation

A key aspect of bioprinting is the reproducibility and accurate fabrication of scaffolds while maintaining a high viability of the cells within the bioink. Therefore, the characterization of the printing performance consists of two parts, namely, the assessment of the printing accuracy, where the printed structures were compared to the predefined computer-aided design (CAD) model, and the determination of the living and dead cell counts after the extrusion process via fluorescent staining.


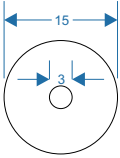
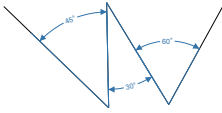
All printing and extrusion experiments were performed with a BioScaffolder 3.1 bioprinter (GeSiM mbH, Radeberg, Germany). The cartridge with the attached stainless-steel nozzle (inner diameter 0.61 mm, length 12.7 mm, Nordson Corp.) was placed on the holder and connected to the air supply. The structures were printed on glass microscopy slides with a distance of 0.5 mm to the nozzle tip. The applied pneumatic pressures were calculated as mentioned in Section 5.2.3. The specific values are listed in Table 5.1. The applied pressure was verified beforehand with a barometer Go Direct® (Vernier Software & Technology, Beaverton, OR, USA), and adjusted, if required.

5.2.4.1 Printing Accuracy Assessment

The aim of the printing accuracy assessment was to find out how accurately the printed structure matches the CAD model. Three single-layer structures, namely a line, a circle, and an object consisting of multiple angles, were printed, imaged, and analyzed. An overview of the objects with corresponding dimensions is given in Table 5.2.

Each structure was printed as a set of 3 biological replicates ($n = 3$) and 8 technical replicates ($n = 8$) resulting in total in 24 objects per bioink and biomaterial ink. The biological replicates of the cell-free experiments consisted of independently prepared biomaterial inks. For the bioinks, cells were additionally harvested directly prior to the mixing step from independent TC flasks. Each object was printed on glass microscope slides. Immediately after printing, each object was individually photographed. For image acquisition, a monochrome camera (DALSA GENIE NANO-M2420, Stemmer Imaging AG, Puchheim, Germany) with 52 pixel/mm was used. The object was placed on a slide on a black background and illuminated with a white light-emitting diode

Table 5.2 Graphic models of the printing path. Images of the printed objects are taken and analyzed as a part of the printing accuracy assessment. The dimensions in the line and circle sketches are given in millimeter (mm), the dimensions in the angle sketch in degrees ($^{\circ}$). Each structure was examined for characteristic parameters, which are shown with the respective formulae for calculation.

Structure	Evaluation Parameter	Formula/Equation
Line 	normalized width	$w_n = \frac{w}{d_{nozzle}}$ (2)
	normalized length	$l_n = \frac{l}{l_{model}}$ (3)
Circle 	normalized width	see Equation (2)
	normalized radii to midline	$r_n = \frac{r_i + r_o}{2r_{model}}$ (4)
Angle 	normalized width	see Equation (2)
	normalized angle to midline	$\alpha_n = \frac{\alpha_i + \alpha_o}{2\alpha_{model}}$ (5)

(LED) ring light (CCS HPR2-150 SW, Stemmer Imaging AG). In order to obtain an objective quantification of the printed geometries, an image processing workflow was developed using Matlab[®] R2022a (TheMathWorks Inc., Natick, MA, USA). In a first step, all images were binarized using local thresholding algorithms. Therefore, each pixel was replaced by the median value of the 3-by-3 surrounding pixels. The image processing workflow is shown schematically in Figure 5.1. Subsequently, the binary images were cropped to the region of interest depending on the structure. From then on, the objects were segmented, and images were evaluated for the specific structure characteristics.

The parameters extracted based on the image files are also listed in Table 5.2. The accuracy of printing all three geometries was evaluated by the normalized width w_n , i.e., the filament width w divided by the diameter of the nozzle. In the case of the line geometry, the filament width was calculated as the mean pixel count along the line. The filament width of the printed circles was measured at 180° from the starting point and 2% of the circle was evaluated. The line width of the angle composite structure was determined at five different points along the printed structure.

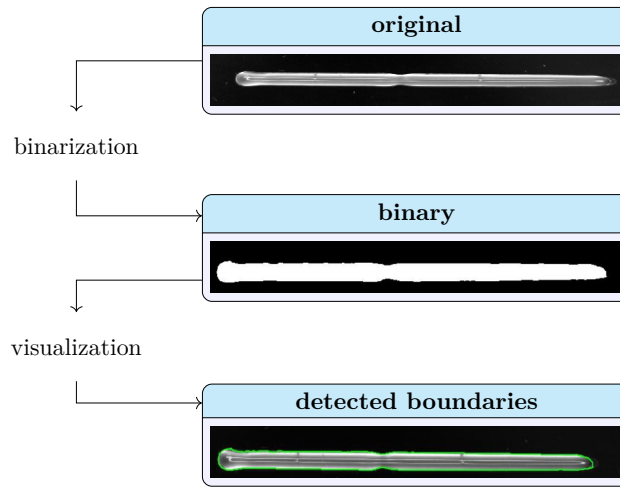


Figure 5.1 Exemplary representation of the object recognition. The original image (**top**) is binarized using local thresholding algorithms (**middle**), and an overlay with the detected boundaries of the identified structure on the original image was created as a visual control (**bottom**).

The analysis of the line also included the normalized length l_n . Therefore, the length of the line l was divided by the length of the CAD model of 30 mm. The assessment of the accuracy of the printed circles and angle composite structures was performed by including a midline as a reference and by combining the inner and outer boundaries of the structure into a single parameter. The midline represents the center of the nozzle, i.e., the axis of movement of the printer equipment. In the case of the circles, the normalized radii to midline r_n were calculated as the sum of inner radius r_i and outer radius r_a detected on the binary image divided by two times the circle radius, i.e., 15 mm as designed in CAD. The 3 mm diameter circle was needed solely as a starting point for the image processing workflow. The angle composite structure was evaluated by the normalized angle α_n . This parameter was calculated as the sum of each inner angle α_i and outer angle α_o of the boundaries on the binary image divided by two times the corresponding angle on the CAD file.

5.2.4.2 Effect of Processing on Cell Viability

A high cell viability is essential throughout the manufacturing process of cell-loaded scaffolds. The effect of processing on the cell viability was determined after a mixing step and after extrusion. The analytical methodology for the determination of the cell viability is schematically shown in Figure 5.2.

The bioink was prepared as mentioned in Section 5.2.2. Three fractions were collected after mixing, weighed, and subsequently diluted 20-fold by weight with DPBS. Similarly, the bioink was extruded as three fractions, which were diluted with DPBS, as well. Fluorescent stains were added to the diluted bioink to a final concentration of 0.1 μM calcein-AM and 1.5 μM propidium iodide (PI); both stains were purchased from Invitrogen (Thermo Fisher Scientific). The samples were analyzed after an incubation of 15 min at room temperature. Data acquisition was performed with a MACSQuant[®] Analyzer 10 flow cytometer (Miltenyi Biotec B.V. & Co. KG, Bergisch Gladbach, Germany) at 100 mL min⁻¹. The acquired data were gated using FlowJo (Becton, Dickinson &

Company, Ashland, OR, USA). This step was used to exclude debris and agglomerates. The distinction between live and dead cells was based on the green and red signals, respectively. Dead cells were gated using a control sample with fixated and permeabilized cells before staining with PI. For fixation, the cells were resuspended in a 3.7% (v/v) paraformaldehyde (AppliChem GmbH, Darmstadt, Germany) in DPBS solution and incubated for 10 min. After a wash step with DPBS, the cells were permeabilized with a 0.1% (v/v) Triton-X (Sigma-Aldrich) in DPBS solution for 15 min. Then, a further wash step proceeded. Fixation and permeabilization were performed at room temperature. The experiment to monitor the effect of the extrusion process on the cells consisted of three biological replicates ($n = 3$); therefore, independently prepared polymer solutions were used. Additionally, cells were harvested directly prior to the mixing step from a separate TC flask. Each fraction of diluted bioink containing stained cells ($n = 3$) was analyzed as technical triplicates ($n = 3$) resulting in data sets of 27 values. The processing steps and the subsequent determination of cell viability were completed before starting a new biological replicate. The cell viability was calculated as the number of viable cells divided by the total number of cells, i.e., both viable and dead cells present in a single technical replicate. The analytical methodology for the determination of the cell viability is schematically shown in Figure 5.2.

5.2.5 Data Handling and Statistical Analysis

Data evaluation, image processing, data visualization, and statistical analysis were performed with Matlab[®] R2022a (TheMathWorks Inc., Natick, MA, USA). Errors related to the calculated parameters were determined after the first-order Taylor series method for uncertainty propagation. The normal distribution of data sets was verified using the Jarque–Bera test with an α -value set to 0.05. A one-way analysis of variance (ANOVA) was carried out in order to find significant differences, and a p -value below 0.05 was classified as statistically significant.

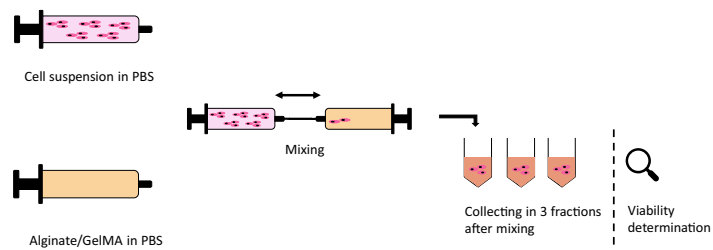
5.3 Results and Discussion

5.3.1 Rheological Characterization

The rheological behavior of the bioink has a great influence on the process as the biomaterial flows through a nozzle and induces stress on the embedded cells. Hence, the viscosity was determined for the cell-free biomaterial inks A3G3 and A4G3 as a function of the shear rate in the range of 1×10^{-1} to $1 \times 10^3 \text{ s}^{-1}$. Figure 5.3 provides the associated results.

Both biomaterial inks showed a similar non-Newtonian behavior at different magnitudes. The course of the viscosity functions showed a plateau at the low range of the shear rate and a shear thinning regime with an increasing shear rate. The viscosity plateaus had values of about 150 Pa s, and 300 Pa s for biomaterial inks A3G3 and A4G3, respectively. The shear thinning regime was fitted using the Ostwald–de Waele relationship to better describe the behavior of the biomaterial inks during extrusion. The power law exponent n and the consistency index K are listed in Table 5.1. The increase in viscosity of A4G3 by a factor of up to 1.9 in comparison to the viscosity of A3G3 can be explained by the higher content of alginate in solution, as a higher amount of water is bound and the entanglement of polymers increases with concentration [220]. In order to set an equal flow rate for both formulations during extrusion, the determined fitting parameters were used to calculate the required pneumatic pressure according to the Hagen–Poiseuille equation shown in Equation (5.1). The results are listed in Table 5.1. The pressure for the extrusion experiments of

(A) Effect of processing on cell viability after mixing



(B) Effect of processing on cell viability after extrusion

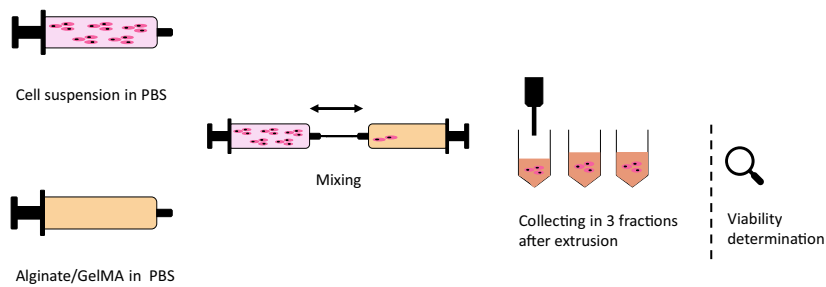


Figure 5.2 Schematic of the workflow applied for the determination of the processing effects on cell viability. A biological replicate consisted of cells harvested independently and mixed with the biomaterial ink. In (A), the processing ended after mixing the cellular material into the biomaterial ink, which was collected in three fractions. In (B), the processing of the bioink consisted of mixing it with the cell suspension and extrusion with the printer. The extruded bioink was collected in three fractions. Each collected fraction was diluted separately before cellular staining and data acquisition with a flow cytometer. Three biological replicates of each process were performed; therefore, each biological replicate was completed before starting the next replicate.

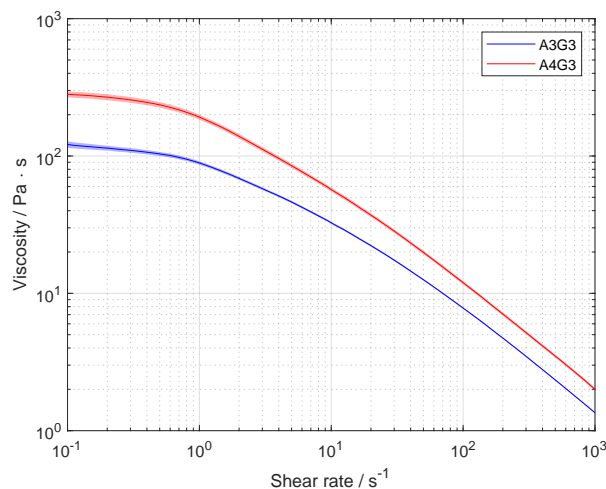


Figure 5.3 Rheological characterization of biomaterial inks A3G3 and A4G3. Viscosity is shown as a function of the shear rate. The results are presented as mean values, the shaded areas, the standard deviation. Each formulation was prepared separately for three times ($n = 3$), and three technical replicates were tested ($n = 3$) from each batch, resulting in data sets of nine values.

the A3G3 biomaterial ink was 80.5 kPa. A higher pressure with a value of 129.1 kPa was required for the extrusion of A4G3 due to the higher viscosity of the biomaterial ink.

5.3.2 Printing Performance

5.3.2.1 Printing Accuracy Assessment

As part of the printing performance studies, printing accuracy was evaluated as the deviation from the set printing path, taking into account the 0.61 mm nozzle diameter as well. Line, circle, and angle structures were printed and characterized by the respective geometrical features. The printed structures and evaluation parameters are presented in Table 5.2. For all results in this section, every structure was printed as a set of 3 biological replicates ($n = 3$) and 8 technical replicates ($n = 8$), resulting in a total of 24 objects per biomaterial ink and bioink. The differences between evaluation parameters were examined for statistical significance. Each bar represents the mean value with the respective standard deviation for one of the four formulations.

In Figure 5.4(A), the normalized width in relation to the nozzle diameter for each formulation is shown. The highest normalized width was found for A4G3 without cells with a value of 1.58 ± 0.11 , the lowest for A3G3 without cells with a value of 1.48 ± 0.17 . Higher standard deviations are shown by the bioinks with values of 0.24 and 0.28 for the A3G3 and A4G3 formulations, respectively. The normalized width of biomaterial inks did not differ significantly. Similarly, the difference between cell-containing bioinks was not significant either. A statistical significance was observed between A3G3 without cells and A4G3 with cells. All determined values are higher than 1, as the filament thickness increases after exiting the nozzle, due to the elastic properties of polymer solutions [220]. The distances between the nozzle tip and printing surface also influence the filament width, as was shown by Habib *et al.* [240]. In this study, the distance was set to 0.5 mm in order for the filament to adhere to the glass surface, thus leading to thicker filaments than nozzle. In general, it is expected

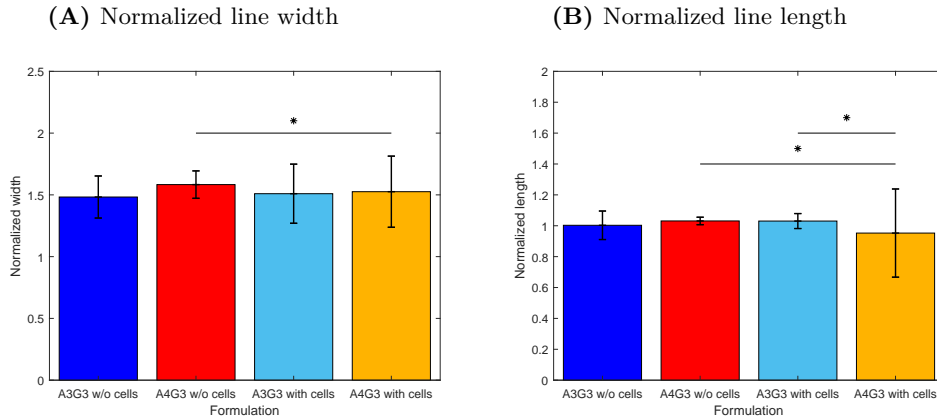


Figure 5.4 Printing accuracy study line structure. In (A), the normalized line width is shown, and in (B), the normalized line length. For all four formulations, three biological replicates ($n = 3$) were produced, and eight technical replicates ($n = 8$) printed for each structure, resulting in a total of 24 objects, of which the mean is shown in a bar with the associated standard deviation. Significant differences are denoted with an asterisk ($p < 0.05$).

that the increasing viscosity of the bioink leads to thinner filaments as shown by other studies [179, 240, 242, 250]. The increasing printing pressure is also known to increase the filament width [240, 251]. In the presented study, the printing pressure was calculated according to the individual viscosity of each formulation in order to control the flow rate. The comparable normalized widths of both formulations can be attributed to the similar amount of material deposition. This approach increases the comparability of results, as printing parameters are objectively set on the basis of rheological data and not determined according to user-dependent impressions. Further methods to control the flow rate as performed by Wenger *et al.* [171] showed increasing reproducibility during extrusion-based bioprinting. The higher standard deviations shown by the cell-containing bioinks can be explained by air entrapment when the cells are mixed into the polymer solution between two syringes. This process is not reproducible, and air bubbles lead to inhomogeneity within the cartridge, resulting in fluctuations of the filament width. Air bubbles entrapped after the mixing steps have been addressed in the literature [172, 175, 204, 244]. The mentioned studies implement strategies by either mixing, using a spatula or centrifuge, the cartridges or syringes to remove the entrapped air. The first imposes a non-reproducible step, while the latter can lead to redistribution or even to complete sedimentation of the cells in the bioink. For future medical applications, it is a basic requirement to develop reproducible mixing processes [244, 252].

In Figure 5.4(B), the length of the printed lines normalized to the full length of the planned structure, i.e., 3 mm, is presented for all four formulations. The highest deviation from 1 and the highest standard deviation with a value of 0.95 ± 0.29 are shown by the bioink A4G3 containing cells. The length of the line of this bioink is significantly different than that of A3G3 without cells and A3G3 with cells. The sample set of printed lines of the A4G3 bioink containing cells includes four interrupted lines, and the cell-laden A3G3 bioink includes one interrupted structure, while both cell-free formulations could be printed to the full length. Values higher than 1 can be attributed to post-flow of the formulation after releasing the air pressure. The printing of non-continuous filaments can be attributed to heterogeneities in the printing cartridge that arise during the mixing

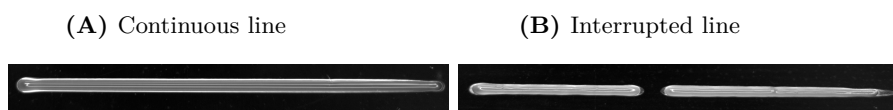


Figure 5.5 Exemplary raw images of printed lines with bioink A4G3 containing cells. In (A), a continuous and, in (B), an interrupted line is shown.

of cells by the two-syringe method as air is introduced into and entrapped in the mixture. Exemplary images of a continuous as well as an interrupted line are depicted in Figure 5.5.

The width of the filament in the printed circle was also determined, and was normalized to the nozzle diameter. The results are shown in Figure 5.6(A). The greatest deviation from 1 was measured for A3G3 without cells with a value of 1.62 ± 0.03 . A4G3 containing cells showed the lowest deviation with a value of 1.51 ± 0.03 . A statistically significance difference was found between both values. Comparing the normalized width of the bioinks containing cells, the values did not differ significantly. Similarly, no statistically significant differences were observed between the cell-free biomaterial inks. Figure 5.6(B) presents the normalized radii to the midline. This parameter offers the advantage of combining two parameters, namely the inner and outer radii. The midline corresponds to the printing path, i.e., the radius of the model. In the ideal case, the inner and outer radii of the filament overlap the path line \pm half nozzle diameter. Here, the comparability of the deviation is easier with one output. Similar to the normalized width of the printed circle, the largest deviation from 1 was measured for A3G3 without cells with a value of 1.02 ± 0.0008 , and the lowest, for A4G3 containing cells with a value of 1.01 ± 0.0007 . The radii normalized to the midline of both compositions differed significantly, as well.

The lack of differences between the normalized widths of formulations that differ in alginate content is explained by the selection of the printing pressure to set an equal flow rate for both biomaterial inks, as previously described. The standard deviations of the normalized width are smaller compared to the standard deviations of the width of the line structure. This is due to the fact that the width of the circle is measured at only a small portion of the filament, namely 2% of the circle at 180° from the starting point and, thus, measures fewer data points than the line structure, where the width is determined in the middle third. The higher values of the A3G3 can be explained by the lower viscosity of the A3G3 biomaterial ink, as bioinks tend to keep flowing after printing, especially as no crosslinking was performed after printing. All values are higher than 1 due to the elasticity of the polymer solution [220].

As a final part of this study, the accuracy of printed angles was characterized by means of the normalized filament width and the normalized angle to the midline. The corresponding data are shown in Figure 5.7(A), (B), respectively. The printed structure consisted of a continuous structure with angles of 30° , 45° , and 60° . Considering the normalized filament width, the highest deviation from 1 was observed for the A3G3 without cells with a value of 1.74 ± 0.02 . The lowest normalized width was produced with A4G3 containing cells with a value of 1.62 ± 0.01 . No statistically significant differences between the normalized filament widths were proven between any of the tested formulations. As previously explained, there are no differences in printing accuracy due to the normalization of the volumetric flow rate.

Comparing the normalized width of the filament determined in the angle structure to the normalized width of the simple line structure, it is noteworthy that the standard deviation of the first is lower than that of the latter. The reason lies in the analytical method itself since the width of

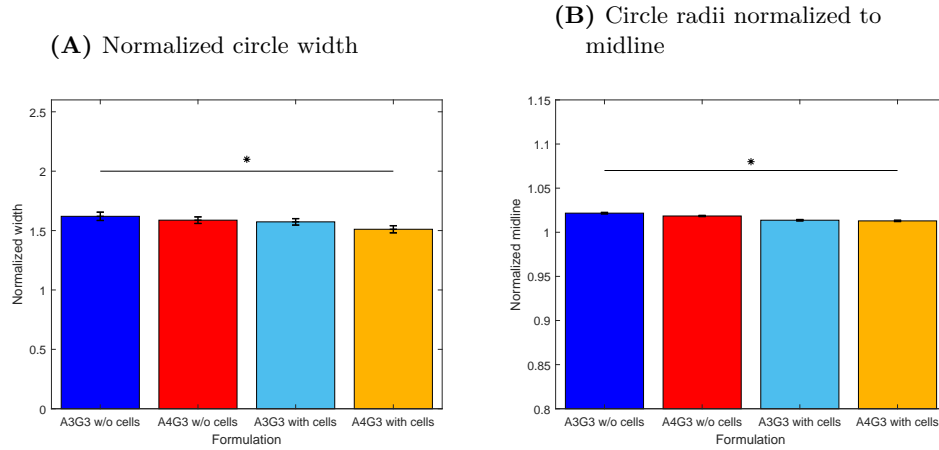


Figure 5.6 Printing accuracy study for the circle structure. In **(A)**, the normalized line width is shown, and in **(B)**, the normalized radius to the midline. For all four formulations, three biological replicates ($n = 3$) were produced and eight technical replicates ($n = 8$) printed for each structure resulting in total in 24 objects, of which the mean is shown in a bar with the associated standard deviation. Significant differences are denoted with an asterisk ($p < 0.05$).

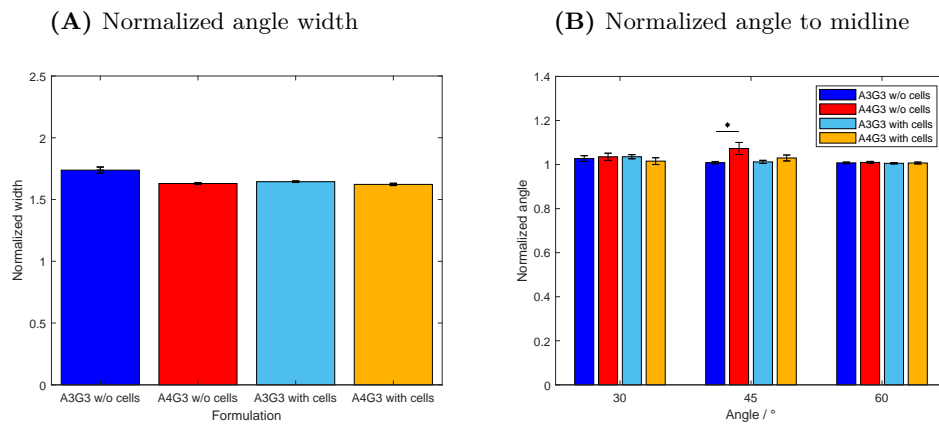


Figure 5.7 Printing accuracy study for the angle structure. In **(A)**, the normalized line width is shown and, in **(B)**, the normalized angle to the midline. For all four formulations, three biological replicates ($n = 3$) were produced, and eight technical replicates ($n = 8$) printed for each structure, resulting in a total of 24 objects, of which the mean is shown in a bar with the associated standard deviation. Significant differences are denoted with an asterisk ($p < 0.05$).

the filament of the angle structure was measured at five points along the whole structure. This data set is smaller compared to the data set used to determine the filament width along the line structure at every pixel of the evaluated section of the image. The quantification along the angle structure is less accurate, but the output serves as a rough estimate to compare whether the more complex movement of the print head has an effect on the produced structure. During the angle analysis shown in (B), the inner and outer angles were again combined together to one parameter; hence, the angles were normalized to the angle of the trajectory of the print head. The cell-free A4G3 showed the highest deviation from 1 with a value of 1.07 ± 0.03 overall. There were no significant differences between the normalized angles of all four formulations printed as a 30° angle. Similarly, no effect of the formulation on the normalized angle was observed while printing 60° angles. By comparing the 45° angle, the values of the biomaterial inks A3G3 and A4G3, both without cells, differed significantly. The differences can be explained by the different alginate concentrations, as the bioinks tend to keep flowing after printing. The analysis of the printed angles was performed with an automated image processing workflow. There have been similar studies regarding printing and characterizing angular structures by He *et al.* [177] and Naghieh *et al.* [92]. Both studies state the importance of characterizing such angular patterns, as these simple patterns build up the bases of printed structures of higher complexity. However, the studies fail to give precise information on the estimation of the angles, which is a basic requirement for the standardization of processes.

It must be noted that the air pressure acting on the cartridge and the set pressure of the printing software did not match. The air pressure was, therefore, controlled with a pneumatic sensor before printing processes were started. Especially when it comes to medical applications, it is a basic requirement for the construction of 3D bioprinters that they work reliably and that the air supply is stable and not affected by the position of the printhead. There is still great potential on the side of the bioprinter manufacturers that needs to be improved. The single-layer structures characterized in this study represent the starting point since later complex geometries can be broken down into them. Characterizing the first layer is important, as defects in the base layer can prevent all subsequent layers from adhering to it. Similarly, defects on the layer can lead to the collapsing of the structure, especially with an increasing amount on layers piling on top of the basis. Future studies should include the characterization of the effect of the amount of extruded material in top of the base layer. Additionally, the strategies should be developed for the evaluation of 3D structures using automated image processing. At the moment, image acquisition takes place externally and not within the bioprinting system online. It would be desirable in the future to integrate the camera into the bioprinter with a suitable and adaptable illumination setup, as the transparency of bioinks is an issue during image acquisition that is particularly important in the choice of lighting and background to reach enough contrast. Regarding image processing, local thresholding should be preferred so that as little information as possible is lost. Such an image processing step is of particular interest if even illumination cannot be performed. Even though there were slight limitations on the imaging methods, the field of bioprinting can benefit from the application of automated image processing and analysis. The presented method proved to be robust for printed object evaluation, as it saves analytical time and reduces observer-dependent errors.

The aim of bioprinting is the production of scaffolds with high accuracy. Simultaneously, the printing of bioinks should meet the requirement of maintaining high cell viability after this process, as shear stress can induce irreversible cell damage.

5.3.2.2 Effect of Processing on Cell Viability

Besides the printing accuracy, the effect of processing on cell viability after the mixing process and after the extrusion process was further studied. Here, three biological replicates for A3G3 with cells and A4G3 with cells were produced and analyzed. Each cartridge containing bioink was collected in three fractions. Each fraction was diluted with DPBS, and cells were stained in the resulting suspension. For the detection of fluorescent signals and, thus, the determination of cell viability, flow cytometry was used. Each diluted fraction was analyzed in technical triplicate. The respective results are presented in Figure 5.8. The bar chart shows the cell viability for both tested bioinks directly after the mixing step and after the extrusion process.

The increasing alginate content of the bioinks led to a decreasing cell viability. This effect was observed after the mixing step as well as after mixing and subsequent extrusion. The viability of cells mixed into the A3G3 formulation and into the A4G3 formulation showed a value of $96.3 \pm 4.9\%$, and $77.9 \pm 16.4\%$, respectively. Both values differed significantly. The viability of cells extruded within the A3G3 bioink was slightly reduced to $95.3 \pm 3.0\%$. However, the difference was not statistically significant. Considering cells in the A4G3 formulation, viability decreased in a significant manner to $66.4 \pm 12.7\%$. After mixing and extrusion, the viability of cells contained in the A3G3 formulation differed significantly from that of cells present in the A4G3 bioink. As cells were harvested directly prior to both processes and the proceeding analysis, the contact between cells and biomaterial was the same for each sample, i.e., effects on cell viability arose from the processing steps. The decreasing amount of viable cells can be explained by the shear stress during mixing and extrusion that leads to cell disruption. The shear stress increases with the viscosity of the polymer solution as well as with increasing pneumatic pressure. The effect of the alginate concentration and thus the increasing viscosity on decreasing cell viability is in accordance with similar studies [241, 247, 253]. Increasing printing pressure leading to lower cell viability was also demonstrated in further studies [241, 247, 254, 255]. Moreover, the use of flow cytometry for data acquisition increased the precision of the determined cell viability as this value was calculated with larger amounts of counted cells. Other studies in the field of bioprinting and tissue engineering analyze a low number of microscopy images containing a low number of cells [179, 185, 247]. Commercially available assays, such as live/dead staining kits, lactate dehydrogenase assay, and alamar blue staining, are commonly applied in order to evaluate cell viability [256]. The assays are developed for culture methods where cells adhere to planar surfaces, i.e., two-dimensional cell culture, or cells are suspended in cell culture media. The assay components are added to the fluid phase and the molecules diffuse easily to the cells, and the absorbance or fluorescence are measured in plate readers. In tissue engineering and biofabrication, cells are embedded within a polymeric network, and the diffusion of solutes within the structures is limited. This is an issue to be considered in the application of commercially available kits. The protocols can be adapted to 3D cell culture substrates by adjusting incubation times or implementing the permeabilization of the hydrogels. By dilution of the bioink to a low viscosity cell suspension, the fast diffusion of the used stains is enabled as well as the use of the flow cytometer. Each technical replicate of this study part of the study regarding the assessment of the processing effects on viability consists of cell numbers in the range of 450 up to about 10,000. Considering the 20-fold dilution required for analysis with flow cytometry, the cell count in the bioink is calculated to be in the range between $9 \times 10^3 \text{ cells mL}^{-1}$ and $0.2 \times 10^6 \text{ cells mL}^{-1}$, considerably lower than the cell count of $2 \times 10^6 \text{ cells mL}^{-1}$ to be set in the bioink. The amount of cells in each fraction differed due to the inhomogeneous mixing of the used method, where a syringe containing the cell suspension is connected to a second syringe containing the polymer solution, and a mixing effect

is produced by transferring the solution back and forth between both syringes. Even though this method requires significant improvement, it was applied in the presented study, as it is commonly used in studies [257, 258], and it shows the benefits of low biomaterial loss compared to static mixer components. Additionally, mixing of cells in this manner can be compliant to good manufacturing practice (GMP) conditions compared to the mixing of cells in open containers. The reduction in waste of biomaterial by improvement of the static mixing units was studied by Dani *et al.* [244] and should be implemented in further studies. The quantified number of cells did differ in each technical sample due to inhomogeneous mixing; however, the viability was in a similar range, as it is the ratio between viable and dead cells. As mentioned in Section 5.3.2.1, bioprinting can benefit from standardization of the mixing method as air bubbles are introduced in the bioink [172, 244]. A further benefit is the comparability of data regarding cell viability, as the mixing method proved to be a critical step. The use of flow cytometry can also reduce observer-dependent errors while increasing reproducibility, as image acquisition mostly relies on the manual focusing of the samples during image acquisition. It is noteworthy that the use of flow cytometry is a destructive method, as the bioink has to be diluted in order to be analyzed. Microscopy is still required as a supplementary cell analytical method regarding cell adhesion, morphology, and migration during longer periods of cultivation.

Gillespie *et al.* [172] mentioned the limitation of the lack of control of the extruded amount of biomaterial. Measured characteristics of printed structures could differ either due to the mechanical properties of the used bioinks, or due to different amounts of bioinks deposited during printing. This presented method overcomes the mentioned difficulty by controlling the volumetric flow rate according to the specific flow behavior of each bioink. Additionally, the printing speed was set equal to the mean velocity of the biomaterial ink based on the rheological properties; thus, this parameter is directly related to the pneumatic pressure. Furthermore, the alginate content of both bioinks differed by 1% (w/v) and, thus, showed different values of viscosity. By controlling the flow rate, no differences were observed regarding the printing accuracy between both bioinks. In contrast, the increasing viscosity led to a significant decrease in cell viability directly after mixing and after extrusion. Bioinks should enable the accurate production of scaffolds while maintaining high viability and supporting biological needs. Meeting both requirements is accepted as a limitation, as increasing the concentration and thus viscosity leads to higher structural stability but increases the resulting cell disruption [234, 236, 250]. In this study, the bioink with the lower alginate content showed better printing performance overall, as the method compared the samples printed with a controlled flow rate. The presented methods show further advantages. The setting of printing parameters did not include the screening of printability by an observer, which is still commonly used in the bioprinting field. There are many printing parameters that can be set during a study on printing performance, and each affects the accuracy of the product in a different magnitude. Therefore, the setting of printing speed in relation to the pneumatic pressure increases the objectivity of the study, as only one was chosen arbitrarily and not both of them. The use of automated image processing to characterize printed structures reduces observer-dependent errors while saving the time required for image analysis. The presented methods increase the comparability of data between bioinks and can allow the transfer of gained knowledge between laboratories.

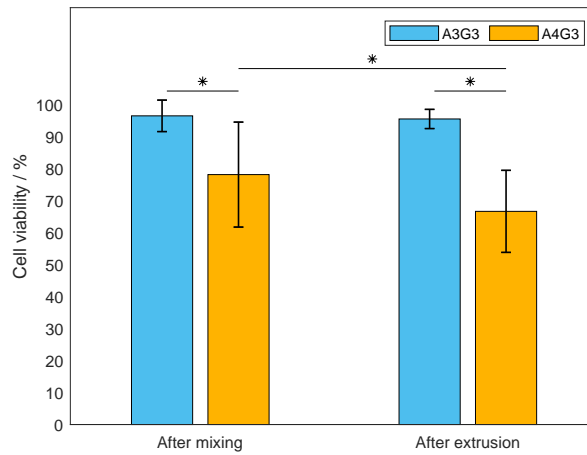


Figure 5.8 Characterization of the effect of processing on cells. The viability was determined after the mixing step and after the extrusion process. For both bioinks, the mean viability is shown as a bar with the associated standard deviation. The experiments were performed as biological triplicates ($n = 3$). For both bioinks, each biological replicate was divided into three fractions, diluted separately ($n = 3$), and analyzed as technical triplicates ($n = 3$), resulting in data sets consisting of 27 values. Significant differences are denoted with an asterisk ($p < 0.05$).

5.4 Conclusions

Universal methodologies should be developed and applied starting from the bioink preparation, including process analytical technology (PAT) strategies as well as standardized analytical methodologies. In this study, the focus lies on the development of analytical methods that enable the comparability of bioprinting processes regarding the metrics of printed structures as well as the effect on cell viability. First, the used bioinks and biomaterial inks were printed with the same flow rate, thus enabling the comparison of structures with the same amount of extruded material. The required pneumatic pressure was determined and set according to the specific flow behavior of each biomaterial ink that differed in alginate concentration by 1 % (w/v) with a constant GelMA concentration. Additionally, the printing speed was directly related the pneumatic pressure applied during printing. This setting of printing parameters enabled the adequate comparison of printed structures produced with an equal amount of material. Second, image-processing tools were developed in order to accurately characterize the printed structures in an automated manner. The application of automated image analysis allowed the time-saving assessment of printed geometries while reducing observer-dependent variations, and therefore, the robustness of the analytical method was enhanced. The study focused on the analysis of the first layer, as this is the base of any multi-layered structure. In the future, the developed image processing should be expanded and implemented into the characterization of 3D structures. Using the developed tools, no effect of the increasing viscosity on the structural features was shown. However, the cell mixing process did have an effect on the geometrical characteristics of the printed structures, as air was entrapped while mixing the biomaterial ink with the cellular material. Future research should include testing the control of flow rate in 3D objects, as, here, only single-layer structures were investigated. Third, cell viability was determined by flow cytometry, thereby increasing the amount of quantified cells

and enhancing the precision of the acquired data compared to the conventionally used microscopy. Moreover, the increasing alginate content showed a significantly negative impact on viability during both processing steps, mixing as well as extrusion. Some issues still have to be studied, e.g., the lack of standardized and effective cell mixing processes. The used mixing strategy was the transfer of biomaterial ink and cells back and forth between two syringes, which is commonly used in the field of bioprinting. This method proved to produce an inhomogeneous cell distribution and air bubbles entrapment in the cartridge. The proposed methods show great potential for saving time and costs by eliminating the need for user-dependent print parameter screenings and enables an easy transfer between devices and laboratories. The lack of standardized methods will constitute an issue in bioprinting by the stage prior to clinical applications when meeting with regulatory agencies. The requirements include robust production processes that lead to quality attributes, independent of the location and operator.

Conflict of interest

The authors declare that the research was conducted in the absence of any commercial or financial relationships that could be construed as a potential conflict of interest.

Author contributions

Conceptualization: S.S., D.G.G. and J.H.; Data curation: S.S. and D.G.G.; Formal analysis: S.S. and D.G.G.; Funding acquisition: J.H.; Investigation: S.S. and D.G.G.; Methodology: S.S. and D.G.G.; Project administration: J.H.; Resources: J.H.; Software: S.S. and D.G.G.; Supervision: J.H.; Validation: S.S. and D.G.G.; Writing—original draft: S.S. and D.G.G.; Writing—review and editing: J.H. All authors have read and agreed to the published version of the manuscript.

Acknowledgments

We would like to thank Lea Bensinger, Jasmin Egner, and Christian Lachmuth for their valuable contribution in form of experimental work for this project. We acknowledge support by the KIT-Publication Fund of the Karlsruhe Institute of Technology.

Data availability statement

The raw data supporting the conclusions of this article will be made available by the authors, without undue reservation.

Chapter references

- [38] J. Malda *et al.*, „25th Anniversary Article: Engineering Hydrogels for Biofabrication“, *Advanced Materials*, vol. 25, no. 36, pp. 5011–5028, 09/2013.
- [92] S. Naghieh, M. Sarker, N. K. Sharma, Z. Barhoumi, and X. Chen, „Printability of 3D Printed Hydrogel Scaffolds: Influence of Hydrogel Composition and Printing Parameters“, *Applied Sciences*, vol. 10, no. 1, p. 292, 2019.
- [122] A. Habeeb, „Determination of free amino groups in proteins by trinitrobenzenesulfonic acid“, *Analytical Biochemistry*, vol. 14, no. 3, pp. 328–336, 03/1966.
- [138] W. Liu *et al.*, „Extrusion Bioprinting of Shear-Thinning Gelatin Methacryloyl Bioinks“, *Advanced Healthcare Materials*, vol. 6, no. 12, pp. 1–11, 06/2017.
- [148] S. Gretzinger, N. Beckert, A. Gleadall, C. Lee-Thedieck, and J. Hubbuch, „3D bioprinting – Flow cytometry as analytical strategy for 3D cell structures“, *Bioprinting*, vol. 11, no. March, e00023, 09/2018.
- [167] J. Groll *et al.*, „A definition of bioinks and their distinction from biomaterial inks“, *Biofabrication*, vol. 11, no. 1, p. 013001, 11/2018.
- [171] L. Wenger, S. Strauß, and J. Hubbuch, „Automated and dynamic extrusion pressure adjustment based on real-time flow rate measurements for precise ink dispensing in 3D bioprinting“, *Bioprinting*, vol. 28, no. July, e00229, 12/2022.
- [172] G. Gillispie *et al.*, „Assessment methodologies for extrusion-based bioink printability“, *Biofabrication*, vol. 12, no. 2, p. 022003, 02/2020.
- [175] N. Paxton, W. Smolan, T. Böck, F. Melchels, J. Groll, and T. Jungst, „Proposal to assess printability of bioinks for extrusion-based bioprinting and evaluation of rheological properties governing bioprintability“, *Biofabrication*, vol. 9, no. 4, p. 044107, 11/2017.
- [177] Y. He, F. Yang, H. Zhao, Q. Gao, B. Xia, and J. Fu, „Research on the printability of hydrogels in 3D bioprinting“, *Scientific Reports*, vol. 6, no. 1, p. 29977, 07/2016.
- [178] T. Gao *et al.*, „Optimization of gelatin–alginate composite bioink printability using rheological parameters: a systematic approach“, *Biofabrication*, vol. 10, no. 3, p. 034106, 06/2018.
- [179] A. A. Aldana, F. Valente, R. Dilley, and B. Doyle, „Development of 3D bioprinted GelMA-alginate hydrogels with tunable mechanical properties“, *Bioprinting*, vol. 21, no. June 2020, e00105, 03/2021.
- [181] B. V. Slaughter, S. S. Khurshid, O. Z. Fisher, A. Khademhosseini, and N. A. Peppas, „Hydrogels in Regenerative Medicine“, *Advanced Materials*, vol. 21, no. 32-33, pp. 3307–3329, 09/2009.
- [185] W. Schuurman *et al.*, „Gelatin-Methacrylamide Hydrogels as Potential Biomaterials for Fabrication of Tissue-Engineered Cartilage Constructs“, *Macromolecular Bioscience*, vol. 13, no. 5, pp. 551–561, 05/2013.
- [195] B. Lee, N. Lum, L. Seow, P. Lim, and L. Tan, „Synthesis and Characterization of Types A and B Gelatin Methacryloyl for Bioink Applications“, *Materials*, vol. 9, no. 10, p. 797, 09/2016.
- [204] S. Eggert and D. W. Huttmacher, „In vitro disease models 4.0 via automation and high-throughput processing“, *Biofabrication*, vol. 11, no. 4, p. 043002, 07/2019.
- [210] D. Grijalva Garces, C. P. Radtke, and J. Hubbuch, „A Novel Approach for the Manufacturing of Gelatin-Methacryloyl“, *Polymers*, vol. 14, no. 24, p. 5424, 12/2022.
- [220] H. Münstedt and F. R. Schwarzl, *Deformation and Flow of Polymeric Materials*. Berlin/Heidelberg, Germany: Springer Berlin Heidelberg, 2014.
- [233] S. V. Murphy and A. Atala, „3D bioprinting of tissues and organs“, *Nature Biotechnology*, vol. 32, no. 8, pp. 773–785, 08/2014.
- [234] I. T. Ozbolat and M. Hospodiuk, „Current advances and future perspectives in extrusion-based bioprinting“, *Biomaterials*, vol. 76, pp. 321–343, 01/2016.
- [235] J. Thiele, Y. Ma, S. M. C. Bruekers, S. Ma, and W. T. S. Huck, „25th Anniversary Article: Designer Hydrogels for Cell Cultures: A Materials Selection Guide“, *Advanced Materials*, vol. 26, no. 1, pp. 125–148, 01/2014.
- [236] Y. Zhao, Y. Li, S. Mao, W. Sun, and R. Yao, „The influence of printing parameters on cell survival rate and printability in microextrusion-based 3D cell printing technology“, *Biofabrication*, vol. 7, no. 4, p. 045002, 11/2015.
- [237] A. S. Theus *et al.*, „Bioprintability: Physiomechanical and Biological Requirements of Materials for 3D Bioprinting Processes“, *Polymers*, vol. 12, no. 10, p. 2262, 10/2020.
- [238] A. Erdem *et al.*, „3D Bioprinting of Oxygenated Cell-Laden Gelatin Methacryloyl Constructs“, *Advanced Healthcare Materials*, vol. 9, no. 15, pp. 1–12, 08/2020.
- [239] H. Jongprasitkul, S. Turunen, V. S. Parihar, and M. Kellomäki, „Two-step crosslinking to enhance the printability of methacrylated gellan gum biomaterial ink for extrusion-based 3D bioprinting“, *Bioprinting*, vol. 25, no. September 2021, e00185, 03/2022.

- [240] A. Habib, V. Sathish, S. Mallik, and B. Khoda, „3D Printability of Alginate-Carboxymethyl Cellulose Hydrogel“, *Materials*, vol. 11, no. 3, p. 454, 03/2018.
- [241] A. Mondal *et al.*, „Characterization and printability of Sodium alginate -Gelatin hydrogel for bioprinting NSCLC co-culture“, *Scientific Reports*, vol. 9, no. 1, p. 19914, 12/2019.
- [242] M. D. Giuseppe *et al.*, „Mechanical behaviour of alginate-gelatin hydrogels for 3D bioprinting“, *Journal of the Mechanical Behavior of Biomedical Materials*, vol. 79, pp. 150–157, 03/2018.
- [243] M. Uzun-Per *et al.*, „Automated Image Analysis Methodologies to Compute Bioink Printability“, *Advanced Engineering Materials*, vol. 23, no. 4, pp. 1–12, 04/2021.
- [244] S. Dani *et al.*, „Homogeneous and Reproducible Mixing of Highly Viscous Biomaterial Inks and Cell Suspensions to Create Bioinks“, *Gels*, vol. 7, no. 4, p. 227, 11/2021.
- [245] E. N. Malamas, E. G. Petrakis, M. Zervakis, L. Petit, and J.-D. Legat, „A survey on industrial vision systems, applications and tools“, *Image and Vision Computing*, vol. 21, no. 2, pp. 171–188, 02/2003.
- [246] O. Semeniuta, S. Dransfeld, K. Martinsen, and P. Falkman, „Towards increased intelligence and automatic improvement in industrial vision systems“, *Procedia CIRP*, vol. 67, pp. 256–261, 2018.
- [247] F. Koch, K. Tröndle, G. Finkenzeller, R. Zengerle, S. Zimmermann, and P. Koltay, „Generic method of printing window adjustment for extrusion-based 3D-bioprinting to maintain high viability of mesenchymal stem cells in an alginate-gelatin hydrogel“, *Bioprinting*, vol. 20, e00094, 12/2020.
- [248] Z. Di *et al.*, „Ultra High Content Image Analysis and Phenotype Profiling of 3D Cultured Micro-Tissues“, *PLoS ONE*, vol. 9, no. 10, R. Oshima, Ed., e109688, 10/2014.
- [249] D. E. Godar, „3D Bioprinting: Surviving under Pressure“, in *Tissue Regeneration*, Rijeka, Croatia: InTech, 06/2018.
- [250] J. H. Y. Chung *et al.*, „Bio-ink properties and printability for extrusion printing living cells“, *Biomaterials Science*, vol. 1, no. 7, p. 763, 2013.
- [251] B. Webb and B. J. Doyle, „Parameter optimization for 3D bioprinting of hydrogels“, *Bioprinting*, vol. 8, no. July, pp. 8–12, 12/2017.
- [252] D. L. Cohen, W. Lo, A. Tsavaris, D. Peng, H. Lipson, and L. J. Bonassar, „Increased Mixing Improves Hydrogel Homogeneity and Quality of Three-Dimensional Printed Constructs“, *Tissue Engineering Part C: Methods*, vol. 17, no. 2, pp. 239–248, 02/2011.
- [253] A. G. Tabriz, M. A. Hermida, N. R. Leslie, and W. Shu, „Three-dimensional bioprinting of complex cell laden alginate hydrogel structures“, *Biofabrication*, vol. 7, no. 4, p. 045012, 12/2015.
- [254] K. Nair *et al.*, „Characterization of cell viability during bioprinting processes“, *Biotechnology Journal*, vol. 4, no. 8, pp. 1168–1177, 08/2009.
- [255] J. Snyder, A. Rin Son, Q. Hamid, C. Wang, Y. Lui, and W. Sun, „Mesenchymal stem cell printing and process regulated cell properties“, *Biofabrication*, vol. 7, no. 4, p. 044106, 12/2015.
- [256] J. Marzi *et al.*, „Non-Invasive Three-Dimensional Cell Analysis in Bioinks by Raman Imaging“, *ACS Applied Materials & Interfaces*, vol. 14, no. 27, pp. 30455–30465, 07/2022.
- [257] H. Park, S.-W. Kang, B.-S. Kim, D. J. Mooney, and K. Y. Lee, „Shear-reversibly Crosslinked Alginate Hydrogels for Tissue Engineering“, *Macromolecular Bioscience*, vol. 9, no. 9, pp. 895–901, 09/2009.
- [258] F. Hafezi *et al.*, „Bioprinting and Preliminary Testing of Highly Reproducible Novel Bioink for Potential Skin Regeneration“, *Pharmaceutics*, no. 6, p. 550, 06/2020.

6

On the reproducibility of extrusion-based bioprinting: round robin study on standardization in the field

David Grijalva Garces^{1,2}, Svenja Strauß^{1,2}, Sarah Gretzinger^{1,2}, Barbara Schmiegl^{1,2}, Tomasz Jüngst^{3,4}, Jürgen Groll^{3,4}, Lorenz Meinel⁵, Isabelle Schmidt⁶, Hanna Hartmann⁶, Katja Schenke-Layland^{6,7}, Nico Brandt⁸, Michael Selzer⁹, Stefan Zimmermann¹⁰, Peter Koltay¹⁰, Alexander Southan^{11,12}, Günter E. M. Tovar^{11,12}, Sarah Schmidt¹², Achim Weber¹², Tilman Ahlfeld¹³, Michael Gelinsky¹³, Thomas Scheibel^{4,14}, Rainer Detsch¹⁵, Aldo R. Boccaccini¹⁵, Toufik Naolou¹⁶, Cornelia Lee-Thedieck¹⁶, Christian Willems¹⁷, Thomas Groth¹⁷, Stephan Allgeier¹⁸, Bernd Köhler¹⁸, Tiaan Friedrich¹⁹, Heiko Briesen¹⁹, Janine Buchholz²⁰, Dietrich Paulus²⁰, Anselm von Gladiss²⁰ and Jürgen Hubbuch^{1,2}

- ¹ Institute of Functional Interfaces, Karlsruhe Institute of Technology (KIT), Eggenstein-Leopoldshafen, Germany
- ² Institute of Engineering in Life Sciences, Section IV: Biomolecular Separation Engineering, Karlsruhe Institute of Technology (KIT), Karlsruhe, Germany
- ³ Department for Functional Materials in Medicine and Dentistry, Institute of Functional Materials and Biofabrication, University of Würzburg, Würzburg, Germany
- ⁴ Bavarian Polymer Institute, University of Bayreuth, Bayreuth, Germany
- ⁵ Institute of Pharmacy and Food Chemistry, University of Würzburg, Würzburg, Germany
- ⁶ NMI Natural and Medical Sciences Institute at the University of Tübingen, Reutlingen, Germany
- ⁷ Institute of Biomedical Engineering, Department for Medical Technologies and Regenerative Medicine, Eberhard Karls University of Tübingen, Tübingen, Germany
- ⁸ Institute for Applied Materials, Karlsruhe Institute of Technology (KIT), Karlsruhe, Germany
- ⁹ Institute for Nanotechnology, Karlsruhe Institute of Technology (KIT), Karlsruhe, Germany
- ¹⁰ Laboratory for MEMS Applications, Department of Microsystems Engineering, University of Freiburg, Freiburg, Germany
- ¹¹ Institute of Interfacial Process Engineering and Plasma Technology, University of Stuttgart, Stuttgart, Germany
- ¹² Functional Surfaces and Materials, Fraunhofer Institute for Interfacial Engineering and Biotechnology, Stuttgart, Germany
- ¹³ Center for Translational Bone, Joint, and Soft Tissue Research, Faculty of Medicine, Technische Universität Dresden, Dresden, Germany
- ¹⁴ Chair of Biomaterials, University of Bayreuth, Bayreuth, Germany
- ¹⁵ Institute of Biomaterials, Friedrich-Alexander University Erlangen-Nuremberg, Erlangen, Germany
- ¹⁶ Institute of Cell Biology and Biophysics, Leibniz University Hannover, Hannover, Germany
- ¹⁷ Department Biomedical Materials, Martin Luther University Halle-Wittenberg, Halle (Saale), Germany
- ¹⁸ Institute for Automation and Applied Informatics, Karlsruhe Institute of Technology (KIT), Eggenstein-Leopoldshafen, Germany
- ¹⁹ Process Systems Engineering, School of Life Sciences, Technical University of Munich, Freising, Germany
- ²⁰ Institute for Computational Visualistics, Active Vision Group, University of Koblenz, Koblenz, Germany
- * Contributed equally

Abstract

The outcome of three-dimensional (3D) bioprinting heavily depends, amongst others, on the interaction between the developed bioink, the printing process, and the printing equipment. However, if this interplay is ensured, bioprinting promises unmatched possibilities in the health care area. To pave the way for comparing newly developed biomaterials, clinical studies, and medical applications (i.e. printed organs, patient-specific tissues), there is a great need for standardization of manufacturing methods in order to enable technology transfers. Despite the importance of such standardization, there is currently a tremendous lack of empirical data that examines the reproducibility and robustness of production in more than one location at a time. In this work, we present data derived from a round robin test for extrusion-based 3D printing performance comprising 12 different academic laboratories throughout Germany and analyze the respective prints using automated image analysis (IA) in three independent academic groups. The fabrication of objects from polymer solutions was standardized as much as currently possible to allow studying the comparability of results from different laboratories. This study has led to the conclusion that current standardization conditions still leave room for the intervention of operators due to missing automation of the equipment. This affects significantly the reproducibility and comparability of bioprinting experiments in multiple laboratories. Nevertheless, automated IA proved to be a suitable methodology for quality assurance as three independently developed workflows achieved similar results. Moreover, the extracted data describing geometric features showed how the function of printers affects the quality of the printed object. A significant step toward standardization of the process was made as an infrastructure for distribution of material and methods, as well as for data transfer and storage was successfully established.

6.1 Introduction

3D bioprinting is attracting widespread interest due to the possibility to manufacture customized artificial tissues in regards to individual patient treatment, designing models for medical studies or organ-on-a-chip applications [39, 259]. For these products to be approved by authorities for medical application or clinical studies, high reproducibility and robust processes will inevitably be a challenge. The safety of the products should be guaranteed by standards and norms. In the field of bioprinting, there is still a need for universally applicable guidelines and standard operating procedures (SOPs). These should be included from the very beginning of the production of bioinks through to process analytical technology (PAT) strategies and standardized analytical methodologies. In order to be able to compare, for example, bioinks or bioprinter setups in interlaboratory tests or prepare technology transfers, standardized methodologies are a prerequisite. Due to the missing guidelines, research groups develop own expertise and there is hardly any exchange of information between groups. This said, the use of interlaboratory data bases as advocated by the research community is still in its infancy. In this regard, there have been advances in the field of bioprinting, where the Kadi4Mat infrastructure was used for process design, documentation, data storage, and exchange [260]. Looking at other related research areas such as tissue engineering, the International Organization for Standardization (ISO) has already constituted a technical committee (TC) for tissue engineering of medical products, i.e., ISO/TC 150/SC 7, aiming to implement relevant standards for testing and manufacturing methods. Therefore, it is only a matter of time before such subcommittees for bioprinting form. At the local level, for example, policy committees have

already been formed as part of the Verein Deutscher Ingenieure (VDI), the Association of German Engineers. The VDI guidelines committee (Richtlinienausschuss 5708) aims for the definition of basic terminology, device requirements, and bioink testing methodologies. The development of robust protocols and standards is of crucial importance for a successful clinical translation of biomaterials and bioprinting as has been mentioned in literature [261].

With regard to future application in clinical studies, there are some process steps which would benefit from standardization. The first aspect is the production and characterization of newly developed bioinks which consist of biomaterials, cells, and other additives [167, 262]. It is, for example, not an easy undertaking to homogeneously introduce cells into the highly viscous solution to complete the bioink because air bubbles present a common challenge [263–265]. One suggestion is to introduce the cells above the gelation temperature of the solution [227]. The second aspect includes the printing process itself and the equipment of the bioprinters. There are different techniques for extrusion-based bioprinters, such as pneumatically operated or piston-driven methods [38, 233]. In addition, there are bioprinters where the cartridge or nozzle can be tempered including different principles, such as the use of a cooling agent or thermoelectric control. Another feature that not every bioprinter is equipped with is the automatic calibration of the coordinates of the nozzle tip which can have an influence on the printing result and thus on the reproducibility.

To ensure the quality and reproducibility of bioprinted structures, the performance of bioprinting evaluation is already being discussed [266, 267]. Filament collapse, fusion and grid tests are three commonly suggested evaluation methods. These evaluation methods are useful for both developers and users of bioprinting processes. The filament collapse test evaluates the printer's ability to deposit a filament on a platform with pillars at increasing intervals without the strand collapsing [268, 269]. This is important for the production of stable and reproducible complex structures. The yield stress of the material used can be derived here, which plays an important role in the design of bioinks as it defines the shear stress for initiating the material flow. The filament fusion test evaluates the printer's ability to deposit filaments meander-like at different distances, which can be used to determine the accuracy of the print test [270, 271]. The grid test evaluates the accuracy and precision of the printer by printing a grid pattern. The distance between the lines, pore diameter, pore geometry and the crossing point of struts are analyzed here for assessment [272]. Special attention should be given to the methodologies for quantitative analysis as the printed objects are evaluated and the outcome is translated into numbers. Image analysis (IA) is a suitable tool as it is fast, non-invasive, can be automated and, thus increases objectivity. Currently, there are still publications where 'the printability was judged by eyes' [177], or the images were cropped, and subsequently analyzed manually by a person [178]. This is a time-consuming procedure and dependent on the subjective impression of one observer only. Furthermore, acquired photographs were 'analysed in ImageJ where the width of the strand was measured at multiple locations and averaged' [179]. Hence, the number and location of measurements are variable and depend on a subjective decision by the observer. There have been advances toward automation of IA, however, the study still includes several manual steps for detection and cropping of artifacts [243]. In conclusion, the studies listed above show user-dependent methodologies based on subjective decisions which limit the overall comparison. So far, cell analytics in the field of bioprinting is also lacking standardization. Microscopy is a commonly used method for investigating cell viability and morphology, however, this method is user-dependent as well due to manual focusing and manual counting of observations [185, 195]. A more advanced alternative for cell analytics is offered by raman imaging, which has been used for the analysis of cells within 3D printed objects [256]. Even though this topic is out of the scope of the present study, in which no cells were used, it should be

standardized as well. Throughout this work, we use the term ink to refer to the applied polymeric solutions in our studies as all experiments were cell-free.

To date and to the best of our knowledge, no studies of the reproducibility and comparison of bioprinting experiments in multiple laboratories have been reported. In this round robin study, we tested how consistent printed-geometry results can be obtained with 12 laboratories cooperating. Therefore, an infrastructure for central distribution of SOPs with information regarding the preparation procedure for inks, and parameters for printing experiments was established. Additionally, the consumables and biomaterials were distributed by the organizing laboratory. A device for standardized image acquisition was developed and used within the round robin experiments. In total 10 prototypes of this so called Bioprinting Fidelity Imager (BioFI) were fabricated and used by different laboratories to record images of the printed objects. For quantitative assessment of the recorded images automated IA was included in order to extract features from the images of the printed objects. Finally, based on the experimental results, several factors that can be improved to increase reproducibility have been identified in order to make bioprinting more reliable and reproducible for future medical applications.

6.2 Materials and methods

6.2.1 Round robin workflow and design

The round robin test was designed and performed to provide a general overview of to which extent bioprinting experiments concur in different laboratories. A compact schematic of the workflow of the project is depicted in Figure 6.1. As already suggested by the name of the project SOP_BioPrint, SOPs for the individual stages were developed in advance and distributed to all participating entities by the organizing laboratory.

6.2.2 Biomaterials, labware, and geometries

In order to achieve a high degree of standardization, the organizing laboratory provided the participating laboratories with the biomaterials, labware, and the files of the designed geometries including orientation to be printed. Three different polymeric solutions were used, two of which were provided by research institutions including preparation instructions. Alginate was provided by the Department for Functional Materials in Medicine and Dentistry from the University of Würzburg (Würzburg, Germany) with instructions for preparing a 4% (w/v) alginate ink in ultrapure water. The properties of this biomaterial in bioprinting is summarized by Karakaya *et al.* [273]. The biomaterials for the gelatin-based ink and guidelines on its preparation were provided by the Department of Functional Surfaces and Materials at Fraunhofer Institute for Interfacial Engineering and Biotechnology (Stuttgart, Germany). The methacrylation of gelatin and its subsequent use as an ink was performed according to Wenz *et al.* [274]. Briefly, the ink consisted of 12% (w/w) functionalized gelatin, i.e., a mixture of 7% (w/w), and 5% (w/w) gelatin with degrees of methacrylation of 0.62 mmol g^{-1} , 0.82 mmol g^{-1} , respectively, and 0.84% (w/w) of LAP photo initiator dissolved in Dulbecco's phosphate-buffered saline (DPBS). The commercially available Cellink Bioink was used as a third ink and purchased from Cellink (Gothenburg, Sweden). This alginate nanocellulose bioink [275] was delivered as ready-to-use cartridges and procured from a single batch. Labware used in the printing experiment consisted of a single-use conic 25G (0.25 mm inner diameter) nozzle from Cellink and six-well glass bottom plates from iBL (Gerasdorf, Austria).

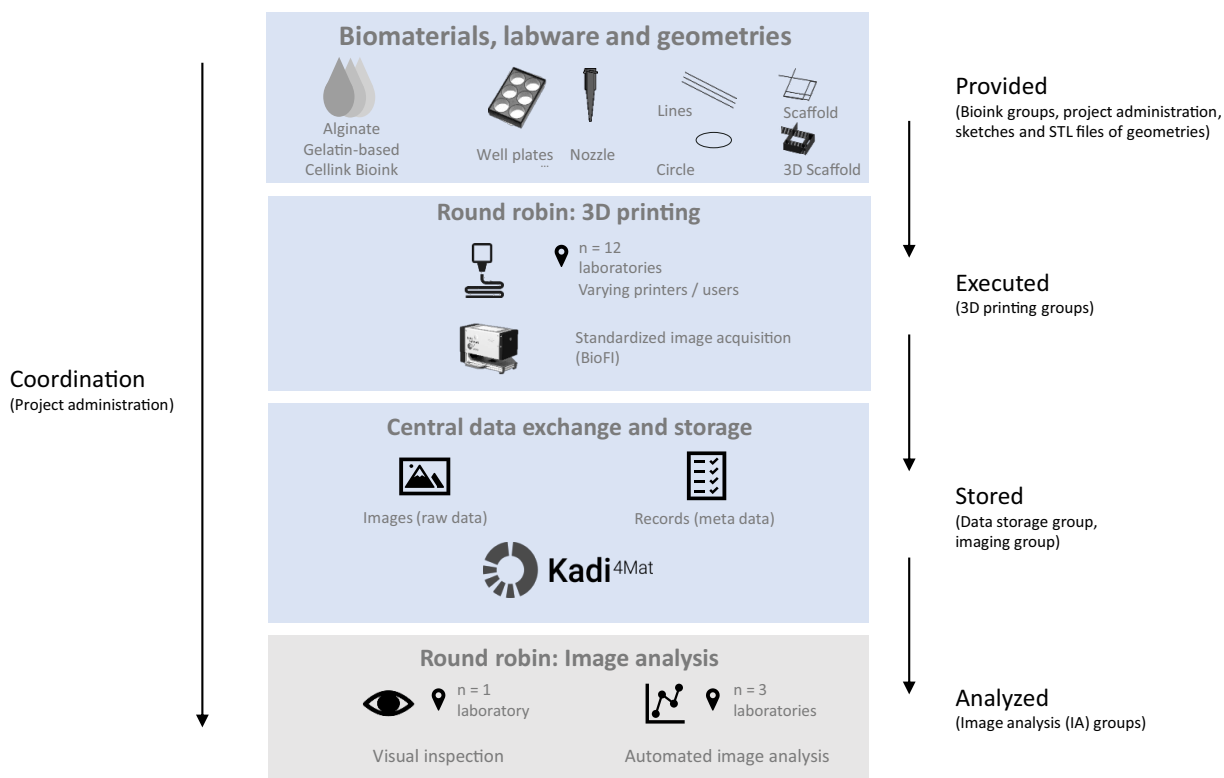


Figure 6.1 Illustrative scheme summarizing the workflow in the round robin tests. Biomaterials, labware, and geometries as well as detailed standard operation procedures (SOPs) regarding the preparation and use of materials were distributed. The Round robin - 3D printing was performed in 12 independent laboratories and comprised the 3D printing experiments and documentation. Subsequently, images of the printed geometries were acquired using the Bioprinting Fidelity Imager (BioFI) system. The Kadi4Mat platform was used for central data exchange and storage. The Round robin - Image analysis was divided into two parts. A qualitative evaluation of the images was performed by the organizing laboratory and extraction of quantitative geometric features was done individually by three image analysis groups independently. Statistical analysis and data visualization in the presented study were performed by the organizing laboratory.

An SOP specified the procurement details (part number, manufacturer, distributor) for well plates and nozzles. Additionally, the STL files, or in case of problems during slicing, the sketches of the objects were provided by the organizing laboratory. A larger sketch of the geometries is presented in the supplementary section (see Figure A5.1). The first model was a pattern of three parallel 25 mm long lines with a distance of 2 mm between the lines. These were to be printed in parallel to the short edge of the well plate. The second object was a circle with a diameter of 12 mm. The first and second models both consisted of a single layer. The third model was designed as a rectangle with two layers. There were two meandering lines printed in two separate layers rotated by 90°. To create a closed square, there was a start up line with the length $l = 5$ mm in each layer. The fourth and last model was a stack of several layers of the scaffold, resulting in a total height of 1.2 mm. The start up filaments of both structures had to be printed oriented to the top left corner of each well plate.

6.2.3 Round robin - 3D printing

The experimental design in the Round robin - 3D printing test is summarized schematically in Figure 6.2. The twelve participating laboratories located in Germany are listed alphabetically below:

- Center for Translational Bone, Joint, and Soft Tissue Research, Technische Universität Dresden, Dresden
- Chair of Biomaterials, University of Bayreuth, Bayreuth
- Department of Functional Materials in Medicine and Dentistry, University of Würzburg, Würzburg
- Functional Surfaces and Materials, Fraunhofer Institute for Interfacial Engineering and Biotechnology, Stuttgart
- Institute of Biomaterials, Friedrich-Alexander University Erlangen-Nuremberg, Erlangen
- Institute of Cell Biology and Biophysics, Leibniz University Hannover, Hannover
- Institute of Functional Interfaces, Karlsruhe Institute of Technology, Eggenstein-Leopoldshafen
- Institute of Interfacial Process Engineering and Plasma Technology, University of Stuttgart, Stuttgart
- Institute of Pharmacy, Martin Luther University Halle-Wittenberg, Halle (Saale)
- Institute of Pharmacy and Food Chemistry, University of Würzburg, Würzburg
- Laboratory for MEMS Applications, Department of Microsystems Engineering, University of Freiburg, Freiburg
- NMI Natural and Medical Sciences Institute at the University of Tübingen, Reutlingen

Training of participants with respect to SOPs was executed virtually. Regarding the conception of SOPs, the 3D printing comprised the largest operational window and proved to be the most difficult to standardize. This was due to the fact that the participating entities used different printing equipment with varying specifications. Local adaptations were done by the respective lab teams within the SOP. Table 6.1 provides relevant information of printers used in the Round robin - 3D printing test. The equipment included three custom-designed printers, five BioX™ and one Inkredible+™ (Cellink), two 3D Discovery™ (regenHU Ltd, Villaz-St-Pierre, Switzerland), and a BioScaffolder® (GeSiM mbH, Radeberg, Germany). Laboratory identification numbers were generated randomly and are used as Lab 1 to Lab 12 throughout this study for the analysis of the produced data sets.

The biomaterials for gelatin-based ink and alginate were distributed as dry materials by the organizing laboratory. Both inks were prepared independently as three batches prior to the printing experiments in the laboratories of the participating entities. The commercially available Cellink Bioink was purchased as specified in the SOP. Three ready-to-use cartridges containing the ink were used. As the 3D-printing experiments were performed without cells, independently prepared inks from the same batch were considered as analogs of biological replicates. Six samples of each structure, e.g. line, circles, and rectangle, were printed using each ink (i.e. technical replicates). Additionally, a 3D scaffold was printed using Cellink Bioink as six samples of the structure (i.e. technical replicates). This resulted in a number of 180 objects per laboratory and in a total number of 2160 for the entire Round robin - 3D printing test. For the printing process, a window of operation regarding printing parameters was set by the organizing laboratory in order to print filaments in a similar metric range. These printing parameters were dependent on the used inks. They are listed in Table 6.2. For the case of the mechanically driven printers, the printing parameter was the axial speed of the piston. Therefore, a target width of 1 mm should be met. Once a parameter was set, it should not be changed over the complete series of printing experiments. Moreover, a standardized

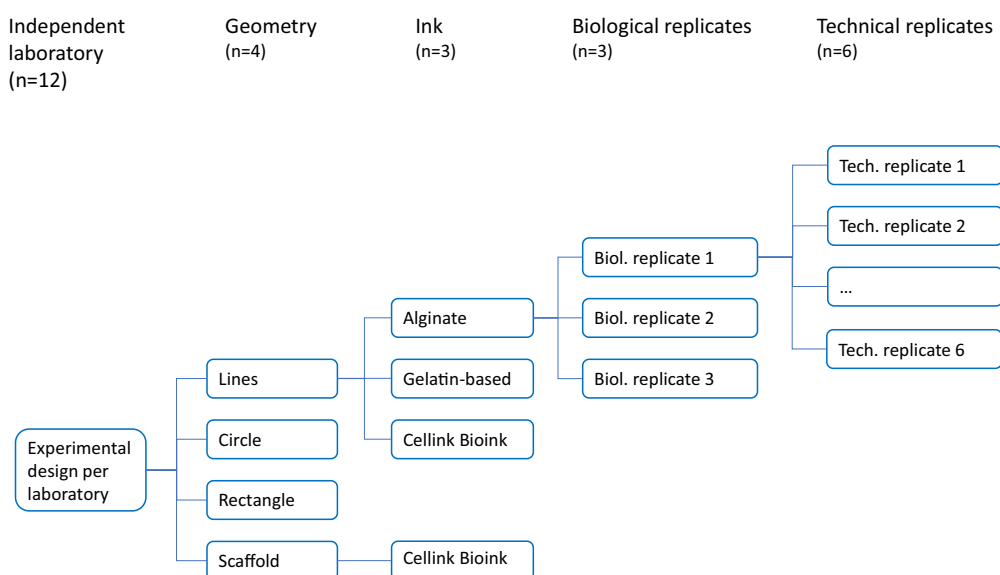


Figure 6.2 Scheme of the experimental design of the Round robin - 3D printing. Twelve different academic laboratories throughout Germany participated in the Round robin - 3D printing test ($n = 12$). Line, circle, and rectangle ($n = 3$) geometries were printed using three different inks ($n = 3$). Additionally, a three-dimensional (3D) scaffold was printed using Cellink Bioink ($n = 1$). As the experiments were performed without cells, independently prepared inks from the same batch were considered as analogs of biological replicates. In the case of Cellink Bioink, the use of an independent cartridge was considered as a biological replicate. For each biological replicate ($n = 3$), the ink was used in order to print six samples as technical replicates ($n = 6$). The resulting data sets contained 180 images for each individual laboratory. Exemplary images of the printed geometries with each ink are provided in the supplementary section (see Figure A5.3).

record was filled by each participating laboratory for documentation [260]. After the printing process, the well plates containing the six objects of a single structure were imaged externally. The BioFI system was specially developed for this purpose by the Laboratory for MEMS Applications, Department of Microsystems Engineering of the University of Freiburg (Freiburg, Germany) and Hahn-Schickard-Gesellschaft für Angewandte Forschung e.V. (Villingen-Schwenningen, Germany). Imaging equipment and methods are specially adapted to polymeric solutions showing low contrast to the background. Simply speaking, the BioFI consisted of calibrated digital image sensor with fixed magnification optics and illumination, that enables acquisition of microscopy images in bright field and dark field mode. The whole equipment works as a stand alone device controlled by an embedded Linux system. The BioFI contained a bracket to hold the well plate in a proper position. Size scales were integrated below each single well for size determination. Imaging settings including lighting and exposure time were standardized and could not be modified by the operator. Printing records and acquired images were uploaded in the central database [260].

Table 6.1 Extrusion principles and specifications of printing equipment used by the participating laboratories in the Round robin - 3D printing test. Laboratory identification numbers were generated randomly.

Lab	Extrusion principle	Temperature control	Z-height calibration
1	mechanical piston	fluid circulation	user-controlled
2	mechanical piston	none	user-controlled
3	pneumatic	electric heating	user-controlled
4	pneumatic	none	user-controlled
5	pneumatic	none	user-controlled
6	pneumatic	fluid circulation	automated
7	pneumatic	none	automated
8	pneumatic	electric heating	user-controlled
9	mechanical piston	electric heating	user-controlled
10	pneumatic	fluid circulation	automated
11	pneumatic	electric heating	user-controlled
12	pneumatic	electric heating	user-controlled

Table 6.2 Materials employed in the Round robin - 3D printing test with recommendations of printing parameters.

Ink	Extrusion pressure (kPa)	xy Speed (mm s ⁻¹)	Temperature (°C)
Alginate ink	50-120	20	RT
Gelatin-based ink	70-80	20	22-28
Cellink Bioink	20-30	20	RT

6.2.4 Central data exchange and storage

The distribution of SOPs and storage of documentation of the printing experiments of the Round robin test was implemented in a research data management system named Kadi4Mat [276]. Furthermore, all images were uploaded systematically so that, in combination with the relevant records, every step can be retrieved and analyzed at a later point in time. This systematic data storage was not only used for the purpose referred to, it simultaneously fulfilled the function of an electronic lab notebook (ELN) and proved to be important to the development toward digital laboratory. The detailed use of the Kadi4Mat database used in this study is described by Schmieg *et al.* [260]. After completing the experimental part in the laboratories, the analysis of the images of printed structures was divided into two parts. Hereby, the database allowed the quantitative analysis of objects using automated IA with the target to extract geometric features of the printed structures and to store them systematically again.

6.2.5 Round robin - Image analysis

A qualitative analysis was performed by the organizing laboratory in order to explore possible challenges which may complicate an automated evaluation and the extent of occurrence. To do so, two independent observers studied all images and classified them into categories. The categories used

were offset position, orientation of structure, additional paths, non-continuous filaments, material excess, off focus, and weak contrast. In addition to the qualitative analysis, a quantitative assessment was carried out independently from the qualitative analysis. Three IA groups were included in the study for the quantitative assessment of the printed structures. Throughout this study, group identification numbers are used as IA Group 1, IA Group 2, and IA Group 3 regarding IA. The academic entities are given alphabetically in the list below:

- Chair of Process Systems Engineering, Technical University of Munich, Freising
- Institute for Automation and Applied Informatics, Karlsruhe Institute of Technology, Eggenstein-Leopoldshafen
- Institute for Computational Visualistics, University of Koblenz, Koblenz

This study was designed as a randomized and double-blinded multicenter study. The IA groups had access to the submitted images, and were able to freely develop a workflow to extract sets of parameters. It is noteworthy that the three groups were chosen to have different backgrounds and have not worked previously in the field of bioprinting or tissue engineering to avoid any bias. The backgrounds of the chosen groups were active vision where sensor data is processed and reacted to, application-oriented information including process automation, and development of process systems engineering concepts, among other things, also for biological processes. The extracted geometric features include but are not limited to determinations of line width and length, circle inner and outer radius, and circle gap size. To ensure a non-biased analysis, the IA groups did not receive any information about the categorization performed in the qualitative analysis. All images were analyzed and the data sets were extracted using the three IA methodologies as presented below.

The first IA process consisted of four consecutive steps. The same general four-step process chain was used for all patterns, but the specific implementation of each step may differ between the lines, circle, and rectangle patterns. A manual preliminary step rotated all images by 0, 90, 180, and 270° in order to bring them into the expected orientation as specified in the STL template. Step (I) of the automated process chain estimated the location of the printed structure based on a search for geometric primitives. For the circle and rectangle structures, the inner contours of the circle and of the large square cavity were used, respectively. A fixed ROI (region of interest) was formed around the calculated coordinates. For the lines structure, the small crosses of the substrate were used instead as lateral delimiters of the ROI. Step (II) consisted in tracing the contours of the printed structures in the estimated ROI. For the lines structure and the circle structure, both contours of each line and of the circle were extracted. For the rectangle structure, only the inner contours of the four cavities were traced. For the circle and rectangle structures, the nominal position of the extracted contours was defined by the pattern position detected in the previous step. For the lines structure, the six strongest step edges in a vertical projection profile of the ROI were used as reference contour locations. Step (III) analyzed the contour traces and removed parts that are classified as artifacts, e.g., from dust particles, rather than actual printed contours. Step (IV) calculated quantitative feature metrics. The printed line width and circle width were calculated as the distance between corresponding contour pairs, measured horizontally, and radially. For the rectangle structure, the areas of the square and rectangular cavities were calculated as numbers of pixels inside the cavity contours, if the contours were closed. Steps (I) and (II) were implemented in Visual C# 9.0 (Microsoft, Redmond, USA) using the Matrox Imaging Library MIL X 22H1 (Matrox Electronic Systems, Montreal, Canada). Steps (III) and (IV) were implemented in MATLAB® R2022a (TheMathWorks Inc., Natick, USA).

The second IA workflow started with determining the conversion factor from pixel to millimeter. Locations of the size scales which were integrated in the pictures were obtained by correlating binarized reference images and the input grayscale image. This factor was determined by summing up the rows or columns belonging to the 10 mm scale. Thereby, another reference image containing the printed geometry was drawn with the measurements of the construction sketches. The ROI for each geometry just as printing angle for lines and scaffolds were determined by rotating the reference and calculating the highest correlation to the input image. Contour detection was performed using a canny edge detector returning a binary edge image. Next up, small impurities were filtered by deleting all contours with a smaller area than a given threshold. To single out each strand of the line geometry individually, the image was subdivided. If necessary, the recognized edges were closed by active contours creating the segmentation outlines of the printed geometry, allowing images for each individual contour. A full segmentation as well as images of each scaffold hole were preserved by filling the contours with a flood fill procedure. These images enabled the calculation of different geometry characteristics such as area and line width. For the area calculation, all pixels of the filled segmentation were summed up. The first step of the line width computation was the partition of the segment outlines into two matching contours by the medial axis of the geometry. Circle geometries were divided to an inner and outer contour whereas line geometries were separated to left and right. Scaffolds were split to multiple parts, resulting in several upper and lower as well as right and left relating contours. Afterwards, the smallest distance from each pixel of one contour to all pixels of the matching contour was computed and stored as an array. As a last step, the mean and median line widths of the complete geometry were calculated using the mean and median values of the entire array. Additionally, the results were transferred into the metric system by multiplication with the conversion factor. The program was implemented in Python 3.8.13 (Python Software Foundation, Delaware, USA) using the libraries OpenCV 4.6.0, NumPy 1.22.4, and Scikit-image 0.19.3[277].

The third IA approach for evaluating print quality consisted of four main steps: (I) segmentation of the printed geometry, (II) edge detection, (III) matching of the target geometry, and (IV) the evaluation of its quality. For the segmentation step (I), the scaled geometry and blank images were denoised with guided filtering [278] under self-guidance, resulting in edge-preserving noise reduction. KAZE features [279] were then computed and the blank image was aligned with the image of the printed geometry. By subtracting the aligned blank image from the image of the geometry, the marks on the plate and the backlight were removed. For edge detection (II), the gradient of the segmented geometry image is calculated. Local minima were reduced in order to be able to detect edges with the watershed algorithm. For this purpose, the 0.9 quantile of the gradient distribution was calculated. This 0.9 quantile was then used as a threshold for an H-minima transformation, where all local minima with a depth below this threshold were removed. Subsequently, the edges were extracted as watershed ridge lines, and small artifacts were removed by area opening with a minimum area of 0.25 mm^2 . The next step was to match the given geometry templates to the edge image (III). For this purpose, points on the inner and outer edges of the geometries were sampled. On the edge image, edge pixels of parallel lines with distances between 0.25 mm and 2 mm were selected. This selection was done by finding the maximum response of a Frangi filter [280]. Finally, the geometry template was aligned with the selected edge pixels by kernel correlation registration [281], and all edge pixels not connected to the region covered by the matched template were removed. Finally, for the quantitative evaluation of the printed structure (IV), the width of the detected structure was measured for the line and circle geometries. Missing segments were defined by zero width. For the rectangle and scaffold geometries, a flood fill was seeded to the expected center of the hole, and the centroid, as well as the covered area were measured. The program was implemented in

MATLAB[®] R2022a used with the libraries Signal Processing Toolbox 9.0, Image Processing Toolbox 11.5, Statistics and Machine Learning Toolbox 12.3, Global Optimization Toolbox 4.7, Computer Vision Toolbox 10.2, and Parallel Computing Toolbox 7.6.

The data sets extracted by the IA groups were evaluated by the organizing laboratory. Outliers were detected and compared to the corresponding image. Only for the case of outliers arising from artifacts not recognized as such by the image processing workflows, the corresponding data was not used for further analysis. In terms of metrics regarding the printed structures, line and circle width were used in this study for the purpose of clarity. For the calculation of both parameters, filament width of each printed geometry were determined at several point along the complete structure. Data provided below is the mean and the corresponding standard deviation of the mean width of single printed geometries. Both parameters were used for the calculation of the percentage coefficient of variation (CV) as the ratio of mean value to the associated standard deviation. A schematic representation of the two parameters is shown in the supplementary section (see Figure A5.2).

6.2.6 Data handling and visualization

Data processing and evaluation including the calculation of mean and standard deviation as well as CV of the data sets, and data visualization were performed with MATLAB[®] R2022a.

6.3 Results and discussion

6.3.1 Round robin - 3D printing

The experimental part of the round robin study was conducted in twelve independent research institutions. After completion of the printing experiments, each laboratory submitted the acquired images and reports on Kadi4Mat. Thereby, support from the organizing laboratory was provided during data submission if required, as the project participants used this platform for the first time. It is noteworthy to mention that the experiments were not performed simultaneously as only a limited amount of BioFi imaging systems were used. The experimental part took place in a time frame of five months.

6.3.2 Round robin - Image analysis: qualitative

After having completed the practical part of the elaborate Round robin - 3D printing test, a visual inspection of images of printed structures was performed to get a first impression of the data quality. Some deviations from the specifications were found and sorted into five categories, and a possible root cause of the deviation was defined. However, not every deviation can be clearly traced back to a single cause, which is why there are some overlapping causes. The results are shown in Figure 6.3 by exemplary images.

Category C1 includes samples where the orientation was different from the original STL file or samples with an offset position in relation to the center of the plate. Images that qualified for this category showed one of both of the named conditions. As can be seen in Figure 6.3 (A), the line structures were deposited in a horizontal orientation, i.e., parallel to the long edge of the well plate, whereas the intended STL files contained structures aligned vertically. Category C2 contains printed structures showing additional paths other than the expected structure. Figure 6.3 (B) shows the circle geometry with an excentric strand connecting the middle of the circle and

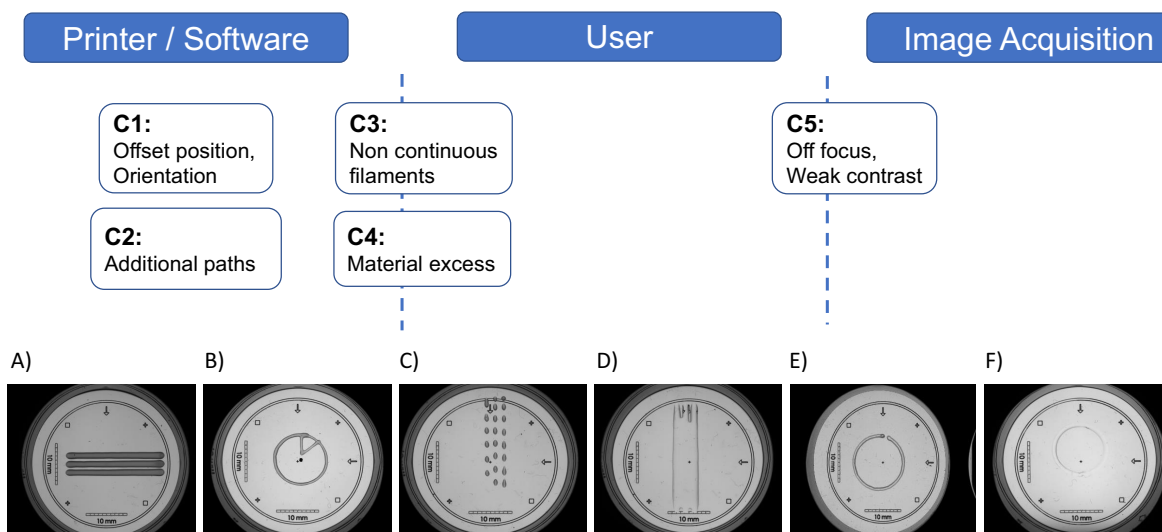


Figure 6.3 Overview of deviations with images shown as examples that occurred during the printing experiments. These can be caused by the setup (printer and software), the operator, or problems during image acquisition. Not every deviation can be traced back to a single cause. Therefore, some deviations are assigned to several causes and are in-between. (A) Lines are rotated 90° compared to the original STL file, categorized as C1. (B) Additional paths printed within the circle, categorized as C2. (C) Discontinuous lines and simultaneously off-centered positioning, categorized as C1 and C3. (D) Lines merged together due to excessive material corresponding to category C4. (E) Substrate not properly placed in the BioFI imaging system, categorized as C5. (F) Weak contrast between background and printed material as well as printed in an offset position, categorized as C5 and C1. Scale bars left and below printed geometries: 10 mm.

the circumference. Both categories were probably produced by mistakes in the printing setup, i.e., software and printer. Category C3, and Category C4 are comprised of samples with non-continuous filaments, and material excess, respectively. Category C3 can be caused by a printing system that cannot keep the set pneumatic pressure stable or it can be the product of nozzle clogging. Corresponding to this category, Figure 6.3 (C) exemplifies an intermittent line structure. Category C4 can arise due some printer equipment not having the feature to set a defined temperature leading to a lower viscosity of the ink. Similarly, a further origin of issues concerning this category can be an excessively high pneumatic pressure applied by the printer equipment. Figure 6.3 (D) displays an excessive amount of material deposited on the substrate to the extent that all three intended strands fuse together to a single outspread shape without any specific geometry. Both categories C3 and C4 might also be affected by the inappropriate setting of printing parameters, which could be originated both by the user and by the printing setup. Category C5 consists of images lacking high contrast between printed structures and structures out off focus. This can occur if the well plate is not properly placed in the bracket in the imaging system as seen in Figure 6.3 (E) and (F). Each image was classified into the categories of the presented challenges. The ratio of images found in each category to the total amount of images is presented in Figure 6.4 (A).

C1 with 73.1 % represents rotation and/or shifts from the origin and C2 with 6.1 % the amount of additional paths. C3 with 39 % is the percentage of non-continuous filaments, and C4 with 13.3 %

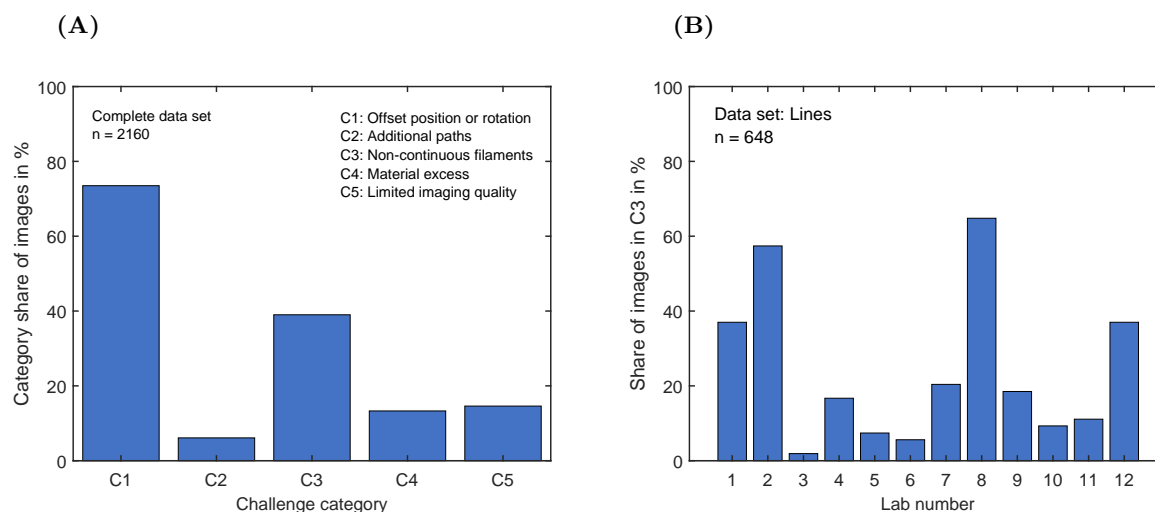


Figure 6.4 Deviations of the images from the specifications taken in the round robin test. The deviations presented in the images were divided into challenge categories. Single images could qualify for more than one challenge category. The respective share of the total image data set is shown in (A) (n = 2160). In (B), the subset of images of printed line geometries that were classified as category 3 is shown by occurrence in the 12 laboratories (n = 648).

shows the occurrence of material excess. The fifth category - C5 - with 14.6% includes images of limited image quality.

At first sight, the C1 category seems to be a big issue, however, this issue could be overcome by the development of algorithms that identify the ROI by matching the imaged structure to the expected structure and rotate the image as required. Similarly, the matching of the expected geometry with the binarized images enabled the selection of ROIs avoiding additional paths present in images categorized as C2. Remarkably, only a subset of images showed the geometry as it was designed regarding the intended orientation. C5 contained images of limited acquisition quality, which could also be analyzed by the developed workflows as denoising steps. Sensitive thresholding was included. These steps could overcome artifacts such as dust or scratches on the substrate. The deposition of excessive amounts of material leading to fusing of the filaments or random geometries was categorized as C4. The images in this category did not resemble the expected geometries and could therefore not be analyzed. Regarding category C3, non-continuous filaments resembled the intended structure and could therefore be analyzed by the algorithms used. It is noteworthy that even though a sequence of dots can resemble a line, the intended structure was not complete. All in all, this evaluation of the images shows what kind of issues are to be expected in the future and helps with the development of analysis methods to distinguish between the various cases and the challenges to be reckoned with.

The subset of data of line geometries consisted of 648 images of line geometries, i.e., data sets of 54 images per laboratory. The share of images of printed line geometries showing broken filaments, thus classified as category C3, is presented in Figure 6.4 (B). An exemplary image is shown in Figure 6.3 (C). What can be clearly seen here is that there is a scatter in the laboratories between 2 to 65%. Which leads to the conclusion that even a simple structure like a single line or circle could not be printed by any laboratory with 100% reliability. This indicates that there are still significant challenges to be overcome regarding reliability and reproducibility of bioprinting, before

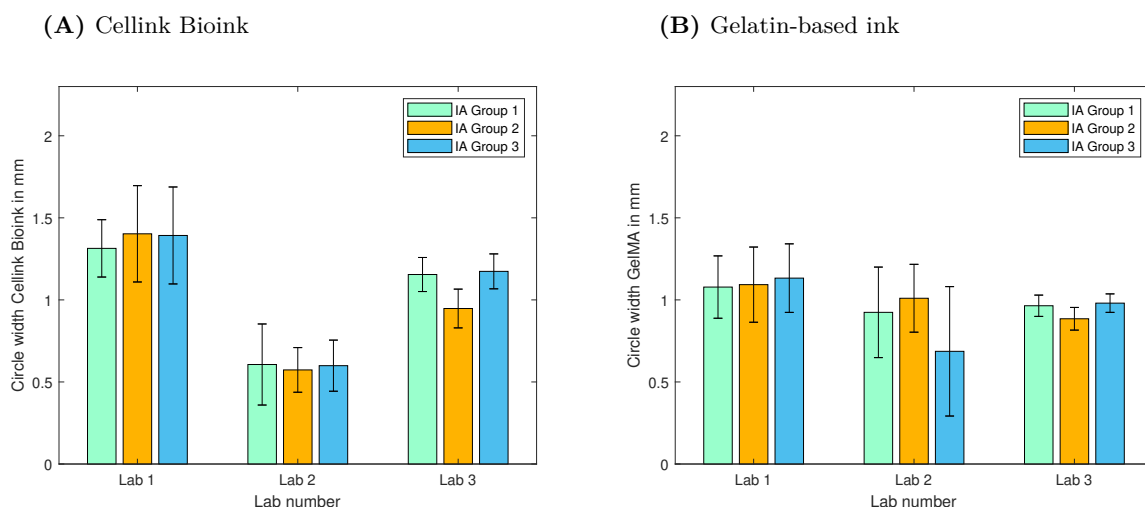


Figure 6.5 Filament width of circle geometries extracted by the three image analysis groups 1-3. In (A), the circle width printed with Cellink Bioink, and in (B), the circle width printed with gelatin-based ink are depicted with the respective standard deviations. The data of laboratories 1 to 3 are shown as exemplars. Each image analysis groups analyzed every single printed structure by all laboratories ($n = 108$), and the geometric parameters were determined where possible.

medical applications with high regulatory requirements are intended. Although the entire process was standardized as much as possible, the results differed significantly between the laboratories. This large scatter might be a clear indicator of the results being nevertheless still highly dependent on the operator and printer. However, it was not feasible to determine which of both factors is the main cause of variability. After having conducted the visual qualitative analysis, the main deviations were identified and can be considered to be applied in the future development of analytics. Possible countermeasures for future round robins might be (a) further improvement of the SOPs, (b) training of the laboratory staff along the SOPs, and (c) refinement of the IA procedures towards potential outliers.

6.3.3 Round robin - Image analysis: quantitative

Following printing and data storage, three groups specialized in IA developed an image processing workflow to extract the features of the objects without prior knowledge of the categorized deviations. In order to investigate whether the three methods developed by the IA groups might lead to different results, the geometric features of each group extracted per laboratory were compared. For simplification, exemplary results of one analysis parameter, i.e. the circle width (see Figure A5.2 in the supplementary section) printed with Cellink Bioink and with gelatin-based ink for three laboratories, are presented in Figure 6.5.

In Figure 6.5, the results as regards circle width and variation of the 'strand' when printing a circle and the associated standard deviations printed by three laboratories and extracted by all three IA groups are shown, Cellink Bioink in A) and the gelatin-based ink in B). For Cellink Bioink, the circle width determined by the different IA groups were: (a) Lab 1 1.4 mm, (b) Lab 2 0.6 mm, (c) Lab 3 1.1 mm. Comparing single laboratories, the results extracted by the IA groups are in the

same range. The largest difference of extracted data was observed for Lab 3 ranging from a circle width of 0.95 ± 0.10 mm, to a circle width of 1.17 ± 0.10 mm. The extracted measurements regarding filament width of line and circle structures differed slightly when comparing the data extracted by the different IA workflows. The deviations in the metrics might originate from the different methodologies used in the preprocessing of the images, where background noise and artifacts are removed. Similarly, the edges of the printed structures were not detected in an equal manner by all IA groups. The extraction of data was thus affected. As mentioned above, the acquired images showed issues such as weak contrast between ink and background. These issues regarding image quality also influence the extraction capability of automated image processing. Future studies should include the assessment of performance of automated IA including a comparison of images by determination of the Jaccard index or the Sorensen-Dice coefficient. These parameters enable quantification of the similarity between the analyzed image and the ground-truth presented as the desired geometry. This might not be an easy task, as the designed geometry is transferred as STL file between locations. The geometry to be printed is sliced by each printer software in different manner. Especially for more complex structures, this could lead to differences in the printing path and therefore in the produced geometry. It must be noted, that the image processing groups were not included in the development of the imaging setup. This can be improved in future studies. Nevertheless, all three independently developed methods delivered results in similar ranges which in turn emphasizes the suitability and robustness of automated image processing as an evaluation tool. Here, the focus was initially placed on single-layer objects, since the first layer is crucial because all other layers are applied on top of it. Automated image processing should also be applied to three-dimensional structures in future studies.

In the following, for a quantitative analysis of printed structures and the assessment of the reproducibility of printing processes, only a subset of data is presented. Several hypotheses were tested and only data of qualified laboratories were selected. Any variations in mean and standard deviations of the geometric features account for the effects proceeding from the printing process or the used ink. The exemplary data is presented in three case studies comparing extrusion mechanism, coordinate calibration, and temperature control of the printing equipment used (chapters 6.3.4.1-6.3.4.3). Additionally, the selection of inks was also limited to Cellink Bioink and gelatin-based ink, since these differ most in terms of appearance. Furthermore, the gelatin-based ink shows a thermo-sensitive property due to the sol-gel transition of the protein solution [119].

6.3.4 Assessment of the reproducibility in 3D bioprinting

6.3.4.1 Case study 1: pneumatic vs. mechanical extrusion

In the design of the round robin test and the conception of SOPs, the utmost possible standardization was used. The printers represented the parameter with the greatest leeway, since not all laboratories had the same models available. Thus, factors influencing the reproducibility of 3D bioprinting in different laboratories were examined by grouping the data from different laboratories that presented similarities in terms of the function of the used printing equipment. A first aspect to be examined was the extrusion mechanism of the used equipment. Therefore, data sets of laboratories using the same device model were compared with those of laboratories that used custom models. The Cellink BioX printer is equipped with pneumatic powered printheads. Lab 3, Lab 4, Lab 8, Lab 11, and Lab 12 set the pneumatic pressure to 23, 25, 20, 23, and 20 kPa, respectively. In contrast, all three custom models used piston-driven extrusion using the velocity of axial movement of the piston as a

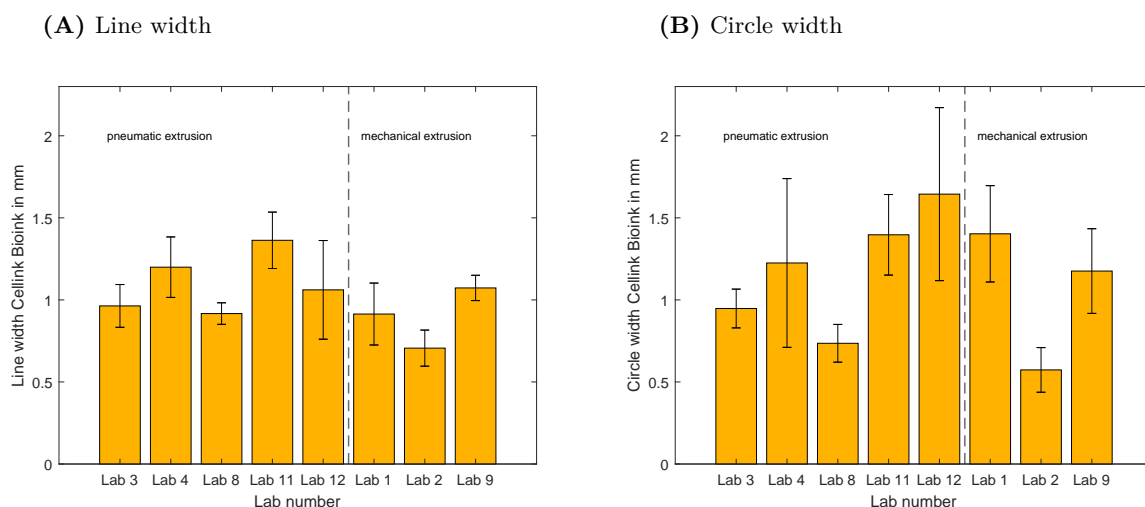


Figure 6.6 Filament width of geometries printed with Cellink Bioink. In (A), the mean line width, and in (B), the mean circle width are presented. The laboratories are classified according to the extrusion mechanism of the used printers. On the left side of each diagram, data is shown from laboratories using pneumatically driven printers. On the right side, data is presented from laboratories using custom-made printers based on the movement of a piston.

Table 6.3 Summary of the coefficients of variation (CV) for each laboratory regarding the examination of the effects of the extrusion mechanism on the filament width.

Lab	Pneumatic extrusion					Mechanical extrusion		
	3	4	8	11	12	1	2	9
	Line width Cellink Bioink							
CV in %	13.5	15.4	7.2	12.6	28.3	20.7	15.6	7.2
	Circle width Cellink Bioink							
CV in %	12.5	42.0	15.6	17.6	32.1	20.9	23.7	21.9

printing setting. In Figure 6.6, the line and circle structures were selected and quantified in terms of filament width.

The widths of the lines and circles printed with Cellink Bioink are presented in Figure 6.6 (A) and (B), respectively. The printed lines by the laboratories using the pneumatically driven mechanism showed a width in the range of 0.96 to 1.36 mm with standard deviations between 0.07 mm and 0.3 mm. The line widths extracted from geometries printed with the mechanical extrusion systems were in the range of 0.71 to 1.07 mm, and the associated standard deviations showed values varying from 0.08 to 0.19 mm. The widths of printed circles by the group of laboratories using pneumatic extrusion had a minimal mean value of 0.74 mm achieved by Lab 8 with a standard deviation of 0.12 mm. The maximum mean circle width and standard deviation were produced by Lab 12 with values of 1.64 mm and 0.53 mm, respectively. The circle width extracted from the samples printed with the piston-driven devices presented mean values between 0.57 mm and 1.4 mm. The related standard deviations are within the range of 0.14 to 0.29 mm. The effect of the extrusion mechanism

was compared by calculation of the CV, and the values are provided in Table 6.3. The CVs of the pneumatically driven process are in a wide range between 7.2 to 42.0%. In contrast, the CVs of the mechanical piston printers are within a clearly narrower range from 7.2 to 23.7%. The filament width should be independent of the trajectory of the printhead, as long as the printing velocity is the same. Therefore, low variability should be the case in the comparison between line and circle width. The higher variabilities of the widths of lines and circles printed with all five pneumatically driven systems was shown although the same experimental setup was used using pressures within the range of 20 to 25 kPa. All five bioprinters are the same model, windows of printing parameters were the same in all laboratories, and the labware used was provided centrally by the organizing laboratory. Additionally, the ink was acquired centrally from a single batch and distributed to the participating laboratories. It is noteworthy that the biomaterial is delivered in a filled cartridge ready to use. The high inter- and intralaboratory variability of the printed structures might be related to the function of the device where the extrusion pressure is supplied by a compact, built-in compressor that might not be able to hold the set pressure over the whole processing time. Furthermore, the tubes connecting the air supply with the cartridge are loose in the housing and, depending on the tube length, might get squeezed depending on the position of the printhead in relation to the housing. Additionally, several laboratories reported occasional clogging of the nozzles when using this ink. Such deficiency can occur when the material is not homogeneously mixed, leading to an aggregation of the nanocellulose used as a thickener. Similar issues regarding heterogeneities of bioinks and the effect on printing have been shown by Chung *et al.* [250]. Regarding the mean values of the filament width produced in the laboratories, the difference can be explained by the round robin setup and the functionality of the printers. The organizing laboratory set a minimum and maximum target filament width with additional information as to which pressure values were necessary to produce these strand widths with a representative printer during the test design. As the mechanical extrusion printers used in the round robin test were custom-manufactured devices, the respective laboratories had to determine the printer parameters necessary to reach the target filament width individually with regard to the individual printer. The lower variability in the data produced by the single laboratories could be explained by the extrusion mechanism where the piston displacement pushes the ink out of the cartridge. In contrast to pneumatic extrusion, material heterogeneities do not affect the ink flow as this is defined by the chosen speed of the displacement of the piston. The presented data in this comparison demonstrated the influence of the extrusion mechanism leading to non-reproducible printing processes, and showed the advantages of piston-operated extrusions systems used in the field of bioprinting. Alternatively, further methods to increase the reproducibility of pneumatic extrusion have been presented by Armstrong *et al.* [282] and by Wenger *et al.* [171]. Both studies involve the process monitoring and adaptation of the pneumatic pressure. The first method uses a laser scanner to measure the deposited filament width and corrects the printing parameter to reach a certain width. The latter monitors the flow rate and corrects the pneumatic pressure to overcome fluctuations. A further aspect of printing systems that can highly influence the printed geometry is the calibration of coordinates, i.e., the distance between the tip of the nozzle and the surface of the used substrate.

6.3.4.2 Case study 2: coordinate calibration

In terms of the investigation of the effect of coordinate calibration on the reproducibility of bioprinting, the five laboratories operating with the same printer were grouped again. This model requires the operator to set the z-height manually. A second group of laboratories was considered

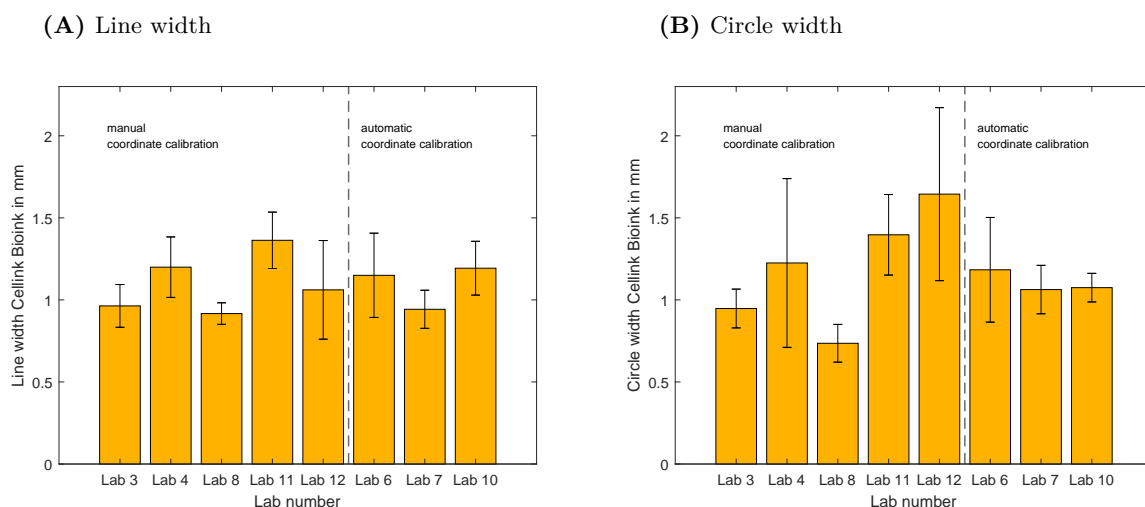


Figure 6.7 Filament width of geometries printed with Cellink Bioprint. In (A), the mean line width, and in (B), the mean circle width are presented. The laboratories are classified according to the mechanism used for coordinate calibration. On the left side of each diagram, data is shown from laboratories using a printer where the position of the tip of the nozzle is calibrated manually by the operator. On the right side, the process of coordinate calibration is performed automatically using an optical sensor.

Table 6.4 Summary of the coefficients of variation (CV) for each laboratory regarding the examination of the effects of the method used for coordinate calibration on the filament width.

Lab	Manual coordinate calibration					Automatic coordinate calibration		
	3	4	8	11	12	6	7	10
	Line width Cellink Bioprint							
CV in %	13.5	15.4	7.2	12.6	28.3	22.3	12.3	13.7
	Circle width Cellink Bioprint							
CV in %	12.5	42.0	15.6	17.6	32.1	27.0	13.9	8.1

for comparison, these used printing systems equipped with optical sensors for determination of the coordinates of the nozzle tip, i.e., the process was automated. In Figure 6.7, the results of line width (A), and circle width (B) are shown, both structures were printed with Cellink Bioprint. The CV was also calculated for each laboratory and is given in Table 6.4.

The range of the mean line width printed after manual calibration of the coordinates was 0.92 to 1.36 mm, and the line width range for the automated setting of coordinates was 0.94 to 1.19 mm. In terms of standard deviation, the highest value was 0.3 mm, shown by the data from equipment where manual coordination calibration was performed, and was generally in the range of 0.07 to 0.3 mm. For the printers equipped with automated coordinate calibration features, the standard deviation with a value of 0.26 mm was the highest. Deviations from the mean were in a lower range with 0.12 to 0.26 mm compared to the group of printers with manual calibration procedures. Regarding the data from circle mean width, the range is even larger with a range of 0.74 to 1.64 mm for the data produced with the manually calibrated printers. A smaller range was detected for automatic

Table 6.5 Summary of the coefficients of variation (CV) for each laboratory regarding the examination of the effects of the mechanism for temperature control on the filament width.

Lab	No heating				Electric heating					Fluid circulation		
	2	4	5	7	3	8	9	11	12	1	6	10
	Line width gelatin-based ink											
CV in %	22.2	32.5	17.1	9.8	4.5	14.7	13.1	7.1	21.3	24.6	14.0	15.4
	Circle width gelatin-based ink											
CV in %	20.5	46.2	27.4	8.8	7.8	16.7	15.1	38.6	29.0	21.0	7.2	21.6

calibration with a range of 1.06 to 1.18 mm. Similarly to the mean width of the printed circle, the standard deviation increases as well for the first group, i.e., printers required to be manually calibrated regarding the z-height. The values of the standard deviation were in the range of 0.12 to 0.53 mm. The standard deviation of the circle width produced by the printers of the second group was in the range of 0.09 to 0.32 mm. The CVs of the line width printed with Cellink Bioink using manually calibrated printers showed a maximum value of 28.3%. The maximum value of the CVs was lower in the group of automated calibration printers with 22.3%. The difference between CVs was larger when circle geometries were printed. The first group and second group showed CVs up to 42.0% and 27%, respectively. Overall, the results regarding filament width and CVs are an indication of the fact that the operator-dependent calibration step introduces variations into the printing process as the distance between surface of the substrate and nozzle tip cannot be manually set to a standard value. The effect of varying distance between the tip of the nozzle and the surface of the substrate on the filament width has been shown by Naghieh *et al.* [92]. Therefore, the automation of the coordinate calibration enhances the robustness of the printing process. In the first and second case studies, Cellink Bioink was used. This ink shows viscoelastic properties such as shear-thinning, as reported in literature [137, 283]. A more complex rheological behavior is presented by the gelatin-based ink which was used as a third case study. The protein solution undergoes gelation under physiological temperatures [119, 138], and, therefore, the printing process using gelatin-based ink is challenged by the ability of the printer to heat and control the temperature at the cartridge.

6.3.4.3 Case study 3: temperature control

To examine the impact of the different printer configurations influencing the reproducibility of printed geometries with gelatin-based ink, the laboratories were grouped according to the types of temperature control of the respective printers. The extracted data is shown in Figure 6.8, where the line width is shown again in (A), and the circle width in (B) from the different laboratories. The four bioprinters on the left side have no cartridge temperature control, the five in the middle have an electric heating, and the three bioprinters on the right side are equipped with a fluid circulation heating, where the fluid temperature is set externally. In Lab 3, Lab 9, Lab 12, Lab 1, Lab 6, Lab 10 a temperature of 23 °C, 23.5 °C, 23 °C, 21 °C, 24 °C and 22.5 °C was used respectively. Two laboratories increased the temperature during the experiments. Lab 8 performed the experiments in a range of 23 °C to 26 °C and Lab 11 in a range of 21 °C to 25 °C. The respective CVs are given in Table 6.5.

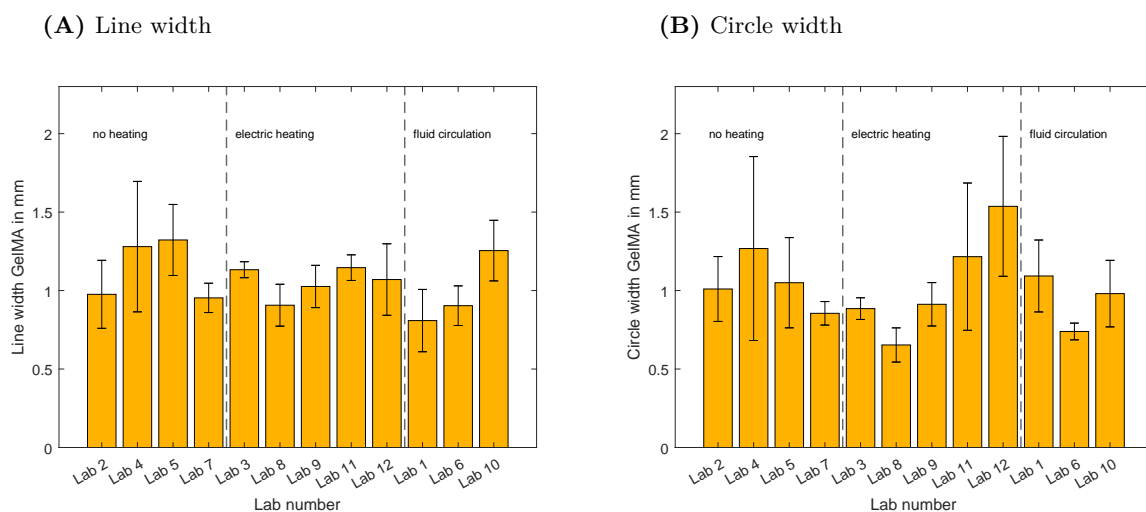


Figure 6.8 Filament width of geometries printed with gelatin-based ink. In (A), the mean line width, and in (B), the mean circle width are presented. The laboratories are classified according to the mechanism used for temperature control. On the left side of each diagram, data is shown from laboratories using equipment without heating elements. In the middle, data is shown from the devices equipped with electric heating in the cartridge holder. On the right side, the temperature control uses fluid circulation and an external setting of the fluid temperature.

The results of the mean line width of the group with no temperature control showed values in the range from 0.95 to 1.32 mm and standard deviations in a range of 0.09 to 0.42 mm. In the second group of printers, i.e., devices equipped with electric heating, the mean line widths were in the range of 0.91 to 1.15 mm with standard deviations in the range of 0.05 to 0.23 mm. The mean widths of lines printed with equipment where the temperature is controlled by fluid circulation were in the range of 0.86 to 1.27 mm with standard deviations between 0.07 mm and 0.59 mm. The results of mean circle width are in the range of 0.89 to 1.54 mm with standard deviations between 0.08 to 0.59 mm without heating, in the range of 0.65 to 1.54 mm with standard deviations between 0.07 to 0.47 mm for electric heating, and in the range of 0.74 to 1.09 mm with standard deviations between 0.05 to 0.23 mm for fluid circulation. The variability of the intralaboratory comparison is reflected in the respective CV. The highest variability was observed in the samples produced by the group of laboratories using printers without the capability of heating the cartridge during the process, where the CVs show values in the range of 9.8 to 32.5% regarding the line geometry, and the variability according to the CVs increased to 8.8 to 46.2% regarding the circle geometry. The same trend was observed in the group of printers with electric heating elements. The CVs of the printed line structures are in the range of 4.5 to 21.3%, and in the range of 7.8 to 38.6% regarding printed circles. The variability of the width of printed geometries produced with printers with temperature control over fluid circulation was lower both for lines and circles where the calculated CVs were 14.0 to 24.6%, and 7.2 to 21.6%, respectively. As solutions containing gelatin and gelatin derivatives undergo a sol-gel transition around physiological temperatures [119], the heating of the cartridge containing bioinks is essential. Without the control of temperature, the gelatin-based ink undergoes a transition into a gel state where the viscosity increases during processing time. This process has been shown to be time-dependent and to be affected by the temperature difference

between solution and environment [284, 285]. A further challenge regarding the use of gelatin-based inks is the possible clogging of nozzles which is mentioned in further bioprinting studies [130, 188]. The SOPs indicated that the printing parameters should be kept constant during a printing session, i.e., printing of six technical replicates. However, it was mentioned as well that it is possible to increase the pneumatic pressure as a measure to counteract the gelation of the gelatin-based ink. The low variability of the structures, both lines and circles, produced by Lab 7 without heating can be explained by the fact that the pressure was adjusted, i.e., increased, during the printing process. In contrast, Lab 5 increased the pneumatic pressure during printing as well, which did not improve the variability of printed geometries. A second possibility to counteract gelation of the gelatin-based ink was the possibility to increase the temperature of the cartridge holder. This measure was taken by Lab 8 and Lab 11. Both groups used printers equipped with electric heating. While the CV of printed lines and circles by Lab 8 stayed in the same range, the CVs of printed lines and circles by Lab 11 differed notably. This shows the important effect of the individual operators on the printing process and printed geometries. Laboratories using printers of the third group, i.e., where the temperature is regulated over fluid circulation, completed the experimental series without the adjustment of printing parameters, both pneumatic pressure and printing temperature. Over the external setting of fluid temperature, the cooling of the cartridge is possible in contrast to the electric elements that are only able to heat the cartridge. It is noteworthy that the lowest variability was shown by the results by Lab 3. Overall, it can be stated that individual operators, and the different equipment of the printer affect the results and, thus, limit the comparability of the provided data. In order to provide robust printing processes, there is still a need for process control and higher degrees of automation in the printing equipment.

6.4 Conclusions

The presented study highlights the successful collaboration of 15 groups nationwide with the shared goal of analyzing reproducibility and introducing standards to the bioprinting field in order to accelerate the transition from laboratory practice to production for clinical applications. For this round robin study, SOPs were written containing information about material preparation, use of labware, and experimental printing setup. Materials were acquired and distributed centrally by the organizing laboratory. Identical imaging conditions were provided by use of the BioFI prototype instrument and the data was centrally managed in the Kadi4Mat platform. During the evaluation process, a distinction was made between a qualitative and a quantitative IA. In the qualitative investigation, it was shown that several deviations in the printing and imaging processes occurred. This study provides an up-to-date overview of possible deviations and helps to analyze where the process needs to be enhanced. An important outcome was that the individual operators still had a significant impact on the resulting structure. Similarly, the recognition of possible factors diminishing the reproducibility of the process after imaging can be differentiated and included in the development of automated IA. These issues were not considered by the three IA groups because the analysis was performed simultaneously and independently. Three different methods obtained results in the similar range regarding geometric features of the printed samples. This proved that automated IA is a suitable tool for the assessment of printing process reproducibility and quantitative comparability in the bioprinting field is by far not achieved, yet, due to lack of standardization in terms of bioprinting equipment. Hereby, devices equipped with pistons for mechanical extrusion, automated calibration of coordinates, especially z-height, and temperature-controlled printheads

proved to be advantageous. Although target line widths were used in this study as a method for device-independent transfer, the product equivalency between locations could not be shown. In the future development of bioprinters, the above-mentioned problems need to be addressed. Ultimately, different cell types must be included in the process and the effects of cellular material on the reproducibility need to be characterized. Thereby, a significant effect is expected. The production of bioprinted structures might face requirements imposed by regulatory agencies when trying to make the leap into clinical stages. These agencies require information on the range of operating conditions that will result in the products and materials meeting certain quality criteria. This preliminary round robin test identified significant present challenges to be overcome in order to provide robust bioprinting processes. Furthermore, a nationwide infrastructure and network is now established, which can be used for material evaluation and evaluation of standards in the field of bioprinting.

Conflict of interest

The authors declare that the research was conducted in the absence of any commercial or financial relationships that could be construed as a potential conflict of interest.

Author contributions

Conceptualization: DG, SS, SG, BS, and JH; Data curation - metadata production: DG, SS, SG, BS, TJ, JG, LM, IS, HH, KSL, SZ, PK, SSc, AW, AS, GEMT, TA, MG, TS, RD, ARB, TN, CLT, CW, and TG; Data curation - interpretation of research data : DG, SS, SG, and BS; Formal analysis: DG, and SS; Funding acquisition: JH; Investigation - performance of experiments: DG, SS, SG, BS, TJ, JG, LM, IS, HH, KSL, SZ, PK, SSc, AW, AS, GEMT, TA, MG, TS, RD, ARB, TN, CLT, CW, and TG; Methodology - experimental design: DG, SS, SG and BS; Methodology - material development: TJ, JG, SZ, PK, AW, SSc, TA, and MG; Project administration: JH; Resources: JH; Software: DG, SS, NB, MS, SA, BK, TF, HB, JB, AVG, and DP; Supervision: JH; Validation: DG, and SS; Visualization: DG, and SS; Writing - original draft: DG, and SS; Writing - review & editing: SG, BS, TJ, JG, LM, IS, HH, KSL, NB, MS, SZ, PK, AS, GEMT, SSc, AW, TA, MG, TS, RD, ARB, TN, CLT, CW, TG, SA, BK, TF, HB, JB, DP, AVG, and JH.

All authors have read and agreed to the published version of the manuscript.

Acknowledgments

The authors wish to express their thanks for the support the following scientists of the institutions mentioned above for the collaboration during the experimental and analysis part in this study: Ellena Fuhrmann, Markus Germann, Fritz Koch, Lukas Kornelius, Annika Lechner, Klaus-Martin Reichert, and Matthias Ruopp. We acknowledge support by the KIT-Publication Fund of the Karlsruhe Institute of Technology.

Data availability statement

The data cannot be made publicly available upon publication because no suitable repository exists for hosting data in this field of study. The data that support the findings of this study are available upon reasonable request from the authors

Chapter references

- [38] J. Malda *et al.*, „25th Anniversary Article: Engineering Hydrogels for Biofabrication“, *Advanced Materials*, vol. 25, no. 36, pp. 5011–5028, 09/2013.
- [39] W. Sun *et al.*, „The bioprinting roadmap“, *Biofabrication*, vol. 12, no. 2, p. 022002, 04/2020.
- [92] S. Naghieh, M. Sarker, N. K. Sharma, Z. Barhomi, and X. Chen, „Printability of 3D Printed Hydrogel Scaffolds: Influence of Hydrogel Composition and Printing Parameters“, *Applied Sciences*, vol. 10, no. 1, p. 292, 2019.
- [119] K. Y. Lee and D. J. Mooney, „Hydrogels for Tissue Engineering“, *Chemical Reviews*, vol. 101, no. 7, pp. 1869–1880, 07/2001.
- [130] E. Hoch, T. Hirth, G. E. Tovar, and K. Borchers, „Chemical tailoring of gelatin to adjust its chemical and physical properties for functional bioprinting“, *Journal of Materials Chemistry B*, vol. 1, no. 41, pp. 5675–5685, 2013.
- [137] K. Hölzl, S. Lin, L. Tytgat, S. Van Vlierberghe, L. Gu, and A. Ovsianikov, „Bioink properties before, during and after 3D bioprinting“, *Biofabrication*, vol. 8, no. 3, p. 032002, 09/2016.
- [138] W. Liu *et al.*, „Extrusion Bioprinting of Shear-Thinning Gelatin Methacryloyl Bioinks“, *Advanced Healthcare Materials*, vol. 6, no. 12, pp. 1–11, 06/2017.
- [167] J. Groll *et al.*, „A definition of bioinks and their distinction from biomaterial inks“, *Biofabrication*, vol. 11, no. 1, p. 013001, 11/2018.
- [171] L. Wenger, S. Strauß, and J. Hubbuch, „Automated and dynamic extrusion pressure adjustment based on real-time flow rate measurements for precise ink dispensing in 3D bioprinting“, *Bioprinting*, vol. 28, no. July, e00229, 12/2022.
- [177] Y. He, F. Yang, H. Zhao, Q. Gao, B. Xia, and J. Fu, „Research on the printability of hydrogels in 3D bioprinting“, *Scientific Reports*, vol. 6, no. 1, p. 29977, 07/2016.
- [178] T. Gao *et al.*, „Optimization of gelatin–alginate composite bioink printability using rheological parameters: a systematic approach“, *Biofabrication*, vol. 10, no. 3, p. 034106, 06/2018.
- [179] A. A. Aldana, F. Valente, R. Dilley, and B. Doyle, „Development of 3D bioprinted GelMA-alginate hydrogels with tunable mechanical properties“, *Bioprinting*, vol. 21, no. June 2020, e00105, 03/2021.
- [185] W. Schuurman *et al.*, „Gelatin-Methacrylamide Hydrogels as Potential Biomaterials for Fabrication of Tissue-Engineered Cartilage Constructs“, *Macromolecular Bioscience*, vol. 13, no. 5, pp. 551–561, 05/2013.
- [188] I. Pepelanova, K. Kruppa, T. Scheper, and A. Lavrentieva, „Gelatin-Methacryloyl (GelMA) Hydrogels with Defined Degree of Functionalization as a Versatile Toolkit for 3D Cell Culture and Extrusion Bioprinting“, *Bioengineering*, vol. 5, no. 3, p. 55, 07/2018.
- [195] B. Lee, N. Lum, L. Seow, P. Lim, and L. Tan, „Synthesis and Characterization of Types A and B Gelatin Methacryloyl for Bioink Applications“, *Materials*, vol. 9, no. 10, p. 797, 09/2016.
- [227] F. P. Melchels, W. J. Dhert, D. W. Hutmacher, and J. Malda, „Development and characterisation of a new bioink for additive tissue manufacturing“, *Journal of Materials Chemistry B*, vol. 2, no. 16, pp. 2282–2289, 2014.
- [233] S. V. Murphy and A. Atala, „3D bioprinting of tissues and organs“, *Nature Biotechnology*, vol. 32, no. 8, pp. 773–785, 08/2014.
- [243] M. Uzun-Per *et al.*, „Automated Image Analysis Methodologies to Compute Bioink Printability“, *Advanced Engineering Materials*, vol. 23, no. 4, pp. 1–12, 04/2021.
- [250] J. H. Y. Chung *et al.*, „Bio-ink properties and printability for extrusion printing living cells“, *Biomaterials Science*, vol. 1, no. 7, p. 763, 2013.
- [256] J. Marzi *et al.*, „Non-Invasive Three-Dimensional Cell Analysis in Bioinks by Raman Imaging“, *ACS Applied Materials & Interfaces*, vol. 14, no. 27, pp. 30455–30465, 07/2022.
- [259] K. Tröndle *et al.*, „Scalable fabrication of renal spheroids and nephron-like tubules by bioprinting and controlled self-assembly of epithelial cells“, *Biofabrication*, vol. 13, no. 3, p. 035019, 07/2021.
- [260] B. Schmiege *et al.*, „Structured Data Storage for Data-Driven Process Optimisation in Bioprinting“, *Applied Sciences*, vol. 12, no. 15, p. 7728, 08/2022.
- [261] P. Bartolo, A. Malshe, E. Ferraris, and B. Koc, „3D bioprinting: Materials, processes, and applications“, *CIRP Annals*, vol. 71, no. 2, pp. 577–597, 2022.
- [262] M. Hospodiuk, M. Dey, D. Sosnoski, and I. T. Ozbolat, „The bioink: A comprehensive review on bioprintable materials“, *Biotechnology Advances*, vol. 35, no. 2, pp. 217–239, 2017.
- [263] S. Seiffert and J. Sprakel, „Physical chemistry of supramolecular polymer networks“, *Chemical Society Reviews*, vol. 41, no. 2, pp. 909–930, 2012.
- [264] J. Chrenek, R. Kirsch, K. Scheck, and S. M. Willerth, „Protocol for printing 3D neural tissues using the BIO X equipped with a pneumatic printhead“, *STAR Protocols*, vol. 3, no. 2, p. 101348, 2022.

- [265] S. Strauß, D. Grijalva Garces, and J. Hubbuch, „Analytics in Extrusion-Based Bioprinting: Standardized Methods Improving Quantification and Comparability of the Performance of Bioinks“, *Polymers*, vol. 15, no. 8, p. 1829, 04/2023.
- [266] L. Ouyang, R. Yao, Y. Zhao, and W. Sun, „Effect of bioink properties on printability and cell viability for 3D bioplotting of embryonic stem cells“, *Biofabrication*, vol. 8, no. 3, p. 035 020, 09/2016.
- [267] E. Karakaya, L. Fischer, J. Hazur, A. R. Boccaccini, I. Thievensen, and R. Detsch, „Strategies to evaluate alginate based bioinks applying extrusion printing for biofabrication“, *Transactions on Additive Manufacturing Meets Medicine*, vol. 2, no. 1, pp. 1–2, 2020.
- [268] A. Ribeiro *et al.*, „Assessing bioink shape fidelity to aid material development in 3D bioprinting“, *Biofabrication*, vol. 10, no. 1, p. 014 102, 11/2017.
- [269] J. M. Rodríguez-Rego, L. Mendoza-Cerezo, A. Macías-García, J. P. Carrasco-Amador, and A. C. Marcos-Romero, „Methodology for characterizing the printability of hydrogels“, *International Journal of Bioprinting*, vol. 9, no. 2, pp. 280–291, 01/2023.
- [270] A. Schwab, R. Levato, M. D’Este, S. Piluso, D. Eglin, and J. Malda, „Printability and Shape Fidelity of Bioinks in 3D Bioprinting“, *Chemical Reviews*, vol. 120, no. 19, pp. 11 028–11 055, 10/2020.
- [271] T. Kreller, T. Distler, S. Heid, S. Gerth, R. Detsch, and A. Boccaccini, „Physico-chemical modification of gelatine for the improvement of 3D printability of oxidized alginate-gelatine hydrogels towards cartilage tissue engineering“, *Materials & Design*, vol. 208, p. 109 877, 10/2021.
- [272] V. Bednarzig, S. Schrüfer, T. C. Schneider, D. W. Schubert, R. Detsch, and A. R. Boccaccini, „Improved 3D Printing and Cell Biology Characterization of Inorganic-Filler Containing Alginate-Based Composites for Bone Regeneration: Particle Shape and Effective Surface Area Are the Dominant Factors for Printing Performance“, *International Journal of Molecular Sciences*, vol. 23, no. 9, p. 4750, 04/2022.
- [273] E. Karakaya *et al.*, „How to Determine a Suitable Alginate for Biofabrication Approaches using an Extensive Alginate Library?“, *Biomacromolecules*, vol. 24, no. 7, pp. 2982–2997, 07/2023.
- [274] A. Wenz, K. Borchers, G. E. M. Tovar, and P. J. Kluger, „Bone matrix production in hydroxyapatite-modified hydrogels suitable for bone bioprinting“, *Biofabrication*, vol. 9, no. 4, p. 044 103, 11/2017.
- [275] K. Markstedt, A. Mantas, I. Tournier, H. Martínez Ávila, D. Hägg, and P. Gatenholm, „3D bioprinting human chondrocytes with nanocellulose-alginate bioink for cartilage tissue engineering applications“, *Biomacromolecules*, vol. 16, no. 5, pp. 1489–1496, 2015.
- [276] N. Brandt *et al.*, „Kadi4Mat: A Research Data Infrastructure for Materials Science“, *Data Science Journal*, vol. 20, no. 1, pp. 1–14, 02/2021.
- [277] S. van der Walt *et al.*, „scikit-image: image processing in Python“, *PeerJ*, vol. 2, no. 1, e453, 06/2014.
- [278] K. He, J. Sun, and X. Tang, „Guided image filtering“, *IEEE Transactions on Pattern Analysis and Machine Intelligence*, vol. 35, no. 6, pp. 1397–1409, 2013.
- [279] P. F. Alcantarilla, A. Bartoli, and A. J. Davison, „KAZE Features“, in *Computer Vision – ECCV 2011*, Berlin/Heidelberg, Germany: Springer Berlin Heidelberg, 2012, pp. 214–227.
- [280] A. F. Frangi, W. J. Niessen, K. L. Vincken, and M. A. Viergever, „Multiscale vessel enhancement filtering“, in *Medical Image Computing and Computer-Assisted Intervention — MICCAI’98*, Berlin/Heidelberg, Germany: Springer Berlin Heidelberg, 1998, pp. 130–137.
- [281] Y. Tsin and T. Kanade, „A Correlation-Based Approach to Robust Point Set Registration“, in *Computer Vision - ECCV 2004*, Berlin/Heidelberg, Germany: Springer Berlin Heidelberg, 2004, pp. 558–569.
- [282] A. A. Armstrong, A. G. Alleyne, and A. J. Wagoner Johnson, „1D and 2D error assessment and correction for extrusion-based bioprinting using process sensing and control strategies“, *Biofabrication*, vol. 12, no. 4, p. 045 023, 10/2020.
- [283] M. Kesti, P. Fisch, M. Pensalfini, E. Mazza, and M. Zenobi-Wong, „Guidelines for standardization of bioprinting: A systematic study of process parameters and their effect on bioprinted structures“, *BioNanoMaterials*, vol. 17, no. 3-4, pp. 193–204, 2016.
- [284] M. Djabourov, J. Leblond, and P. Papon, „Gelation of aqueous gelatin solutions. I. Structural investigation“, *Journal de Physique*, vol. 49, no. 2, pp. 319–332, 1988.
- [285] Y. Maki and M. Annaka, „Gelation of fish gelatin studied by multi-particle tracking method“, *Food Hydrocolloids*, vol. 101, no. October 2019, p. 105 525, 04/2020.

Conclusion and Outlook

Biomaterials as a multidisciplinary field upholds the potential to improve biomanufacturing processes for pharmaceutical proteins and cell therapies. However, the lack of effective transfer of knowledge and associated methodologies has resulted in limited comparability and reproducibility, impeding the translation of research findings into clinical applications. Versatile biomaterials covering a wide range of applications are advantageous since many options are available in the formulations. Gelatin methacryloyl (GelMA) is a suitable candidate as it can fulfill macroscopic and microscopic requirements in several applications, which include structural stability and biocompatibility. This thesis aims to gain better knowledge regarding GelMA and its applications and strengthen the concept of interdisciplinary research while developing robust processes and analytical methods.

The first part of the thesis covered the production of GelMA and the characterization of GelMA-based hydrogels. Chapter 3 presented a suitable approach for the functionalization of gelatin at room temperature, therefore enhancing the robustness of the process as no heating was required. As the study focused on processing the single most used gelatin product, the principle was transferred to further raw materials in research presented in Chapter 4. Eight different gelatin products of varying species and bloom strength were modified here. The degree of functionalization of the protein depended on gelatin origin, bloom value, and reactant ratio. Furthermore, even batch-to-batch variations proved to affect the reaction. Due to the immiscibility of the reactant methacrylic anhydride with the aqueous phase, the adsorption and, hence, the functionalization of gelatin highly depends on molecular weight, its distribution, and surface charge. Therefore, it was shown that the reaction process has to be adapted if the raw material is changed. In both studies, the viscoelastic properties of the hydrogel were determined. Hydrogels with tunable elasticity were prepared by varying the protein concentration and degree of functionalization. Furthermore, the raw materials also affected the elasticity since bloom strength increases with molecular weight, influencing crosslink density. The methodology for determining the degree of functionalization consisted of offline analytics. Process analytical technologies could be applied to better describe the production of GelMA. For instance, Raman spectroscopy could be implemented as inline analytics

of the conversion of the double bonds. Hence, determining optimal reaction parameters, including reaction time.

Furthermore, the biocompatibility of hydrogels was evaluated in Chapter 3. NIH 3T3 fibroblasts were seeded onto hydrogels, and the viability was determined during a three-day period. Cellular staining and microscopy were performed for this purpose. The staining consisted of three components for detecting three cell populations, living death, and all cells. This experimental strategy and a developed image processing workflow enabled the recognition of single cells in overlapping regions. The automated quantification improved the analytical time and increased the size of the data sets as a more significant number of images could be evaluated. In addition, the biocompatibility GelMA hydrogels prepared with the presented approach showed no difference compared to those prepared using a conventional process. In Chapter 4, the application of GelMA for the microfluidic production of droplets and the crosslinking to hydrogel microparticles is shown. With precise formulation of the aqueous phase, the microfluidic fabrication was enabled at room temperature at high GelMA concentrations. Both droplet and particle sizes were determined using automated image analysis. Droplet size increased with decreasing feed rate ratio of the continuous to disperse phase. The swelling behavior of hydrogel microparticles increased with decreasing protein concentration. Future studies should characterize the droplet generation process thoroughly. A better understanding of dripping and jetting regimes can be accomplished using dimensionless numbers. Furthermore, inline particle size monitoring can be implemented to regulate the feed rates and set the desired droplet size. In general, automated image analysis was confirmed to be a reliable tool for quantifying cells at a microscopic level and determining the macroscopic size of droplets and particles.

The second part of this study consists of two studies examining the printing performance of GelMA-containing bioinks. As comparability across studies in the literature is restricted, establishing a comparable experimental setup and implementing robust analytical strategies were the aims of the study shown in Chapter 5. The rheological characterization of two bioinks was performed, and the acquired data was used to calculate the required pneumatic pressure for an extrusion-based bioprinter. As the viscosity of the bioinks differed, the pneumatic pressure for each formulation also differed. This approach enabled the setting of equal flow rates and, hence, the comparison of printed structures with the same amount of deposited biomaterial. The overall performance of a bioink includes printing accuracy and the processing effects on cells. The accuracy was determined by extracting geometric features of the printed structures using automated image analysis. The impact of bioink mixing and printing on cells was determined using cell fluorescent staining and flow cytometry. Both image analysis and flow cytometry enabled the quantification of large numbers of structures and cells compared to the literature and increased the statistical accuracy of the studies. Moreover, while the printed geometries exhibited no structural differences, the bioink of the higher viscosity had a detrimental effect on cells. Further studies should characterize the effects of equal flow rates on the accuracy of three-dimensional structures. Additionally, non-destructive analytics should be implemented to study the short- and long-term impact of printing processes on cells. One possible method for this purpose is Raman imaging, which also does not require cellular stains.

Similarly, reproducibility and replicability have also been a concern in biomaterials science and bioprinting. This is due to the lack of standardized materials, procedures, and analysis strategies. The study presented in Chapter 6 evaluated whether bioprinting processes can be standardized. Twelve groups in academia received standardized operational procedures, biomaterials, labware, and printing supplies. Additionally, the imaging equipment for the data generation was the same in every facility. Solely, the bioprinters differed. After the printing and imaging the basic geometries, images, and manufacturing records were centrally stored. A qualitative inspection of the images

revealed common issues in printing and analysis. Quantitative data was extracted from the images by three independent groups. Moreover, data analysis led to the conclusion that data reproducibility is not yet possible. High variability was demonstrated overall in an inter-laboratory comparison. Intra-laboratory variability depended on the printing equipment. Features of printers that enabled a more reproducible experimental procedure include mechanically driven mechanisms, fluid circulating heaters, and automated determination of nozzle coordinates. Records showed that the operator still plays a crucial role in the printing process results. Studies in the future should focus on the reproducibility of three-dimensional structures and the characterization of the effect that cell-laden bioinks have on the final structures.

Overall, the present work provides an improved understanding of the manufacturing process of GelMA, and the effect of the raw materials was achieved. Moreover, a processing workflow was proposed that enhanced the robustness of widening the operating range. Additionally, a microfluidic method was successfully established, enabling the use of droplets with high GelMA concentrations as templates for particles in a single-stage process. Furthermore, implementing principles and adapting analytical techniques already available in other fields is the core of interdisciplinary research. This included the development of automated image processing and analysis strategies to reveal microscopic and macroscopic characteristics of biomaterials. The statistical accuracy of cell viability increased due to large numbers of analyzed cells in images or by implementing flow cytometry. In addition, methodological variability was reduced by setting comparable experimental setups based on rheological properties and calculating the flow rate of bioinks. Critical features of bioprinting equipment that enhance reproducible processes were identified. The presented methodological procedures can be used to characterize further biomaterials. By reintroducing the original multidisciplinary approach, research can contribute to meaningful advancements.

References

- [1] E. L. S. Fong, B. M. Watson, F. K. Kasper, and A. G. Mikos, „Building Bridges: Leveraging Interdisciplinary Collaborations in the Development of Biomaterials to Meet Clinical Needs“, *Advanced Materials*, vol. 24, no. 36, pp. 4995–5013, 09/2012.
- [2] Y. Xu, C. Chen, P. B. Hellwarth, and X. Bao, „Biomaterials for stem cell engineering and biomanufacturing“, *Bioactive Materials*, vol. 4, no. July 2019, pp. 366–379, 2019.
- [3] W. R. Wagner, S. E. Sakiyama-Elbert, G. Zhang, and M. J. Yaszemski, *Biomaterials Science: An Introduction to Materials in Medicine*, 4th ed., W. R. Wagner, S. E. Sakiyama-Elbert, G. Zhang, and M. J. Yaszemski, Eds. London, United Kingdom: Academic Press, 2020, pp. 1–1586.
- [4] D. F. Williams, „On the nature of biomaterials“, *Biomaterials*, vol. 30, no. 30, pp. 5897–5909, 10/2009.
- [5] R. J. Wade and J. A. Burdick, „Engineering ECM signals into biomaterials“, *Materials Today*, vol. 15, no. 10, pp. 454–459, 10/2012.
- [6] F. Ruedinger, A. Lavrentieva, C. Blume, I. Pepelanova, and T. Scheper, „Hydrogels for 3D mammalian cell culture: a starting guide for laboratory practice“, *Applied Microbiology and Biotechnology*, vol. 99, no. 2, pp. 623–636, 01/2015.
- [7] S. Xiao *et al.*, „Gelatin Methacrylate (GelMA)-Based Hydrogels for Cell Transplantation: an Effective Strategy for Tissue Engineering“, *Stem Cell Reviews and Reports*, vol. 15, no. 5, pp. 664–679, 10/2019.
- [8] S. O’Brien, Y. Park, S. Azarin, and W.-S. Hu, „Cell Culture Bioprocess Technology: Biologics and Beyond“, in *Cell Culture Technology*, C. Kasper, V. Charwat, and A. Lavrentieva, Eds., Cham, Switzerland: Springer, 2018, ch. 1, pp. 1–21.
- [9] F. Eberhardt *et al.*, „Impact of serum-free media on the expansion and functionality of CD19.CAR T-cells“, *International Journal of Molecular Medicine*, vol. 52, no. 1, p. 58, 05/2023.
- [10] K. E. Wellen and C. B. Thompson, „Cellular Metabolic Stress: Considering How Cells Respond to Nutrient Excess“, *Molecular Cell*, vol. 40, no. 2, pp. 323–332, 10/2010.

- [11] V. Charwat and D. Egger, „The Third Dimension in Cell Culture: From 2D to 3D Culture Formats“, in *Cell Culture Technology*, C. Kasper, V. Charwat, and A. Lavrentieva, Eds., Cham, Switzerland: Springer, 2018, ch. 5, pp. 75–90.
- [12] J. W. Deitmer, S. M. Theparambil, I. Ruminot, S. I. Noor, and H. M. Becker, „Energy Dynamics in the Brain: Contributions of Astrocytes to Metabolism and pH Homeostasis“, *Frontiers in Neuroscience*, vol. 13, no. December, pp. 1–7, 12/2019.
- [13] R. C. Vergara *et al.*, „The Energy Homeostasis Principle: Neuronal Energy Regulation Drives Local Network Dynamics Generating Behavior“, *Frontiers in Computational Neuroscience*, vol. 13, no. July, pp. 1–18, 07/2019.
- [14] G. Kroemer and J. Pouyssegur, „Tumor Cell Metabolism: Cancer’s Achilles’ Heel“, *Cancer Cell*, vol. 13, no. 6, pp. 472–482, 06/2008.
- [15] W. G. Kaelin and C. B. Thompson, „Clues from cell metabolism“, *Nature*, vol. 465, no. 7298, pp. 562–564, 06/2010.
- [16] M. Teifel, „Transfektion von Säugerzellen“, in *Gentechnische Methoden*, 1944, Heidelberg, Germany: Spektrum Akademischer Verlag, 2012, pp. 351–383.
- [17] A. Lavrentieva, „Essentials in Cell Culture“, in *Cell Culture Technology*, C. Kasper, V. Charwat, and A. Lavrentieva, Eds., Cham, Switzerland: Springer, 2018, ch. 2, pp. 23–48.
- [18] T. Criswell *et al.*, „Shipping and Logistics Considerations for Regenerative Medicine Therapies“, *Stem Cells Translational Medicine*, vol. 11, no. 2, pp. 107–113, 03/2022.
- [19] B. Rubinsky, „Principles of Low Temperature Cell Preservation“, *Heart Failure Reviews*, vol. 8, no. 3, pp. 277–284, 2003.
- [20] F. Li, N. Vijayasankaran, A. (Shen, R. Kiss, and A. Amanullah, „Cell culture processes for monoclonal antibody production“, *mAbs*, vol. 2, no. 5, pp. 466–479, 09/2010.
- [21] K. R. Kim and W.-H. Yeo, „Advances in sensor developments for cell culture monitoring“, *BMEMat*, vol. 1, no. 4, 12/2023.
- [22] S. Elmore, „Apoptosis: A Review of Programmed Cell Death“, *Toxicologic Pathology*, vol. 35, no. 4, pp. 495–516, 2007.
- [23] M. Ghasemi, T. Turnbull, S. Sebastian, and I. Kempson, „The MTT Assay: Utility, Limitations, Pitfalls, and Interpretation in Bulk and Single-Cell Analysis“, *International Journal of Molecular Sciences*, vol. 22, no. 23, p. 12 827, 11/2021.
- [24] A. Adan, G. Alizada, Y. Kiraz, Y. Baran, and A. Nalbant, „Flow cytometry: basic principles and applications“, *Critical Reviews in Biotechnology*, vol. 37, no. 2, pp. 163–176, 02/2017.
- [25] P. Bikmulina *et al.*, „3D or not 3D: a guide to assess cell viability in 3D cell systems“, *Soft Matter*, vol. 18, no. 11, pp. 2222–2233, 2022.
- [26] J. R. Masters, „HeLa cells 50 years on: the good, the bad and the ugly“, *Nature Reviews Cancer*, vol. 2, no. 4, pp. 315–319, 04/2002.
- [27] E. Tan, C. S. H. Chin, Z. F. S. Lim, and S. K. Ng, „HEK293 Cell Line as a Platform to Produce Recombinant Proteins and Viral Vectors“, *Frontiers in Bioengineering and Biotechnology*, vol. 9, no. 12, pp. 1–9, 12/2021.

- [28] S. Derakhti, S. H. Safiabadi-Tali, G. Amoabediny, and M. Sheikhpour, „Attachment and detachment strategies in microcarrier-based cell culture technology: A comprehensive review“, *Materials Science and Engineering: C*, vol. 103, no. 4, p. 109782, 10/2019.
- [29] C. F. Bellani, J. Ajeian, L. Duffy, M. Miotto, L. Groenewegen, and C. J. Cannon, „Scale-Up Technologies for the Manufacture of Adherent Cells“, *Frontiers in Nutrition*, vol. 7, no. November, 11/2020.
- [30] A. D. Henn *et al.*, „Cytocentric measurement for regenerative medicine“, *Frontiers in Medical Technology*, vol. 5, no. April, pp. 1–6, 04/2023.
- [31] „CellProfiler: Image analysis software for identifying and quantifying cell phenotypes“, *Genome Biology*, vol. 7, no. 10, R100, 2006.
- [32] M. A. Bray *et al.*, „Cell Painting, a high-content image-based assay for morphological profiling using multiplexed fluorescent dyes“, *Nature Protocols*, vol. 11, no. 9, pp. 1757–1774, 2016.
- [33] E. Cukierman, R. Pankov, and K. M. Yamada, „Cell interactions with three-dimensional matrices“, *Current Opinion in Cell Biology*, vol. 14, no. 5, pp. 633–640, 10/2002.
- [34] F. Pampaloni, E. G. Reynaud, and E. H. K. Stelzer, „The third dimension bridges the gap between cell culture and live tissue“, *Nature Reviews Molecular Cell Biology*, vol. 8, no. 10, pp. 839–845, 10/2007.
- [35] M. J. Gomez-Lechón *et al.*, „Long-term expression of differentiated functions in hepatocytes cultured in three-dimensional collagen matrix“, *Journal of Cellular Physiology*, vol. 177, no. 4, pp. 553–562, 12/1998.
- [36] J. Lee, M. J. Cuddihy, and N. A. Kotov, „Three-Dimensional Cell Culture Matrices: State of the Art“, *Tissue Engineering Part B: Reviews*, vol. 14, no. 1, pp. 61–86, 03/2008.
- [37] J. L. Drury and D. J. Mooney, „Hydrogels for tissue engineering: scaffold design variables and applications“, *Biomaterials*, vol. 24, no. 24, pp. 4337–4351, 11/2003.
- [38] J. Malda *et al.*, „25th Anniversary Article: Engineering Hydrogels for Biofabrication“, *Advanced Materials*, vol. 25, no. 36, pp. 5011–5028, 09/2013.
- [39] W. Sun *et al.*, „The bioprinting roadmap“, *Biofabrication*, vol. 12, no. 2, p. 022002, 04/2020.
- [40] M. Gargotti, U. Lopez-Gonzalez, H. J. Byrne, and A. Casey, „Comparative studies of cellular viability levels on 2D and 3D in vitro culture matrices“, *Cytotechnology*, vol. 70, no. 1, pp. 261–273, 02/2018.
- [41] F. Bonnier *et al.*, „Cell viability assessment using the Alamar blue assay: A comparison of 2D and 3D cell culture models“, *Toxicology in Vitro*, vol. 29, no. 1, pp. 124–131, 02/2015.
- [42] P. Chandra, J. J. Yoo, and S. J. Lee, „Biomaterials in regenerative medicine: Challenges in technology transfer from science to process development“, in *Translational Regenerative Medicine*, Cambridge, United Kingdom: Elsevier, 2015, ch. 13, pp. 151–167.
- [43] M. Vallet-Regí, „Evolution of Biomaterials“, *Frontiers in Materials*, vol. 9, no. March, pp. 1–5, 03/2022.
- [44] D. F. Williams, „On the mechanisms of biocompatibility“, *Biomaterials*, vol. 29, no. 20, pp. 2941–2953, 07/2008.

- [45] A. J. Ryan and F. J. O'Brien, „Insoluble elastin reduces collagen scaffold stiffness, improves viscoelastic properties, and induces a contractile phenotype in smooth muscle cells“, *Biomaterials*, vol. 73, pp. 296–307, 12/2015.
- [46] C. Bason, M. Gallorini, and A. C. Berardi, „The Extracellular Matrix, Growth Factors and Morphogens in Biomaterial Design and Tissue Engineering“, in *Extracellular Matrix for Tissue Engineering and Biomaterials*, A. C. Berardi, Ed., 1st ed., Cham, Switzerland: Humana Cham, 2018, ch. 1, pp. 3–26.
- [47] C. F. Guimarães, L. Gasperini, A. P. Marques, and R. L. Reis, „The stiffness of living tissues and its implications for tissue engineering“, *Nature Reviews Materials*, vol. 5, no. 5, pp. 351–370, 02/2020.
- [48] M. Gómez-Florit, R. M. Domingues, S. M. Bakht, B. B. Mendes, R. L. Reis, and M. E. Gomes, „Natural Materials“, in *Biomaterials Science*, Fourth Edi, London, United Kingdom: Elsevier, 2020, pp. 361–375.
- [49] K. Schenke-Layland, S. Liebscher, and S. L. Layland, „Use of Extracellular Matrix Proteins and Natural Materials in Bioengineering“, in *Biomaterials Science*, Fourth Edi, London, United Kingdom: Elsevier, 2020, pp. 401–413.
- [50] G. Singh and A. Chanda, „Mechanical properties of whole-body soft human tissues: a review“, *Biomedical Materials*, vol. 16, no. 6, p. 062004, 11/2021.
- [51] T. H. Qazi *et al.*, „Programming hydrogels to probe spatiotemporal cell biology“, *Cell Stem Cell*, vol. 29, no. 5, pp. 678–691, 05/2022.
- [52] L. G. Griffith and M. A. Swartz, „Capturing complex 3D tissue physiology in vitro“, *Nature Reviews Molecular Cell Biology*, vol. 7, no. 3, pp. 211–224, 03/2006.
- [53] C. Sobacchi, E. Palagano, A. Villa, and C. Menale, „Soluble Factors on Stage to Direct Mesenchymal Stem Cells Fate“, *Frontiers in Bioengineering and Biotechnology*, vol. 5, no. MAY, pp. 1–9, 05/2017.
- [54] E. Cukierman, R. Pankov, D. R. Stevens, and K. M. Yamada, „Taking Cell-Matrix Adhesions to the Third Dimension“, *Science*, vol. 294, no. 5547, pp. 1708–1712, 11/2001.
- [55] V. Vogel and M. Sheetz, „Local force and geometry sensing regulate cell functions“, *Nature Reviews Molecular Cell Biology*, vol. 7, no. 4, pp. 265–275, 04/2006.
- [56] K. A. Jansen, D. M. Donato, H. E. Balcioglu, T. Schmidt, E. H. Danen, and G. H. Koenderink, „A guide to mechanobiology: Where biology and physics meet“, *Biochimica et Biophysica Acta (BBA) - Molecular Cell Research*, vol. 1853, no. 11, pp. 3043–3052, 11/2015.
- [57] P. Kollmannsberger, C. M. Bidan, J. W. C. Dunlop, and P. Fratzl, „The physics of tissue patterning and extracellular matrix organisation: how cells join forces“, *Soft Matter*, vol. 7, no. 20, p. 9549, 2011.
- [58] K. Burridge and C. Guilly, „Focal adhesions, stress fibers and mechanical tension“, *Experimental Cell Research*, vol. 343, no. 1, pp. 14–20, 04/2016.
- [59] C.-M. Lo, H.-B. Wang, M. Dembo, and Y.-l. Wang, „Cell Movement Is Guided by the Rigidity of the Substrate“, *Biophysical Journal*, vol. 79, no. 1, pp. 144–152, 07/2000.
- [60] A. J. Engler, S. Sen, H. L. Sweeney, and D. E. Discher, „Matrix Elasticity Directs Stem Cell Lineage Specification“, *Cell*, vol. 126, no. 4, pp. 677–689, 08/2006.

- [61] G. Broughton, J. E. Janis, and C. E. Attinger, „The Basic Science of Wound Healing“, *Plastic and Reconstructive Surgery*, vol. 117, no. SUPPLEMENT, 12S–34S, 06/2006.
- [62] B. Li and J. H. Wang, „Fibroblasts and myofibroblasts in wound healing: Force generation and measurement“, *Journal of Tissue Viability*, vol. 20, no. 4, pp. 108–120, 11/2011.
- [63] D. Dado and S. Levenberg, „Cell–scaffold mechanical interplay within engineered tissue“, *Seminars in Cell & Developmental Biology*, vol. 20, no. 6, pp. 656–664, 08/2009.
- [64] P. E. Rouse, „A Theory of the Linear Viscoelastic Properties of Dilute Solutions of Coiling Polymers“, *The Journal of Chemical Physics*, vol. 21, no. 7, pp. 1272–1280, 07/1953.
- [65] R. H. Colby, „Structure and linear viscoelasticity of flexible polymer solutions: comparison of polyelectrolyte and neutral polymer solutions“, *Rheologica Acta*, vol. 49, no. 5, pp. 425–442, 05/2010.
- [66] M. Rubinstein, R. H. Colby, and A. V. Dobrynin, „Dynamics of semidilute polyelectrolyte solutions“, *Physical Review Letters*, vol. 73, no. 20, pp. 2776–2779, 1994.
- [67] B. A. Miller-Chou and J. L. Koenig, „A review of polymer dissolution“, *Progress in Polymer Science*, vol. 28, no. 8, pp. 1223–1270, 08/2003.
- [68] T. Osswald and N. Rudolph, *Polymer Rheology*. München, Germany: Carl Hanser Verlag GmbH & Co. KG, 11/2014, pp. 101–141.
- [69] F. Irgens, *Rheology and non-newtonian fluids*. Berlin, Heidelberg, Germany: Springer International Publishing, 2013, vol. 9783319010533, pp. 1–190.
- [70] N. A. Peppas and A. S. Hoffman, „Hydrogels“, in *Biomaterials Science*, 1, Fourth Edi, London: Elsevier, 2020, pp. 153–166.
- [71] K. S. Lim, J. H. Galarraga, X. Cui, G. C. J. Lindberg, J. A. Burdick, and T. B. F. Woodfield, „Fundamentals and Applications of Photo-Cross-Linking in Bioprinting“, *Chemical Reviews*, vol. 120, no. 19, pp. 10662–10694, 10/2020.
- [72] N. Peppas, „Hydrogels in pharmaceutical formulations“, *European Journal of Pharmaceutics and Biopharmaceutics*, vol. 50, no. 1, pp. 27–46, 07/2000.
- [73] J. Jung and J. Oh, „Swelling characterization of photo-cross-linked gelatin methacrylate spherical microgels for bioencapsulation“, *e-Polymers*, vol. 14, no. 3, pp. 161–168, 05/2014.
- [74] Z. Wang, Z. Tian, F. Menard, and K. Kim, „Comparative study of gelatin methacrylate hydrogels from different sources for biofabrication applications“, *Biofabrication*, vol. 9, no. 4, p. 044101, 08/2017.
- [75] M. B. Aljaber, F. Verisqa, Z. Keskin-Erdogan, K. D. Patel, D. Y. S. Chau, and J. C. Knowles, „Influence of Gelatin Source and Bloom Number on Gelatin Methacryloyl Hydrogels Mechanical and Biological Properties for Muscle Regeneration“, *Biomolecules*, vol. 13, no. 5, p. 811, 05/2023.
- [76] N. A. Peppas, J. Z. Hilt, A. Khademhosseini, and R. Langer, „Hydrogels in Biology and Medicine: From Molecular Principles to Bionanotechnology“, *Advanced Materials*, vol. 18, no. 11, pp. 1345–1360, 06/2006.
- [77] M. Sutter, J. Siepmann, W. E. Hennink, and W. Jiskoot, „Recombinant gelatin hydrogels for the sustained release of proteins“, *Journal of Controlled Release*, vol. 119, no. 3, pp. 301–312, 2007.

- [78] T. Nii, „Strategies using gelatin microparticles for regenerative therapy and drug screening applications“, *Molecules*, vol. 26, no. 22, pp. 1–10, 2021.
- [79] P. Kofinas, „Hydrogels prepared by electron irradiation of poly(ethylene oxide) in water solution: unexpected dependence of cross-link density and protein diffusion coefficients on initial PEO molecular weight“, *Biomaterials*, vol. 17, no. 15, pp. 1547–1550, 1996.
- [80] L. Wenger and J. Hubbuch, „Investigation of Lysozyme Diffusion in Agarose Hydrogels Employing a Microfluidics-Based UV Imaging Approach“, *Frontiers in Bioengineering and Biotechnology*, vol. 10, no. March, pp. 1–12, 03/2022.
- [81] K. S. Anseth, C. N. Bowman, and L. Brannon-Peppas, „Mechanical properties of hydrogels and their experimental determination“, *Biomaterials*, vol. 17, no. 17, pp. 1647–1657, 01/1996.
- [82] J. R. Tse and A. J. Engler, „Preparation of Hydrogel Substrates with Tunable Mechanical Properties“, *Current Protocols in Cell Biology*, vol. 47, no. 1, pp. 1–16, 06/2010.
- [83] C. T. McKee, J. A. Last, P. Russell, and C. J. Murphy, „Indentation Versus Tensile Measurements of Young’s Modulus for Soft Biological Tissues“, *Tissue Engineering Part B: Reviews*, vol. 17, no. 3, pp. 155–164, 06/2011.
- [84] M. A. Kotlarchyk, E. L. Botvinick, and A. J. Putnam, „Characterization of hydrogel microstructure using laser tweezers particle tracking and confocal reflection imaging“, *Journal of Physics: Condensed Matter*, vol. 22, no. 19, p. 194 121, 05/2010.
- [85] A. Sheikhi and R. J. Hill, „Hydrogel–colloid interfacial interactions: a study of tailored adhesion using optical tweezers“, *Soft Matter*, vol. 12, no. 31, pp. 6575–6587, 2016.
- [86] K. M. Schultz and E. M. Furst, „Microrheology of biomaterial hydrogelators“, *Soft Matter*, vol. 8, no. 23, p. 6198, 2012.
- [87] J. Roether, S. Bertels, C. Oelschlaeger, M. Bastmeyer, and N. Willenbacher, „Microstructure, local viscoelasticity and cell culture suitability of 3D hybrid HA/collagen scaffolds“, *PLOS ONE*, vol. 13, no. 12, J. D. Schieber, Ed., e0207397, 12/2018.
- [88] J. Hafner *et al.*, „Monitoring matrix remodeling in the cellular microenvironment using microrheology for complex cellular systems“, *Acta Biomaterialia*, vol. 111, pp. 254–266, 07/2020.
- [89] M. W. Tibbitt and K. S. Anseth, „Hydrogels as extracellular matrix mimics for 3D cell culture“, *Biotechnology and Bioengineering*, vol. 103, no. 4, pp. 655–663, 07/2009.
- [90] R. Ravichandran *et al.*, „Functionalised type-I collagen as a hydrogel building block for bio-orthogonal tissue engineering applications“, *Journal of Materials Chemistry B*, vol. 4, no. 2, pp. 318–326, 2016.
- [91] Z. Li *et al.*, „Tuning Alginate-Gelatin Bioink Properties by Varying Solvent and Their Impact on Stem Cell Behavior“, *Scientific Reports*, vol. 8, no. 1, p. 8020, 05/2018.
- [92] S. Naghieh, M. Sarker, N. K. Sharma, Z. Barhoumi, and X. Chen, „Printability of 3D Printed Hydrogel Scaffolds: Influence of Hydrogel Composition and Printing Parameters“, *Applied Sciences*, vol. 10, no. 1, p. 292, 2019.
- [93] J. A. Burdick, C. Chung, X. Jia, M. A. Randolph, and R. Langer, „Controlled Degradation and Mechanical Behavior of Photopolymerized Hyaluronic Acid Networks“, *Biomacromolecules*, vol. 6, no. 1, pp. 386–391, 01/2005.

- [94] B. Sarker *et al.*, „Evaluation of Fibroblasts Adhesion and Proliferation on Alginate-Gelatin Crosslinked Hydrogel“, *PLoS ONE*, vol. 9, no. 9, M. Yamamoto, Ed., e107952, 09/2014.
- [95] M. K. Cowman, H.-G. Lee, K. L. Schwertfeger, J. B. McCarthy, and E. A. Turley, „The Content and Size of Hyaluronan in Biological Fluids and Tissues“, *Frontiers in Immunology*, vol. 6, no. JUN, pp. 1–8, 06/2015.
- [96] G. Kogan, L. Šoltés, R. Stern, and P. Gemeiner, „Hyaluronic acid: a natural biopolymer with a broad range of biomedical and industrial applications“, *Biotechnology Letters*, vol. 29, no. 1, pp. 17–25, 12/2006.
- [97] M. A. Torres-Acosta *et al.*, „Comparative Economic Analysis Between Endogenous and Recombinant Production of Hyaluronic Acid“, *Frontiers in Bioengineering and Biotechnology*, vol. 9, no. July, pp. 1–14, 07/2021.
- [98] J. A. Burdick and G. D. Prestwich, „Hyaluronic Acid Hydrogels for Biomedical Applications“, *Advanced Materials*, vol. 23, no. 12, pp. 41–56, 03/2011.
- [99] B. P. Toole, „Hyaluronan: from extracellular glue to pericellular cue“, *Nature Reviews Cancer*, vol. 4, no. 7, pp. 528–539, 07/2004.
- [100] A. B. Csoka, G. I. Frost, and R. Stern, „The six hyaluronidase-like genes in the human and mouse genomes“, *Matrix Biology*, vol. 20, no. 8, pp. 499–508, 12/2001.
- [101] M. N. Collins and C. Birkinshaw, „Hyaluronic acid based scaffolds for tissue engineering—A review“, *Carbohydrate Polymers*, vol. 92, no. 2, pp. 1262–1279, 02/2013.
- [102] K. A. Smeds and M. W. Grinstaff, „Photocrosslinkable polysaccharides for in situ hydrogel formation“, *Journal of Biomedical Materials Research*, vol. 54, no. 1, pp. 115–121, 01/2001.
- [103] I. Donati and S. Paoletti, „Material Properties of Alginates“, in *Biology and Applications*, B. H. A. Rehm, Ed., Springer Berlin Heidelberg, 2009, ch. 1, pp. 1–53.
- [104] K. Y. Lee and D. J. Mooney, „Alginate: Properties and biomedical applications“, *Progress in Polymer Science*, vol. 37, no. 1, pp. 106–126, 01/2012.
- [105] M. B. Łabowska, I. Michalak, and J. Detyna, „Methods of extraction, physicochemical properties of alginates and their applications in biomedical field - A review“, *Open Chemistry*, vol. 17, no. 1, pp. 738–762, 2019.
- [106] A. D. Augst, H. J. Kong, and D. J. Mooney, „Alginate Hydrogels as Biomaterials“, *Macromolecular Bioscience*, vol. 6, no. 8, pp. 623–633, 08/2006.
- [107] R. Schrieber and H. Gareis, *Gelatine Handbook*. Weinheim, Germany: Wiley, 02/2007.
- [108] P. Privalov, E. Tiktopulo, and V. Tischenko, „Stability and mobility of the collagen structure“, *Journal of Molecular Biology*, vol. 127, no. 2, pp. 203–216, 01/1979.
- [109] M. Djabourov, J.-P. Lechère, and F. Gaill, „Structure and rheology of gelatin and collagen gels“, *Biorheology*, vol. 30, no. 3-4, pp. 191–205, 08/1993.
- [110] J. Brinckmann, „Collagens at a Glance“, in *Topics in Current Chemistry*, vol. 247, 04/2005, pp. 1–6.
- [111] „The Collagen Suprafamily: From Biosynthesis to Advanced Biomaterial Development“, *Advanced Materials*, vol. 31, no. 1, 2019.

- [112] A. Tirella, T. Liberto, and A. Ahluwalia, „Riboflavin and collagen: New crosslinking methods to tailor the stiffness of hydrogels“, *Materials Letters*, vol. 74, pp. 58–61, 05/2012.
- [113] H. Liang, S. J. Russell, D. J. Wood, and G. Tronci, „Monomer-Induced Customization of UV-Cured Atelocollagen Hydrogel Networks“, *Frontiers in Chemistry*, vol. 6, no. DEC, pp. 1–14, 12/2018.
- [114] J. M. Lee, S. K. Q. Suen, W. L. Ng, W. C. Ma, and W. Y. Yeong, „Bioprinting of Collagen: Considerations, Potentials, and Applications“, *Macromolecular Bioscience*, vol. 21, no. 1, pp. 1–18, 01/2021.
- [115] N. J. Bulleid, D. C. A. John, and K. E. Kadler, „Recombinant expression systems for the production of collagen“, *Biochemical Society Transactions*, vol. 28, no. 4, pp. 350–353, 08/2000.
- [116] S. Browne, D. I. Zeugolis, and A. Pandit, „Collagen: Finding a Solution for the Source“, *Tissue Engineering Part A*, vol. 19, no. 13-14, pp. 1491–1494, 07/2013.
- [117] A. A. Karim and R. Bhat, „Fish gelatin: properties, challenges, and prospects as an alternative to mammalian gelatins“, *Food Hydrocolloids*, vol. 23, no. 3, pp. 563–576, 2009.
- [118] I. Haug and K. Draget, „Gelatin“, in *Handbook of Food Proteins*, 1964, G. Phillips and P. Williams, Eds., Woodhead Publishing, 2011, pp. 92–115.
- [119] K. Y. Lee and D. J. Mooney, „Hydrogels for Tissue Engineering“, *Chemical Reviews*, vol. 101, no. 7, pp. 1869–1880, 07/2001.
- [120] T. Göckler *et al.*, „Tuning Superfast Curing Thiol-Norbornene-Functionalized Gelatin Hydrogels for 3D Bioprinting“, *Advanced Healthcare Materials*, vol. 10, no. 14, pp. 1–13, 07/2021.
- [121] A. I. Van Den Bulcke, B. Bogdanov, N. De Rooze, E. H. Schacht, M. Cornelissen, and H. Berghmans, „Structural and rheological properties of methacrylamide modified gelatin hydrogels“, *Biomacromolecules*, vol. 1, no. 1, pp. 31–38, 2000.
- [122] A. Habeeb, „Determination of free amino groups in proteins by trinitrobenzenesulfonic acid“, *Analytical Biochemistry*, vol. 14, no. 3, pp. 328–336, 03/1966.
- [123] B. H. Lee, H. Shirahama, N.-J. Cho, and L. P. Tan, „Efficient and controllable synthesis of highly substituted gelatin methacrylamide for mechanically stiff hydrogels“, *RSC Advances*, vol. 5, no. 128, pp. 106 094–106 097, 2015.
- [124] H. Shirahama, B. H. Lee, L. P. Tan, and N.-J. Cho, „Precise Tuning of Facile One-Pot Gelatin Methacryloyl (GelMA) Synthesis“, *Scientific Reports*, vol. 6, no. 1, p. 31 036, 08/2016.
- [125] H. Xu, J. Casillas, S. Krishnamoorthy, and C. Xu, „Effects of Irgacure 2959 and lithium phenyl-2,4,6-trimethylbenzoylphosphinate on cell viability, physical properties, and microstructure in 3D bioprinting of vascular-like constructs“, *Biomedical Materials*, vol. 15, no. 5, p. 055 021, 08/2020.
- [126] A. K. Nguyen, P. L. Goering, R. K. Elespuru, S. Sarkar Das, and R. J. Narayan, „The Photoinitiator Lithium Phenyl (2,4,6-Trimethylbenzoyl) Phosphinate with Exposure to 405 nm Light Is Cytotoxic to Mammalian Cells but Not Mutagenic in Bacterial Reverse Mutation Assays“, *Polymers*, vol. 12, no. 7, p. 1489, 07/2020.
- [127] M. Kirsch *et al.*, „Gelatin-Methacryloyl (GelMA) Formulated with Human Platelet Lysate Supports Mesenchymal Stem Cell Proliferation and Differentiation and Enhances the Hydrogel’s Mechanical Properties“, *Bioengineering*, vol. 6, no. 3, p. 76, 08/2019.

- [128] S.-B. Han, J.-K. Kim, G. Lee, and D.-H. Kim, „Mechanical Properties of Materials for Stem Cell Differentiation“, *Advanced Biosystems*, vol. 4, no. 11, pp. 1–17, 11/2020.
- [129] S. Liu, M. Jin, Y. Chen, L. Teng, D. Qi, and L. Ren, „Air-In-Water Emulsion Solely Stabilized by Gelatin Methacryloyl and Templating for Macroporous Nanocomposite Hydrogels“, *Macromolecular Chemistry and Physics*, vol. 220, no. 9, pp. 1–9, 05/2019.
- [130] E. Hoch, T. Hirth, G. E. Tovar, and K. Borchers, „Chemical tailoring of gelatin to adjust its chemical and physical properties for functional bioprinting“, *Journal of Materials Chemistry B*, vol. 1, no. 41, pp. 5675–5685, 2013.
- [131] M. Cuvellier *et al.*, „3D culture of HepaRG cells in GelMa and its application to bioprinting of a multicellular hepatic model“, *Biomaterials*, vol. 269, p. 120 611, 2021.
- [132] Z. Wang, R. Abdulla, B. Parker, R. Samanipour, S. Ghosh, and K. Kim, „A simple and high-resolution stereolithography-based 3D bioprinting system using visible light crosslinkable bioinks“, *Biofabrication*, vol. 7, no. 4, p. 045 009, 12/2015.
- [133] T. Tang *et al.*, „Microfluidic Fabrication of Gelatin Acrylamide Microgels through Visible Light Photopolymerization for Cell Encapsulation“, *ACS Applied Bio Materials*, vol. 6, no. 6, pp. 2496–2504, 06/2023.
- [134] J. Liu, T. Tagami, and T. Ozeki, „Fabrication of 3D-Printed Fish-Gelatin-Based Polymer Hydrogel Patches for Local Delivery of PEGylated Liposomal Doxorubicin“, *Marine Drugs*, vol. 18, no. 6, p. 325, 06/2020.
- [135] M. Vigata, C. Meinert, N. Bock, B. L. Dargaville, and D. W. Hutmacher, „Deciphering the Molecular Mechanism of Water Interaction with Gelatin Methacryloyl Hydrogels: Role of Ionic Strength, pH, Drug Loading and Hydrogel Network Characteristics“, *Biomedicines*, vol. 9, no. 5, p. 574, 05/2021.
- [136] A. H. Nguyen, J. McKinney, T. Miller, T. Bongiorno, and T. C. McDevitt, „Gelatin methacrylate microspheres for controlled growth factor release“, *Acta Biomaterialia*, vol. 13, pp. 101–110, 02/2015.
- [137] K. Hözl, S. Lin, L. Tytgat, S. Van Vlierberghe, L. Gu, and A. Ovsianikov, „Bioink properties before, during and after 3D bioprinting“, *Biofabrication*, vol. 8, no. 3, p. 032 002, 09/2016.
- [138] W. Liu *et al.*, „Extrusion Bioprinting of Shear-Thinning Gelatin Methacryloyl Bioinks“, *Advanced Healthcare Materials*, vol. 6, no. 12, pp. 1–11, 06/2017.
- [139] R. Gauvin *et al.*, „Microfabrication of complex porous tissue engineering scaffolds using 3D projection stereolithography“, *Biomaterials*, vol. 33, no. 15, pp. 3824–3834, 05/2012.
- [140] Z. Wang *et al.*, „Visible Light Photoinitiation of Cell-Adhesive Gelatin Methacryloyl Hydrogels for Stereolithography 3D Bioprinting“, *ACS Applied Materials & Interfaces*, vol. 10, no. 32, pp. 26 859–26 869, 08/2018.
- [141] J. Visser *et al.*, „Reinforcement of hydrogels using three-dimensionally printed microfibrils“, *Nature Communications*, vol. 6, no. 1, p. 6933, 04/2015.
- [142] J. Liang, H. Chen, Z. Guo, P. Dijkstra, D. Grijpma, and A. Poot, „Tough fibrous mats prepared by electrospinning mixtures of methacrylated poly(trimethylene carbonate) and methacrylated gelatin“, *European Polymer Journal*, vol. 152, no. February, 2021.

- [143] W. J. Seeto, Y. Tian, S. Pradhan, P. Kerscher, and E. A. Lipke, „Rapid Production of Cell-Laden Microspheres Using a Flexible Microfluidic Encapsulation Platform“, *Small*, vol. 15, no. 47, pp. 1–13, 11/2019.
- [144] K. Yue, G. Trujillo-de Santiago, M. M. Alvarez, A. Tamayol, N. Annabi, and A. Khademhosseini, „Synthesis, properties, and biomedical applications of gelatin methacryloyl (GelMA) hydrogels“, *Biomaterials*, vol. 73, pp. 254–271, 2015.
- [145] F. Piccinini, A. Tesei, C. Arienti, and A. Bevilacqua, „Cell Counting and Viability Assessment of 2D and 3D Cell Cultures: Expected Reliability of the Trypan Blue Assay“, *Biological Procedures Online*, vol. 19, no. 1, p. 8, 12/2017.
- [146] R. Szeliski, *Computer Vision* (Texts in Computer Science May). Cham, Switzerland: Springer International Publishing, 2022, ch. 3, pp. 85–151.
- [147] V. Wiesmann, D. Franz, C. Held, C. Münzenmayer, R. Palmisano, and T. Wittenberg, „Review of free software tools for image analysis of fluorescence cell micrographs“, *Journal of Microscopy*, vol. 257, no. 1, pp. 39–53, 01/2015.
- [148] S. Gretzinger, N. Beckert, A. Gleadall, C. Lee-Thedieck, and J. Hubbuch, „3D bioprinting – Flow cytometry as analytical strategy for 3D cell structures“, *Bioprinting*, vol. 11, no. March, e00023, 09/2018.
- [149] A. C. Daly, L. Riley, T. Segura, and J. A. Burdick, „Hydrogel microparticles for biomedical applications“, *Nature Reviews Materials*, vol. 5, no. 1, pp. 20–43, 2020.
- [150] A. L. Liu and A. J. García, „Methods for Generating Hydrogel Particles for Protein Delivery“, *Annals of Biomedical Engineering*, vol. 44, no. 6, pp. 1946–1958, 06/2016.
- [151] E. Amstad, „Emulsion Drops as Templates for the Fabrication of Microparticles and Capsules“, in *Droplet Microfluidics*, C. Ren and A. Lee, Eds., The Royal Society of Chemistry, 11/2020, pp. 261–289.
- [152] A. Dewandre, J. Rivero-Rodriguez, Y. Vitry, B. Sobac, and B. Scheid, „Microfluidic droplet generation based on non-embedded co-flow-focusing using 3D printed nozzle“, *Scientific Reports*, vol. 10, no. 1, p. 21 616, 12/2020.
- [153] N. Qin, „Fundamentals“, in *Droplet Microfluidics*, C. Ren and A. Lee, Eds., The Royal Society of Chemistry, 11/2020, pp. 15–44.
- [154] A. S. Utada, L.-Y. Chu, A. Fernandez-Nieves, D. R. Link, C. Holtze, and D. A. Weitz, „Dripping, Jetting, Drops, and Wetting: The Magic of Microfluidics“, *MRS Bulletin*, vol. 32, no. 9, pp. 702–708, 09/2007.
- [155] A. S. Utada, A. Fernandez-Nieves, J. M. Gordillo, and D. A. Weitz, „Absolute Instability of a Liquid Jet in a Coflowing Stream“, *Physical Review Letters*, vol. 100, no. 1, p. 014 502, 01/2008.
- [156] T. F. Tadros, *Volume 1 Interfacial Phenomena and Colloid Stability, Basic Principles*. Berlin, Germany: De Gruyter, 12/2015.
- [157] C. B. Highley, K. H. Song, A. C. Daly, and J. A. Burdick, „Jammed Microgel Inks for 3D Printing Applications“, *Advanced Science*, vol. 6, no. 1, p. 1 801 076, 01/2019.
- [158] E. X. Ng, M. Wang, S. H. Neo, C. A. Tee, C. H. Chen, and K. J. Van Vliet, „Dissolvable Gelatin-Based Microcarriers Generated through Droplet Microfluidics for Expansion and Culture of Mesenchymal Stromal Cells“, *Biotechnology Journal*, vol. 16, no. 3, pp. 1–10, 2021.

- [159] J. Huang *et al.*, „One-step generation of core–shell biomimetic microspheres encapsulating double-layer cells using microfluidics for hair regeneration“, *Biofabrication*, vol. 15, no. 2, p. 025 007, 04/2023.
- [160] Z. Lin *et al.*, „Bioactive Decellularized Extracellular Matrix Hydrogel Microspheres Fabricated Using a Temperature-Controlling Microfluidic System“, *ACS Biomaterials Science and Engineering*, vol. 8, no. 4, pp. 1644–1655, 2022.
- [161] S. Dutta, S. K. Pal, and R. Sen, „Digital Image Processing in Machining“, in *Modern Mechanical Engineering*, J. P. Davim, Ed., 1st ed., Berlin, Heidelberg, Germany: Springer, 2014, pp. 367–410.
- [162] B. L. DeCost and E. A. Holm, „A computer vision approach for automated analysis and classification of microstructural image data“, *Computational Materials Science*, vol. 110, pp. 126–133, 12/2015.
- [163] A. S. Basu, „Droplet morphometry and velocimetry (DMV): A video processing software for time-resolved, label-free tracking of droplet parameters“, *Lab on a Chip*, vol. 13, no. 10, pp. 1892–1901, 2013.
- [164] J.-C. Baret *et al.*, „Fluorescence-activated droplet sorting (FADS): efficient microfluidic cell sorting based on enzymatic activity“, *Lab on a Chip*, vol. 9, no. 13, p. 1850, 2009.
- [165] M. Chabert and J.-L. Viovy, „Microfluidic high-throughput encapsulation and hydrodynamic self-sorting of single cells“, *Proceedings of the National Academy of Sciences*, vol. 105, no. 9, pp. 3191–3196, 03/2008.
- [166] J. Groll *et al.*, „A definition of bioinks and their distinction from biomaterial inks“, *Biofabrication*, vol. 11, no. 1, p. 013 001, 11/2018.
- [167] J. Groll *et al.*, „A definition of bioinks and their distinction from biomaterial inks“, *Biofabrication*, vol. 11, no. 1, p. 013 001, 11/2018.
- [168] K. Dubbin, A. Tabet, and S. C. Heilshorn, „Quantitative criteria to benchmark new and existing bio-inks for cell compatibility“, *Biofabrication*, vol. 9, no. 4, p. 044 102, 09/2017.
- [169] „Biofabrication: A Guide to Technology and Terminology“, *Trends in Biotechnology*, vol. 36, no. 4, pp. 384–402, 04/2018.
- [170] F. Wulle *et al.*, „Multi-axis 3D printing of gelatin methacryloyl hydrogels on a non-planar surface obtained from magnetic resonance imaging“, *Additive Manufacturing*, vol. 50, no. December 2021, p. 102 566, 02/2022.
- [171] L. Wenger, S. Strauß, and J. Hubbuch, „Automated and dynamic extrusion pressure adjustment based on real-time flow rate measurements for precise ink dispensing in 3D bioprinting“, *Bioprinting*, vol. 28, no. July, e00229, 12/2022.
- [172] G. Gillispie *et al.*, „Assessment methodologies for extrusion-based bioink printability“, *Biofabrication*, vol. 12, no. 2, p. 022 003, 02/2020.
- [173] R. Chang, J. Nam, and W. Sun, „Effects of Dispensing Pressure and Nozzle Diameter on Cell Survival from Solid Freeform Fabrication–Based Direct Cell Writing“, *Tissue Engineering Part A*, vol. 14, no. 1, pp. 41–48, 01/2008.
- [174] A. A. Foster, L. M. Marquardt, and S. C. Heilshorn, „The diverse roles of hydrogel mechanics in injectable stem cell transplantation“, *Current Opinion in Chemical Engineering*, vol. 15, pp. 15–23, 02/2017.

- [175] N. Paxton, W. Smolan, T. Böck, F. Melchels, J. Groll, and T. Jungst, „Proposal to assess printability of bioinks for extrusion-based bioprinting and evaluation of rheological properties governing bioprintability“, *Biofabrication*, vol. 9, no. 4, p. 044 107, 11/2017.
- [176] A. Blaeser, D. F. Duarte Campos, U. Puster, W. Richtering, M. M. Stevens, and H. Fischer, „Controlling Shear Stress in 3D Bioprinting is a Key Factor to Balance Printing Resolution and Stem Cell Integrity“, *Advanced Healthcare Materials*, vol. 5, no. 3, pp. 326–333, 02/2016.
- [177] Y. He, F. Yang, H. Zhao, Q. Gao, B. Xia, and J. Fu, „Research on the printability of hydrogels in 3D bioprinting“, *Scientific Reports*, vol. 6, no. 1, p. 29 977, 07/2016.
- [178] T. Gao *et al.*, „Optimization of gelatin–alginate composite bioink printability using rheological parameters: a systematic approach“, *Biofabrication*, vol. 10, no. 3, p. 034 106, 06/2018.
- [179] A. A. Aldana, F. Valente, R. Dilley, and B. Doyle, „Development of 3D bioprinted GelMA–alginate hydrogels with tunable mechanical properties“, *Bioprinting*, vol. 21, no. June 2020, e00105, 03/2021.
- [180] T. Brosnan and D. W. Sun, „Improving quality inspection of food products by computer vision - A review“, *Journal of Food Engineering*, vol. 61, no. 1 SPEC. Pp. 3–16, 2004.
- [181] B. V. Slaughter, S. S. Khurshid, O. Z. Fisher, A. Khademhosseini, and N. A. Peppas, „Hydrogels in Regenerative Medicine“, *Advanced Materials*, vol. 21, no. 32-33, pp. 3307–3329, 09/2009.
- [182] D. E. Ingber, „Cellular mechanotransduction: putting all the pieces together again“, *The FASEB Journal*, vol. 20, no. 7, pp. 811–827, 05/2006.
- [183] B. J. Klotz, D. Gawlitta, A. J. Rosenberg, J. Malda, and F. P. Melchels, „Gelatin-Methacryloyl Hydrogels: Towards Biofabrication-Based Tissue Repair“, *Trends in Biotechnology*, vol. 34, no. 5, pp. 394–407, 05/2016.
- [184] E. Kaemmerer, F. P. Melchels, B. M. Holzapfel, T. Meckel, D. W. Hutmacher, and D. Loessner, „Gelatine methacrylamide-based hydrogels: An alternative three-dimensional cancer cell culture system“, *Acta Biomaterialia*, vol. 10, no. 6, pp. 2551–2562, 06/2014.
- [185] W. Schuurman *et al.*, „Gelatin-Methacrylamide Hydrogels as Potential Biomaterials for Fabrication of Tissue-Engineered Cartilage Constructs“, *Macromolecular Bioscience*, vol. 13, no. 5, pp. 551–561, 05/2013.
- [186] H. Stratesteffen, M. Köpf, F. Kreimendahl, A. Blaeser, S. Jockenhoevel, and H. Fischer, „GelMA-collagen blends enable drop-on-demand 3D printability and promote angiogenesis“, *Biofabrication*, vol. 9, no. 4, p. 045 002, 09/2017.
- [187] V. H. M. Mouser, F. P. W. Melchels, J. Visser, W. J. A. Dhert, D. Gawlitta, and J. Malda, „Yield stress determines bioprintability of hydrogels based on gelatin-methacryloyl and gellan gum for cartilage bioprinting“, *Biofabrication*, vol. 8, no. 3, p. 035 003, 07/2016.
- [188] I. Pepelanova, K. Kruppa, T. Scheper, and A. Lavrentieva, „Gelatin-Methacryloyl (GelMA) Hydrogels with Defined Degree of Functionalization as a Versatile Toolkit for 3D Cell Culture and Extrusion Bioprinting“, *Bioengineering*, vol. 5, no. 3, p. 55, 07/2018.
- [189] M. Zhu, Y. Wang, G. Ferracci, J. Zheng, N.-J. Cho, and B. H. Lee, „Gelatin methacryloyl and its hydrogels with an exceptional degree of controllability and batch-to-batch consistency“, *Scientific Reports*, vol. 9, no. 1, p. 6863, 05/2019.

- [190] I. Pezron, M. Djabourov, and J. Leblond, „Conformation of gelatin chains in aqueous solutions: 1. A light and small-angle neutron scattering study“, *Polymer*, vol. 32, no. 17, pp. 3201–3210, 01/1991.
- [191] S. B. Ross-Murphy, „Structure and rheology of gelatin gels: recent progress“, *Polymer*, vol. 33, no. 12, pp. 2622–2627, 01/1992.
- [192] Q. Zou, S. M. Habermann-Rottinghaus, and K. P. Murphy, „Urea effects on protein stability: Hydrogen bonding and the hydrophobic effect“, *Proteins: Structure, Function, and Genetics*, vol. 31, no. 2, pp. 107–115, 05/1998.
- [193] M. C. Stumpe and H. Grubmüller, „Interaction of Urea with Amino Acids: Implications for Urea-Induced Protein Denaturation“, *Journal of the American Chemical Society*, vol. 129, no. 51, pp. 16 126–16 131, 12/2007.
- [194] A. Das and C. Mukhopadhyay, „Urea-Mediated Protein Denaturation: A Consensus View“, *The Journal of Physical Chemistry B*, vol. 113, no. 38, pp. 12 816–12 824, 09/2009.
- [195] B. Lee, N. Lum, L. Seow, P. Lim, and L. Tan, „Synthesis and Characterization of Types A and B Gelatin Methacryloyl for Bioink Applications“, *Materials*, vol. 9, no. 10, p. 797, 09/2016.
- [196] E. Hadjipanayi, V. Mudera, and R. A. Brown, „Close dependence of fibroblast proliferation on collagen scaffold matrix stiffness“, *Journal of Tissue Engineering and Regenerative Medicine*, vol. 3, no. 2, pp. 77–84, 02/2009.
- [197] R. A. Marklein and J. A. Burdick, „Controlling Stem Cell Fate with Material Design“, *Advanced Materials*, vol. 22, no. 2, pp. 175–189, 01/2010.
- [198] J. W. Nichol, S. T. Koshy, H. Bae, C. M. Hwang, S. Yamanlar, and A. Khademhosseini, „Cell-laden microengineered gelatin methacrylate hydrogels“, *Biomaterials*, vol. 31, no. 21, pp. 5536–5544, 07/2010.
- [199] C. D. O’Connell *et al.*, „Tailoring the mechanical properties of gelatin methacryloyl hydrogels through manipulation of the photocrosslinking conditions“, *Soft Matter*, vol. 14, no. 11, pp. 2142–2151, 2018.
- [200] S. Krishnamoorthy, B. Noorani, and C. Xu, „Effects of Encapsulated Cells on the Physical–Mechanical Properties and Microstructure of Gelatin Methacrylate Hydrogels“, *International Journal of Molecular Sciences*, vol. 20, no. 20, p. 5061, 10/2019.
- [201] J. Ricka and T. Tanaka, „Swelling of ionic gels: quantitative performance of the Donnan theory“, *Macromolecules*, vol. 17, no. 12, pp. 2916–2921, 12/1984.
- [202] M.-Y. Shie, J.-J. Lee, C.-C. Ho, S.-Y. Yen, H. Y. Ng, and Y.-W. Chen, „Effects of Gelatin Methacrylate Bio-ink Concentration on Mechano-Physical Properties and Human Dermal Fibroblast Behavior“, *Polymers*, vol. 12, no. 9, p. 1930, 08/2020.
- [203] N. Malpica *et al.*, „Applying watershed algorithms to the segmentation of clustered nuclei“, *Cytometry*, vol. 28, no. 4, pp. 289–297, 12/1998.
- [204] S. Eggert and D. W. Hutmacher, „In vitro disease models 4.0 via automation and high-throughput processing“, *Biofabrication*, vol. 11, no. 4, p. 043 002, 07/2019.
- [205] S. Sharifi, H. Sharifi, A. Akbari, and J. Chodosh, „Systematic optimization of visible light-induced crosslinking conditions of gelatin methacryloyl (GelMA)“, *Scientific Reports*, vol. 11, no. 1, p. 23 276, 12/2021.

- [206] J. Kunkel and P. Asuri, „Function, Structure, and Stability of Enzymes Confined in Agarose Gels“, *PLoS ONE*, vol. 9, no. 1, P. K. Agarwal, Ed., e86785, 01/2014.
- [207] M. C. Gutiérrez *et al.*, „Hydrogel scaffolds with immobilized bacteria for 3D cultures“, *Chemistry of Materials*, vol. 19, no. 8, pp. 1968–1973, 2007.
- [208] T. Takei, K. Ikeda, H. Ijima, and K. Kawakami, „Fabrication of poly(vinyl alcohol) hydrogel beads crosslinked using sodium sulfate for microorganism immobilization“, *Process Biochemistry*, vol. 46, no. 2, pp. 566–571, 2011.
- [209] S. V. Murphy and A. Atala, „3D bioprinting of tissues and organs“, *Nature Biotechnology*, vol. 32, no. 8, pp. 773–785, 08/2014.
- [210] D. Grijalva Garces, C. P. Radtke, and J. Hubbuch, „A Novel Approach for the Manufacturing of Gelatin-Methacryloyl“, *Polymers*, vol. 14, no. 24, p. 5424, 12/2022.
- [211] L. Sewald *et al.*, „Beyond the Modification Degree: Impact of Raw Material on Physicochemical Properties of Gelatin Type A and Type B Methacryloyls“, *Macromolecular Bioscience*, vol. 18, no. 12, pp. 1–10, 2018.
- [212] S. Pahoff, C. Meinert, O. Bas, L. Nguyen, T. J. Klein, and D. W. Hutmacher, „Effect of gelatin source and photoinitiator type on chondrocyte redifferentiation in gelatin methacryloyl-based tissue-engineered cartilage constructs“, *Journal of Materials Chemistry B*, vol. 7, no. 10, pp. 1761–1772, 2019.
- [213] A. T. Young, O. C. White, and M. A. Daniele, „Rheological Properties of Coordinated Physical Gelation and Chemical Crosslinking in Gelatin Methacryloyl (GelMA) Hydrogels“, *Macromolecular Bioscience*, vol. 20, no. 12, pp. 1–15, 12/2020.
- [214] H. Tavassoli, S. N. Alhosseini, A. Tay, P. P. Chan, S. K. Weng Oh, and M. E. Warkiani, „Large-scale production of stem cells utilizing microcarriers: A biomaterials engineering perspective from academic research to commercialized products“, *Biomaterials*, vol. 181, pp. 333–346, 10/2018.
- [215] R. Samanipour, Z. Wang, A. Ahmadi, and K. Kim, „Experimental and computational study of microfluidic flow-focusing generation of gelatin methacrylate hydrogel droplets“, *Journal of Applied Polymer Science*, vol. 133, no. 29, p. 43 701, 08/2016.
- [216] N. Leister, C. Yan, and H. P. Karbstein, „Oil Droplet Coalescence in W/O/W Double Emulsions Examined in Models from Micrometer- to Millimeter-Sized Droplets“, *Colloids and Interfaces*, vol. 6, no. 1, p. 12, 02/2022.
- [217] M. V. Bandulasena, G. T. Vladislavljević, and B. Benyahia, „Versatile reconfigurable glass capillary microfluidic devices with Lego® inspired blocks for drop generation and micromixing“, *Journal of Colloid and Interface Science*, vol. 542, pp. 23–32, 2019.
- [218] B. H. Leuenberger, „Investigation of viscosity and gelation properties of different mammalian and fish gelatins“, *Topics in Catalysis*, vol. 5, no. 4, pp. 353–361, 1991.
- [219] E. Van Den Bosch and C. Gielens, „Gelatin degradation at elevated temperature“, *International Journal of Biological Macromolecules*, vol. 32, no. 3-5, pp. 129–138, 2003.
- [220] H. Münstedt and F. R. Schwarzl, *Deformation and Flow of Polymeric Materials*. Berlin/Heidelberg, Germany: Springer Berlin Heidelberg, 2014.

- [221] D. Loessner *et al.*, „Functionalization, preparation and use of cell-laden gelatin methacryloyl-based hydrogels as modular tissue culture platforms“, *Nature Protocols*, vol. 11, no. 4, pp. 727–746, 2016.
- [222] A. Duconseille, D. Andueza, F. Picard, V. Santé-Lhoutellier, and T. Astruc, „Variability in pig skin gelatin properties related to production site: A near infrared and fluorescence spectroscopy study“, *Food Hydrocolloids*, vol. 63, pp. 108–119, 2017.
- [223] J. Olijve, F. Mori, and Y. Toda, „Influence of the molecular-weight distribution of gelatin on emulsion stability“, *Journal of Colloid and Interface Science*, vol. 243, no. 2, pp. 476–482, 2001.
- [224] J. O’Sullivan, B. Murray, C. Flynn, and I. Norton, „The effect of ultrasound treatment on the structural, physical and emulsifying properties of animal and vegetable proteins“, *Food Hydrocolloids*, vol. 53, pp. 141–154, 02/2016.
- [225] T. F. Tadros, *Volume 2 Interfacial Phenomena and Colloid Stability, Industrial Applications*. Berlin, Germany: De Gruyter, 12/2015.
- [226] E. Hoch, C. Schuh, T. Hirth, G. E. Tovar, and K. Borchers, „Stiff gelatin hydrogels can be photo-chemically synthesized from low viscous gelatin solutions using molecularly functionalized gelatin with a high degree of methacrylation“, *Journal of Materials Science: Materials in Medicine*, vol. 23, no. 11, pp. 2607–2617, 2012.
- [227] F. P. Melchels, W. J. Dhert, D. W. Hutmacher, and J. Malda, „Development and characterisation of a new bioink for additive tissue manufacturing“, *Journal of Materials Chemistry B*, vol. 2, no. 16, pp. 2282–2289, 2014.
- [228] Y. Yang, T. Xu, Q. Zhang, Y. Piao, H. P. Bei, and X. Zhao, „Biomimetic, Stiff, and Adhesive Periosteum with Osteogenic–Angiogenic Coupling Effect for Bone Regeneration“, *Small*, vol. 17, no. 14, pp. 1–10, 04/2021.
- [229] C. Colosi *et al.*, „Microfluidic Bioprinting of Heterogeneous 3D Tissue Constructs Using Low-Viscosity Bioink“, *Advanced Materials*, vol. 28, no. 4, pp. 677–684, 01/2016.
- [230] S. Halonen, T. Kangas, M. Haataja, and U. Lassi, „Urea-Water-Solution Properties: Density, Viscosity, and Surface Tension in an Under-Saturated Solution“, *Emission Control Science and Technology*, vol. 3, no. 2, pp. 161–170, 06/2017.
- [231] J. Guerrero, Y.-W. Chang, A. A. Fragkopoulos, and A. Fernandez-Nieves, „Capillary-Based Microfluidics—Coflow, Flow-Focusing, Electro-Coflow, Drops, Jets, and Instabilities“, *Small*, vol. 16, no. 9, p. 1904344, 03/2020.
- [232] A. S. Utada, A. Fernandez-Nieves, H. A. Stone, and D. A. Weitz, „Dripping to jetting transitions in coflowing liquid streams“, *Physical Review Letters*, vol. 99, no. 9, pp. 1–4, 2007.
- [233] S. V. Murphy and A. Atala, „3D bioprinting of tissues and organs“, *Nature Biotechnology*, vol. 32, no. 8, pp. 773–785, 08/2014.
- [234] I. T. Ozbolat and M. Hospodiuk, „Current advances and future perspectives in extrusion-based bioprinting“, *Biomaterials*, vol. 76, pp. 321–343, 01/2016.
- [235] J. Thiele, Y. Ma, S. M. C. Bruekers, S. Ma, and W. T. S. Huck, „25th Anniversary Article: Designer Hydrogels for Cell Cultures: A Materials Selection Guide“, *Advanced Materials*, vol. 26, no. 1, pp. 125–148, 01/2014.

- [236] Y. Zhao, Y. Li, S. Mao, W. Sun, and R. Yao, „The influence of printing parameters on cell survival rate and printability in microextrusion-based 3D cell printing technology“, *Biofabrication*, vol. 7, no. 4, p. 045 002, 11/2015.
- [237] A. S. Theus *et al.*, „Bioprintability: Physiomechanical and Biological Requirements of Materials for 3D Bioprinting Processes“, *Polymers*, vol. 12, no. 10, p. 2262, 10/2020.
- [238] A. Erdem *et al.*, „3D Bioprinting of Oxygenated Cell-Laden Gelatin Methacryloyl Constructs“, *Advanced Healthcare Materials*, vol. 9, no. 15, pp. 1–12, 08/2020.
- [239] H. Jongprasitkul, S. Turunen, V. S. Parihar, and M. Kellomäki, „Two-step crosslinking to enhance the printability of methacrylated gellan gum biomaterial ink for extrusion-based 3D bioprinting“, *Bioprinting*, vol. 25, no. September 2021, e00185, 03/2022.
- [240] A. Habib, V. Sathish, S. Mallik, and B. Khoda, „3D Printability of Alginate-Carboxymethyl Cellulose Hydrogel“, *Materials*, vol. 11, no. 3, p. 454, 03/2018.
- [241] A. Mondal *et al.*, „Characterization and printability of Sodium alginate -Gelatin hydrogel for bioprinting NSCLC co-culture“, *Scientific Reports*, vol. 9, no. 1, p. 19 914, 12/2019.
- [242] M. D. Giuseppe *et al.*, „Mechanical behaviour of alginate-gelatin hydrogels for 3D bioprinting“, *Journal of the Mechanical Behavior of Biomedical Materials*, vol. 79, pp. 150–157, 03/2018.
- [243] M. Uzun-Per *et al.*, „Automated Image Analysis Methodologies to Compute Bioink Printability“, *Advanced Engineering Materials*, vol. 23, no. 4, pp. 1–12, 04/2021.
- [244] S. Dani *et al.*, „Homogeneous and Reproducible Mixing of Highly Viscous Biomaterial Inks and Cell Suspensions to Create Bioinks“, *Gels*, vol. 7, no. 4, p. 227, 11/2021.
- [245] E. N. Malamas, E. G. Petrakis, M. Zervakis, L. Petit, and J.-D. Legat, „A survey on industrial vision systems, applications and tools“, *Image and Vision Computing*, vol. 21, no. 2, pp. 171–188, 02/2003.
- [246] O. Semeniuta, S. Dransfeld, K. Martinsen, and P. Falkman, „Towards increased intelligence and automatic improvement in industrial vision systems“, *Procedia CIRP*, vol. 67, pp. 256–261, 2018.
- [247] F. Koch, K. Tröndle, G. Finkenzeller, R. Zengerle, S. Zimmermann, and P. Koltay, „Generic method of printing window adjustment for extrusion-based 3D-bioprinting to maintain high viability of mesenchymal stem cells in an alginate-gelatin hydrogel“, *Bioprinting*, vol. 20, e00094, 12/2020.
- [248] Z. Di *et al.*, „Ultra High Content Image Analysis and Phenotype Profiling of 3D Cultured Micro-Tissues“, *PLoS ONE*, vol. 9, no. 10, R. Oshima, Ed., e109688, 10/2014.
- [249] D. E. Godar, „3D Bioprinting: Surviving under Pressure“, in *Tissue Regeneration*, Rijeka, Croatia: InTech, 06/2018.
- [250] J. H. Y. Chung *et al.*, „Bio-ink properties and printability for extrusion printing living cells“, *Biomaterials Science*, vol. 1, no. 7, p. 763, 2013.
- [251] B. Webb and B. J. Doyle, „Parameter optimization for 3D bioprinting of hydrogels“, *Bioprinting*, vol. 8, no. July, pp. 8–12, 12/2017.
- [252] D. L. Cohen, W. Lo, A. Tsavaris, D. Peng, H. Lipson, and L. J. Bonassar, „Increased Mixing Improves Hydrogel Homogeneity and Quality of Three-Dimensional Printed Constructs“, *Tissue Engineering Part C: Methods*, vol. 17, no. 2, pp. 239–248, 02/2011.

- [253] A. G. Tabriz, M. A. Hermida, N. R. Leslie, and W. Shu, „Three-dimensional bioprinting of complex cell laden alginate hydrogel structures“, *Biofabrication*, vol. 7, no. 4, p. 045 012, 12/2015.
- [254] K. Nair *et al.*, „Characterization of cell viability during bioprinting processes“, *Biotechnology Journal*, vol. 4, no. 8, pp. 1168–1177, 08/2009.
- [255] J. Snyder, A. Rin Son, Q. Hamid, C. Wang, Y. Lui, and W. Sun, „Mesenchymal stem cell printing and process regulated cell properties“, *Biofabrication*, vol. 7, no. 4, p. 044 106, 12/2015.
- [256] J. Marzi *et al.*, „Non-Invasive Three-Dimensional Cell Analysis in Bioinks by Raman Imaging“, *ACS Applied Materials & Interfaces*, vol. 14, no. 27, pp. 30 455–30 465, 07/2022.
- [257] H. Park, S.-W. Kang, B.-S. Kim, D. J. Mooney, and K. Y. Lee, „Shear-reversibly Crosslinked Alginate Hydrogels for Tissue Engineering“, *Macromolecular Bioscience*, vol. 9, no. 9, pp. 895–901, 09/2009.
- [258] F. Hafezi *et al.*, „Bioprinting and Preliminary Testing of Highly Reproducible Novel Bioink for Potential Skin Regeneration“, *Pharmaceutics*, no. 6, p. 550, 06/2020.
- [259] K. Tröndle *et al.*, „Scalable fabrication of renal spheroids and nephron-like tubules by bioprinting and controlled self-assembly of epithelial cells“, *Biofabrication*, vol. 13, no. 3, p. 035 019, 07/2021.
- [260] B. Schmieg *et al.*, „Structured Data Storage for Data-Driven Process Optimisation in Bioprinting“, *Applied Sciences*, vol. 12, no. 15, p. 7728, 08/2022.
- [261] P. Bartolo, A. Malshe, E. Ferraris, and B. Koc, „3D bioprinting: Materials, processes, and applications“, *CIRP Annals*, vol. 71, no. 2, pp. 577–597, 2022.
- [262] M. Hospodiuk, M. Dey, D. Sosnoski, and I. T. Ozbolat, „The bioink: A comprehensive review on bioprintable materials“, *Biotechnology Advances*, vol. 35, no. 2, pp. 217–239, 2017.
- [263] S. Seiffert and J. Sprakel, „Physical chemistry of supramolecular polymer networks“, *Chemical Society Reviews*, vol. 41, no. 2, pp. 909–930, 2012.
- [264] J. Chrenek, R. Kirsch, K. Scheck, and S. M. Willerth, „Protocol for printing 3D neural tissues using the BIO X equipped with a pneumatic printhead“, *STAR Protocols*, vol. 3, no. 2, p. 101 348, 2022.
- [265] S. Strauß, D. Grijalva Garces, and J. Hubbuch, „Analytics in Extrusion-Based Bioprinting: Standardized Methods Improving Quantification and Comparability of the Performance of Bioinks“, *Polymers*, vol. 15, no. 8, p. 1829, 04/2023.
- [266] L. Ouyang, R. Yao, Y. Zhao, and W. Sun, „Effect of bioink properties on printability and cell viability for 3D bioplotting of embryonic stem cells“, *Biofabrication*, vol. 8, no. 3, p. 035 020, 09/2016.
- [267] E. Karakaya, L. Fischer, J. Hazur, A. R. Boccaccini, I. Thievensen, and R. Detsch, „Strategies to evaluate alginate based bioinks applying extrusion printing for biofabrication“, *Transactions on Additive Manufacturing Meets Medicine*, vol. 2, no. 1, pp. 1–2, 2020.
- [268] A. Ribeiro *et al.*, „Assessing bioink shape fidelity to aid material development in 3D bioprinting“, *Biofabrication*, vol. 10, no. 1, p. 014 102, 11/2017.

- [269] J. M. Rodríguez-Rego, L. Mendoza-Cerezo, A. Macías-García, J. P. Carrasco-Amador, and A. C. Marcos-Romero, „Methodology for characterizing the printability of hydrogels“, *International Journal of Bioprinting*, vol. 9, no. 2, pp. 280–291, 01/2023.
- [270] A. Schwab, R. Levato, M. D’Este, S. Piluso, D. Eglin, and J. Malda, „Printability and Shape Fidelity of Bioinks in 3D Bioprinting“, *Chemical Reviews*, vol. 120, no. 19, pp. 11 028–11 055, 10/2020.
- [271] T. Kreller, T. Distler, S. Heid, S. Gerth, R. Detsch, and A. Boccaccini, „Physico-chemical modification of gelatine for the improvement of 3D printability of oxidized alginate-gelatine hydrogels towards cartilage tissue engineering“, *Materials & Design*, vol. 208, p. 109 877, 10/2021.
- [272] V. Bednarzig, S. Schrüfer, T. C. Schneider, D. W. Schubert, R. Detsch, and A. R. Boccaccini, „Improved 3D Printing and Cell Biology Characterization of Inorganic-Filler Containing Alginate-Based Composites for Bone Regeneration: Particle Shape and Effective Surface Area Are the Dominant Factors for Printing Performance“, *International Journal of Molecular Sciences*, vol. 23, no. 9, p. 4750, 04/2022.
- [273] E. Karakaya *et al.*, „How to Determine a Suitable Alginate for Biofabrication Approaches using an Extensive Alginate Library?“, *Biomacromolecules*, vol. 24, no. 7, pp. 2982–2997, 07/2023.
- [274] A. Wenz, K. Borchers, G. E. M. Tovar, and P. J. Kluger, „Bone matrix production in hydroxyapatite-modified hydrogels suitable for bone bioprinting“, *Biofabrication*, vol. 9, no. 4, p. 044 103, 11/2017.
- [275] K. Markstedt, A. Mantas, I. Tournier, H. Martínez Ávila, D. Hägg, and P. Gatenholm, „3D bioprinting human chondrocytes with nanocellulose-alginate bioink for cartilage tissue engineering applications“, *Biomacromolecules*, vol. 16, no. 5, pp. 1489–1496, 2015.
- [276] N. Brandt *et al.*, „Kadi4Mat: A Research Data Infrastructure for Materials Science“, *Data Science Journal*, vol. 20, no. 1, pp. 1–14, 02/2021.
- [277] S. van der Walt *et al.*, „scikit-image: image processing in Python“, *PeerJ*, vol. 2, no. 1, e453, 06/2014.
- [278] K. He, J. Sun, and X. Tang, „Guided image filtering“, *IEEE Transactions on Pattern Analysis and Machine Intelligence*, vol. 35, no. 6, pp. 1397–1409, 2013.
- [279] P. F. Alcantarilla, A. Bartoli, and A. J. Davison, „KAZE Features“, in *Computer Vision – ECCV 2012*, Berlin/Heidelberg, Germany: Springer Berlin Heidelberg, 2012, pp. 214–227.
- [280] A. F. Frangi, W. J. Niessen, K. L. Vincken, and M. A. Viergever, „Multiscale vessel enhancement filtering“, in *Medical Image Computing and Computer-Assisted Intervention – MICCAI’98*, Berlin/Heidelberg, Germany: Springer Berlin Heidelberg, 1998, pp. 130–137.
- [281] Y. Tsai and T. Kanade, „A Correlation-Based Approach to Robust Point Set Registration“, in *Computer Vision - ECCV 2004*, Berlin/Heidelberg, Germany: Springer Berlin Heidelberg, 2004, pp. 558–569.
- [282] A. A. Armstrong, A. G. Alleyne, and A. J. Wagoner Johnson, „1D and 2D error assessment and correction for extrusion-based bioprinting using process sensing and control strategies“, *Biofabrication*, vol. 12, no. 4, p. 045 023, 10/2020.

- [283] M. Kesti, P. Fisch, M. Pensalfini, E. Mazza, and M. Zenobi-Wong, „Guidelines for standardization of bioprinting: A systematic study of process parameters and their effect on bioprinted structures“, *BioNanoMaterials*, vol. 17, no. 3-4, pp. 193–204, 2016.
- [284] M. Djabourov, J. Leblond, and P. Papon, „Gelation of aqueous gelatin solutions. I. Structural investigation“, *Journal de Physique*, vol. 49, no. 2, pp. 319–332, 1988.
- [285] Y. Maki and M. Annaka, „Gelation of fish gelatin studied by multi-particle tracking method“, *Food Hydrocolloids*, vol. 101, no. October 2019, p. 105 525, 04/2020.

List of Figures

3.1	Synthesis and purification of gelatin methacryloyl (GelMA)	38
3.2	Image processing workflow for cell counting.	42
3.3	Degree of functionalization (DoF) of produced gelatin methacryloyl (GelMA) batches the DoF was determined by the TNBS method	43
3.4	Elastic plateau modulus of gelatin methacryloyl (GelMA) hydrogels at various concentrations	45
3.5	Equilibrium swelling ratio of gelatin methacryloyl (GelMA) hydrogels at various concentrations	46
3.6	Cell viability of NIH 3T3 fibroblasts on gelatin methacryloyl (GelMA) coated well plates	47
4.1	Viscosity of solution comprising gelatin at 10 % (w/v) in reaction buffer measured at room temperature	61
4.2	Degree of functionalization (DoF) of produced gelatin methacryloyl (GelMA) of various sources.	62
4.3	Elastic plateau modulus of gelatin methacryloyl (GelMA) hydrogels of various sources at 10 % (w/v)	65
4.4	Schematic of the microfluidic setup used in the study on the production of gelatin methacryloyl (GelMA) droplets of various sources	67
4.5	Viscosity of gelatin methacryloyl (GelMA) solutions of various sources and sunflower seed oil measured at room temperature	68
4.6	Production of gelatin methacryloyl (GelMA) droplets in a microfluidic device	70
4.7	Volumetric swelling ratio of gelatin methacryloyl (GelMA) microparticles	72
5.1	Exemplary representation of the object recognition	85
5.2	Schematic of the workflow applied for the determination of the processing effects on cell viability	87
5.3	Rheological characterization of biomaterial inks	88
5.4	Printing accuracy study line structure	89
5.5	Exemplary raw images of printed lines with bioink containing cells.	90
5.6	Printing accuracy study for the circle structure	91
5.7	Printing accuracy study for the angle structure	91
5.8	Characterization of the effect of processing on cells	95

6.1	Illustrative scheme summarizing the workflow in the round robin tests	104
6.2	Scheme of the experimental design of the Round robin - 3D printing	106
6.3	Overview of deviations with images shown as examples that occurred during the printing experiments	111
6.4	Deviations of the images from the specifications taken in the round robin test	112
6.5	Filament width of circle geometries extracted by the three image analysis groups	113
6.6	Filament width of geometries printed with Cellink Bioink	115
6.7	Filament width of geometries printed with Cellink Bioink.	117
6.8	Filament width of geometries printed with gelatin-based ink	119
A5.1	Designed models used during the Round robin - 3D printing test	157
A5.2	Schematic draft of features describing the geometries used in the results from the Round robin - Image analysis study	158
A5.3	Exemplary raw images of each printed geometry and bioink during the Round robin - 3D printing test	159

List of Tables

1.1	Dimensionless number for characterizing droplet generation in microfluidic systems. ρ : fluid density, L : characteristic length, v : characteristic velocity, η : viscosity, σ : interfacial tension.	17
3.1	Overview of the experimental set-up for the synthesis of gelatin methacryloyl (GelMA) .	38
4.1	Overview of gelatin types for the synthesis of gelatin methacryloyl (GelMA)	60
4.2	Composition of disperse phase as employed for the production of hydrogel microparticles as well as the feed rate and feed ratio of continuous phase to disperse phase.	68
5.1	Biomaterial ink compositions as employed in this study and abbreviations used throughout this work	82
5.2	Graphic models of the printing path.	84
6.1	Extrusion principles and specifications of printing equipment used by the participating laboratories in the Round robin - 3D printing test	107
6.2	Materials employed in the Round robin - 3D printing test with recommendations of printing parameters	107
6.3	Summary of the coefficients of variation for each laboratory regarding the examination of the effects of the extrusion mechanism on the filament width	115
6.4	Summary of the coefficients of variation for each laboratory regarding the examination of the effects of the method used for coordinate calibration on the filament width	117
6.5	Summary of the coefficients of variation for each laboratory regarding the examination of the effects of the mechanism for temperature control on the filament width	118

Abbreviations

Acronym	Meaning
2D	Two-dimensional
3D	Three-dimensional
IA	Image analysis
BioFI	Bioprinting Fidelity Imager
CAD	Computer-aided design
CAM	Calcein-AM
CB	Carbonate-bicarbonate
CCM	Cell culture media
CV	Coefficient of variation
DoF	Degree of functionalization
DPBS	Dulbecco's phosphate buffered saline
DMEM	Dulbecco's Modified Eagle Medium
DMV	Droplet morphometry and velocimetry
EBB	Extrusion-based bioprinting
ECM	Extracellular matrix
EDTA	Ethylenediaminetetraacetic acid
ESB	European Society of Biomaterials
ESC	Embryonic stem cell
FA	Focal adhesion
FBS	Fetal bovine serum
G	L-guluronic acid
GAG	Glycosaminoglycan
GelMA	Gelatin-methacryloyl
GMP	Good manufacturing practice
HA	Hyaluronic acid
HEK	Human Embryonic Kidney
HMP	Hydrogel microparticle

Continued on next page

Acronym	Meaning
IA	Image analysis
IEP	Isoelectric point
ISO	International Organization for Standardization
LAP	lithium phenyl-2,4,6- trimethyl- benzoylphosphinate
LED	Light-emitting diode
LVE	Linear viscoelastic
M	D-mannuronic acid
MAA	Methacrylic anhydride
MTT	3-(4,5-dimethylthiazol-2-yl)-2,5-diphenyltetrazolium bromide
MSC	Mesenchymal stem cell
MW	Molecular weight
NIH	National Institutes of Health
PAT	Process analytical technology
PG	Proteoglycan
PI	Propidium iodide
PTFE	Polytetrafluoroethylen
RGD	Arginine-Glycine-Aspartic acid
ROI	region of interest
RT	Room temperature
SOP	Standard operating procedure
TC	tissue culture
TE	Tissue engineering
TFF	Tangential flow filtration
TNBS	2,4,6-Trinitrobenzenesulfonic acid solution
UV	Ultraviolet
VDI	Verein deutsch Ingenieure, the Association of German Engineers
VSR	Volumetric swelling ratio

Symbols

Symbol	Meaning
α	Angle
α_n	Normalized angle
$\dot{\gamma}$	Shear rate
η	Viscosity
ρ	Density
σ	Interfacial tension
c	Concentration
d	Diameter
K	Consistency index
l	Length
l_n	Normalized length
L	Characteristic length
m	Weight
n	Power law exponent
N	Number
p	Pneumatic pressure
Q	Volumetric flow rate
r	Radius
r_n	Normalized radius
\bar{v}	Mean velocity
T	Temperature
v	Characteristic velocity
w	Width

A5

Appendix Chapter 5

On the reproducibility of extrusion-based bioprinting: round robin study on standardization in the field

David Grijalva Garces^{1,2}, Svenja Strauß^{1,2}, Sarah Gretzinger^{1,2}, Barbara Schmiegl^{1,2}, Tomasz Jüngst^{3,4}, Jürgen Groll^{3,4}, Lorenz Meinel⁵, Isabelle Schmidt⁶, Hanna Hartmann⁶, Katja Schenke-Layland^{6,7}, Nico Brandt⁸, Michael Selzer⁹, Stefan Zimmermann¹⁰, Peter Koltay¹⁰, Alexander Southan^{11,12}, Günter E. M. Tovar^{11,12}, Sarah Schmidt¹², Achim Weber¹², Tilman Ahlfeld¹³, Michael Gelinsky¹³, Thomas Scheibel^{4,14}, Rainer Detsch¹⁵, Aldo R. Boccaccini¹⁵, Toufik Naolou¹⁶, Cornelia Lee-Thedieck¹⁶, Christian Willems¹⁷, Thomas Groth¹⁷, Stephan Allgeier¹⁸, Bernd Köhler¹⁸, Tiaan Friedrich¹⁹, Heiko Briesen¹⁹, Janine Buchholz²⁰, Dietrich Paulus²⁰, Anselm von Gladiss²⁰ and Jürgen Hubbuch^{1,2}

- ¹ Institute of Functional Interfaces, Karlsruhe Institute of Technology (KIT), Eggenstein-Leopoldshafen, Germany
- ² Institute of Engineering in Life Sciences, Section IV: Biomolecular Separation Engineering, Karlsruhe Institute of Technology (KIT), Karlsruhe, Germany
- ³ Department for Functional Materials in Medicine and Dentistry, Institute of Functional Materials and Biofabrication, University of Würzburg, Würzburg, Germany
- ⁴ Bavarian Polymer Institute, University of Bayreuth, Bayreuth, Germany
- ⁵ Institute of Pharmacy and Food Chemistry, University of Würzburg, Würzburg, Germany
- ⁶ NMI Natural and Medical Sciences Institute at the University of Tübingen, Reutlingen, Germany
- ⁷ Institute of Biomedical Engineering, Department for Medical Technologies and Regenerative Medicine, Eberhard Karls University of Tübingen, Tübingen, Germany
- ⁸ Institute for Applied Materials, Karlsruhe Institute of Technology (KIT), Karlsruhe, Germany
- ⁹ Institute for Nanotechnology, Karlsruhe Institute of Technology (KIT), Karlsruhe, Germany
- ¹⁰ Laboratory for MEMS Applications, Department of Microsystems Engineering, University of Freiburg, Freiburg, Germany
- ¹¹ Institute of Interfacial Process Engineering and Plasma Technology, University of Stuttgart, Stuttgart, Germany
- ¹² Functional Surfaces and Materials, Fraunhofer Institute for Interfacial Engineering and Biotechnology, Stuttgart, Germany
- ¹³ Center for Translational Bone, Joint, and Soft Tissue Research, Faculty of Medicine, Technische Universität Dresden, Dresden, Germany
- ¹⁴ Chair of Biomaterials, University of Bayreuth, Bayreuth, Germany
- ¹⁵ Institute of Biomaterials, Friedrich-Alexander University Erlangen-Nuremberg, Erlangen, Germany
- ¹⁶ Institute of Cell Biology and Biophysics, Leibniz University Hannover, Hannover, Germany
- ¹⁷ Department Biomedical Materials, Martin Luther University Halle-Wittenberg, Halle (Saale), Germany
- ¹⁸ Institute for Automation and Applied Informatics, Karlsruhe Institute of Technology (KIT), Eggenstein-Leopoldshafen, Germany
- ¹⁹ Process Systems Engineering, School of Life Sciences, Technical University of Munich, Freising, Germany
- ²⁰ Institute for Computational Visualistics, Active Vision Group, University of Koblenz, Koblenz, Germany
- * Contributed equally

A5.1 CAD models used during the Round robin – 3D printing test



Figure A5.1 Designed models used during the Round robin - 3D printing test. (A) single layer line, (B) single layer circle, (C) two layer rectangle geometries, and (D) scaffold which equaled the rectangle geometry with several printed layers.

A5.2 Schematic draft of line and circle width

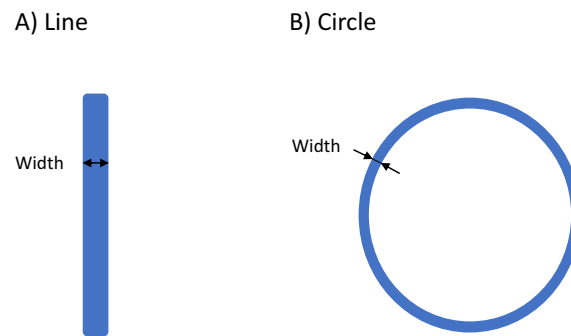


Figure A5.2 Schematic draft of features describing the geometries used in the results from the Round robin - Image analysis study, namely line width (**A**) and circle width (**B**).

A5.3 Exemplary raw images

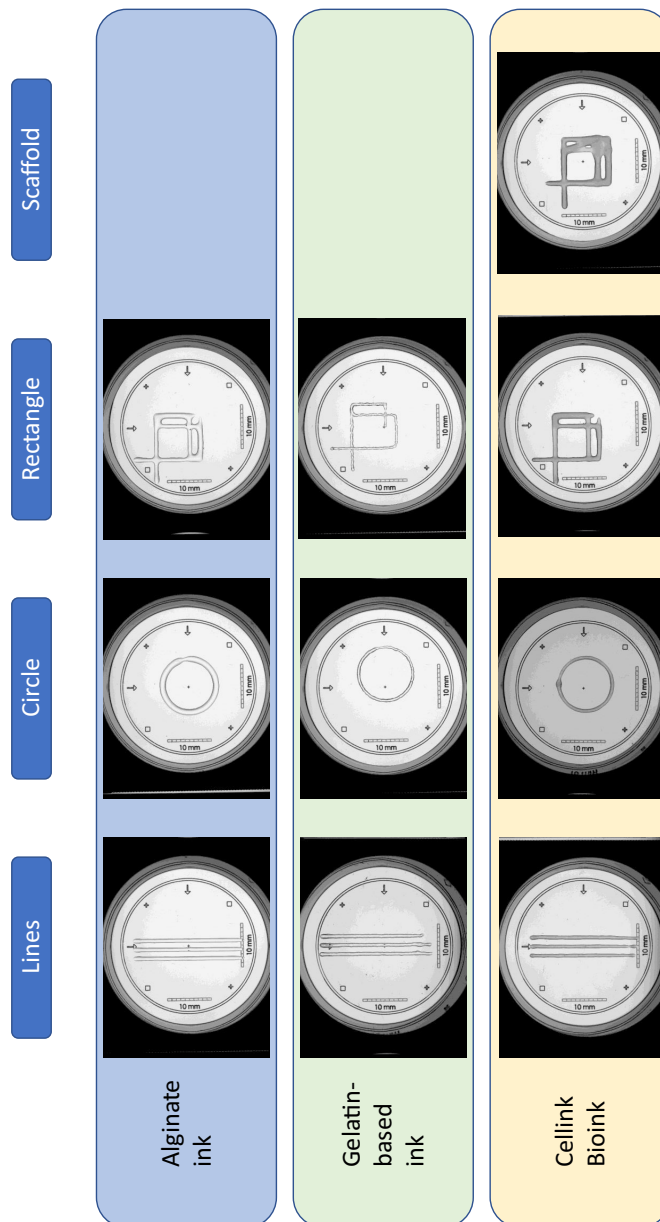


Figure A5.3 Exemplary raw images of each printed geometry and bioink during the Round robin - 3D printing test. The designed models are shown in Figure 6.1. Scale bars left and below printed geometries: 10 mm

